

# **Topology Optimisation for Fluid Flow and Heat Transfer Applications**

**Mani Sekaran Santhanakrishnan**

Department of Mathematical Sciences

University of Greenwich

A thesis submitted in partial fulfilment of the  
requirements of the University of Greenwich  
for the Degree of Doctor of Philosophy

September 2018

## Declaration

I certify that the work contained in this thesis, or any part of it, has not been accepted in substance for any previous degree awarded to me, and is not concurrently being submitted for any degree other than that of Doctor of Philosophy in Mathematical Sciences, being studied at the University of Greenwich. I also declare that this work is the result of my own investigations except where otherwise identified by references and that the contents are not the outcome of any form of research misconduct.

.....

Mani Sekaran Santhanakrishnan ( Ph.D. Student)

Date :

.....

Dr. Timothy Tilford (1<sup>st</sup> Supervisor)

Date :

.....

Professor Christopher Bailey (2<sup>nd</sup> Supervisor)

Date :

## **Acknowledgements**

Firstly I would like to thank my supervisors Dr. Timothy Tilford and Prof. Christopher Bailey for their continued, invaluable advice and support throughout the duration of this research. Without their support and encouragement this research work may not have been feasible. In addition, I would like to thank the University of Greenwich, who has funded this study through Vice Chancellor's Scholarship.

I would like to thank Dr. Mayur Patel, Dr. Stoyan Stoyanov, Dr. Hua Lu, Dr. Erwin George and Dr. Andrew Kao for their valuable advice and assistance relating to the research and for providing the softwares required for this study.

I would also like to extend my sincere gratitude to the examiners Dr. Robin Bornoff, Mentor Graphics and Dr. Alan J. Soper, University of Greenwich for critically evaluating this thesis and for providing valuable feedback to improve its quality.

I would also like to thank Dr. Georgios Michailidis of Ecole Polytechnique, Paris, Dr. Kristian Ejlebjærg Jensen, Dr. Joe Alexanderson, and Dr. Jan HK Haertel of DTU, Denmark for their invaluable help and support during this research work.

Finally, I would also like to thank my family and friends who always supported and encouraged me.

# Abstract

In this study, we apply the two most prevalent topological optimisation algorithms to the design of single material heat sinks and heat exchangers. We aim to determine the merits and drawbacks of each method, extend the most suitable method to consider multi-material structures and to subsequently apply this method to design heat recovery structures subject to fluid convection. The two optimisation methods assessed were the density method and the level-set topological optimisation method.

This study presents a review of the current state-of-the-art in topology optimisation, identifying gaps and limitations in current knowledge relating to the application of these methods to fluid-flow and heat transfer problems. Both topological optimisation approaches have been implemented in a numerical framework consisting of a combination of the Matlab package and the Comsol Multiphysics package. The optimisation algorithms have been implemented in Matlab while Comsol is used to perform thermofluid analyses. The implementation has been validated against standard test cases. Comparison of the two methods indicated that the level-set method developed designs performed better than those developed by the density method, and that the level-set method had a number of additional advantages stemming from its superior handling of fluid-solid interface boundary. The relative performance of the approaches is fully discussed.

The level-set approach was extended through implementation of a regular re-initialisation capability to increase the accuracy of interface boundary and through implementation of an adjoint-based sensitivity evaluation to enhance the computational efficiency. This framework is applied to the design of heat-recovery channels, particularly assessing the effect of solid-to-fluid thermal conductivity ratio and flow Reynolds number on the optimised shapes.

This framework is subsequently extended to consider multi-material problems through development of the underlying level-set formulation. The optimal design of copper-aluminium and copper-steel heatsinks are assessed and results and observations are discussed. Potential areas for further works are discussed after drawing conclusions.



# Contents

1	Introduction .....	20
1.1	Motivation for study.....	22
1.2	Aim and Objectives .....	22
1.3	State of the Art.....	23
1.4	Novel contributions .....	25
1.5	Thesis outline .....	26
2	Literature Review .....	29
2.1	Background .....	29
2.2	Topology Optimisation methods.....	29
2.2.1	Density method.....	29
2.2.2	Level-set methods .....	31
2.2.3	Topological derivative method .....	35
2.2.4	Phase field approaches .....	35
2.2.5	Evolutionary structural optimisation method (ESO) .....	36
2.3	Optimisation algorithms .....	36
2.4	Applications of the Density method.....	37
2.4.1	Structural problems.....	37
2.4.2	Fluid flow problems.....	37
2.4.3	Multi-material optimisation problems.....	41
2.5	Applications of the Level-set method .....	41
2.5.1	Structural problems.....	41
2.5.2	Fluid flow problems.....	42
2.5.3	High Reynolds number flow problems.....	43
2.5.4	Thermal problems.....	44
2.5.5	Multi-material optimisation problems.....	45
2.6	Applications of other TO methods.....	46
2.7	Summary .....	46
3	Theory of Topology Optimisation Methods.....	48
3.1	Density method.....	48
3.1.1	Methodology .....	48

3.1.2	Penalisation technique.....	49
3.1.3	Sensitivity evaluation .....	51
3.1.4	Regularisation.....	52
3.2	Level-set method .....	53
3.2.1	Geometry mapping .....	56
3.2.2	Adjoint method for topology optimisation.....	57
3.2.3	Shape sensitivity evaluation.....	60
3.2.4	Topological sensitivity evaluation .....	63
3.2.5	Solving the Hamilton-Jacobi equation .....	65
3.2.6	Re-initialisation methods.....	66
3.2.7	Hole nucleation methods .....	67
3.2.8	Thickness control.....	68
3.2.9	Parametric level-set methods.....	69
3.3	Optimisation algorithms .....	70
3.3.1	Constrained optimisation methods.....	70
3.3.2	Sequential Quadratic Programming (SQP) .....	71
3.3.3	Convex linearization method (CONLIN).....	72
3.3.4	Method of Moving Asymptotes (MMA) .....	74
3.3.5	Optimality criteria method .....	76
3.4	Finite element method .....	77
3.1	Summary .....	78
4	Density and Level-set Method Implementation.....	79
4.1	Introduction.....	79
4.2	Density method based convectively cooled heat sink design – Case 1 .....	79
4.2.1	Numerical model.....	79
4.2.2	Computational details .....	81
4.2.3	Results .....	83
4.2.4	Summary .....	86
4.3	Density method based convectively cooled heat sink design – Case 2 .....	86
4.3.1	Numerical model.....	86
4.3.2	Computational details .....	87
4.3.3	Results .....	87
4.3.4	Summary .....	89
4.4	Coupled Level-set method using Hamilton-Jacobi equation .....	89

4.4.1	Optimisation of Stokes flow diffuser .....	90
4.4.2	Level-set formulation .....	90
4.4.3	Solution methodology .....	92
4.4.4	Results .....	93
4.4.5	Mesh sensitivity .....	96
4.4.6	Summary .....	96
4.5	Summary .....	97
5	Performance Assessment of Density and Level-set Methods .....	98
5.1	Heat sink design through density method .....	98
5.2	Results of the density method.....	101
5.3	Heat sink design through coupled level-set method.....	106
5.4	Results of the level-set method.....	110
5.5	CFD based validation.....	113
5.5.1	Validation of the highly conductive solid case ( $k_f/k_s=0.001$ ) .....	113
5.5.2	Validation of low conductivity solid case ( $k_f/k_s=0.1$ ) .....	119
5.6	Discussion .....	121
5.7	Summary .....	122
6	Enhancement of Level-Set Optimisation Framework .....	124
6.1	Introduction.....	124
6.2	Level-set advection.....	124
6.3	Re-initialisation of level-sets.....	125
6.3.1	Numerical implementation .....	126
6.4	Heat sink design with re-initialisation of level-set .....	128
6.4.1	Computational details .....	128
6.4.2	2D Heat sink results and discussion .....	131
6.4.3	3D Heat sink results and discussion .....	134
6.4.4	Summary .....	136
6.5	Adjoint based shape sensitivity evaluation .....	136
6.6	Topology optimisation of 'Bend channel' using adjoint sensitivity .....	140
6.6.1	Computational details .....	140
6.6.2	Results .....	141
6.7	Topology derivative based optimisation .....	143

6.8	Topology optimisation of irregular design domain .....	145
6.9	Summary .....	147
7	Topology Optimisation of Heat Recovery Channel.....	148
7.1	Introduction.....	148
7.2	Two-dimensional optimisation.....	149
7.3	Two-dimensional results and discussion.....	154
7.3.1	$k_s/k_f=10$ case:.....	154
7.3.2	$k_s/k_f=1$ case:.....	156
7.3.3	$k_s/k_f=1$ case with $k_s=k_f=0.4$ [W/m/K]: .....	158
7.3.4	$k_s/k_f=1$ case with $k_f=k_s=0.04$ [W/m/K]:.....	160
7.4	Three-dimensional optimisation .....	163
7.4.1	Three-dimensional numerical model .....	163
7.4.2	Three-dimensional results and discussion ( $k_s/k_f=1$ ).....	165
7.5	Summary .....	168
8	Topology Optimisation of Multi-material Heat Sink.....	170
8.1	Introduction.....	170
8.2	Two-material topology optimisation formulation .....	170
8.3	Three-material topology optimisation formulation.....	174
8.4	Computational details .....	175
8.5	Two dimensional study results .....	179
8.6	Three dimensional study results: .....	184
8.7	Summary .....	190
9	Conclusions and Future Work.....	191
10	References.....	194

## List of Figures

Figure 1- 1 Iterative progression of structural topological optimisation of a mechanical structure .....	20
Figure 1- 2 Bridge support structures design using topological optimisation [2].....	21
Figure 1- 3 Thesis Outline .....	28
Figure 2-1 Density based Topology optimisation process flowchart .....	31
Figure 2-2 Level-set based Topology optimisation process flow chart.....	33
Figure 3-1 Comparison of SIMP and RAMP interpolation functions .....	50
Figure 3-2 Convex interpolation function for fluid flow .....	51
Figure 3-3 Level-set function boundary (left) and full function (right) .....	54
Figure 3-4 Signed distance function (red cone) of a disk (grey colour) .....	55
Figure 3-5 Design domain and the level-set model .....	55
Figure 3-6 Cantilever problem with boundary conditions .....	62
Figure 4-1 Computational domain details .....	81
Figure 4-2: Evolution of heat sink shape during the optimisation process .....	84
Figure 4-3: Convergence plot of objective function.....	84
Figure 4-4: Optimised (porous) solid material layout with velocity contour (top) and temperature contours (bottom) for $Re=12$ .....	85
Figure 4-5: Optimised (porous) solid material layout with velocity (top) and temperature contour (bottom) for $Re=70$ .....	86
Figure 4-6 Optimised shape and Temperature contour with coarse mesh for $k_f/k_s=0.1$ at $\gamma_{initial}=0.2$ .....	87
Figure 4-7 Optimisation results with fine mesh for $k_f/k_s=0.1$ at $\gamma_{initial}=0.2$ .....	88
Figure 4-8 Optimised shapes for $\gamma_{initial}$ values of 0.5 (Top), 0.7 (Centre) and 1.0 (Bottom).....	88
Figure 4-9 Convergence history for $\gamma_{initial}= 0.5$ case, and the corresponding Temperature contour.....	89
Figure 4-10 Design domain and boundary conditions .....	91
Figure 4-11 Different LS initialisations tried in this study: Uniform circles (left), Full fluid (centre) and Fluid in the middle rectangle (right). (Blue=solid, Red=fluid).....	93
Figure 4-12 Optimised shape & Velocity contour obtained for uniform circle LS.....	94
Figure 4-13 Optimised shape & Velocity contour obtained for full fluid LS.....	94

Figure 4-14 Optimised shape & Velocity contour obtained for middle fluid LS on mesh 51x51 .....	94
Figure 4-15 Optimised shape & Convergence plot obtained for middle fluid LS on 101x101 mesh.....	95
Figure 4-16 Pressure and Velocity contour for middle fluid LS on 101x101 mesh .....	95
Figure 4-17 Velocity contour on CFD simulation of approximately equivalent diffuser shape .....	96
Figure 5-1 Computational domain of 3D heat sink design study.....	100
Figure 5-2 Density method optimised heat sink for $k_f/k_s = 0.001$ at initial $\gamma$ of 0.1 and 0.25	102
Figure 5-3 Density method optimised heat sink for $k_f/k_s = 0.001$ at initial $\gamma$ of 0.45 and 0.55 .....	102
Figure 5-4 Full view of the best optimised heat sink (Isometric, Top view) by Density method for $k_f/k_s = 0.001$ . .....	103
Figure 5-5 Temperature contour in the design domain for $k_f/k_s = 0.001$ at initial $\gamma$ of 0.55...	103
Figure 5-6 Density method optimised heat sink for $k_f/k_s = 0.1$ at initial $\gamma$ of 0.1 and 0.25.....	104
Figure 5-7 Density method optimised heat sink for $k_f/k_s = 0.1$ at initial $\gamma$ of 0.45 and 0.55...	104
Figure 5-8 Full view of best optimised heat sink by Density method for $k_f/k_s = 0.1$ .....	105
Figure 5-9 Temperature contour in the design domain for best optimised heat sink by DM for $k_f/k_s = 0.1$ (Top & Bottom view) .....	105
Figure 5-10 Convergence of objective function for $k_f/k_s = 0.001$ ( $\gamma$ initial=0.25) and $k_f/k_s$ 0.1 ( $\gamma$ initial=0.55).....	105
Figure 5-11 Initial Level-set distribution (A) in the design domain (Red- solid, Blue-Fluid). 109	
Figure 5-12 Cube like level-set initialisation (B).....	110
Figure 5-13 Optimised shape for $k_f/k_s = 0.001$ through Level-set method with initialisation A and the convergence plot.....	111
Figure 5-14 Optimised shape for $k_f/k_s = 0.001$ through Level-set method with initialisation B .....	111
Figure 5-15 Temperature contour on design domain for $k_f/k_s = 0.001$ through LSM with initialisation B.....	112
Figure 5-16 Optimised shape for $k_f/k_s = 0.1$ through Level-set method with initialisation B .	112
Figure 5-17 3Dimensional Pin-fin heat sink geometry .....	115
Figure 5-18 Temperature distribution from CFD study on Standard heatsink for $k_f/k_s = 0.001$ .....	116
Figure 5-19 Temperature distribution from CFD study on DM heatsink for $k_f/k_s = 0.001$ .....	116
Figure 5-20 Temperature distribution from CFD study on LS heatsink for $k_f/k_s = 0.001$ .....	117

Figure 5-21 Temperature gradient comparison between Standard heatsink, DM & LS heatsinks for $k_f/k_s=0.001$ .....	118
Figure 5-22 CFD based Temperature contour of Standard and DM heat sinks .....	120
Figure 5-23 Temperature gradient comparison between Standard heatsink and DM heatsink for $K_f/K_s =0.1$ .....	120
Figure 6-1 Design domain mesh with surrounding ghost elements used for LS advection	125
Figure 6- 2 Level-set topology optimisation procedure .....	127
Figure 6- 3 Level-set function before and after re- initialisation .....	128
Figure 6- 4 2D Computational domain details .....	128
Figure 6- 5 Three dimensional computational domain.....	131
Figure 6- 6 Optimised shape for higher solid conductivity case and Temperature (K) distribution .....	132
Figure 6- 7 Convergence history of 2D heat sink design using re-initialised LSM.....	132
Figure 6- 8 Optimised shape for lower solid conductivity case ( $k_f/k_s=0.1$ ) and Temperature (K) distribution .....	133
Figure 6- 9 Optimised shape for minimum viscous dissipation and Velocity (m/s) contour	133
Figure 6- 10 Results of combined TC and VD optimisation: Shape, velocity (m/s) and temperature (K) contours .....	134
Figure 6- 11 Front and top view of 3D optimised heat sink.....	135
Figure 6- 12 Temperature (K) distribution in the diagonal plane and convergence history.	135
Figure 6- 13 Design domain geometry for 90° bend channel and initial LS distribution.....	140
Figure 6- 14 Adjoint velocity and adjoint pressure at an instant during optimisation .....	141
Figure 6- 15 Optimised level-set function distribution at Re5.33, Re266.7 and Re622.2 ...	142
Figure 6- 16 Velocity contours on optimised shapes for Re5.33 and Re 622.2.....	142
Figure 6- 17 Pressure (Pa) distribution over optimised shape at Re5.33, Re266.7 and Re622.2 .....	143
Figure 6- 18 Convergence history .....	144
Figure 6- 19 Optimised pipe bend and the velocity contour.....	145
Figure 6- 20 Irregular geometry for topology optimisation .....	146
Figure 6- 21 Multi-block mesh and initial level-set distribution in the design domain .....	146
Figure 6- 22 Optimised flow path shape and its pressure (Pa) contour .....	147
Figure 7- 1 Computational domain of 2D study and initial LS function.....	151
Figure 7- 2 Computational domain with boundary conditions for adjoint equations.....	151

Figure 7- 3 Schematic of Quadrilateral and Linear elements for Finite element discretisation .....	152
Figure 7- 4 Convergence history of a TO run .....	153
Figure 7- 5 Optimised shape (LSF contour) and velocity contour for total pressure drop minimisation at Re=140 .....	154
Figure 7- 6 Optimised shapes and corresponding temperature contour for Re=35 (Left) and Re=70 (Right) for $k_s/k_f = 10$ .....	155
Figure 7- 7 Optimised shapes for Re=70 with $F_2=1e4$ (Left) and $F_2=1e5$ (Right) for $k_s/k_f = 10$ .....	155
Figure 7- 8 Optimised shapes for Re=174 (Left) and 521 (Right) for $F_1=1$ (Top row) and 100 (Bottom row) for $k = 4$ [W/m/K].....	157
Figure 7- 9 Temperature (K) distribution on optimised shapes at Re=174 (Left) and 521 (Right) for $F_1=1$ (Top row) and 100 (Bottom row) for $k = 4$ [W/m/K].....	158
Figure 7- 10 Velocity contour in the design domain for Re=174, $F_1=100$ for $k_f = 4$ [W/m/K] .....	158
Figure 7- 11 Optimised shapes for Re=70 (Left), Re=174 (centre) and 326 (Right) for $F_1=1$ (Top row) and 100 (Bottom row) for $k_f = 0.4$ [W/m/K] .....	159
Figure 7- 12 Temperature (K) distribution on optimised shapes at Re=70 (left), Re=174 (centre) and Re=326 (right).....	160
Figure 7- 13 Optimised shapes for Re=70 (Left), Re=174 (Centre) and 326 (Right) for $F_1=1$ (Top row) & 100 (Bottom row) for $k_f = 0.04$ [W/m/K].....	161
Figure 7- 14 Temperature (K) distribution on optimised shapes for Re=70 (Left), Re=174 (Centre) and 326 (Right) for $F_1=1$ (Top row) & 100 (Bottom row) at $k_f = 0.04$ [W/m/K].....	161
Figure 7- 15 Evolution of optimised shapes during optimisation for $k_s/k_f=1000$ , $F_1=100$ at Re=70.....	163
Figure 7- 16 Full domain with initial LSF and computational domain for 3D heat recovery channel design.....	164
Figure 7- 17 Optimised shapes for glycol ( $k_s=k_f$ ) at Re=19 (Top) and Re=38 (Bottom) and their velocity iso-surface.....	166
Figure 7- 18 Velocity and temperature contour for glycol ( $k_s=k_f$ ) at Re=38 .....	166
Figure 7- 19 Optimised shapes for low conductivity material ( $k_s=k_f$ ) at Re=19 and Re=38 and its velocity iso-surface.....	167
Figure 8- 1 Design domain with level-set representation for two-material structure .....	172
Figure 8- 2 Design domain with level-set representation for three-material structure .....	174
Figure 8- 3 Computational domain and initial distribution of two LSFs.....	175
Figure 8- 4 Convergence history of two material topology optimisation .....	177

Figure 8- 5 Evolution of two-material heat sink shape with iterations.....	178
Figure 8- 6 Optimised shape and the Temperature contour (K) for single material heat sink .....	179
Figure 8- 7 Optimised shape and its temperature contour for case2 .....	180
Figure 8- 8 Optimised shape and its temperature contour for case3 .....	180
Figure 8- 9 Optimised shapes and its temperature contour for case6.....	182
Figure 8- 10 Optimised shapes and its temperature contour for case7.....	182
Figure 8- 11 Optimised shape and its temperature contours for case4.....	183
Figure 8- 12 Optimised shape and its temperature contour for case5 .....	183
Figure 8- 13 Optimised shape and its temperature contour for case8 .....	184
Figure 8- 14 Optimised shape of single material (Cu) 3D heat sink (Front view & Top view) (Case1).....	185
Figure 8- 15 Illustration of initial set-up 'A' (left, Case2) and initial set-up 'B' (right, Case3) .....	185
Figure 8- 16 Optimised copper-aluminium heat sink shape for set-up 'A' (Case2). Top row: Front & topview of Al layout; Bottom row: Complete view and diagonal plane view of Cu-Al heat sink .....	186
Figure 8- 17 Optimised copper-aluminium heat sink shape for set-up 'B'(Case3). Top row: Copper layout and aluminium layout; Bottom row: Complete view & diagonal plane view of Cu-Al heat sink. ....	186
Figure 8- 18 Optimised copper-steel heat sink shape for set-up 'A'(Case4). Top row: Front & topview of steel; Bottom row: Complete view and diagonal plane view of Cu-steel heat sink. .....	188
Figure 8- 19 Optimised copper-steel heat sink for high conductivity fluid with initial set-up 'B' (Case5). Top row: Copper front & top view; Bottom row: Complete view and diagonal plane view of Cu-steel heat sink. ....	189

## List of Tables

Table 4-1 Material property values .....	80
Table 4-2 Parameter values used for Heat sink design .....	82
Table 4-3 Thermal compliance results .....	83
Table 4-4 Parameter values used for Heat sink design .....	87
Table 4-5 Objective values of different $\gamma$ initial simulations .....	88
Table 4-6 Parameter values used for the coupled level-set optimisation .....	91
Table 4-7 Minimum Objective value obtained in different simulations.....	95
Table 5-1 Material property interpolation relations for the Density based 3D heat sink design .....	99
Table 5-2 Parameter values used for the Density based 3D heat sink design .....	99
Table 5-3 Summary of density method results .....	106
Table 5-4 Thermal properties interpolation formula in LS method .....	107
Table 5-5 Comparison of DM and LS results (Volume fraction 0.25).....	113
Table 5-6 Validation of DM TO results for $k_f/k_s=0.001$ for volume fraction 19%.....	116
Table 5-7 Surface area of different heat sinks for volume fraction 19%.....	117
Table 5-8 Validation of DM TO results for $K_f/K_s=0.1$ for volume fraction 25%.....	119
Table 6- 1 Material interpolation formulas .....	129
Table 6- 2 Material properties for 2D heat sink design .....	129
Table 6- 3 Results of minimum thermal compliance objective optimisations.....	133
Table 6- 4 Combined TC and VD optimisation results.....	134
Table 7-1 Thermal properties interpolation for heat recovery channel design.....	150
Table 7- 2 Properties of solid and fluid used in the 2D heat recovery channel design .....	152
Table 7-3 Objective values of optimised shapes for $k_s/k_f=10$ .....	156
Table 7- 4 Optimised objective values of optimised shapes for $k_f =4$ [W/m/K] .....	158
Table 7- 5 Objective values of optimised shapes for $k_f =0.4$ [W/m/K] .....	160
Table 7- 6 Objective values of optimised shapes for $k_f =0.04$ [W/m/K] .....	162
Table 7- 7 Objective values of optimised shapes for $k_s/k_f=1000$ , $F_1=100$ at $Re=70$ .....	162
Table 7- 8 Thermal properties of materials used for 3D heat recovery channel design .....	164
Table 7- 9 Objective values obtained for optimised 3D heat recovery channels .....	167

Table 8- 1 Thermal properties interpolation formula for two-material LSM.....	172
Table 8- 2 Material properties .....	176
Table 8- 3 Thermal conductivity used in different simulations .....	177
Table 8- 4 Summary of 2D multi-material heat sink design results .....	181
Table 8- 5 3D multi-material heat sink design results .....	187

# Nomenclature

$Al$	Aluminium
$c$	Structural compliance
$CFL$	Courant-Friedrichs-Lewy condition
$C_p$	Specific heat capacity at constant pressure
$C_{p\gamma}$	Specific heat capacity at a point in design domain; function of design variable
$Cu$	Copper
$D$	Thermal diffusivity
$DM$	Density Method
$E$	Youngs modulus of a material
$ESO$	Evolutionary Structural Optimisation
$F$	Objective function
$F_1, F_2$	Weightage factors for 'temperature drop' and 'pressure drop' objectives
$FEM$	Finite Element Method
$GMRES$	Generalized Minimum Residual Method
$GCMMA$	Globally Convergent Method of Moving Asymptotes
$H$	Heaviside function
$h$	Width of Heaviside function over which it varies from 0 to 1
$HJ$	Hamilton Jacobi equation
$k$	Thermal conductivity
$K$	Stiffness of a structural member
$k_\gamma$	Thermal conductivity at a point in the design domain; function of design variable.
$L$	Lagrangian of an optimisation problem
$LSF$	Level-set function
$LSM$	Level-set Method
$MMA$	Method of Moving Asymptotes
$N$	Number of level-set cubes

NS	Navier-Stokes equation
$p$	Pressure
<i>PDE</i>	Partial Differential Equation
$Q$	Heat flux
$Q_0$	Temperature dependent heat source
RAMP	Rational Approximation of Material Properties
RD	Reaction Diffusion equation
$S$	Smoothed sign function in Eikonal equation
<i>SDF</i>	Signed distance function
SIMP	Solid Isotropic Material with Penalization
$t$	Time
$T$	Temperature
<i>TC</i>	Thermal Compliance
TEG	Thermoelectric Generators
<i>TO</i>	Topology optimisation
$u$	Velocity vector
$V$	Volume constraint
<i>VD</i>	Viscous Dissipation
$V_n$	Propagation velocity (normal component) of level-set function
$w, q, T\hat{a}$	Adjoint variables for velocity, pressure and temperature
$x, y, z$	Three spatial directions
<i>xFEM</i>	Extended Finite element method
$\rho_\gamma$	Density at a point in design domain; function of design variable

### **Greek letters**

$\Lambda$	Area Penalty factor
$\rho$	Density

$\gamma$	Design variable
$\mu$	Viscosity
$\alpha$	Impermeability factor
$\delta$	Dirac delta function
$\lambda$	Lagrange multiplier
$\lambda_1, \mu_1$	Lame's constant
$\Psi$	Level-set function
$\Omega$	Design domain
$\partial\Omega$	Boundary of design domain
$\Gamma$	Design boundary with specific boundary condition
$\Phi$	Phase field function

### Dimensionless Groups

Re	Reynolds number
Pr	Prandtl number
Biot	Biot number

### Subscripts

f	Fluid
max	Maximum
min	Minimum
n	Normal component
i	Node number in x direction
j	Node number in y direction
k	Node number in z direction
s	solid

### Superscripts

tr	Transpose
----	-----------

# 1 Introduction

Topological optimisation is a numerical approach which aims to determine the distribution of a defined volume of material within a defined space to minimise/maximise a specified objective within a given set of constraints. An illustrative example of the general concept would be a cantilever beam optimisation study presented in Figure 1-1. This work, carried out by Luo et al [1], uses a topological optimisation algorithm to determine the arrangement of material that minimises the displacement of the tip of the beam subject to a specified load. The analysis is subject to constraints defining linear elasticity equations and the volume of material that can be used. We can observe the transition of the design from an initialisation pattern through to an optimal solution. During the optimisation process, the shape of the beam varies a lot. The final optimal design differs quite considerably from ‘traditional’ designs in that it has an organic nature.

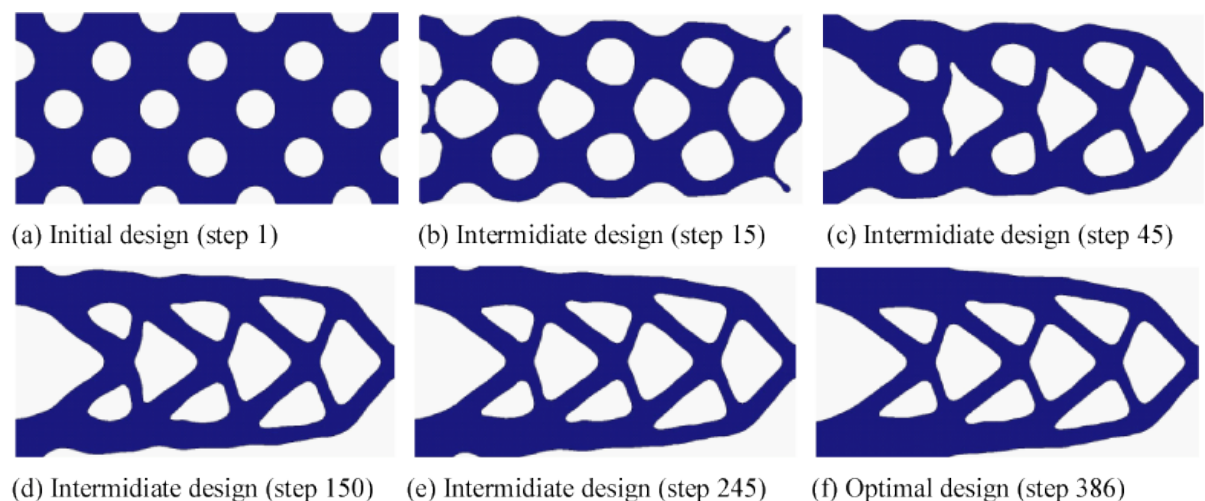


Figure 1- 1 Iterative progression of structural topological optimisation of a mechanical structure



Figure 1- 2 Bridge support structures design using topological optimisation [2]

Figure 1-2 shows a bridge support structure which has been designed using topological optimisation [2], with the organic nature of the design again evident. While the design of the bridge may result in excellent mechanical performance and be aesthetically pleasing there are clearly issues regarding the costs and complexity of making such a structure. Recent advances in additive manufacturing would seem to provide a solution to this issue. Indeed, additive manufacturing and topological optimisation would seem to be highly synergistic technologies.

While topological optimization is now becoming increasingly widely adopted for structural design its use in problems including fluid flow are still very much in their infancy. This is predominantly due to issues relating to complexity, stability and computational expense. In this study, we aim to apply topological optimisation algorithms to the design of heat transfer structures such as heat sinks and heat exchanger systems subject to convective fluid flow. This requires advances beyond the current state-of-the-art in the field. The overall objective is to move toward a point

where topological optimisation algorithms can be utilised to design heat transfer structures that can be fabricated using modern additive manufacturing approaches that provide superior performance to conventional designs. Furthermore, this study assesses the viability of developing designs comprising multiple materials (e.g. copper-aluminium heatsinks) that may enhance cost-performance design trade-offs.

## 1.1 Motivation for study

Heat exchangers are the critical components used in variety of fields, including power generators, aircraft and automobile engines, microelectronics, etc. Increasing demand on the effectiveness of heat exchangers, forces researchers to look for novel design methodologies. Topology optimisation is a novel design method which is capable of giving superior, non-intuitive designs hence it started to find industrial applications in the field of structural engineering. In spite of its advantages, it is not explored much for fluid flow problems because of the complex nature of physics and its modelling. The motivation of this study is to identify the best topology optimisation method for fluid flow problems and developing a state of the art numerical framework for this method. Then this numerical framework will be used for the design of heat exchangers which involves the coupling of two physics namely fluid flow and heat transfer.

Currently most of the micro-electronic heat sinks are made of aluminium; though copper has superior thermal properties it is sparingly used because of its high cost. These low cost aluminium heat sinks become highly incapable with increasing current density and miniaturisation of micro-electronic devices. Hence, there is a need to design alternate heat sinks which will have low cost and superior heat dissipating properties. One possible avenue for this is designing composite heatsinks which use a large amount of aluminium and small amount of copper to enhance its heat dissipating properties. Since topology optimisation is a promising design technique, this will be explored for the design of cost effective multi-material heat sinks which are critically needed for the electronics industry.

## 1.2 Aim and Objectives

The aim of this work is to assess the popular topology optimisation methods and to develop a numerical framework for the suitable topology optimisation method for the

design of fluid flow and heat transfer problems. Using the developed framework, heat recovery channels for different solid-fluid material sets and highly efficient multi-material heat sinks made up of copper, aluminium and steel have to be designed.

The numerical framework is intended to be fixed mesh based, and should be accurate for fluid flow applications. The major objectives of this work are listed below.

- Review and document the current state-of-the-art in topology optimisation and identify gaps and limitations in current knowledge for applying these methods to fluid-flow and heat transfer problems (Chapter 2 & 3).
- Implement both level-set and density topology optimisation methods using Matlab and Comsol and validate with standard test cases (Chapter 4). Compare and contrast the two methods, by designing 3D convectively cooled heat sinks, and hence document their advantages and disadvantages (Chapter 5).
- Develop the level-set numerical framework by implementing a re-initialisation capability and adjoint-based sensitivity evaluation capability. The re-initialisation of level-sets improves the accuracy of interface prediction and adjoint-based sensitivity evaluation reduces the computational cost and improves the accuracy. (Chapter 6).
- Utilise the above framework for the design of heat-recovery channels and study the effect of solid-to-fluid thermal conductivity ratio and Reynolds number on the optimised shapes (Chapter 7).
- Update the above framework to handle multi-material problems, and utilise it for the design of convectively cooled multi-material heat-sinks (Chapter 8).

### 1.3 State of the Art

The state of the art in topology optimisation will be fully outlined in the review chapter of this thesis. However, a brief overview is given in this section. The Density method and level-set method are the two popular methods used for topology optimisation of fluid flow problems. The density method based fluid flow optimisation started with the pioneering work of Borrvall and Petersson [3] whereas the level-set based fluid flow optimisation started with the work of Duan [4]. It is reported in the literature that, for fluid flow problems, the level-set method is better as it can crisply capture the material boundary between the solid and fluid. But apart from this qualitative comparison no

back-to-back comparison has been made between the two methods for any practical design problem analysing in terms of the objective value of the results obtained, computational time, etc.

Though the density method and level-set method are conceptually very different, they both use a gradient based optimising strategy. For finding the gradient or sensitivity of the objective with respect to the design variables, the adjoint sensitivity method is very cost effective. Othmer [5] has evaluated the sensitivity for Navier-Stokes (NS) flows and this has been used widely in conjunction with the density method but very few researchers have used the adjoint sensitivity for the level-set topology optimisation.

The level-set TO is slowly evolving and it is still not extensively utilised for designing complex coupled fluid flow and heat transfer applications. For example, currently heat exchangers or heat recovery channels are designed by conventional design techniques. The use of level-set TO in combination with the adjoint sensitivity, for designing heat recovery channels, can yield significantly better shapes at low computational cost.

Since the TO has the possibility to produce superior designs compared to conventional design methods, it is increasingly applied in various physics, namely structures, structural dynamics, mechanisms, optics, materials, etc. Further, TO methods are also suitable for designing multi-material structures, i.e., using more than one solid material for the design. In this case, the TO not only optimises the outer shape but also determines internal distribution or layout of each of the solid materials involved. Sigmund [6] and Wang [7] pioneered this approach respectively for density method and level-set method for structural problems. The developments taking place in 3D printing technology, especially the selective deposition technique, enables the manufacturability of multi-material structures. Currently most of the heat sinks are made up of aluminium; though copper heat sinks are superior in performance, it is sparingly used because of the cost constraints. Hence there is a strong need for designing copper-aluminium or copper-steel composite heat sinks, as this will improve the heat sink performance yet keeping the cost low. So exploring the TO technique for the design of multi-material heat sinks can pave the way for the design of low cost copper-aluminium heat sinks with superior performance.

## 1.4 Novel contributions

The summary of novel contributions of this thesis are given below.

- **Performance assessment of Density and Level-set method for 3D heat sink design**

Developed Comsol and Matlab based numerical framework for Density and Level-set based TO methods. By using these frameworks, 3D convectively cooled heat sinks were designed for two different material set. Assessed the performance of the two methods in terms of the quality of the design, objective value, computation time taken and robustness.

- **Application of the Level-set TO to the design of heat recovery channels**

Heat exchange or heat recovery channels, which are used in the transportation and energy industry to recover the waste heat, are designed using the adjoint sensitivity based Level-set TO for different solid-fluid conductivity ratios and for different flow Reynolds numbers in 2D and 3D. The design of these channels are challenging as the heat exchange capability has to be maximised without penalising the pumping pressure requirements. Deeper insights on the effect of solid-fluid thermal conductivity value and Reynolds number on the shape of optimised channels have been provided. Capability and limitations of the Level-set method to this application are also discussed.

- **Application of the Level-set TO to the design of multi-material heat sinks**

Extended the multi-material level-set optimisation techniques which are currently used in the field of structural mechanics, to the design of two and three solid material convectively cooled heat sinks. This will pave the way for the design of composite copper-aluminium or copper-steel heat sinks which will be cheap but yet very effective in heat dissipation. Effect of solid-to-solid and solid-to-fluid thermal conductivity ratio on the optimised heat sink shape is studied in detail. Effect of the solid material volume constraint is also studied in detail.

## Publications

The research presented in this document has contributed to 2 journal papers and 3 conference papers and they are listed below. An additional journal article titled “Adjoint based Level-set Topology Optimisation for Heat Recovery Channel Design” is under preparation.

- i. “Performance assessment of Density and Level-set Topology Optimisation methods for 3D Heat sink design”, **Journal of Algorithms and Technology**, June, 2018.
- ii. “Multi-material Heat sink Design using Level-set Topology Optimisation”, Journal article submitted to **IEEE Transactions on Components, Packaging and Manufacturing Technology**, on Aug., 2018.

### Conference Papers:

- i. “On the application of Topology optimisation techniques to the thermal management of microelectronics systems”, 17th **EurosimE IEEE** conference, Montpellier, 2016.
- ii. “Level-set based topology optimisation of convectively cooled heatsinks” **Comsol Conference**, Rotterdam, Netherlands, Oct, 2017.
- iii. “Multi-material Level-set based topology optimisation of convectively cooled heat sinks”, **ECCM-ECFD** 2018 conference, Glasgow, June, 2018.

## 1.5 Thesis outline

This document is split into nine chapters and the schematic outline of this thesis is given in Figure 1-3. The first chapter gives an overview of the topology optimisation process and presents aims and objectives of this research work. The second chapter contains the literature review and considers the current state of the art in topology

optimisation methods and their application to various fields and in particular to fluid flow and heat transfer.

The third chapter discusses the theory behind the density method and level-set method. Further, different optimisation algorithms are explained in detail along with a brief note on finite element methods.

The fourth chapter presents the density and level-set method numerical framework and their validation on standard test cases. The fifth chapter concerns the use of the density and level-set method in designing three dimensional convectively cooled heat sink and the performance assessment of the two methods.

The sixth chapter discusses the various features implemented in the Level-set TO framework. Implementation details about the re-initialisation of level-sets, adjoint based shape sensitivity evaluation and topological derivative for fluid flow cases are presented and the results of validation cases are also explained.

The seventh chapter discusses the design of heat recovery channels using the level-set method. The eighth chapter discusses the design of multi-material convectively cooled heat sink design using the level-set method.

The ninth chapter summarises the other chapters and also discusses possible potential extensions of the present work.

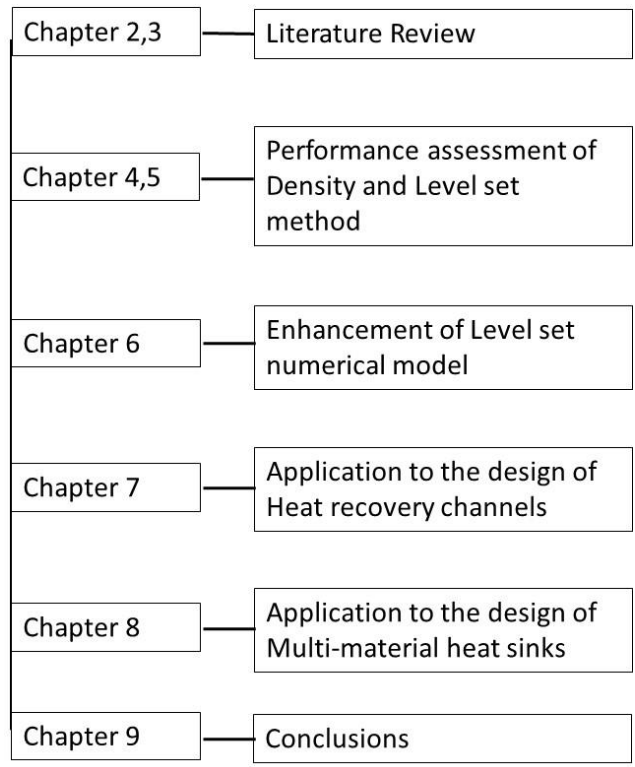


Figure 1- 3 Thesis Outline

## 2 Literature Review

### 2.1 Background

Currently, topology optimisation techniques find lots of applications in structural mechanics mainly for compliance minimisation of structures. Recently, this method is being applied to other fields, including structural dynamics, heat transfer, fluid flows, electromagnetics, optics and their combinations. A seminal paper on numerical topology optimisation was published by Bendsoe and Kikuchi in 1988 [8]. This was a finite element method based topology optimisation using a homogenisation method wherein the heterogeneous medium is replaced with a homogeneous medium to compute the solution. Following this, many researchers worked in this area to propose new methods for topology optimisation and to extend the existing TO methods to new physics. The popular TO methods are the density method, level-set method, evolutionary shape optimisation and topology derivative method. In this section, each of the methods is briefly described and an elaborate review of the TO work carried out in fluid flow and heat transfer is also reported.

### 2.2 Topology Optimisation methods

In the following chapters the literature pertaining to different topology optimisation approaches and optimisation algorithms are reviewed and discussed.

#### 2.2.1 Density method

This method was introduced by Bendsoe in 1989 [9]. It is a relatively simple and fast method. In this method, critical parameters of physics and the objective function are modelled as a function of material density ( $\rho$ ), which acts as the design variable for the optimisation problem. In earlier days, the optimisation problem was solved as a variable thickness problem for compliance constraints. The topology optimisation

method could be thought of as an improvement over variable thickness optimisation. Here, thickness is replaced with density of the material in a given finite element cell and the density is made to take a 0 or 1 value by penalising the intermediate density values. A density value of 0 represents no material and 1 represents material in the given finite element cell. Bendsoe proposed a simple and effective power law approach for penalisation (Eqn 2.1).

$$E = E_o \rho_i^p \quad (2.1)$$

Where  $E_o$  is the material property and ' $p$ ' is the power factor and it generally takes a value of 3. This method of penalisation of intermediate densities is called Solid Isotropic Material with Penalisation or SIMP.

The Density method is mostly implemented using finite element solvers. In the finite element method, each mesh element stores state variables and density variables and they are solved during each iteration. For given initial values of density, the physics of the problem is solved, then the objective function and sensitivity of objective function with respect to density are calculated. A gradient based optimiser solves for the new density values based on the sensitivity information. This procedure is repeated until change in density distribution becomes negligible. The various steps involved in the density based topology optimisation [10] is depicted in Figure 2-1.

Sensitivity analysis is the process of finding the rate of change of objective value with respect to design variable. This information is fed into the gradient based optimiser to find the new set of design variables. Regularisation is a process, in which intermediate density values are filtered out to get discrete 0-1 densities. To carry out each step of the TO, different methods are available. For instance, sensitivity analysis can be performed by the adjoint method, finite difference method and regularisation can be performed by the neighbourhood method, PDE based filtering, density filtering methods and optimisation can be performed by any of the gradient based optimisers. As mentioned earlier for structural mechanics problems, Young's modulus is modelled as a function of density. Likewise, for fluid flow problems material impermeability and for thermal problems thermal conductivity, are modelled in terms of the design variable. Two noted drawbacks of this method are intermediate density regions or grey regions found in the final design and pressure diffusion found across

solid walls formed by the TO in fluid flow problems. The pressure diffusion leads to inaccuracies in the final value of the objective function (viscous loss, total pressure, etc.). More details about this method and the steps involved can be found in section 3.1.

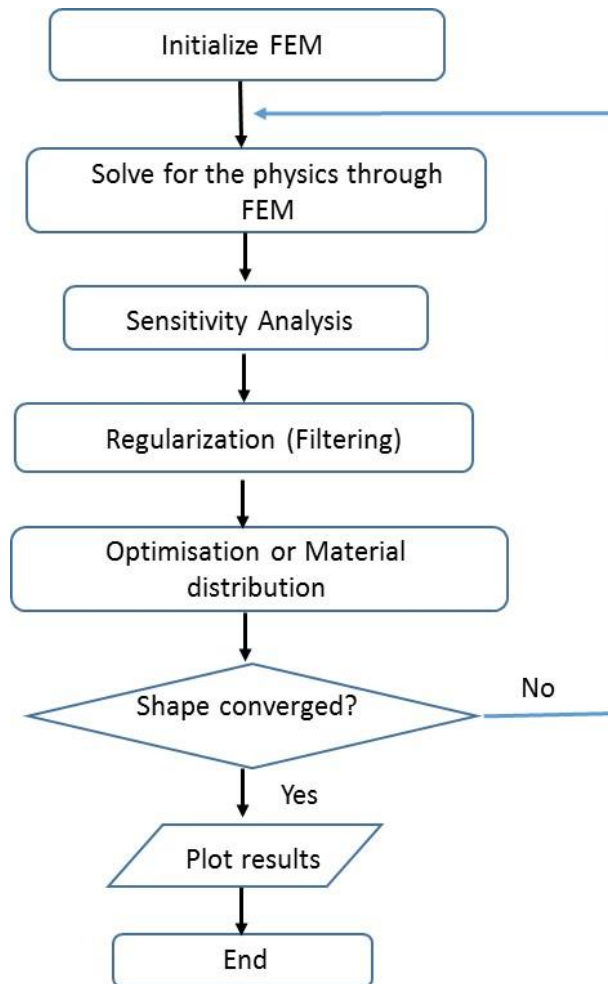


Figure 2-1 Density based Topology optimisation process flowchart

### 2.2.2 Level-set methods

The level-set functions (LSF) were initially used to model crack propagation and evolution of interphases [11]. Later, Osher [12] and Sethian [13] used these functions for topology optimisation. The currently used level-set based topology optimisation was first proposed by Allaire [14] and Wang [15] independently. In mathematics, “level-set” is a function which can take a set of possible values but one value at a time. Usually Signed Distance Functions (SDF) are used as level-set functions. The level-sets are topologically flexible, they can form holes, split to form multiple boundaries or

merge with other boundaries to form a single surface. In topology optimisation, a positive value of the level-set is modelled to represent a material domain and a negative value is modelled to represent a void. The domain boundary is evolved in time in the direction of maximum descent of the objective function till convergence is achieved.

The level-sets are evolved in time by solving the Hamilton Jacobi (HJ) equation (Eqn 2.2) and the boundary evolving direction is found through shape sensitivity analysis. Shape sensitivity is the response of an objective function to changes of the shape of the material domain. Changes to the material domain are made in infinitesimal amounts in the normal direction to the boundary. In the simplest level-set topology optimisation formulation, the material properties (Young's modulus, Impermeability, etc.) are projected on to the level-set function through a Heaviside function. The Heaviside function is a step function which takes value 1 in the material domain and 0 in the void domain.

$$\frac{\partial \psi}{\partial t} - V_n |\nabla \psi| = 0 \quad (2. 2)$$

The speed of evolution or normal velocity  $V_n$ , of the level-set function is equal to the shape sensitivity of the Lagrangian. From the solution of the physics of the problem, shape sensitivity is evaluated.

Allaire [14] and Wang [15] independently applied the level-set methods for the topology optimisation of compliance minimisation problems. The idea is to move the design boundary represented by the level-set model according to its shape sensitivity in the decreasing direction of objective function. The Hamilton Jacobi equation is solved using an upwind scheme to find the new evolved level-set shape. The time step for time marching the HJ equation should satisfy the Courant-Friedrichs-Lewy (CFL) number criteria with respect to mesh size. As the level-set functions are evolved in time, their gradient changes from 1. This leads to inaccuracies in interface boundary and formation of grey regions in the design. To avoid this, their gradient is brought back to 1 by a process called re-initialisation.

The HJ equation doesn't have a capability to nucleate new holes in the material domain in two dimensions. So the final optimised shape obtained depends very much on the initial level-set function used. To alleviate this difficulty, a topology gradient (key concept of Bubble method) term is added to the HJ equation. The topology gradient can be defined as the measure of change in the objective function when an infinitesimal hole is inserted in the design domain. The level-set method is slightly more complicated than the density method and there are multiple ways to do each step of the optimisation process. A vast amount of research is currently taking place in this field.

For nucleating new holes in the material domain, the HJ equation in (2.2) is modified to have a topology derivative term in addition. The modified HJ equation is shown in Eqn 2.3 and it was suggested by Allaire [16] in 2005. He has tested this method for different 2D and 3D structural problems and also for mechanisms design.

$$\frac{\partial \psi}{\partial t} + V \cdot \nabla \psi = -wG \quad (2.3)$$

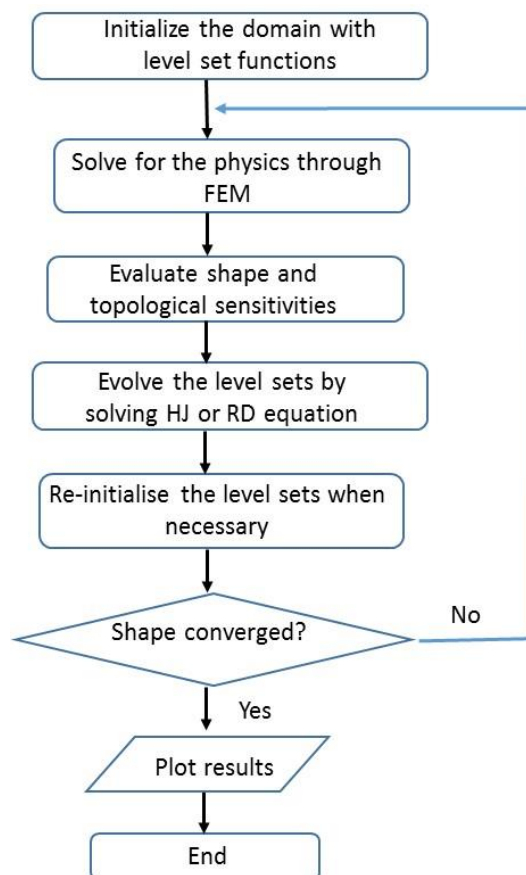


Figure 2-2 Level-set based Topology optimisation process flow chart

In the equation (2.3), 'w' is a weighting factor and 'G' is a topology derivative. Different steps involved in the level-set based topology optimisation is given in Figure 2-2. For mapping the geometry and the level-set function to a mechanical model two different approaches are used: they are density method approach and extended finite element method (xFEM) approach. The density method like approach is also called an ersatz material mapping. Each step in the topology optimisation process could be carried out in multiple ways and each way has its own merits and demerits (refer to chapter 3.2).

Yamada [17] proposed a new level-set method wherein the level-sets are evolved using a Reaction Diffusion equation (Eqn 2.4) and the method is regularised using a fictitious interface energy. Unlike the HJ equation based level-set evolution, this method has the capability to nucleate new holes in the solid domain and the final optimised shapes obtained are smooth and has less dependency on the initial level-set function.

$$\begin{aligned} \frac{\partial \psi}{\partial t} &= -K(\psi) \left( -\frac{\partial F}{\partial \psi} - \tau \nabla^2 \psi \right) \quad \text{in } D \\ \frac{\partial \psi}{\partial n} &= 0 \quad \text{on } \partial D \setminus \partial D_N \\ \psi &= 1 \quad \text{on } \partial D_N \end{aligned} \quad (2.4)$$

Where  $K$  is a proportionality constant and  $\partial F / \partial \Psi$  is equivalent to the topological derivative. The final term of the equation (2.4) denotes the interfacial energy term. Note that a shape derivative is not used in this method so it is not considered as a pure level-set method by some researchers. Compared to the density method this converges slowly but it is more advantageous for fluid flow TO because the interface boundary can be crisply captured. By using the extended finite element method along with the level-set method, pressure diffusion across the solid walls can be avoided. Further, the no-slip boundary condition on the solid wall can also be effectively imposed.

### 2.2.3 Topological derivative method

The idea of this method is to predict the influence of introducing an infinitesimal hole at any point 'x' in the design domain on the objective function and use this as the driver for the generation of new holes. This method is also known as the “Bubble method” and Eschenauer first postulated this method [18]. Topological derivatives determine where to place new holes and to either modify the shape of the boundaries of existing holes, or to update the presence of holes element-wise. This is more like a shape optimisation method rather than a topology optimisation method. Amsutz [19] pointed out that for common choices of material properties the topological derivative corresponds to the standard density gradients. He also noticed that the results of the density gradient method and the topology gradient method are equal for suitably chosen penalisation factors. The critical review of this method and its strength and weakness in relation to other methods of optimisation are given in reference [20].

### 2.2.4 Phase field approaches

In this method, similar to the level-set method, the optimised topology is obtained through evolution of implicit functions. This method is in use, for tracking the interface of different materials and in crack propagation, since the 1960s. Unlike the level-set interface, here the interface has finite thickness. So the interface is “diffused” here. The equation used for the evolution of the implicit function is Allen–Cahn equation [21].

$$\frac{\partial \phi}{\partial t} = M(\phi)(\varepsilon \nabla^2 \phi - \left(\frac{1}{\varepsilon}\right) f'(\phi)) \quad (2.5)$$

where  $f(\phi)$  is an implicit function called a double well function and  $M$  is a mobility parameter. The speed of propagation of the interface is determined by the difference between two minimum values of the double well function which is determined by sensitivity analysis. This method doesn't require the re-initialisation of the function as required by the level-set methods [22].

This method has some similarity to the density methods in the sense that they directly act on the density variables. This method penalises intermediate densities by minimising a function which contains a double well function. Phase field methods have

slow convergence rate compared to other methods. The critical review of established topology optimisation methods was done by Rozvany in [23].

### 2.2.5 Evolutionary structural optimisation method (ESO)

This method was first proposed by Xie and Steven [24]; Based on the steps involved, this method may also be called ‘Sequential element rejections and admissions’ [23]. In this method, some finite changes are done on the shape/topology, on the basis of certain heuristic criteria, which may not be based on sensitivities. An appropriate ‘criterion function’ (eg. Mises stress or energy density [23]) is calculated for each element and in each iteration some elements with the lowest criterion function value are eliminated. This procedure is repetitively carried out till convergence.

Along with element elimination, new elements could also be added on the cells where the criterion function is above a certain threshold value. This improved method is called bi-directional ESO or BESO method [25].

## 2.3 Optimisation algorithms

Topology optimisation problems can be classified as constrained optimisation problems. Governing partial differential equations and material volume constraints are the typical constraints specified during optimisation. The minimum of an unconstrained objective function is calculated from the condition that at the minimum the first order derivative of the objective function is equal to zero and second order derivative is positive. Similarly for a constrained objective function, at the minimum, the first order derivative of its Lagrangian is equal to zero.

In general, the Lagrangian for the constrained optimisation problem is defined as,

$$L(x, \lambda) = f(x) - \sum_{i=1, \dots, n} \lambda_i c_i(x) \quad (2.6)$$

where  $f(x)$  is the objective function,  $c(x)$  is the constraint and  $\lambda$  is the Lagrangian multiplier. If  $x^*$  is the solution where the objective function  $f$  is minimum then it should satisfy the following condition.

$$0 = \nabla_x L(x^*, \lambda^*) = \nabla f(x^*) - \sum_{i=1, \dots, n} \lambda_i^* \nabla c_i(x^*) \quad (2.7)$$

Generally in a TO problem, the number of design variables solved for, is higher than the number of constraints. Hence for solving these type of problems, non-gradient based solvers are not suitable and they are prohibitively expensive. So gradient based non-linear programming methods are more widely used to solve these type of optimisation problems. Typically used optimisers are Sequential linear programming (SLP), Sequential quadratic programming (SQP), Optimality criteria method, Convex linearisation (CONLIN) and Method of Moving Asymptotes (MMA). Details of these optimiser algorithms are given in Chapter 3.

## 2.4 Applications of the Density method

### 2.4.1 Structural problems

The numerical topology optimisation method was first invented for structural compliance minimisation problems. Different types of beams were considered, like the MBB beam, L beam with different loading conditions and supports. Later this optimisation technique was applied to many different fields such as structural dynamics problems [26] and compliant mechanism design [27]. Deaton and Grandhi [28] in their review article listed the application of each method of topology optimisation (Density, Level-set etc) to various fields.

### 2.4.2 Fluid flow problems

Fluid optimisation problems were first solved by Borrvall and Petersson [3] wherein they used a fictitious porous term to optimise for Stokes flows. The porous term is modelled in terms of the impermeability factor ( $\alpha$ ) in such a way that in a solid region the impermeability factor takes a very high value and in a fluid region it takes value zero. Intermediate values of alpha are penalised by using a convex expression for it.

Olesen et al. [29] extended Borrvall's work to optimise slightly higher Reynolds number Navier-Stokes flows. They have used Brinkmann's or the porosity approach to represent and model the fluid flow. As per this model, fluid flow is modelled with an additional force term in the Navier-Stokes equation.

$$(\nabla \cdot u) = 0 \quad (2.8)$$

$$\rho(u \cdot \nabla u) = -\nabla p + \nabla \cdot \{\mu \nabla u\} - \alpha u \quad (2.9)$$

here the ‘ $\alpha u$ ’ represents the Brinkmann term. In order to suppress intermediate  $\alpha$  values, the following interpolation function is used.

$$\alpha(\rho) = \alpha_U + (\alpha_L - \alpha_U) \rho \frac{1+q}{\rho+q} \quad (2.10)$$

Olesen et al. used FEMLAB software to solve for the fluid problem and for computing the sensitivities. The FEMLAB results are called in Matlab along with the MMA optimiser to execute the topology optimisation iterations. This paper paved the way for the industrialisation of topology optimisation methodology to many diverse physics problems using the FEMLAB software. Deng [30] carried out the density based topology optimisation of unsteady NS flows. He has used a continuous adjoint method for sensitivity evaluation and demonstrated the methodology with relevant examples.

The TO of thermo-fluidic problems started with Dede [31], who optimised the liquid cooling channels of a rectangular domain with volumetric heat source. Combined minimum pressure loss and minimum thermal compliance is considered as the objective. The TO is carried out on COMSOL multi-physics package combined with a MMA optimiser. As material properties were not interpolated, the solid region created in the optimisation had zero or low thermal conductivity and the fluid region had high thermal conductivity.

Yoon [32] carried out the design of a heat dissipating structure subjected to forced convection and for the first time he interpolated the thermal conductivity and other relevant material properties with respect to design variables. Thereby the resulting solid regions had a non-zero thermal conductivity. Koga et al. [33] carried out a study similar to Dede [31], using their own FEM code and then validating the optimisation results with a 3D computation. Stokes equation is considered to define the fluid flow and material properties are interpolated. The mathematical expression of minimum flow compliance or minimum pressure loss objective and minimum thermal

compliance objective are given in Eqn. 2.11 and 2.12 respectively. The final objective for this study was combination of these two with some weighting factors.

$$\Phi = \frac{1}{2} \mu \int_{\Omega} \nabla u \cdot \nabla u \, d\Omega + \frac{1}{2} \int_{\Omega} \alpha(\rho) u \cdot u \, d\Omega - \int_{\Omega} f \cdot u \, d\Omega \quad (2.11)$$

$$\Gamma = \frac{1}{2} \int_{\Omega} [k \nabla T \cdot \nabla T + \rho_m c_p (u \cdot \nabla T)] \, d\Omega - \int_{\Omega} f_T T \, d\Omega \quad (2.12)$$

Burger et al. [34] carried out the topological optimisation of positioning of high conductivity material in low conductivity material to maximise the overall thermal conductivity subjected to constraints on the percentage of high conductivity material used. For intermediate density penalisation, SIMP method was used. For sensitivity analysis the adjoint method was used. The MMA algorithm was used for optimisation and FVM was used for solving the heat conduction equations. The optimisation was carried out for different boundary conditions, thermal conductivity ratios and volumetric constraints. The results showed that the high conductivity material distribution resembles a tree structure with primary branches leading to the furthest corners.

Van Oevelen et al. [35] applied the topology optimisation to the design of micro heat sinks for cooling a constant temperature heat source. Heat is extracted and removed from the source through convective heat transfer (by water) in the micro heat sink which is attached on the top of the source. The optimisation was done in a two dimensional context using Brinkmann's approach. The design objective is to maximise the total heat transfer  $Q$  from the heat source to the heat sink. The governing equations are discretised using FV formulation. It is observed that, for the objective of maximising the heat transfer, the optimised heat sinks have a tree-like network of channels.

The first work on natural convection cooled heat sink was carried out by Alexandersen [36], [37] who optimised heat sink designs for various Grashof numbers by fully solving the thermo-fluidic governing equations. This study also validated the obtained results through a CFD study. Alexandersen [38] also optimised forced convective heat transfer problems, but they were simple and academic test cases in nature. Matsumori [39] designed liquid cooling channels for constant input power by introducing an additional equation to calculate the inlet pressure and that pressure was kept constant during TO. He designed the channels for two types of heat sources namely temperature dependent heat sources and temperature independent heat sources.

JHK Haertel optimised the heat sink for minimum temperature objective for the prescribed pressure drop of horizontal flow forced convection. This 2D study was carried out using the density method in Comsol software [40]. Extending this work he has topologically optimised the airside surface of power plant condensers for fluid dynamically and thermally fully developed laminar flows in [41]. The condensers are additively manufactured with polymers containing thermally conducting metal filaments and the optimisation is conducted for varying exchanger thermal conductivity and flow pressure drops. It was found that optimised designs tend to require finer feature sizes with increasing polymer conductivities.

Alberto [42] optimised the layout of highly conductive material embedded in a phase change material to maximise the performance of heat exchanger. He handled energy minimisation and time minimisation approaches and both of them converge to the same pareto front of results in 2D. But optimised designs in 3D had features which were not visible in 2D. He maximised the steadiness by optimising the highly conductive material layout and relaxing the discharge time. He observed that an increase in discharge time resulted in an increase of the steadiness.

Alexanderson [43] designed passive coolers for light emitting diodes in horizontal and vertical orientations and compared their effectiveness with a lattice fin design and simple pin-fin design. From the optimisation study, he recommends not to have fins at the core, in order to achieve high velocity of natural convection and hence to have better cooling. He also suggests aerofoil shape for fin cross section, instead of circular section, to reduce drag and to increase the convection velocity. But he has not accounted for the radiative heat transfer and the flow is limited to laminar regime; turbulent flow is not considered. Zhou et al. [44] presented an industrial application of the TO for combined conductive and convective heat transfer problems. Flow solution is carried out in SIMULIA-Abaqus and optimisation is carried out by SIMULIA-Tosca and design dependent convection is modelled. The methodology is validated for different heat sink designs.

C B Dilgen [45] presented a method to optimise turbulent flow problem using automatic differentiation to solve discrete adjoint system of RANS equations. He has compared the frozen turbulence model with a fully resolved  $k-\omega$  turbulence model and S-A turbulence model. He has proved that automatic differentiation can be used to calculate exact sensitivities of 2D and 3D large scale turbulent flows. He has observed

that improved preconditioners are necessary for more robustness of the solution. Dbouk [46] did consolidated review of all the heat transfer related topology optimisation work done till 2016. He has classified the works based on type of problem handled, sensitivity evaluation type and TO method type.

One of the disadvantage of density based topology optimisation methods is that a no-slip condition is not strictly imposed on the solid walls. So power dissipation computed is not very accurate.

### 2.4.3 Multi-material optimisation problems

The simple topology optimisation technique considers two phases, namely material and void. Sigmund [6] extended the technique to optimise physics involving two different phase or two different materials, so in this case the optimisation domain will have material1, material2, and a void. He has modified the power law as follows,

$$E(\rho) = \rho_1^p (\rho_2^p E^1 + (1 - \rho_2)^p E^2) \quad (2.13)$$

Where  $\rho_1$  and  $\rho_2$  are two design variables and  $E^1$  and  $E^2$  are material properties of material 1 and 2 respectively. The volume constraint of material 1 and 2 are given as,

$$\sum_{e=1}^N \rho_1^e \rho_2^e V^e \leq V_1 \quad (2.14)$$

$$\sum_{e=1}^N \rho_1^e (1 - \rho_2^e) V^e \leq V_2 \quad (2.15)$$

## 2.5 Applications of the Level-set method

### 2.5.1 Structural problems

Challis [47] has written a simple Matlab code to demonstrate the level-set based topology optimisation for compliance minimisation problems. The work is mostly based on Wang and Allaire's algorithm but the topological derivative for nucleation of new holes is also implemented in the code. The LSF is evolved in time by solving the

HJ equation. This is a discrete level-set method where material density can take either 0 or 1 and hence the derivative of density distribution with respect to the level-set function is calculated through a variational problem instead of directly from the distribution.

Liu et al. [48] implemented the level-set based topology optimisation formulation in FEMLAB. He solved the Navier's equation of structural mechanics and the HJ equation in a coupled manner. An additional stabilizing diffusion term is added to the HJ equation as it is solved in a finite element method instead of an upwind finite difference method. A volume penalty parameter is added to the Lagrangian in order to satisfy the volume constraint. For the velocity extension purpose a radial basis function of few mesh cell width is used. The optimised solution had grey regions as the re-initialisation of LS was not carried out.

Kawamoto [49] has modelled a Reaction Diffusion (RD) equation based level-set TO in Comsol. The level-set function doesn't require explicit re-initialisation as it was taken care of by an additional term present in the RD equation. The model used an ordinary differential equation to update the Lagrangian multiplier. The model was demonstrated for 2D and 3D compliance minimisation problems.

### **2.5.2 Fluid flow problems**

Recently, Duan et al. [4] have applied a variational level-set method to the shape and topology optimisation of fluid flow problems. The method was demonstrated with two-dimensional examples and proposed a new evolution equation for the level-set function, in order to achieve a smooth evolution without re-initialisation. Zhou and Li [50] have also applied the level-set method for the topology optimisation of steady-state Navier–Stokes flows in both two and three dimensions. The drawback of Duan and Zhou's approach is that the domain needs to be re-meshed after the evolution of the level-set, which is computationally expensive.

Challis and Guest [51] have applied the level-set based topology optimisation method with topology derivative for Stokes flows without the need of remeshing. Both the shape sensitivity and topology sensitivity of Stokes flow, are used in this level-set method. The topology derivative is used for new solid creation in the fluid domain. Kreisli [52] carried out the level-set based topology optimisation of fluid problems

using extended Finite element (xFEM) based geometry mapping. The results showed that the LS with xFEM doesn't experience boundary resolution problems (grey cells) as did by the TO with Brinkmann's approach. Further he also showed that, the solids created using Brinkmann's approach has pressure diffusion within it, but that is absent in solids created using the LSM with xFEM approach.

Deng carried out the level-set topology optimisation of steady Navier Stokes flow subjected to body forces [53] and also the optimisation of unsteady NS flows [54]. He computed the shape sensitivity through the continuous adjoint method and the topology derivative through the asymptotic expansion method. He updated the level-set function taking topology derivative as an additional source term in the HJ equation similar to Burger [55] and Challis [47] approach. The Lagrangian multiplier and the penalty factor are updated algebraically from a random initial guess and are not solved analytically.

### **2.5.3 High Reynolds number flow problems**

Because of the use of a porosity model for modelling solids, there is a limit on the Reynolds number of flow that can be optimised without any instability. Recently suitable models were developed to simulate turbulent topology optimisations. Othmer [5] has derived adjoint NS equations and the sensitivity for cost functions like viscous dissipation and flow uniformity at the outlet. The results are applicable to laminar flow and also to turbulent flow with frozen turbulence. Here frozen turbulence means the eddy viscosity is not computed but assumed constant throughout the flow domain.

Zymaris [56] derived the adjoint equations for Spallart-Almaras (SA) turbulence model and thereby enabled the calculation of shape sensitivity for turbulent flows. Papoutsis [57] and Kontoleontos [58] derived adjoint equations for Spallart-Almaras turbulence model for coupled NS and energy equations considering additional constraints. They considered surface integrated cost function namely minimum total pressure drop and temperature difference between inlet and outlet. Papoutsis validated and applied this model to industrial flow problems in [59].

While Papoutsis and Kontolentis tested the derived equations for density based topology optimisation, Georgios [60] applied the equations for Level-set based topology optimisation for fluid flow problems.

Yoon [61] demonstrated the TO of turbulent flow using SA turbulence model in the density method. He modified the SA equation to satisfy additional boundary conditions during topology optimisation. Similar to the Brinkmann term for penalising velocity, a penalising term for turbulence,  $(\alpha^*v_t)$  is included in the SA equation to make the eddy viscosity zero on the wall region. The turbulence model implementation requires knowledge of nearest wall distance from the computational grid element. To calculate the wall distance, Eikonal equation is solved.

It has to be noted that though, the turbulence model is modified to enforce the zero eddy viscosity in wall, the turbulence computation may not be accurate. For accurate turbulence calculation boundary layer mesh is necessary; since during TO the geometry is evolving, the boundary layer mesh should also evolve. This requires remeshing of the design domain after every iteration which is computationally expensive.

#### **2.5.4 Thermal problems**

Yamada [62] solved generic design dependent heat transfer problems (eg. Problem involving pressure loads) using the LSM with RD equation. This level-set method allows specifying the boundary conditions on the available level-set surfaces and it also allows the increase and decrease of the number of holes. The objective function is written as a sum of actual objective function and an interfacial energy term to regularise the optimisation.

Yaji [63] applied the RD equation based level-set topology optimisation to coupled heat transfer and fluid flow optimisation problem similar to Koga [29] and Dede [27]. But his objective function is not combined minimum thermal compliance and minimum fluid power dissipation, instead maximum internal heat generation in the design domain. Instead of the inlet velocity boundary condition fixed pressure difference is imposed. They also proposed a Tikhonov based regularisation scheme that enables the qualitative control of the geometric complexity of the optimal configurations. By varying the regularisation parameter, optimised geometries with different levels of complexity are generated. One of the limitations of this work is that the solid and fluid are modelled through a porosity approach which has a pressure diffusion problem across the solid walls.

Coffin [64], carried out the topology optimisation of cooling device by approximating convective fluxes through Newton's Law of cooling using the LSM with xFEM. He has compared the results of LSM with xFEM with LSM with porosity approach and the Density method results. He used an explicit feature size control method to prevent the formation of small geometries and to avoid the re-initialisation. The results obtained are better than the density method and LSM with porosity approach but for the convective flux modelling he recommends solving the entire fluid flow equations instead of using Newton's law of cooling. Subsequently Coffin [65], solved natural convection TO problems by solving full flow equations using a LSM with xFEM approach. Coffin also optimised a 3D heat sink subjected to steady low Grashof number natural convection and observed that the optimisation of high Grashof number steady and all unsteady problems are highly computationally expensive.

Yaji [66] presented a new TO method using a Lattice Boltzmann equation and its adjoint equation to optimise the heat exchange channels. He has demonstrated the method for two problems, one for pressure drop minimisation and the other for heat exchange maximisation. However, more details could be given about physical input values (velocity, pressure, temperature etc) considered in his results.

### 2.5.5 Multi-material optimisation problems

MY Wang [7] extended the level-set method to multi-material optimisation problems. It requires 'm' level-set functions to represent a structure of '2<sup>m</sup>' different material phases. The level-set function and Heaviside function are treated as vector quantities and each level-set function is evolved by solving a separate HJ equation. So the computation involves coupled solution of all the HJ equations. Material property at a point is interpolated between different materials properties as follows.

$$E(\rho) = H(\psi_1)(H(\psi_2)E^1 + (1 - H(\psi_2))E^2) \quad (2.16)$$

$$\Psi = [\psi_1, \psi_1, \dots, \psi_m] \text{ and } H(\psi) = [H(\psi_1), H(\psi_2), \dots, H(\psi_m)] \quad (2.17)$$

where  $E^1$  and  $E^2$  are Youngs modulus of two different materials and their corresponding Heaviside functions are  $H_1$  and  $H_2$ . For the two material case, the possible combination values for  $H_1$  and  $H_2$  (denoted as  $[H_1, H_2]$ ) are  $[1,1]$ ,  $[1,0]$ ,  $[0,1]$  and  $[0,0]$ .

Chungang [67] extended the multi-material topology optimisation to heat conduction problems following MY.Wang's work. He derived the Lagrange multipliers from the augmented Lagrangian equation. By solving these equations in coupled manner, multipliers are evaluated. Y Wang [68] devised a scheme for design of meta materials using multiphase level-sets. Using the method he has designed materials with negative Poisson's ratio and negative thermal expansion coefficients.

## 2.6 Applications of other TO methods

Li et al [69] designed heat conducting fields using the ESO method. Thermal conductivity of an individual finite element is considered as a design variable and discrete temperature sensitivity is used as a criterion function. Design is evolved by sequentially removing the element with most negative temperature sensitivity from the design domain.

Bornoff et al [70] proposed a new method for the heat sink design. The heat sink is designed by sequentially adding material at the maximum temperature region. This method is slightly similar to the ESO method; the difference is, instead of removing the material depending on a criterion function, material is sequentially added, in this method. The criterion function used here is temperature, where as in ESO generally temperature sensitivity is used as the criterion function. The performance of the designed heat sink is within 5% of the parametrically designed plate fin heat sink. Bornoff et al [71] carried out another study in which 'thermal bottle neck' number is used as a criterion function, and material is removed sequentially wherever the bottle neck number is lowest. Bottle neck number is the dot product of the heat flux and temperature gradient vectors and it identifies flow path that carry high heat with high resistance.

## 2.7 Summary

This literature review shows that the Density method and Level-set method have been the most widely researched for the topology optimisation of fluid flow and heat transfer applications, while other methods have not developed to this stage. In spite of wide research, density and level-set methods have not developed to the stage of designing

industrial heat sinks and heat exchangers. TO is applied to the design of multi-material structures but it is still not applied to the design of multi-material heat sinks. So exploring topology optimisation for the design of multi-material heat sinks could be rewarding.

Going forward, algorithm of the density and level-set methods will be studied in detail and numerical modelling of simple fluid flow and heat transfer optimisation test cases will be carried out.

## 3 Theory of Topology Optimisation Methods

In the previous section, an overview of the TO, including different methods of TO and their applications to various fields were covered. In this chapter detailed algorithms for the Density method and Level-set method are presented. In this research work, finite element method (FEM) is used to solve the physics involved. Hence a brief introduction to FEM is also provided in this chapter.

### 3.1 Density method

#### 3.1.1 Methodology

In general, topology optimisation is an iterative optimisation process, where the objective and sensitivity are calculated by solving the physics of the problem through FE method and the optimisation is generally carried out through gradient based optimisers. In the density method, the element density ( $\rho$ ) is considered as a design variable and it is combined with a suitable parameters of the physical problem. For instance in structural problems, element density is combined with the Young's modulus as,

$$E(\rho) = \rho^p E_0 \quad (3.1)$$

in fluid flow problems it is combined with a material impermeability term as,

$$\alpha(\rho) = \rho^p \alpha_0 \quad (3.2)$$

Where  $E$  is the elemental Young's modulus which depends on the value of  $\rho$ ,  $E_0$  denotes the material Young's modulus and ' $p$ ' designates a penalisation factor. When the density variable  $\rho = 0$ , the phase is assimilated as void, while  $\rho = 1$  indicates the presence of material. Meanwhile, during the optimisation process,  $\rho$  can take intermediate continuous values. These intermediate density values are penalised by taking  $p \geq 1$  and mostly  $p=3$  is found to be the ideal value, to obtain just solid and void regions. Typically a topology optimisation problem will have an equality constraint (governing equation) and a non-equality constraint coming from the material volume constraint. Initially while starting the iterative solution, the material density of all the cells can be initialised to any value between 0 and 1. As the solution progresses, the cells falling under the optimum layout will have the density value of 1 and rest of the cells will have the value of 0.

Sigmund published an educational article [10] in 2001, to explain the process of topology optimisation using the density method. The major steps involved in the TO are,

- 1 Initialize the design variable (density) throughout the design domain.
- 2 Solve for state variables by solving the physics in FEM.
- 3 Evaluate the objective function and the sensitivity of objective function with respect to design variable.
- 4 Update the design variables using optimiser.
- 5 Repeat the process from step-2 to step-4 till convergence of the design variables.

Typically convergence is decided based on the integrated difference in the design variable value for a range of consecutive iterations. Since gradient based optimisers are used the final solution obtained depends on the initial value. Hence the entire procedure needs to be repeated with different initial values of design variables to conclude that the solution has actually reached the global minimum and not a local minimum [72].

### **3.1.2 Penalisation technique**

From the continuous design variable which can take values between 0 and 1, a discrete solution of design variable with either 0 or 1 value is obtained by penalising

the intermediate design variables. Power law or Solid Isotropic Material with Penalisation (SIMP) approach is commonly used for penalising the intermediate densities (Eqn 3.1). Power factor value  $p = 3$  is usually considered as a good value for convergence of 0-1 solutions. For compliance minimisation problems, the optimisation with  $p=1$  is convex in nature hence it is a good practice to start the optimisation with  $p=1$  and gradually increasing to  $p=3$ . This approach is called continuation approach and it is used not only in compliance minimisation problems but in other physics optimisation also.

Stolpe and Svanberg [73] proposed an alternative interpolation or penalisation scheme (Eqn 3.3) known as the Rational Approximation of Material Properties (RAMP). A desirable feature of the RAMP model is that, unlike the SIMP, it has nonzero sensitivity at zero density (Figure 3-1). As a result, the RAMP material model has been shown to remedy some numerical difficulties in problems related to very low density values in the presence of design dependent loading. However this doesn't seem to play a strong role for practical problems.

$$E(\rho_i) = \frac{\rho_i}{1 + q(1 - \rho_i)} E_o \quad (3.3)$$

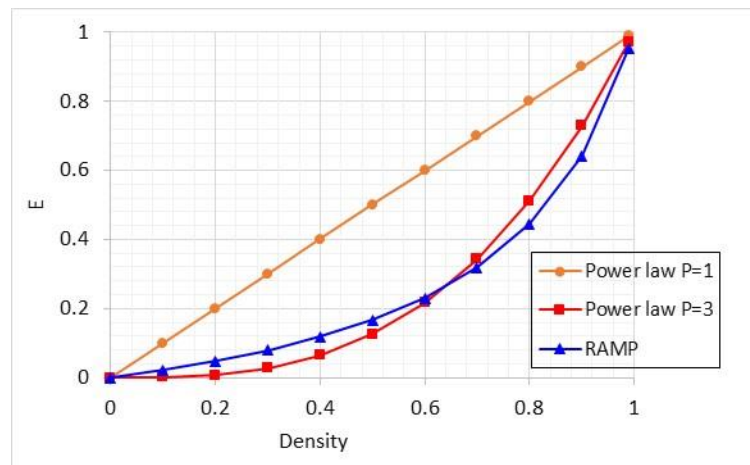


Figure 3-1 Comparison of SIMP and RAMP interpolation functions

where 'q' is the tuning parameter. For the fluid flow optimisation problems, Borrvall [3] proposed a convex interpolation formula for impermeability factor  $\alpha$  in terms of a tuning parameter 'q'. He has proven that when  $\alpha$  is a linear function, the optimal distribution is fully discrete valued. Following this, Olesen suggested an interpolation formula for Navier-Stokes flows, which is given in Eqn (3.4). For large values of 'q' the

interpolation is almost linear and hence a discrete interface is expected. The interpolation function is plotted for different values of  $q$  in Figure 3-2.

$$\alpha(\rho_i) = \alpha_{min} + (\alpha_{max} - \alpha_{min}) \frac{q[1 - \rho_i]}{q + \rho_i} \quad (3.4)$$

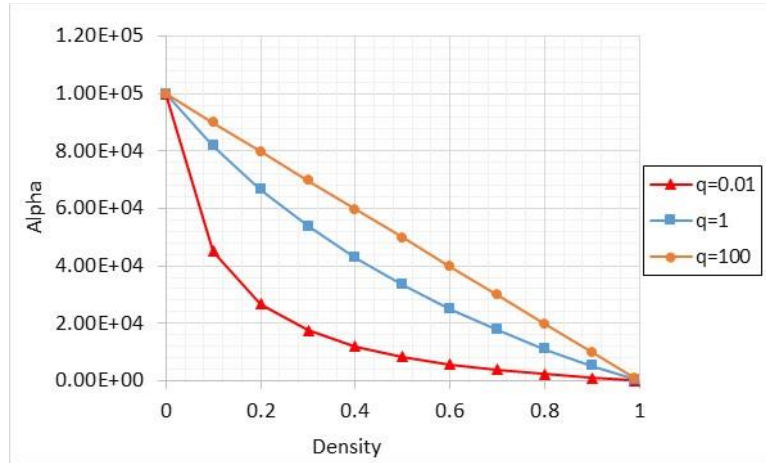


Figure 3-2 Convex interpolation function for fluid flow

### 3.1.3 Sensitivity evaluation

The derivative of the objective function with respect to design variables (density vector) is required to march towards the minimum objective value. The objective function will be an implicit function of the solution vector, so to find the sensitivity of the problem, the physics has to be solved as many times as the size of the design variable vector. To avoid this, the adjoint sensitivity method is evolved, which only requires solving the problem physics once and solving the adjoint problem once.

For structural mechanics problem, sensitivity of compliance 'c' with respect to design variable 'ρ' can be calculated as,

$$\frac{dc}{d\rho_i} = \frac{\partial c}{\partial u} \frac{du}{d\rho_i} \quad \text{where } c = u^T K u \quad (3.5)$$

Where 'u' is the state variable and 'K' is the stiffness matrix. Evaluation of state variable's derivative with respect to each design variable, calls for an individual solution of physics. Hence this step has to be avoided and this is possible if we calculate a variable  $\lambda$  which satisfies the following relation.

$$K^T \lambda = -\left(\frac{\partial c}{\partial u}\right)^T \quad (3.6)$$

Where  $\lambda$  is the adjoint variable or Lagrange multiplier. The above equation is solved to calculate the adjoint variable and using this sensitivity (Eqn 3.5) is calculated as given below.

$$\frac{\partial c}{\partial \rho} = \lambda^T \frac{\partial K}{\partial \rho} U \quad (3.7)$$

Additional information about the adjoint sensitivity method is presented in section 3.2.2. Van Kuelen et al [74] conducted a review of different methods for structural sensitivity calculation and Tortorelli [75] has written a review article on sensitivity analysis wherein he has given simple tutorials on sensitivity evaluation which can be extended to complex systems.

### 3.1.4 Regularisation

The process of ensuring that the stable solution is reached through optimisation by means of filtering, is called regularisation. In order to ensure the existence of a solution to the problem, some sort of restriction or filtering technique is introduced. Numerous previous applications have proved that the filtering produces mesh independent designs in practice. The sensitivity filter is a popular filter used in the density method, this modifies the sensitivity of grid cell as follows.

$$\frac{\partial c}{\partial \rho} = \frac{1}{\rho \sum_{f=1}^N H_f} \sum_{f=1}^N H_f \rho_f \frac{\partial c}{\partial \rho_f} \quad (3.8)$$

Where ' $H_f$ ' is a convolution operator or weight factor, which decays linearly from the centre of the point to chosen radius of averaging ' $r$ '. There are many other filtering techniques like perimeter filtering, density filtering etc. Reference [72] gives more details about these techniques.

Another popular problem faced by the density method is an alternating solid and void pattern found in some cells during the iteration process. This phenomenon is known as the 'Checker board' problem. The checker-boarding is merely a discretisation error of the FE method, which has nothing to do with the SIMP. This error results in an overestimation of the stiffness. A highly efficient but partially heuristic solution to this problem is the filtering method, suggested by Sigmund [72],

[10]. The sensitivity filter is the popular filter used to prevent checker-boarding but the disadvantage of this is it leaves a grey zone of width equal to the filtering radius. An alternative to sensitivity filtering is density based filtering. Bruns [76] suggested a density filter, whose principle is similar to the weighted averaging of density in a neighbourhood of radius  $r$ .

$$\text{Filtered density } \rho = \frac{\sum_j \rho_j \omega_j}{\sum_j \omega_j}, \text{ where } \omega_j = \max\left(1 - \frac{(x_j - x_i)^2 + (y_j - y_i)^2}{r^2}, 0\right) \quad (3.9)$$

Where  $w_j$  is weightage,  $x_i, y_i$  are centroidal coordinates of concerned elements, and  $x_j, y_j$  are coordinates of surrounding element and ' $r$ ' is the filter radius. This filter gives weightage inversely proportional to the distance from the concerned cell. If the cell is outside the filter radius it gets zero weightage. Alexanderson [36] used this filter to get rid of small features which are created during 3D coupled thermal and fluid optimisation problems.

In order to avoid the grey zone associated with filtering, projection schemes (Guest [77]) have been proposed. These methods operate on 3 fields namely design field, filtered field and projection field. The latter field is obtained by smoothed Heaviside projection. An extension of this method is called robust optimisation, wherein minimum and maximum length scales are imposed on the optimised shape.

### 3.2 Level-set method

A Level-set of a differentiable function ' $f$ ' corresponding to a real value ' $c$ ' is the set of points which satisfies the condition  $f=c$ . For a quadratic function in 2D, level-set is a plane curve and in 3D it is a level surface. For example, if the level-set function is  $f=x^2+y^2$  and the real value of ' $c$ ' equals to 4, then the level-set is a circle with radius 2 (Figure 3-3).

The level-set field can either be mapped on to material properties or a geometric interface description between solid and void. The values taken by the level-set function  $\psi$  on different material regions is given below.

$$\psi = \begin{cases} = 0 \forall x \in \partial\Omega \text{ (boundary)} \\ > 0 \forall x \in \Omega^+ \text{ (solid region)} \\ < 0 \forall x \in \Omega^- \text{ (void region)} \end{cases} \quad (3.10)$$

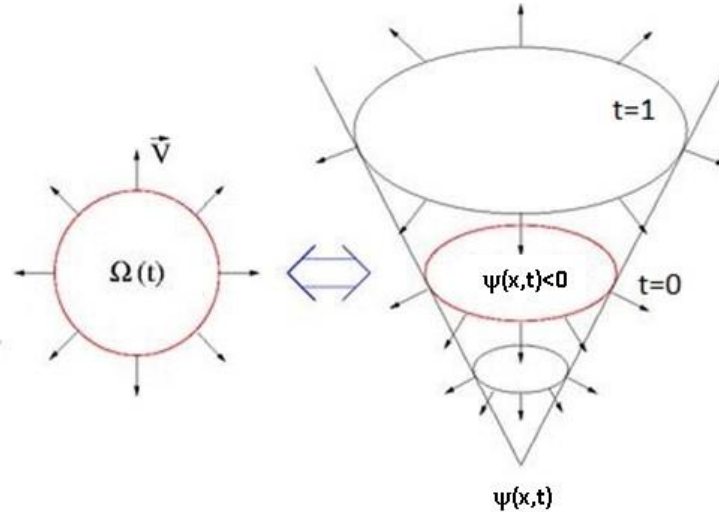


Figure 3-3 Level-set function boundary (left) and full function (right)

The Signed Distance Function (Illustrated in Figure 3-4) is a commonly used level-set function. This function measures the Euclidean distance of a given point relative to a boundary and it takes positive values if the point is inside the boundary and takes negative values if the point is outside the boundary (or vice versa). The signed distance function and its one particular level-set curve, 'a disk' are shown in Figure 3-4. Radial basis function is another function which is also used as a level-set function. Evolution of the geometry interface (represented by level-set function) is obtained by solving the Hamilton-Jacobi equation. The underlying principle of HJ equation is that material derivative (w.r.t. time) of the level-set function is zero.

$$\frac{\partial\psi}{\partial t} + V \cdot \nabla\psi = 0 \quad (3.11)$$

Where  $V$  is the velocity with which the level-set is advected and the normal vector of level-set function is,

$$n = -\frac{\nabla\psi}{|\nabla\psi|} \quad (3.12)$$

where  $\nabla\psi$  is the gradient of the level-set function and  $|\nabla\psi|$  is its magnitude and ' $n$ ' is the normal vector. Substituting the value of  $\nabla\psi$  in equation (3.11), the HJ equation becomes

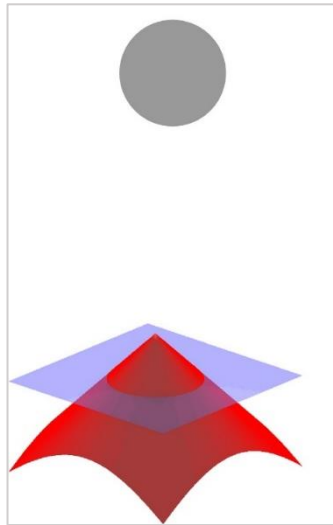


Figure 3-4 Signed distance function (red cone) of a disk (grey colour)

$$\frac{\partial \psi}{\partial t} - V \cdot n |\nabla \psi| = 0 \quad (3.13)$$

$$\frac{\partial \psi}{\partial t} - V_n |\nabla \psi| = 0 \quad (3.14)$$

where  $V_n$  is the normal velocity of the level-set curve with which it propagates. Typically the velocity of propagation  $V_n$ , is found through shape sensitivity analysis.

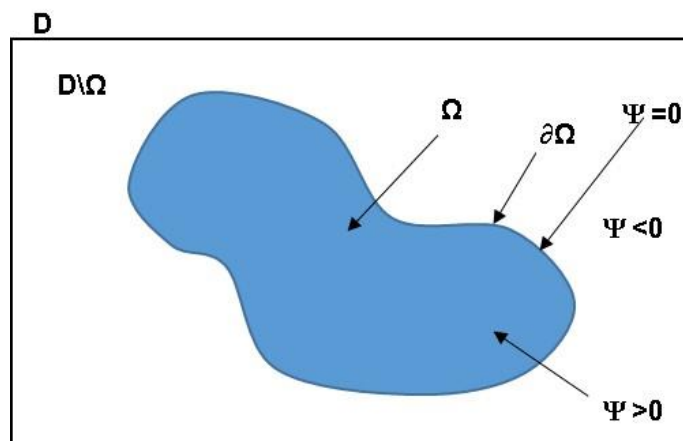


Figure 3-5 Design domain and the level-set model

Typical procedure followed in the level-set based topology optimisation is given below.

1. Mesh the initial structure.
2. Initialize the level-set function to a signed distance function.
3. Map the positive and negative level-set values to the parameters of the physics. (Eg. Youngs modulus, Material conductivity, etc.)
4. Repeat until convergence:
  - (a) Calculate the solution to the governing equation for the current level-set domain.
  - (b) Calculate the shape sensitivity and topological sensitivity based on the solution.
  - (c) Evolve the level-set function using the HJ equation to find a new shape.
  - (d) Reinitialize the level-set function to an approximate signed distance function when necessary (typically after every 5 iterations).

### 3.2.1 Geometry mapping

The evolved level-set geometry has to be mapped on to the finite element mesh. This can be done by 3 different methods, namely i) Conformal discretisation, ii) Density based mapping and iii) Immersed boundary technique or XFEM based mapping. In conformal meshing, each time the level-set function is evolved the material domain is remeshed and void region is excluded from computation. Remeshing is expensive but enables the interface geometry to be very crisply captured and excluding the void region from computation might save some computational cost.

The density based mapping is similar to the density method where parameters of the physics are modelled as a function of level-set function with the help of a Heaviside function. Heaviside function is a unit step function which takes zero value when the LSF is negative and unit value when the LSF is positive. An example of density mapping is given in Equation (3.15).

$$E(\psi)=(E_o-E_{min})H(\psi)+E_{min} \quad (3.15)$$

In the material domain, when  $H$  value is one, Youngs modulus becomes  $E_o$  and in the void region where  $H$  value is zero, Youngs modulus is equal to  $E_{min}$ . A polynomial expression is used for the Heaviside function, so that a finite derivative exists at the

boundary. The derivative of the Heaviside function is a delta function and the expressions for Heaviside and delta functions are given below.

$$H(\psi) = \frac{1}{2} + \frac{15}{16} \left(\frac{\psi}{h}\right) - \frac{5}{8} \left(\frac{\psi}{h}\right)^3 + \frac{3}{16} \left(\frac{\psi}{h}\right)^5 \quad (3.16)$$

$$\delta(\psi) = \frac{15}{16h} \left(1 - \left(\frac{\psi}{h}\right)^2\right)^2 \quad (3.17)$$

The material domain integration and boundary integrations can be calculated using the below formulas which use Heaviside and delta functions.

$$\int_S f(x) dS = \int_{\Omega} f(x) H(\psi) d\Omega \quad (3.18)$$

$$\int_{\Gamma} f(x) d\Gamma = \int_{\Omega} f(x) \delta(\psi) |\nabla\psi| d\Omega \quad (3.19)$$

Like the density method, density mapping method of level-set TO also has grey regions in the optimised geometry.

EXtended FEM (XFEM) is a technique developed for computing crack propagation in materials under loading. In this method, an additional 'enrichment' term is added to the finite element shape function, in order to predict these discontinuities. Suitable enrichment functions are available to predict the growth of a crack and movement of an interface between two materials. This enrichment function avoids the need for remeshing the region to capture these discontinuities. Further, the boundary conditions at the material interface, like the no-slip condition on a solid-wall, can be effectively imposed in this mapping method. Developing an XFEM solver is difficult and time consuming.

### 3.2.2 Adjoint method for topology optimisation

The adjoint method stems from the mathematical theory of 'Functional analysis'. In the field of aeronautical CFD, Jameson pioneered the use of the adjoint method for optimal aero shape design [78]. Typically in engineering optimisation problems, a large number of design variables are involved and this is proportional to the mesh size of FEM. To calculate the sensitivity of all these design variables (say  $n$ )

by means of the finite difference method,  $n+1$  simulations will be required. This is highly expensive, but in the adjoint method only 2 simulations are required to find the sensitivities irrespective of the number of design variables. Because of this significant advantage, this method is increasingly used in engineering optimisation problems [79].

A small recap is provided of some of the Functional analysis terminologies here.

Banach space: Normed space, note norm can be defined in any fashion.

Hilbert space: Complete inner product space.

Every inner product space is a normed space; Every Hilbert space is a Banach space, but the converse need not be true.

Lebesgue space: Function space defined using natural generalisation of 'p' norm for finite dimensional vector spaces.

Sobolev space: Vector function space of weak form solutions.

Frechet derivative: Strong derivative; generalisation of the gradient of vector space. Usual derivative is known as the Gateaux derivative.

Suppose that the objective function,  $F = g^T u$  and ' $u$ ' is the state variable which satisfies the equilibrium equation,  $Au = f$ . Then as per adjoint theory, there exists an adjoint variable ' $v$ ' such that,  $F = v^T f$  and it satisfies the equation,  $A^T v = g$ . The adjoint problem is also known as the dual problem.

Depending on whether the adjoint form is calculated using an analytical form of governing equation or using a discretised form of the governing equations, it is classified as a continuous adjoint method or discrete adjoint method.

For homogenous governing equations with homogeneous boundary conditions, the adjoint equation can be calculated as below. Let the notation  $(V, U)$  denote the integral inner product over some domain  $\Omega$ .

$$(V, U) = \int_{\Omega} V^T U d\Omega \quad (3.20)$$

Then the adjoint operator  $L^*$ , can be calculated through

$$(V,LU) = (L^*V,U) \quad (3.21)$$

Or the more general form for problem with homogeneous boundary condition,

$$(V,LU)_{\Omega} + (C^*V,BU)_{\partial\Omega} = (L^*V,U)_{\Omega} + (B^*V,CU)_{\partial\Omega} \quad (3.22)$$

where  $LU=f$  is the equilibrium equation for the primal problem. By performing the inner product integration of  $LU$  with  $V$ , the governing equation for the adjoint variable ' $v$ ' can be found. It is worth mentioning that, the Laplacian problems are mostly self-adjoint; that is the state variable is equal to the adjoint variable. This simplifies the shape sensitivity calculation very much. For structural compliance minimisation problems the shape sensitivity is equal to negative of structural compliance and for Stokes flow for viscous dissipation minimisation problem the shape sensitivity is equal to negative of viscous dissipation.

Generally, shape sensitivity is calculated from the augmented Lagrangian of a given problem (section 3.2.3). Typically it will be of the form,

$$F'(\Omega)(\Theta) = \int_{\Gamma_N} v \theta \cdot n \, ds \quad (3.23)$$

making use of ' $v$ ' from the above equation, the ' $Vn$ ' of the HJ equation can be calculated as,

$$Vn = -v + \lambda - \Lambda \left( \int_{\Omega} H(\psi) d\Omega - \text{Volume\_req} \right) \quad (3.24)$$

where  $\lambda$  and  $\Lambda$  are Lagrange multiplier and area penalty factor respectively.

Some of the objective functions involve only surface integration over the boundaries of the domain rather than volume integration. For example, the total pressure loss in a diffuser only involves surface integration of total pressure at the boundaries. These objectives influence the adjoint equation system only in the adjoint boundary condition. The objective function involving volume integration will affect the adjoint equation meaning objective related terms will be present in the adjoint equation itself. Adjoint analysis is also useful to find topological sensitivity and the details are given in section 3.2.4.

### 3.2.3 Shape sensitivity evaluation

The shape derivative of the objective function ( $F(\Omega)$ ) is a directional derivative of the objective function under some small perturbation of the design boundary ( $\partial\Omega$ ). It evaluates the change in objective function for a small change in the design boundary [80].

The shape derivative or sensitivity indicates the velocity with which the level-set boundary needs to be evolved. It is like steepest descent direction of the optimisation problem. The shape sensitivity is calculated from the augmented Lagrangian of a given problem. The augmented Lagrangian includes objective function and constraints as given in Eqn (3.25).

$$L = F(x) + \lambda(V - V_{req}) + \frac{1}{2\Lambda}[V - V_{req}]^2 \quad (3.25)$$

Lagrangian also includes a penalty term ' $\Lambda$ ' which accounts for the difference in value of the initialised material volume and the required material volume. The Lagrange multiplier takes the following final form,

$$\lambda = -\frac{\int_{\partial\Omega} v ds}{\int_{\partial\Omega} 1 ds} \quad (3.26)$$

The shape derivative of the volume constraint can be calculated and its value is unity. So the normal velocity for evolving the level-set becomes,

$$Vn = F'(x) + \lambda + \frac{1}{\Lambda}[V - V_{req}] \quad (3.27)$$

#### Shape Sensitivity of Laplacian Equation:

Let the objective function be,

$$F(\Omega) = \int_{\Omega} j(u) dx + \int_{\partial\Omega} l(u) ds \quad (3.28)$$

where ' $j$ ' is a volume integrated objective and ' $l$ ' is a surface integrated objective.

Then the shape sensitivity will be of the form,

$$F'(\Omega)(\Theta) = \int_{\Gamma_N} v \Theta \cdot n ds \quad (3.29)$$

Suppose the governing equation is a Laplacian, as in the case of a structural mechanics problem,

$$-\nabla \cdot Ae(u) = f \quad (3.30)$$

$$\text{Boundary conditions are, } Ae(u)n = g \text{ on } \Gamma_N \quad (3.31)$$

$$u = 0 \text{ on } \Gamma_D \quad (3.32)$$

where 'e(u)' is Strain, 'u' is displacement and 'A' is Young's modulus.

Then the corresponding adjoint equations [14] are,

$$-\nabla \cdot Ae(p) = -j'(u) \quad (3.33)$$

$$Ae(p)n = -l'(u) \text{ on } \Gamma_N \quad (3.34)$$

$$p = 0 \text{ on } \Gamma_D \quad (3.35)$$

The shape derivative is, evaluated from the Frechet derivative of the objective function.

$$\begin{aligned} F'(\Omega) = & \int_{\Gamma_N} \left( j(u) + Ae(u) \cdot e(p) - f \cdot p - \frac{\partial g \cdot p}{\partial n} - Hg \cdot p \right) \theta \cdot \text{nds} \\ & + \int_{\Gamma_D} (j(u) - Ae(u) \cdot e(p)) \theta \cdot \text{nds} + \int_{\partial\Omega} \left( \frac{\partial l(u)}{\partial n} + Hl(u) \right) \theta \cdot \text{nds} \end{aligned} \quad (3.36)$$

Where 'H' is curvature term equal to  $\nabla \cdot n$

The shape derivative expression has 3 terms, the first one for the volume objective with Neuman type boundary condition the second term for the volume objective with Dirichlet type boundary condition and the third term accounting for the boundary objective function.

For compliance minimisation problem with a boundary traction load, the body force  $f$  is zero. Further this is a self adjoint problem with  $p=-u$ , and  $\theta \cdot n = 0$  on  $\Gamma_D$  and on  $\partial\Omega$  where  $g \neq 0$  (Figure 3-6). Then the shape sensitivity equation (3.36) simplifies to,

$$F'(\Omega) = \int_{\Gamma_N} \left[ 2 \left( f \cdot u + \frac{\partial g \cdot u}{\partial n} + Hg \cdot u \right) - Ae(u) \cdot e(u) \right] \theta \cdot \text{nds} + \int_{\Gamma_D} (Ae(u) \cdot e(u)) \theta \cdot \text{nds} \quad (3.37)$$

$$+ \int_{\Gamma_o} \left[ 2 \left( f \cdot u + \frac{\partial g \cdot u}{\partial n} + Hg \cdot u \right) - Ae(u) \cdot e(u) \right] \theta \cdot \text{nds}$$

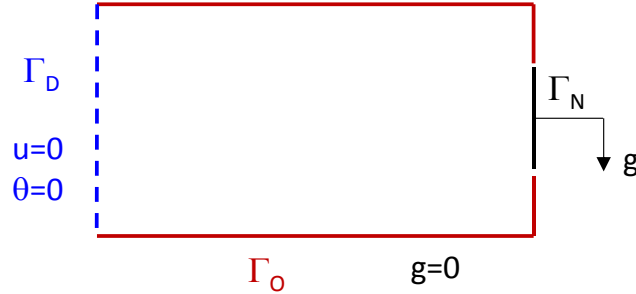


Figure 3-6 Cantilever problem with boundary conditions

where Neumann and Dirichlet boundary integral terms vanish and traction load 'g' is zero on the free boundary. This gives,

$$F'(\Omega) = \int_{\Gamma_o} (-Ae(u) \cdot e(u)) \theta \cdot \text{nds} \quad (3.38)$$

If volume force 'f' is present then shape sensitivity is,

$$F'(\Omega) = \int_{\Gamma_o} (2(f \cdot u) - Ae(u) \cdot e(u)) \theta \cdot \text{nds} \quad (3.39)$$

where  $\Gamma_o$  is a traction free boundary.

For the conductive tree optimisation problem, if volumetric heat source is applied, then  $f \neq 0$ . For this self adjoint problem (applying  $\theta \cdot n = 0$  on  $\Gamma_D$  and  $\Gamma_N$ ) the shape sensitivity is,

$$F'(\Omega) = \int_{\Gamma_o} (2(f \cdot T) - A(\nabla T) \cdot (\nabla T)^T) \theta \cdot \text{nds} \quad (3.40)$$

Note, both state and adjoint variables are represented by 'T', the temperature. The level-sets have to be propagated in the decreasing direction of objective function, which is found to be equal to negative of the shape derivative.

### 3.2.4 Topological sensitivity evaluation

Generally, engineering optimisation problems will have more than one local optimum in the solution domain. The optimiser needs to be flexible enough to search all possible topologies, to find the globally optimum shape from the set of available optimum shapes. The shape sensitivity based level-set evaluation of the HJ equation, can only vary a solid region boundary but cannot create a void region inside the solid region. Hence, the optimised shape obtained will depend on the initial distribution of level-sets. To enable the hole/void nucleation inside the solid region, the HJ equation should also have a topology gradient term.

The topological sensitivity measures the change in objective function for the introduction of an infinitesimal hole in the material domain. It is evaluated through the topological asymptote method in which the objective function is expanded in a series, as given in Eqn (3.41).

$$F(\Omega_r) = F(\Omega) + f(\varepsilon)D_T F(x_o) + o(f(\varepsilon)) \quad (3.41)$$

where,  $D_T F(x_o)$  is the topology derivative and ' $\varepsilon$ ' is the hole radius. The topological derivative value is very specific to the objective function, state equations and the boundary condition imposed on the boundary of a new hole. The topology derivative of a simple compliance minimisation problem is given as [16],

$$g = \begin{cases} \frac{\pi(\lambda_1 + 2\mu_1)(4\mu_1 SE + (\lambda_1 - \mu_1)\text{trace}(\sigma)\text{trace}(\varepsilon))}{2\mu_1(\lambda_1 + \mu_1)} + \lambda(-\pi) & \text{if } \psi > 0 \text{ (solid)} \\ 0 & \text{if } \psi < 0 \text{ (void)} \end{cases} \quad (3.42)$$

where  $\lambda_1$  and  $\mu_1$  are Lamé's constants, ' $SE$ ' is the strain energy and ' $\text{trace}$ ' stands for the trace of a matrix. In this problem, a new hole boundary has a Neuman boundary condition. During optimisation, topology sensitivity of the Lagrangian function has to be used. The Lagrangian is equal to the sum of the objective function, volume constraint and other constraints. The topology sensitivity of the volume constraint is given as

$$D_T V(x) = -|\omega| \quad (3.43)$$

where  $\omega$  is the volume of the inserted hole.

Allaire [16] suggested that alternating the evolution of level-sets based on shape derivative and topology derivative will work well to obtain the global optimum. The HJ equation with both shape and topology derivative is given below.

$$\frac{\partial \psi}{\partial t} + V \cdot \nabla \psi = -wG \quad (3.44)$$

Where ‘ $G$ ’ is the topological sensitivity and ‘ $w$ ’ is a positive parameter indicating the weightage of topology derivative. Allaire also recommended, to do one topology derivative based iteration for every 5 iterations with shape derivative, to obtain better results.

Challis [47] in her Matlab code, simultaneously used both the shape and topology derivative terms for the level-set advection. Researchers observed that more frequent nucleation of holes will slow down the convergence and the solution may lead to local minima.

Topological derivative, in the case of fluid optimisation problems represents inserting an obstacle (solid) in the design domain. Generally, if only, the change in objective function is negative, then a hole will be introduced in the material domain.

Topological derivative for Stokes flow is evaluated by Guillaume [81] through asymptotic expansion method and the same for Navier-Stokes flow is evaluated by Amstutz [82], for different objective functions. Alternatively by using augmented Lagrangian and adjoint equations, Othmer [5] evaluated the topological derivative of the ducted flows. The duct flow topology derivative is a function of state variables and adjoint variables. By solving the state equations and adjoint equations topological derivative can be evaluated (Eqn. 3.45).

$$\frac{\partial L}{\partial \alpha} = (u \cdot w) * Vol \quad (3.45)$$

where ‘ $u$ ’ and ‘ $w$ ’ are state and adjoint velocity vectors and ‘ $Vol$ ’ is the volume of hole inserted. Topological derivative for 2D NS equation is,

$$d_T F(\Omega) = 4\pi\rho\mu(u \cdot w) + d_T F(\Omega) - (\lambda - \Lambda * Vol. Difference)d_T V(\Omega) \quad (3.46)$$

where the second term on the RHS accounts for the topological derivative of objective function and third term accounts for the topological derivative due to difference in volume between the present material volume to the required material volume. Substituting the topological derivative for the viscous dissipation objective function, in Eqn. 3.46, a complete expression for the topology derivative is obtained and it is shown in Eqn. (3.47) [53].

$$d_T F(\Omega) = 4\pi\rho\mu u \cdot w + 4\pi\rho\mu u \cdot u + \pi[\lambda - \Lambda(\text{Vol. Difference})] \quad (3.47)$$

### 3.2.5 Solving the Hamilton-Jacobi equation

Generally, the HJ equation (Eqn 3.14) is solved using a finite difference method. Since the HJ equation is hyperbolic in nature, upwind differencing schemes are used to solve it. The explicit scheme used for time marching is given below.

$$\psi_{ijk}^{n+1} = \psi_{ijk}^n - \Delta t [\max(Vn_{ij}, 0) \nabla^+ + \min(Vn_{ij}, 0) \nabla^-] \quad (3.48)$$

Where superscript 'n' denotes the time level and subscript i,j,k denotes the mesh node numbering in x, y and z directions.

$$\begin{aligned} \nabla^+ = & [\max(D_{ijk}^{-x}, 0)^2 + \min(D_{ijk}^{+x}, 0)^2 + \max(D_{ijk}^{-y}, 0)^2 + \min(D_{ijk}^{+y}, 0)^2 \\ & + \max(D_{ijk}^{-z}, 0)^2 + \min(D_{ijk}^{+z}, 0)^2]^{1/2} \end{aligned} \quad (3.49)$$

$$\begin{aligned} \nabla^- = & [\max(D_{ijk}^{+x}, 0)^2 + \min(D_{ijk}^{-x}, 0)^2 + \max(D_{ijk}^{+y}, 0)^2 + \min(D_{ijk}^{-y}, 0)^2 \\ & + \max(D_{ijk}^{+z}, 0)^2 + \min(D_{ijk}^{-z}, 0)^2]^{1/2} \end{aligned} \quad (3.50)$$

$D_{ijk}^{+x}$ : Forward difference in x

$D_{ijk}^{-x}$ : Backward difference in x

The formula for backward and forward difference are given in Eqn. 3.55 to 3.60. The time step should satisfy the CFL criteria given below.

$$\Delta t \leq \frac{h}{\max |Vn_{ijk}|} \quad (3.51)$$

The level-set ( $\psi$ ) takes Neumann boundary condition on the boundaries.

Xing [83] solved the HJ equation in FE formulation without switching to FD method and without adding diffusion terms to the HJ equation. He has used the stabilised FEM (Streamline Diffusion FEM) to solve the HJ equation. He also reinitialized the level-set function by solving the Eikonal equation and this is also solved through SDFEM. While solving the Eikonal equation, an additional diffusion term is added, to improve the stability near the boundary. The accuracy of FEM method is compared with the FDM method and observed that FEM is comparable to accuracy of first order FDM methods. He pointed out that adding diffusion terms to the HJ equation causes too much dissipation in the cross wind direction.

### 3.2.6 Re-initialisation methods

Typically signed distance functions are used to represent level-set function. The gradient of this function is 1. But when the level-set boundary is updated during the optimisation the gradient of the SDF changes from 1, it could become either steep or very flat. From the steep or flat function obtaining the material boundary (zero level-set function) could be erroneous, hence the SDF needs to be re-initialised frequently in order to ensure its gradient lies close to 1. The frequent re-initialisation also has a disadvantage; it discourages the nucleation of new holes in the material domain.

The Eikonal equation (3.51) is solved to re-initialise the level-set function [84]. The unsteady equation is time marched till steady state is obtained, the steady state ensures the gradient of level-set equals to one.

$$\frac{\partial \psi}{\partial t} + w \cdot \nabla \psi = S(\psi_0) \quad (3.52)$$

$$w = S(\psi_0) \frac{\nabla \psi}{|\nabla \psi|} \quad (3.53)$$

where  $S$  is smoothed sign function.

$$S(\psi)_{i,j} = \frac{\psi_{i,j}}{\sqrt{\psi_{i,j}^2 + \left(\frac{a+b}{2}\right)^2 + \left(\frac{c+d}{2}\right)^2 + \left(\frac{e+f}{2}\right)^2} * \Delta x^2 + \varepsilon} \quad (3.54)$$

Gradients calculated through forward and backward difference formulas are used to solve the equation. Difference formula used for time marching is given below.

$$a = D_x^- \psi_{ijk} = \frac{\psi_{i,jk} - \psi_{i-1,jk}}{\Delta x} \quad (3.55)$$

$$b = D_x^+ \psi_{ijk} = \frac{\psi_{i+1,jk} - \psi_{i,jk}}{\Delta x} \quad (3.56)$$

$$c = D_y^- \psi_{ijk} = \frac{\psi_{ik,j} - \psi_{ik,j-1}}{\Delta y} \quad (3.57)$$

$$d = D_y^+ \psi_{ijk} = \frac{\psi_{ik,j+1} - \psi_{ik,j}}{\Delta y} \quad (3.58)$$

$$e = D_z^- \psi_{ijk} = \frac{\psi_{ij,k} - \psi_{ij,k-1}}{\Delta z} \quad (3.59)$$

$$f = D_z^+ \psi_{ijk} = \frac{\psi_{ij,k+1} - \psi_{ij,k}}{\Delta z} \quad (3.60)$$

$$\Delta t = 0.2 * \min(\Delta x, \Delta y, \Delta z) / \max(\text{abs}(S)) \quad (3.61)$$

$$\psi_{i,j}^{N+1} = \psi_{i,j}^N - \Delta t([\max(S, 0) * \nabla^+ + \min(S, 0) * \nabla^-] - S) \quad (3.62)$$

Due to re-initialisation, the mean line of the boundary might be slightly moved or there may be a phase lag. The nucleation of new holes is not possible if the integration is performed only on the boundary of the level-set function. Hence the level-set propagation velocity needs to be naturally extended in to the interior domain so that new holes can be nucleated. Even then the new holes will be first nucleated only near the domain boundary then they will move to the centre of the domain.

### 3.2.7 Hole nucleation methods

The HJ equation without the topological derivative term is not capable of nucleating new holes in the design domain, in 2 dimensions. Two strategies are proposed to introduce holes using topological gradients. One strategy is after marching the HJ equation only with the shape sensitivity term for a few iterations, if convergence level remains stationary then the HJ equation is time marched with topology gradient term. During the latter evolution, wherever the topology gradient is minimum, there a small hole is introduced and then again the HJ equation is time

marched with shape sensitivity term. This process is repeated till convergence is achieved. The second approach is solving the HJ equation (Eqn 3.44) always with both the gradient terms.

Burger [55] studied the different approaches to use topological gradient for the TO and their effect on convergence. Based on this, he suggested that for every few TO iterations (say 5) with shape sensitivity, an iteration with topology sensitivity should be run. The two different LS evolutions are alternated till final shape is obtained. In the topology sensitivity based evolution, wherever topology gradient is minimum and negative, there a hole is introduced.

### 3.2.8 Thickness control

On many occasions, it is desired to control the thickness of the optimised shape so that the resulting shape is manufacturable or free of disconnected shapes. To achieve this, many feature size control methods are available. Chen [85] employed a quadratic energy functional in the objective of the topology optimisation, to introduce interactions between different points on the structural boundary to favour a strip like shape of specified width. Allaire [86] while comparing different thickness control methods suggested to use the energy functional method (with fine mesh) as its shape derivative can be easily computed. The quadratic energy function given by Chen is,

$$E_q(C) = - \iint dp dp' \vec{t}(p) \cdot \vec{t}(p') \psi(|\vec{C}(p) - \vec{C}(p')|) \quad (3. 63)$$

where  $\psi$  is the weighting function and  $\vec{C}(p')$  is the coordinates of point  $p$ .

Allaire has formulated an energy function in terms of SDF as given below.

$$E(\Omega) = - \int_{\Omega} d_{\Omega}(x)^2 [(d_{\Omega}(x) + \frac{d_{min}}{2})^+]^2 dx \quad (3. 64)$$

Where  $d_{\Omega}(x)$  represents SDF,  $(..)^+$  represents maximum of the bracketed quantity and ' $d_{min}$ ' is the required minimum size of the optimised structure. The optimisation problem is,

$$\min_{\Omega} \int_{\Omega} dx + l_E E(\Omega) \quad (3.65)$$

$$s. t \int_{\partial\Omega} g.uds \leq g_{max} \quad (3.66)$$

' $u$ ' is the solution of the structural problem and  $g_{max}$  is the maximum force applied on the Neuman boundary. The nature of the optimal shape obtained is more influenced by the weighting factor ' $l_E$ '. This quadratic energy method is mostly used for minimum size control rather as a maximum size control.

Guo et al [87] proposed a feature control method based on medial surfaces. The medial surface is set of all centres of the closed maximal balls which is also called as 'skeleton'. Combined Minimum and maximum thickness constraint functional is given as,

$$g^\epsilon = \int_{MS(\Omega)} \mathcal{H}(\psi, \bar{d}, \underline{d}) dV \quad (3.67)$$

With,

$$\mathcal{H}(\psi, \bar{d}, \underline{d}) = \begin{cases} (\psi - \bar{d})^2, & \text{if } \psi > \bar{d} \\ (\psi - \underline{d})^2, & \text{if } \psi < \underline{d} \\ 0, & \text{otherwise} \end{cases} \quad (3.68)$$

where,  $\underline{d}$  represents the minimum thickness,  $\bar{d}$  represents the maximum thickness and  $\mathcal{H}(s)$  represents the medial surface. The shape derivative of the above constraint function is evaluated and used along with the shape derivative of objective function during optimisation.

### 3.2.9 Parametric level-set methods

The level-set algorithm using the HJ equation had the drawbacks of inability to handle multiple constraints and the necessity of re-initialization after every few time steps. So, Zhen Luo [88] discretised the HJ equation into a series of algebraic

equations with unknown coefficients. Then the unknown coefficients are calculated through mathematical programming (MMA) methods. Thereby solving the HJ equation by time marching is avoided. Other researches including Kreissl [52] and Ottomori [89] also used a mathematical programming approach instead of time marching the HJ equation.

The parameterisation of level-set changes the shape optimisation problem into simple size optimisation problem of finding the right values of the level-set function expansion coefficients.

### 3.3 Optimisation algorithms

Optimisation algorithms form the backbone of topology optimisation methods. In this section a review of constrained optimisation methods and gradient based optimiser algorithms are presented. A brief overview of the FE based solution of Partial Differential Equations is also presented.

#### 3.3.1 Constrained optimisation methods

Mathematically, based on the nature of the objective function the optimisation problem can be classified as Linear or Non-linear. The objective function can have two types of constraints i) equality constraints or ii) in-equality constraints. Equality constraint problems can be solved with Lagrangian multipliers. Lagrangian multipliers provide the necessary condition for the solution of equality constrained optimisation problems.

Similar to the Lagrangian condition, Karush, Kuhn and Tucker (KKT) [90] have derived a necessary condition for in-equality constrained optimisation problems. These necessary conditions also become sufficient conditions if the objective function is convex and separable. A function will be said to be convex, if a line connecting any two points within the domain also lies within the domain. The Lagrangian  $L$  of an objective function  $g_o$  and constraints  $g_i$  is written as,

$$L(x, \lambda) = g_o(x) + \sum_{i=1}^l \lambda_i g_i(x) \tag{3. 69}$$

The KKT conditions for 'L' are,

$$\frac{\partial L(x, \lambda)}{\partial x_j} = 0 \text{ if } x_j^{\min} < x_j < x_j^{\max} \quad (3.70)$$

$$\lambda_i g_i(x) = 0, \quad g_i(x) \leq 0, \quad \lambda_i \geq 0 \quad (3.71)$$

Approximating the nonlinear objective function through Taylor's series, yields a method for solving the nonlinear optimisation problem. Sequential Linear programming (SLP) and Sequential Quadratic Programming (SQP) are based on these ideas. In SLP, the linearisation approximation is only valid closer to the design variable  $x$ , so the size of design changes ( $dx$ ) has to be restricted. So, this is not considered to be a good method for engineering applications. Standard books on optimisation [91], [92] covers the SLP method with examples.

Different algorithms used for optimisation are optimality criteria method, convex linearisation method and method of moving asymptotes. In this section, brief description of different algorithms used for optimisation are explained.

### 3.3.2 Sequential Quadratic Programming (SQP)

In this method the objective function is approximated with a Taylor's series upto the second order term and the constraints are linearly approximated. For the given optimisation problem (objective function  $f$ , quadratic objective function 'Q' and design variable  $X$ ), the search direction  $S$  is found by the following quadratic problem.

$$Q = \nabla f(X)^T S + \frac{1}{2} S^T [H] S \quad (3.72)$$

subject to

$$\beta_j g_j(X) + \nabla \beta_j g_j(X)^T S \leq 0, \quad j = 1, 2, \dots, m \quad (3.73)$$

$$\bar{\beta} h_k(X) + \nabla h_k(X)^T S = 0, \quad k = 1, 2, \dots, p \quad (3.74)$$

where  $[H]$  is a positive definite matrix that is taken initially as the identity matrix and is updated in subsequent iterations so as to converge to the Hessian matrix of the Lagrange function and ' $g$ ' is the constraint function. In the above equations,  $\beta_j$  and  $\bar{\beta}$

are constants used to ensure that the linearised constraints do not cut off the feasible space completely. Typical values of these constants are given by

$$\bar{\beta} \approx 0.9; \beta_j = \begin{cases} 1 & \text{if } g_j(X) \leq 0 \\ \bar{\beta} & \text{if } g_j(X) \geq 0 \end{cases} \quad (3.75)$$

This sub-problem can be solved by any of the quadratic programming methods and the solution gives the search direction S. Then the design vector is updated as

$$X_{j+1} = x_j + \alpha^* S \quad (3.76)$$

where  $\alpha^*$  is the optimal step length found using a penalty function approach. After finding  $X_{j+1}$ , for the next iteration, the Hessian matrix is updated to improve the quadratic approximation using a Broyden-Fletcher-Goldfarb-Shanno type formula [91]. With the new Hessian matrix the next iteration is carried out till the optimum  $X$  is reached.

SQP is well-suited method for optimisation with significant non-linearities but it is computationally more expensive.

### 3.3.3 Convex linearization method (CONLIN)

In most engineering problems, the objective function and constraints are complex and they may not be explicit functions of the design variables. In these cases, a sequence of explicit sub problems of the original problem are generated and solved. Convex linearization, proposed by Fleury [93], is one such method.

In this method, some of the objective function and constraints are linearized in terms of  $x_i$  and others are linearized in terms of  $1/x_i$ . The constraint function is approximated as,

$$g_i^{C,k}(x) = g_i(x^k) + \sum_{j \in \Omega_+} g_{ij}^{L,k}(x) + \sum_{j \in \Omega_-} g_{ij}^{R,k}(x) \quad (3.77)$$

where,

$$\Omega_+ = \left\{ j : \frac{\partial g_i(x^k)}{\partial x_j} > 0 \right\} \text{ and } \Omega_- = \left\{ j : \frac{\partial g_i(x^k)}{\partial x_j} \leq 0 \right\} \quad (3.78)$$

Superscript  $L$  (on  $g$ ) represents linearization in  $x_i$ , this is done when the gradient is positive, and superscript  $R$  represents linearization in  $1/x_i$  and this is done when the gradient is negative. This approximation is actually the most conservative approximation, i.e.,

$$g_i^{C,k}(x) \geq g_i^{RL,k}(x) \quad (3.79)$$

These approximations are first order approximations, that is  $g_i$  and their first order derivatives are exact. Further the  $g_i^{C,k}$  are convex and separable. Therefore, the KKT condition becomes the necessary and sufficient condition for optimality. This makes Lagrangian duality a suitable solution method for the approximation. A brief description of the Lagrangian dual method is given below.

Consider a minimisation problem (primal problem) given below.

$$\min_x f^T x \text{ such that } \begin{cases} A \cdot x = b \\ x + s = u \\ x \geq 0, s \geq 0 \end{cases} \quad (3.80)$$

Where 's' is a primal slack variable.

Solving the primal problem is equivalent to solving the dual problem, which is given below.

$$\max [b^T y - u^T w] \text{ such that } \begin{cases} A^T \cdot y - w + z = f \\ z \geq 0, w \geq 0 \end{cases} \quad (3.81)$$

where  $y$  and  $w$  are dual variables and 'z' is a dual slack. The optimality condition of both the primal and dual problem can be written as,

$$F(x, y, z, s, w) = 0 = \begin{cases} A \cdot x - b \\ x + s - u \\ A^T \cdot y - w + z - f \\ x_i z_i \\ s_i w_i \end{cases} \quad (3.82)$$

$$x \geq 0, z \geq 0, s \geq 0, w \geq 0$$

The quadratic equations  $x_i z_i = 0$  and  $s_i w_i = 0$  are called complementarity conditions and the other equations are called feasibility conditions. By solving this matrix equation, the solution to the primal problem can be obtained. These kinds of methods are known as the primal-dual method or the Lagrangian dual method.

### 3.3.4 Method of Moving Asymptotes (MMA)

This method is an improvement over Convex Linearization, such that the degree of conservatism can be controlled to achieve better convergence of optimisation problems. Since the advent of this method (by Svanberg [94]), this has been widely used in topology optimisation of structural problems. In this method, the given problem is approximated as,

$$g_i^k(x) = r_i^k + \sum_{j=1}^n \left( \frac{p_{ij}^k}{U_j^k - x_j} - \frac{q_{ij}^k}{x_j - L_j^k} \right) \quad (3.83)$$

where

$$p_{ij}^k = \begin{cases} (U_j^k - x_j^k)^2 \frac{\partial g_i(x^k)}{\partial x_j} & \text{if } \frac{\partial g_i(x^k)}{\partial x_j} > 0 \\ 0 & \text{Otherwise} \end{cases} \quad (3.84)$$

$$q_{ij}^k = \begin{cases} 0 & \text{if } \frac{\partial g_i(x^k)}{\partial x_j} \geq 0 \\ -(x_j^k - L_j^k)^2 \frac{\partial g_i(x^k)}{\partial x_j} & \text{Otherwise} \end{cases} \quad (3.85)$$

$$r_i^k = g_i(x^k) - \sum_{j=1}^n \left( \frac{p_{ij}^k}{U_j^k - x_j} - \frac{q_{ij}^k}{x_j - L_j^k} \right) \quad (3.86)$$

' $k$ ' denotes the iteration. ' $g_0$ ' is the objective function and ' $g_1$ ', ' $g_2$ ', etc. are constraints. ' $j$ ' denotes the element in the design space and it varies from 1 to  $n$ , where  $n$  is the size of the design variable vector.  $L_j$  and  $U_j$  are moving asymptotes that are changed

during the iterations such that  $x_j$  is always bounded between  $L_j$  and  $U_j$ . Suitably changing the values of  $L_j$  and  $U_j$  changes the level of conservatism and rate of convergence. This convex separable problem can be solved using Lagrangian duality. In broader terms, the sequence of sub problems are solved according to the following iterative scheme.

STEP (0) A starting point  $x^{(0)}$  is chosen for iteration  $k = 0$

STEP (I) For a given iteration,  $k$ , the following are determined:

(i) Constraint function value:  $g_1(x^{(k)})$

(ii) Gradients (in terms of  $x$ ) of the cost function as well as the constraint functions:  $\nabla g_0(x^{(k)})$  and  $\nabla g_1(x^{(k)})$

STEP (II) Generate a sub-problem based on the original problem by replacing the original implicit functions with approximating explicit functions based on the results of STEP (I).

STEP (III) Find the optimal solution of the sub-problem and let this solution be the next iteration point  $x^{(k+1)}$ . Go to STEP (I) and repeat until the convergence criterion is met.

From the lower bound and upper bound of the design variables,  $U_j$  and  $L_j$  values can be calculated for any problem as,

$$L_j^k = x_j^k - s_{init}(x_j^{max} - x_j^{min}) \quad (3.87)$$

$$U_j^k = x_j^k + s_{init}(x_j^{max} - x_j^{min}) \quad (3.88)$$

where  $s_{init}$  is a fixed real number and its value can be altered depending on the nature of solution progress. That is, its value can be suitably chosen to prevent any oscillation in the solution, as well as to improve convergence and monotonicity.

This method works excellently for structural optimisation problems, but still convergence cannot be guaranteed in some cases. So to improve convergence, Svanberg [95] came up with Globally Convergent MMA or GCMMA. Svanberg named this class of methods as Conservative Convex Separable Approximation (CCSA) and MMA is the most famous one. Though this class of methods also solves convex sub-problems, unlike SQP and CONLIN, the method introduces curvature in the objective function and constraints, in order to make it conservative. Thereby this method doesn't

need any line search. In a line search strategy, the minimum of a function is found (iteratively) by calculating the descent direction and the step size of the design variable. The major advantage of CCSA is that it can be successfully applied to problems with a very large number of design variables.

### 3.3.5 Optimality criteria method

This method was developed by Prager and extended by Venkayya, Khot and Berke [96]. This method is an iterative method based on the optimality condition which is derived from Kuhn-Tucker conditions. For instance, let the optimisation problem be stated as follows:

Find  $X$  which minimises,

$$f(x) = \sum_{i=1}^n c_i x_i \quad (3.89)$$

$$\text{subject to } \sum_{i=1}^n \frac{a_i}{x_i} = y_{max} \quad (3.90)$$

where  $c_i$  are constants,  $y_{max}$  is the maximum permissible displacement, and  $a_i$  depends on the force induced in member  $i$  due to the applied loads, length of member and Young's modulus of member. The Lagrangian function can be defined as,

$$L(x, \lambda) = \sum_{i=1}^n c_i x_i + \lambda \left( \sum_{i=1}^n \frac{a_i}{x_i} - y_{max} \right) \quad (3.91)$$

At the optimum solution, we have

$$\frac{\partial L}{\partial x_k} = c_k - \lambda \frac{a_k}{x_k^2} + \lambda \sum_{i=1}^n \frac{1}{x_i} \frac{\partial a_i}{\partial x_k} = 0, \quad k = 1, 2, \dots, n \quad (3.92)$$

From the above relation the optimality criteria that must be satisfied at the optimum solution of the problem can be derived and are given as,

$$x_k = \left( \frac{1}{y^*} \sqrt{\frac{a_k}{c_k} \sum_{i=1}^n \sqrt{a_i c_i}} \right), \quad k=1, 2, \dots, n \quad (3.93)$$

This equation can be used to iteratively update the design variable  $x_k$  as,

$$x_k^{j+1} = \left( \frac{1}{y^*} \sqrt{\frac{a_k}{c_k} \sum_{i=1}^n \sqrt{a_i c_i}} \right), \quad k=1, 2, \dots, n \quad (3.94)$$

Where  $j$  denotes the iteration number. In each iteration the components  $a_k$  and  $c_k$  are assumed to be constants. Optimality criteria methods work very well for single constraint problems. The difficulty of the optimality criteria method for multiple constraints lies in the evaluation of multiple Lagrangian multipliers. More details about this method can be found in the reference [96].

### 3.4 Finite element method

The finite element method is a powerful numerical method used to solve complicated physics and PDEs. In this method, the geometry domain of a problem is represented as a collection of simple subdomains called finite elements. Over each finite element, algebraic equations are deduced from the governing differential equation of physics. Finally, equations of all elements are assembled appropriately and the matrix of equations are solved [97].

The order of an element refers to the degree of polynomial used to represent the solution over the element. As the order of an element increases accuracy increases but computational cost increases. For fluid flow problems, mixed or penalty finite elements can be used. In mixed finite elements, the interpolation polynomial used for pressure must be at least one order lower than that used for the velocity field because pressure is like a Lagrange multiplier which enforces incompressibility equation. So (in mixed finite elements) velocity uses quadratic interpolation and pressure uses linear interpolation functions (Figure 7-6). Finite elements using these types of discretisation for velocity and pressure are called Taylor-Hood elements. Linear elements or discretisation can also be used for both velocity and pressure along with streamwise diffusion stabilisation.

Most of the research on TO is based on the finite element method, though few works are published based on the finite volume method. The primary focus of this research work is to develop and apply the TO methods for fluid flow applications but not to develop solvers for fluid flow equations. Among the commercial solvers available, finite element based solver Comsol, gave lots of freedom to solve user specified equations, coupled multiphysics problems and to modify the material properties as liked. Further,

some of the popular optimising algorithms are already available in Comsol and it is easy to couple the Matlab programming language with Comsol. So this research work is carried out using Comsol finite element solver.

In Comsol, options are available to solve the governing equations in a segregated manner or coupled manner. The linear system of equations are solved using Generalised Minimal RESidual (GMRES) solver. For the coupled solution of fluid flow equation and the HJ equation in Comsol, time step size of a particular iteration is chosen automatically by the Comsol software, depending upon the stability of the numerical system.

### 3.1 Summary

In this section, the algorithm of density and level-set methods and its various formulations proposed by different researchers are reviewed in detail. For the level-set method, XFEM based geometry mapping is more accurate, but its implementation is difficult and time consuming, whereas density-based mapping is slightly approximate but it is simple to implement. For the level-set front propagation, the HJ equation and RD equations are used, but the RD equation doesn't make use of shape-sensitivity term. The HJ equation based level-set method is widely researched and a wealth of literature is available for this. Parametric level-set methods are gaining popularity but this requires an optimiser algorithm like MMA or SQP in addition to the physics solver.

The adjoint method is computationally cheap and accurate for shape sensitivity calculation. There are only few researchers who have used this method for the topology optimisation of fluid flow and heat transfer problems. So there are enough opportunities for further research in this area and its application to topology optimisation methods.

## 4 Density and Level-set Method Implementation

### 4.1 Introduction

Though there are many methods for topology optimisation, Density and Level-set methods are the popular and most widely used methods. A literature review indicates that the density method is popular because of its simplicity and faster convergence, while the level-set method is popular because of its crisp interface capturing ability. In this section, simple numerical models for both the methods will be developed and applied to the optimisation of simple test cases.

### 4.2 Density method based convectively cooled heat sink design – Case 1

In this study topology optimisation of a coupled multi-physics problem is solved using the density method. The convectively cooled heat sink design involves coupling of fluid flow and heat transfer. A simple density based TO model is developed in Comsol, using the MMA optimiser which is in-built in the software, to design the heat sinks.

#### 4.2.1 Numerical model

The objective of this problem is to design two dimensional convectively cooled heat sinks, which minimises the thermal compliance of the given design domain. Thermal compliance is quite similar to structural compliance in concept and this objective tries to uniformly distribute the temperature throughout the design domain. This objective, in effect will bring down the maximum temperature in the design domain.

As mentioned in the literature review, the density method is based on a design variable ' $\gamma$ ', which takes value between 0 and 1. In this case, a  $\gamma$  value of 1 indicates (porous) solid and 0 indicates fluid. In pure heat conduction problems, the thermal conductivity is modelled as a function of  $\gamma$ . For topology optimisation of fluid flow

problems, flow impermeability term is modelled as a function of  $\gamma$ , based on the Brinkman approach (Eqn 4.1). This impermeability based force term is added additionally to the flow momentum equation and it is modelled to take very high value ( $\alpha_{max}$  is 1e6) in the solid regions ( $\gamma=1$ ) and a zero value in the fluid regions ( $\gamma=0$ ).

$$\alpha(\gamma) = \alpha_{max}\gamma^3 \quad (4. 1)$$

Since it is a coupled fluid flow and heat transfer problem, along with an impermeability factor, the thermal conductivity, specific heat capacity and density are also interpolated with respect to the design variable gamma as given in Table 4-1.

Name	Expression
$k_\gamma$	$(k_s - k_f) * \gamma^3 + k_f$
$C_{p\gamma}$	$(C_{ps} - C_{pf}) * \gamma^3 + C_{pf}$
$\rho_\gamma$	$(\rho_s - \rho_f) * \gamma^3 + \rho_f$

Table 4-1 Material property values

The governing equations for the fluid flow and heat transfer are:

$$\rho_\gamma(\nabla \cdot u) = 0 \quad (4. 2)$$

$$\rho_\gamma(u \cdot \nabla u) = -\nabla p + \nabla \cdot \{\mu\{\nabla u + (\nabla u)^{tr}\}\} - \alpha u \quad (4. 3)$$

$$\rho_\gamma C_{p\gamma}(u \cdot \nabla T) = \nabla \cdot (k_\gamma \nabla T) \quad (4. 4)$$

$$\text{Heat flux Boundary condition: } (k_\gamma \nabla T) \cdot n = Q \quad (4. 5)$$

Equation (4.2) is the continuity equation (for steady, incompressible flow) with ' $u$ ' being the velocity vector. The thermal properties,  $k$ ,  $C_p$ , and  $\rho$  are modelled as given in Table 4-1. The momentum conservation equation is given in equation (4.3), which has an additional force term to differentiate (porous) solid and fluid. In (porous) solids,  $\gamma$ 's value is 1, hence the force term takes a very high value and in fluids  $\gamma$ 's value is 0, so the force term vanishes.

The property interpolation given in Table 4-1 follows the SIMP approach, this ensures that when gamma is 1, the parameters are equal to solid material properties and when gamma is zero, these are equal to fluid material properties. The power factor of 3 has been used to penalise intermediate values of gamma. The optimisation problem is defined as given below.

Objective:  $Thermal\ Compliance = \int k_{\gamma} * (\nabla T)^2 d\Omega$  (4. 6)

Constraint:  $\int \gamma dV \leq 0.40V$  (4. 7)

Governing equations 4.2 to 4.5

Note, that since the objective is thermal compliance, the effect of heat transfer due to convection is not considered.

At the start of the optimisation, the chosen initial value of gamma, is assigned on all the finite elements of the design domain. Based on this initial gamma value, physics equations are solved and the objective (thermal compliance) are calculated. Then the optimiser calculates the gradient of objective with respect to design variable and evaluates the optimum distribution of design variable (gamma) to minimise the objective function. This procedure is repeated till convergence is achieved.

#### 4.2.2 Computational details

The 2D computational domain used for this study is shown in Figure 4-1. The design domain is rectangular in shape and at its base a 5 mm thick section of strip of solid material representing a microelectronics heat source is heated by a heat flux of 100 W/m<sup>2</sup>. The top surface of the computational domain is defined as a fluid inlet with a prescribed constant velocity matching the Reynolds number of the study. The fluid inlet temperature (ambient temperature) is 293.15K. The two vertical sides are fluid outlets. The bottom side (excluding the heat source) is considered to be an adiabatic no slip wall.

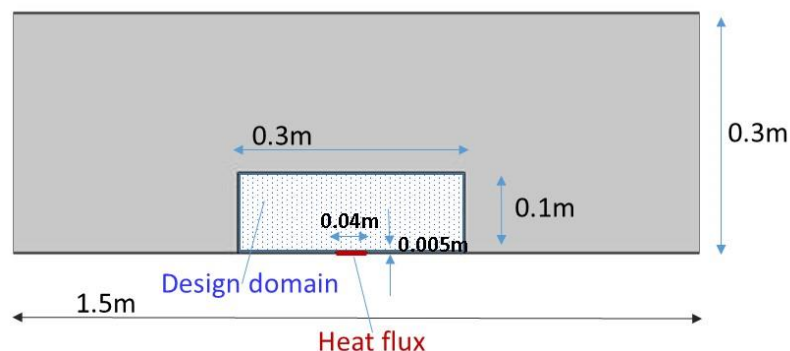


Figure 4-1 Computational domain details

For these types of problem, the thermal conductivity ratio between fluid and solid and Reynolds number of the flow are the most influential parameters. The materials

used in this particular study are copper and air, resulting in a conductivity ratio of  $1.5603 \times 10^4$ . The influence of Reynolds number on the optimal design is studied by conducting the simulations at  $Re=12$  and  $Re=70$  corresponding to velocities  $6.171 \times 10^{-4}$  and  $3.6 \times 10^{-3} \text{ m/s}$  respectively. The design domain length is considered as the characteristics length (0.3m). The Reynolds number ( $Re$ ) plays a significant role in choosing the value of  $\alpha$ ; If  $Re$  is low, higher values of  $\alpha$  can be used thereby solid can be accurately modelled but if  $Re$  is comparatively large, higher  $\alpha$  values poses problems with flow start and flow convergence. Because of this flow instability reason optimisation is not carried out at higher Reynolds numbers. For these low  $Re$  studies, Peclet number, which is a ratio between inertial diffusion to thermal diffusion, is very low compared to Peclet number usually observed in industrial applications. Generally, a low value of Peclet numbers are only observed in microchannel cooling problems.

The parameter values used in the optimisation are tabulated below.

Parameter	Value
$\alpha_{\max}$	1e6
$k_f/k_s$	15603
$\rho_s/\rho_f$	8920/1.225
$C_{p_s}/C_{p_f}$	385/1005

Table 4-2 Parameter values used for Heat sink design

The volume fraction of solid material is constrained at 0.4. The domain is discretised with triangular cells using a Delaunay triangulation method. Typically meshes of the order of 50,000 elements were used, with refinement used to concentrate cells on the design domain of the computational domain.

The approach adopted in this work can be prone to: the checkerboard problem and convergence issues. In order to attempt to mitigate against these, gradient of gamma is limited through imposition of equation (4.8). The global objective value in the design domain is also monitored. Typically in a converged run the relative change in control variable gamma is less than  $1 \times 10^{-5}$ .

$$\left(\frac{\partial \gamma}{\partial x}\right)^2 + \left(\frac{\partial \gamma}{\partial y}\right)^2 \leq 150 \quad (4.8)$$

### 4.2.3 Results

The topological optimisation is an iterative process with the heatsink shape and resulting thermal compliance evolving during the solution process. Figure 4-2 shows the evolution of solid material for the two dimensional simulation at  $Re=12$ . The iterative process is continued until the change in the global objective value decrease below a critical value, defined as  $1e-3$ , in this study.

The convergence of global objective function is shown in Figure 4-3. Figure 4-4 shows the optimised shape ((porous) solid material layout) for the  $Re=12$  case, while results for the  $Re=70$  case are shown in Figure 4-5. The optimal solid material layout resembles a tree-like structure, with the main branch leading towards the corner of the design domain and other secondary branches extending towards the edges of the design domain. The optimal tree shape is in agreement with the constructal theory of Bejan [98], wherein he states that a system will evolve in such a way that it provides easier access to the imposed currents that flow through it. Near the edge of the design domain the branch expands like a fan covering almost the entire length of the domain edge with solid material. This could be to effectively enhance the convective cooling happening by the downward air stream.

The objective value achieved for the optimisation at both Reynolds numbers are of the same order, with results given in Table 4-3. This is because the objective function doesn't account for the convective heat transfer. Simulations with different gamma initialisation lead to different optimal values and the given result had the minimum compliance among all the runs. The results show that values of the design variable  $\gamma$  lie between zero and unity in number of cells, leading to a blurring of the interface. This intermediate region, known as a grey region, is one of the drawbacks of the density methodology.

Case	Thermal Compliance (WK/m)
Re 12	0.0933
Re 70	0.0961

Table 4-3 Thermal compliance results

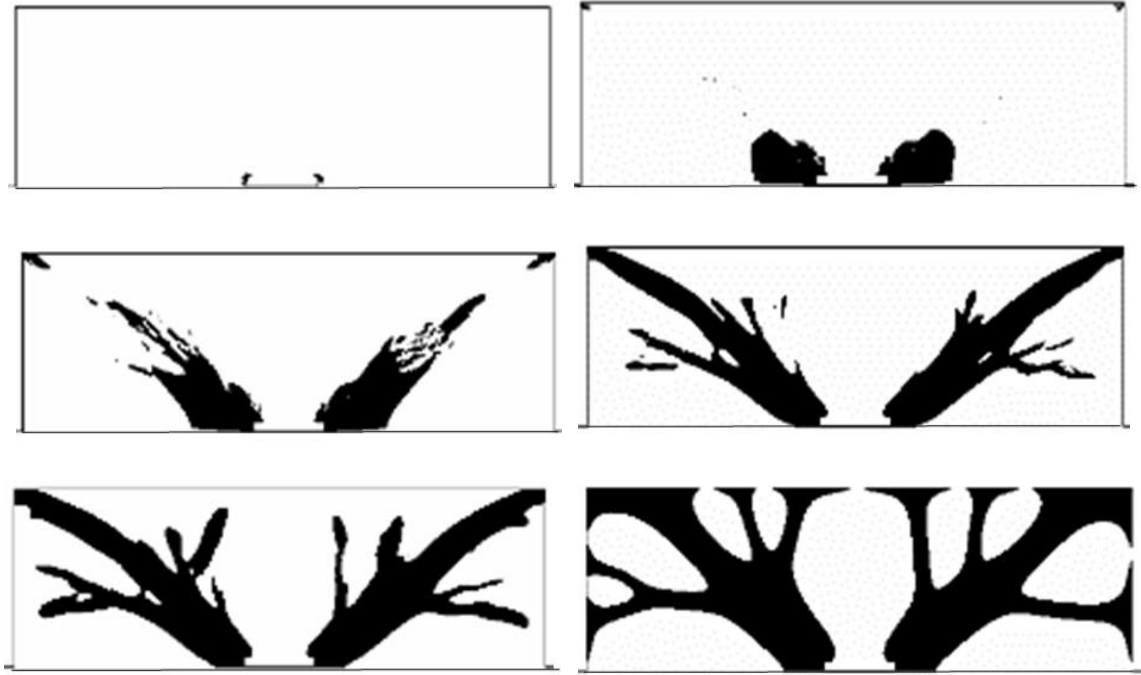


Figure 4-2: Evolution of heat sink shape during the optimisation process

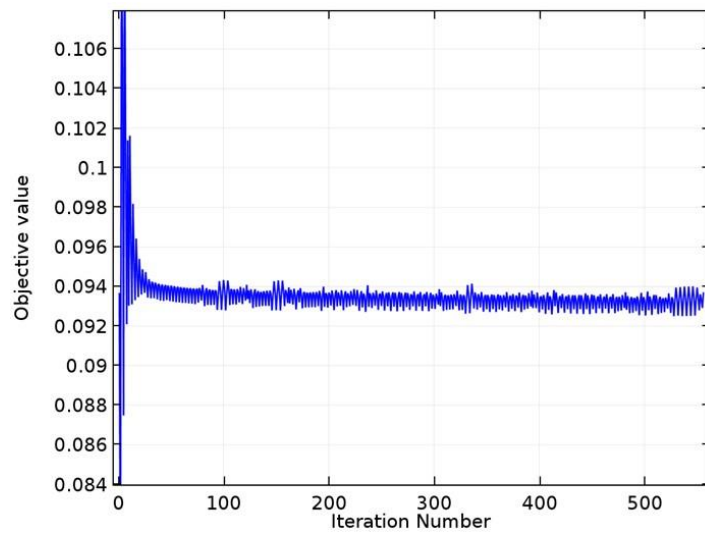


Figure 4-3: Convergence plot of objective function

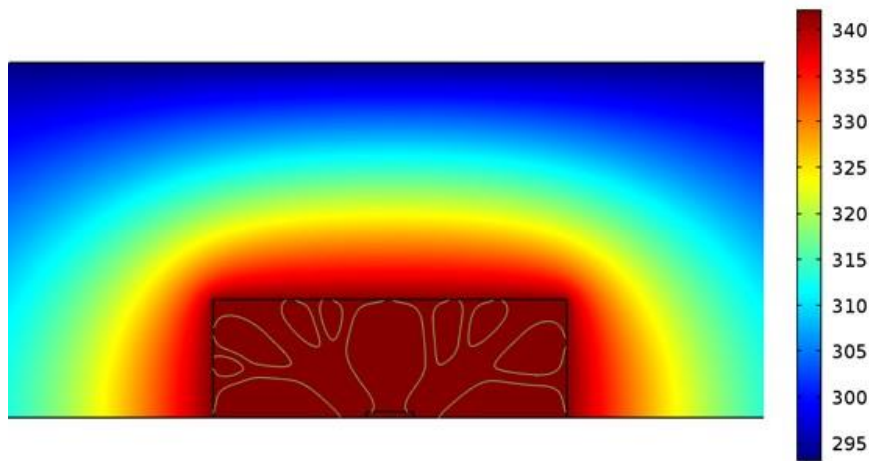
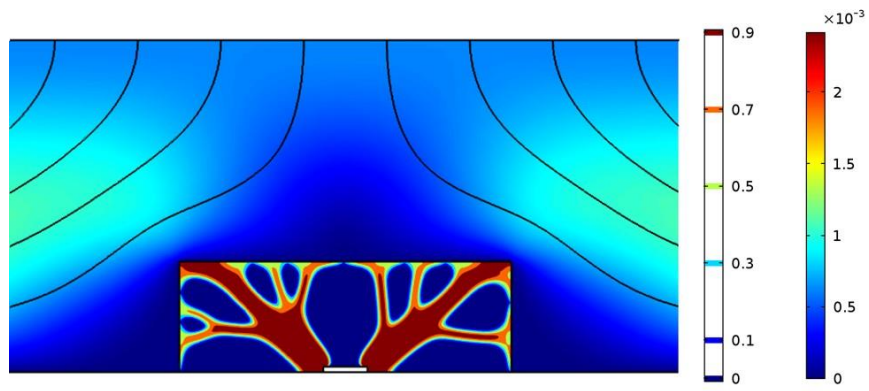
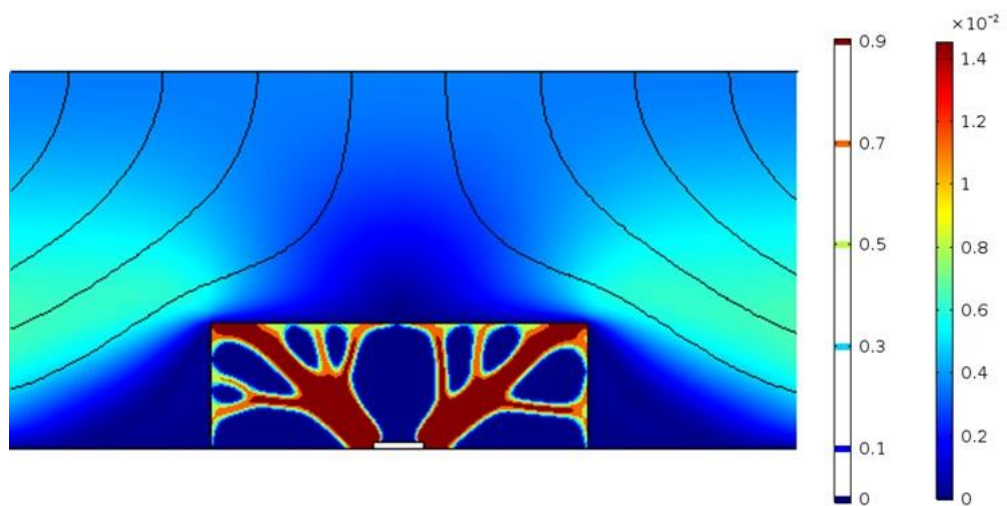


Figure 4-4: Optimised (porous) solid material layout with velocity contour (top) and temperature contours (bottom) for  $Re=12$



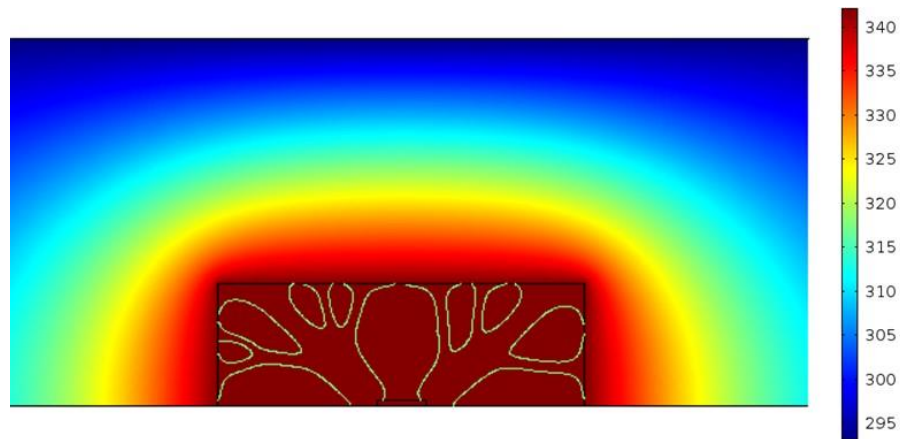


Figure 4-5: Optimised (porous) solid material layout with velocity (top) and temperature contour (bottom) for  $Re=70$

#### 4.2.4 Summary

The design of a copper heat sink subjected to forced convective cooling by air has been demonstrated. Material properties are interpolated following the SIMP approach.

The heatsink design problem was investigated at two different Reynolds numbers. The optimal heatsink shapes resemble tree-like forms as expected. It was found that the Reynolds number variations didn't alter the shape of the optimised heat sink. This is because the objective function only includes thermal compliance and the heat transfer due to fluid velocity is not accounted for.

### 4.3 Density method based convectively cooled heat sink design – Case 2

In the preceding section a heat sink is designed for highly conductive solid (copper) cooled with air convection. In this section, a heat sink will be designed for fluid to solid conductivity ratio ( $k_f/k_s$ ) of 0.1. In heat transfer involving liquid metal cooling, this kind of conductivity ratio is possible. For example, in copper metal and Gallium liquid cooling, the conductivity ratio is  $40.6/401$ , which is equal to 0.1.

#### 4.3.1 Numerical model

The governing equations and density methodology used are same as in section 4.2. Refer to section 4.2 for complete numerical model details.

### 4.3.2 Computational details

The computational domain of the previous study is used here, but the domain is discretised with Cartesian cells. The study is conducted at a Reynolds number of 60 (velocity  $2e-4\text{m/s}$ ) and Prandtl number of 104.6. The other thermal properties of solid and fluid used for this simulation are tabulated below.

Parameter	Value
$\alpha_{\max}$	1e6
$k_f/k_s$	0.04/0.4
$\rho_s/\rho_f$	8920/1000
$C_{p_s}/C_{p_f}$	385/4184

Table 4-4 Parameter values used for Heat sink design

The simulations are carried out at design domain mesh size of  $26 \times 78$  (coarse) and  $50 \times 150$  (fine) to establish the mesh independency.

### 4.3.3 Results

The topology optimisation simulations are carried out at  $\gamma$  initial value of 0.2 with coarse mesh and fine mesh. The optimised shape and temperature contour obtained are shown in Figure 4-6 and 4-7. The coarse mesh results show a shape with steps, clearly indicating the mesh needs further refinement. The finer mesh simulation result shows a smooth shape and the objective and maximum temperature values have dropped by 2.3% and 1.5% respectively from the coarse mesh results. Doubling the mesh size from  $50 \times 150$  to  $100 \times 300$  didn't improve the solution (shape & objective value) much, hence the remaining optimisations are conducted with  $50 \times 150$  mesh.

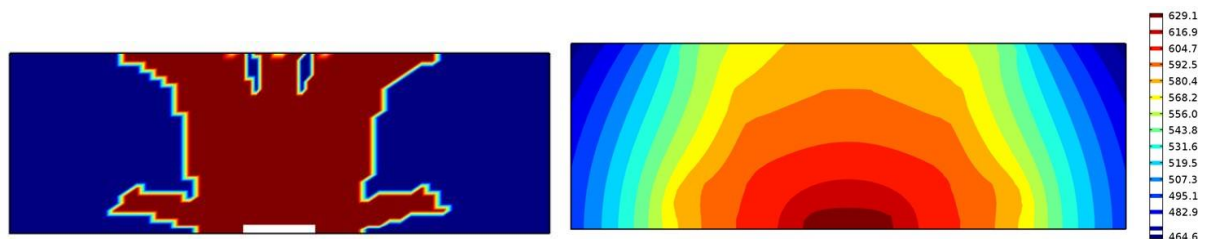


Figure 4-6 Optimised shape and Temperature contour with coarse mesh for  $k_f/k_s=0.1$  at  $\gamma$  initial=0.2

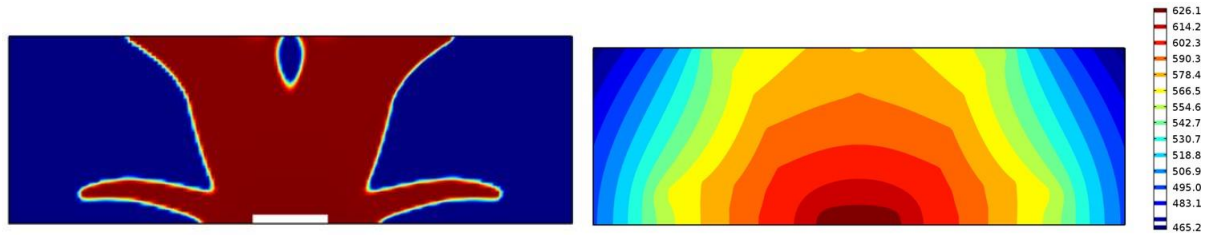


Figure 4-7 Optimisation results with fine mesh for  $k_f/k_s=0.1$  at  $\gamma$  initial=0.2

As the optimisation result depends on the initialization, the study is conducted for  $\gamma$  initial values of 0.2, 0.5, 0.7 and 1.0. The optimised shape obtained for  $\gamma$  initial values of 0.5, 0.7 and 1.0 are shown in Figure 4-8. The objective values obtained for all the simulations are shown in Table 4-6. Results shows that a  $\gamma$  initial value of 0.5 has given the lowest objective value.

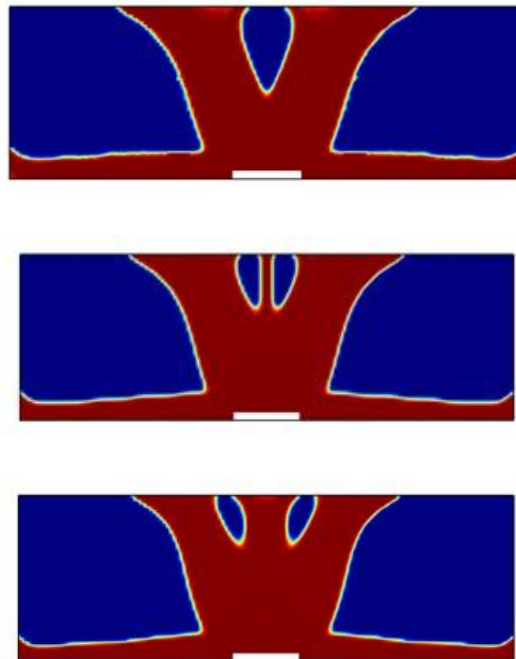


Figure 4-8 Optimised shapes for  $\gamma$  initial values of 0.5 (Top), 0.7 (Centre) and 1.0 (Bottom)

$\gamma$ Initial	Thermal compliance (WK/m)
0.2	2707
0.5	2560
0.7	2569
1.0	2580

Table 4-5 Objective values of different  $\gamma$  initial simulations

The convergence of the objective value for the  $\gamma$  initial value of 0.5 run and the corresponding temperature contours are shown in Figure 4-9. The maximum temperature attained in the design domain is 616K.

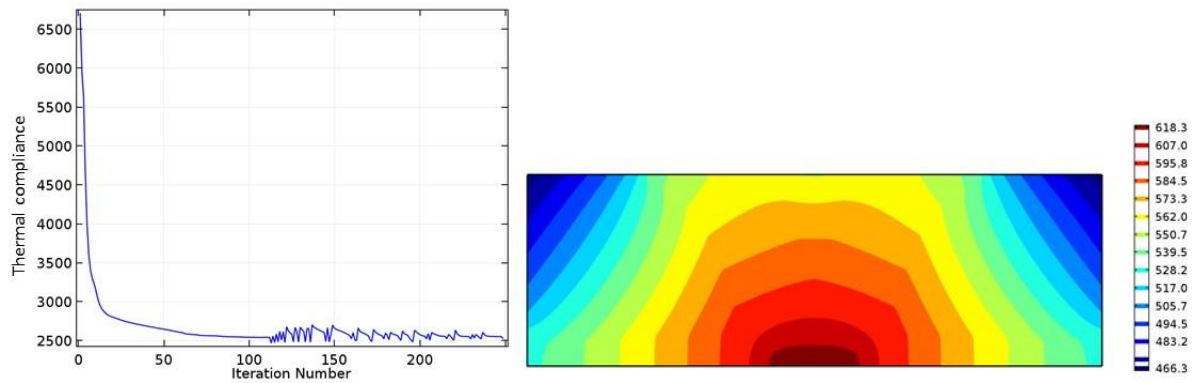


Figure 4-9 Convergence history for  $\gamma_{\text{initial}}=0.5$  case, and the corresponding Temperature contour

#### 4.3.4 Summary

The mesh independency study showed that, as the mesh refined the shape becomes smoother without any staircase like structure but the overall shape of optimum remains the same. And as the solid-to-fluid thermal conductivity ratio is decreased from 15000 to 10, the optimal shape doesn't resemble a tree-like branched structure. Further the grey regions are decreased in this case compared to the high conductivity solid case tested in section 4.2. So for better accuracy of shape capture, grey regions should be avoided and this is possible by implementing density or sensitivity based filters [72].

#### 4.4 Coupled Level-set method using Hamilton-Jacobi equation

A simple HJ equation based level-set topology optimisation model is developed in Comsol using the relevant physics module and general form PDE module present in Comsol. The later module is used to solve the time-dependent HJ equation. The density based TO problem is solved as a steady problem while the level-set based TO problem is solved as an unsteady problem.

#### 4.4.1 Optimisation of Stokes flow diffuser

This problem is aimed at identifying the diffuser shape which will increase the flow velocity by 3 times, while keeping the viscous dissipation to a minimum for the Stokes flow. The design domain is a simple square with inlet on the left hand side and outlet on the right hand side. The velocity boundary conditions are specified at inlet and outlet. For the inlet velocity, a parabolic velocity profile is specified. This is a coupled modelling where the HJ equation and flow physics are solved in Comsol software. The coupled LS formulation is based on the work of Liu et al. [48].

#### 4.4.2 Level-set formulation

A signed distance function (SDF) is used as the level-set function. The positive value of SDF is considered to represent a fluid and the negative value of SDF is considered to represent a solid. This is enforced by the ersatz projection approach, using the Heaviside function.

$$\psi = \begin{cases} = 0 & \forall x \in \partial\Omega \text{ (boundary)} \\ > 0 & \forall x \in \Omega^+ \text{ (Fluid region)} \\ < 0 & \forall x \in \Omega^- \text{ (solid region)} \end{cases} \quad (4.9)$$

Brinkman's porosity term ( $\alpha$ ) is used to differentiate the solid and liquid and it is added to the Stokes equation.

$$\alpha = (\alpha_{\max} - \alpha_{\min}) * (1-H) + \alpha_{\min} \quad (4.10)$$

Here,  $H$  is the Heaviside function, which takes a unit value when the LSF is positive (fluid region) and takes a zero value when the LSF is negative ((porous) solid region) and it has a smooth transition between the two levels, in order to enable its' differentiability. The value of  $\alpha_{\max} = 1e5$  and  $\alpha_{\min} = 0$ . The expression for the Heaviside function in terms of the LSF is given in Eqn 3.16.

#### Problem definition:

The problem statement is,

$$\text{Objective: min. } 0.5 * \int \mu * \left( \left( \frac{\partial u}{\partial x} \right)^2 + \left( \frac{\partial u}{\partial y} \right)^2 + \left( \frac{\partial v}{\partial x} \right)^2 + \left( \frac{\partial v}{\partial y} \right)^2 \right) d\Omega \quad (4.11)$$

$$\text{Subjected to, } \mu \nabla^2 u = \frac{\partial p}{\partial x} + \alpha u \quad (4.12)$$

$$\mu \nabla^2 v = \frac{\partial p}{\partial y} + \alpha v \quad (4.13)$$

$$\frac{\partial u}{\partial x} + \frac{\partial v}{\partial y} = 0 \quad (4.14)$$

Area constraint = 0.50

Where 'u' and 'v' are velocity components in x and y directions.

Figure 4-10, shows the design domain with boundary conditions.

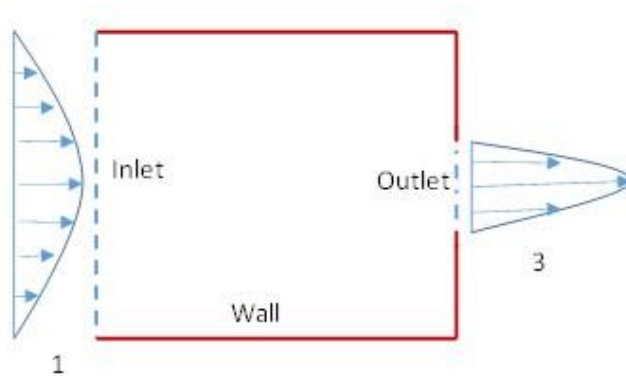


Figure 4-10 Design domain and boundary conditions

$$U_{in} = 0.2y(1-y) \quad (4.15)$$

$$U_{out} = 5.411(y-0.3333)(0.6667-y) \quad (4.16)$$

At the outlet centre point, pressure of 100Pa is specified to reach a unique solution else multiple pressure combinations are possible for the specified velocity boundary conditions. The Reynolds number of this Stokes flow based on the inlet condition is 0.0333.

The other parameters and their values used for this simulation are given in Table 4-6.

Parameter	Value
Density	1 kg/m <sup>3</sup>
Viscosity	1 Pa.s
$\alpha_{max}$	1e5
Average inlet velocity	0.0333m/s

Table 4-6 Parameter values used for the coupled level-set optimisation

#### 4.4.3 Solution methodology

The Hamilton Jacobi equation is marched in time to update the level-set function in the decreasing direction of the objective value. This is done by taking the velocity of convection equal to sum of shape sensitivity, Lagrange multiplier and area constraint term. The Stokes flow with minimum viscous dissipation objective is a self adjoint problem and its shape sensitivity is obtained from [81].

$$\frac{\partial \psi}{\partial t} = V_n |\nabla \psi| \quad (4. 17)$$

$$V_n = (0.5 * \mu * \left( \left( \frac{\partial u}{\partial x} \right)^2 + \left( \frac{\partial u}{\partial y} \right)^2 + \left( \frac{\partial v}{\partial x} \right)^2 + \left( \frac{\partial v}{\partial y} \right)^2 \right) + \lambda + \Lambda(\text{Area difference})) \quad (4. 18)$$

Where  $\lambda$  is the Lagrangian multiplier calculated using Euler-Lagrange equation [91].

$$\lambda = - \frac{\int_{\Omega} \left[ 0.5 * \mu * \left( \left( \frac{\partial u}{\partial x} \right)^2 + \left( \frac{\partial u}{\partial y} \right)^2 + \left( \frac{\partial v}{\partial x} \right)^2 + \left( \frac{\partial v}{\partial y} \right)^2 \right) \right] \delta(\psi) |\nabla \psi| d\Omega}{\int_{\Omega} \delta(\psi) |\nabla \psi| d\Omega} \quad (4. 19)$$

And  $\Lambda$  is the area penalty factor, which needs to be suitably selected to ensure the area constraint is met. This is achieved by trial and error and the suitable value for this problem is -10. It should be noted that the Lagrange multiplier only preserves the area or it assumes that the initial level-set distribution satisfies the area constraint.

The simulations are carried out in Comsol 5.1 on two different mesh sizes (51x51 and 101x101) to identify the ideal mesh size for this optimisation study. Allaire [16] has noted that even if a new hole nucleation capability is introduced in the topology optimisation process, the final optimum shape depends on the initial level-set distribution. So to reach the global optimum it is necessary to do topology optimisation with different initial level-set distributions. Here, in this study, 3 different initial level-set distributions are tried and they are shown in Figure 4-11. They are namely, uniformly distributed circles (left figure), square domain initialized with full fluid (middle figure) and square domain with solid material in the top and bottom rectangle and fluid in the middle rectangle (right figure). Note that shades of red indicate fluid and shades of blue indicate solid region.

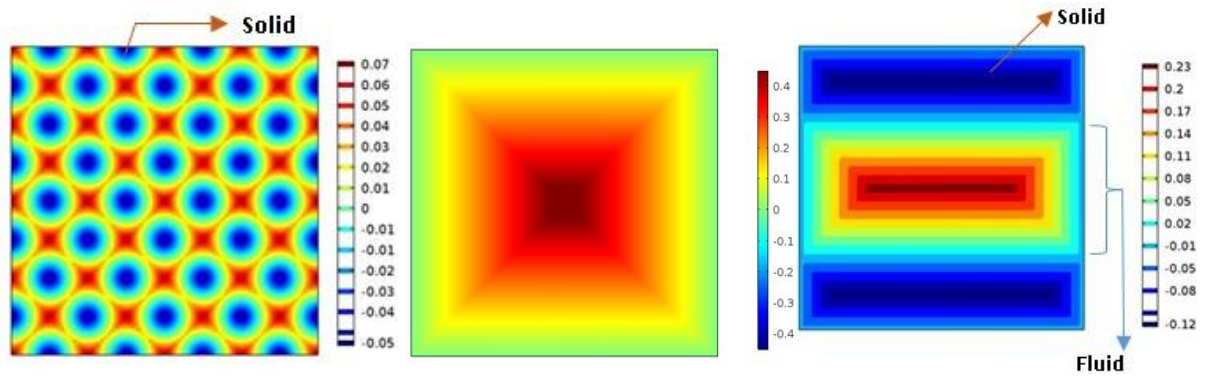


Figure 4-11 Different LS initialisations tried in this study: Uniform circles (left), Full fluid (centre) and Fluid in the middle rectangle (right). (Blue=solid, Red=fluid)

#### 4.4.4 Results

Figure 4-12 to 4-14, show the optimised diffuser shape and velocity contour for the 3 different LS initialisations mentioned earlier. From the figures it can be observed that, middle fluid LS seems to converge to optimum diffuser shape. The objective value (viscous dissipation) obtained for different cases are given in Table 4-7. Full fluid LS case has comparatively lower dissipation value, but optimum shape has (porous) solid wall near the inlet. Since the solid created are actually porous solid, by increasing the inlet pressure significantly, required inlet flow velocity is imposed on the inlet. The optimiser tries to reduce the velocity gradient by transforming the parabolic inlet velocity profile into uniform velocity profile by distributing the porous solid at the inlet. This is supported by the lower viscous dissipation value reported by these configurations than the middle fluid LS case. The same phenomena is also reported by Lee [99] as one of the drawbacks of Brinkmann approach. The uniform circle LS case has lower dissipation than the middle fluid LS case but here a larger (porous) solid region is created near the inlet and this can be inferred by comparing the velocity contour obtained during TO with velocity contour of straight walled subsonic nozzle case given in Figure 4-17. Comparatively, middle fluid LS case seems to achieve a better optimised shape and further the velocity contour of this case looks very close to the CFD case (Figure 4-16). The time where objective function reaches minimum and area constraint is satisfied is considered as the optimised solution, for this case this happens at time 0.4sec.

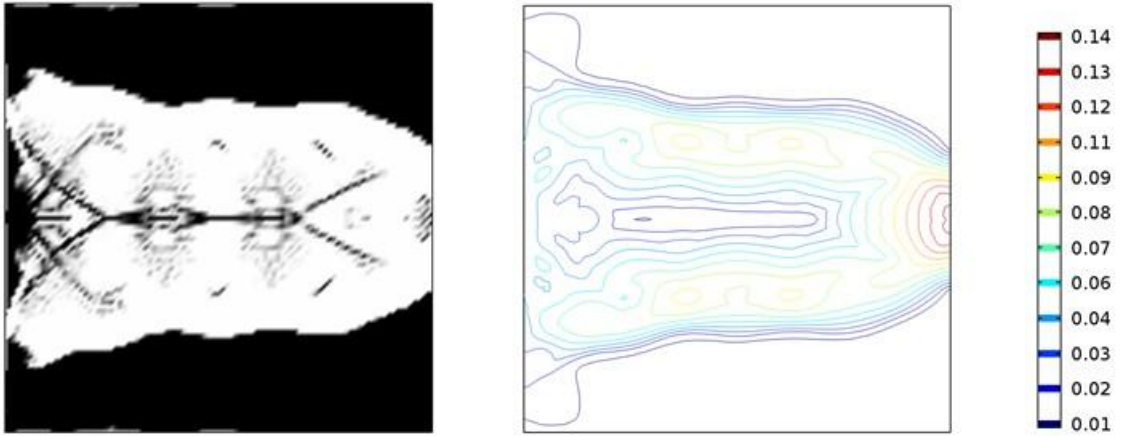


Figure 4-12 Optimised shape & Velocity contour obtained for uniform circle LS

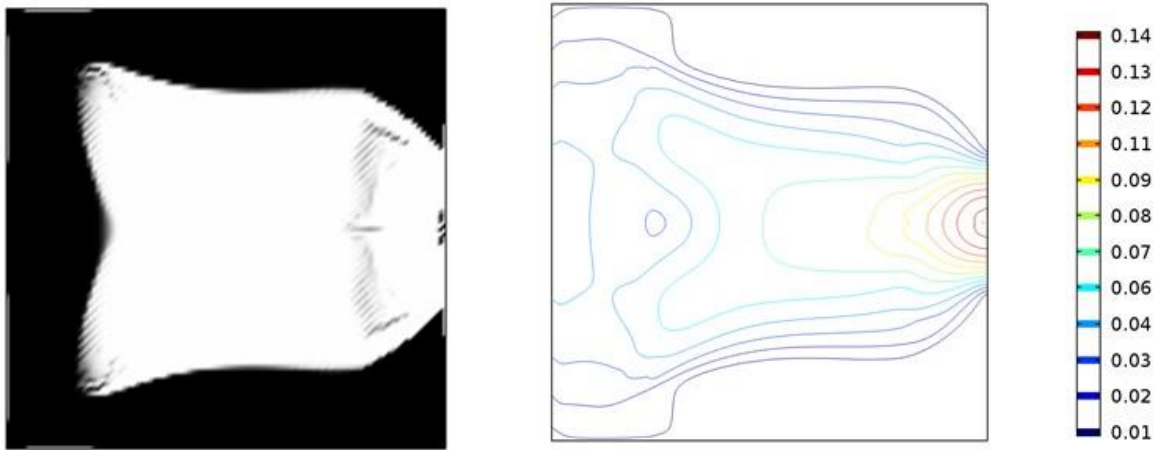


Figure 4-13 Optimised shape & Velocity contour obtained for full fluid LS

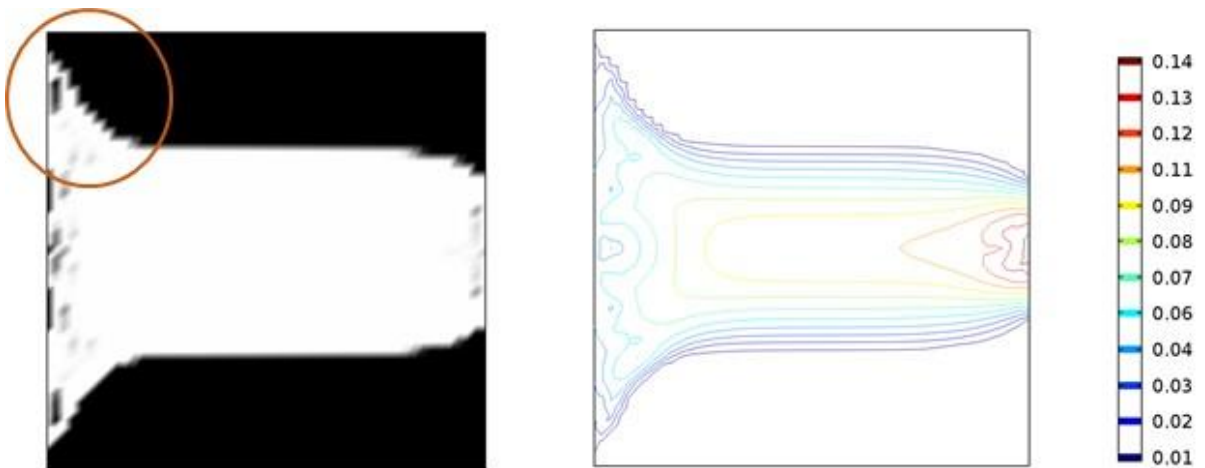


Figure 4-14 Optimised shape & Velocity contour obtained for middle fluid LS on mesh 51x51

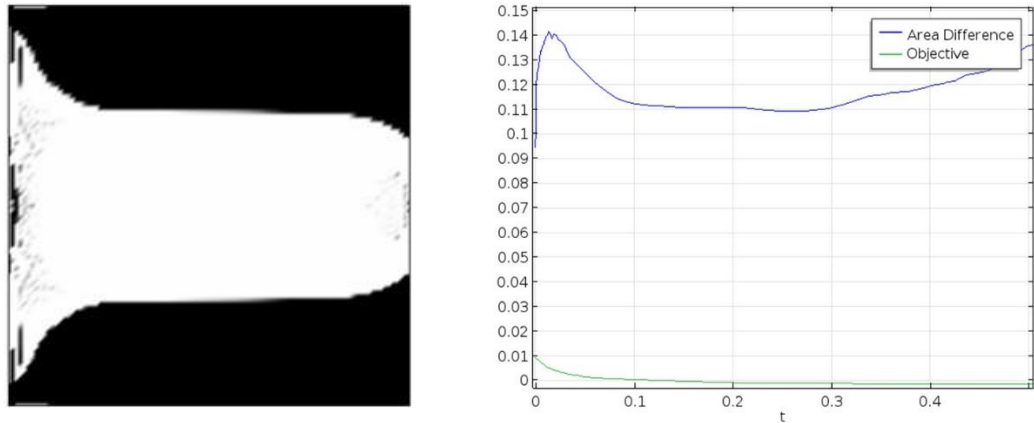


Figure 4-15 Optimised shape & Convergence plot obtained for middle fluid LS on 101x101 mesh

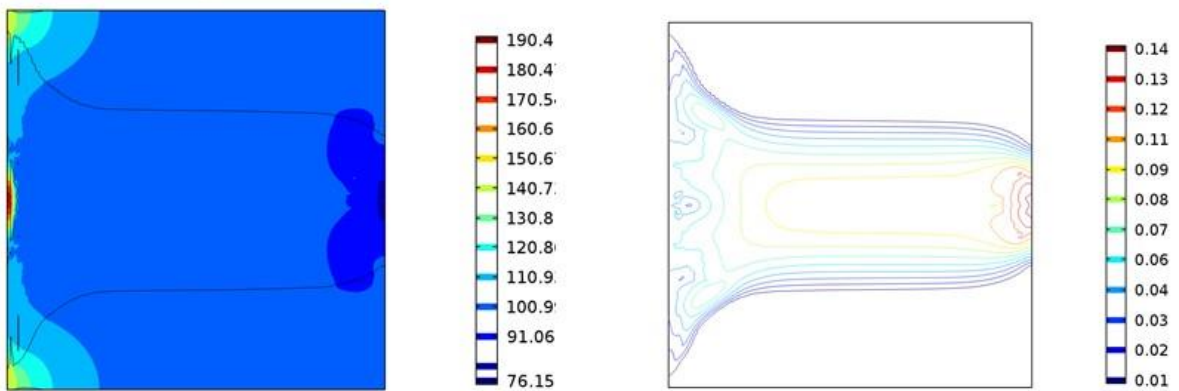


Figure 4-16 Pressure and Velocity contour for middle fluid LS on 101x101 mesh

The viscous dissipation of optimised shape is comparatively higher than the equivalent CFD case, mainly because the solid region is not completely impermeable, hence flow diffuses to larger area than the specified 50% fluid domain. As the fluid to solid contact area is overall higher, the viscous dissipation value is also higher.

	Integrated Viscous Dissipation (N/s)
Uniform circles LS	0.099913
Full fluid LS	0.043242
Middle fluid LS (51x51 mesh)	0.10150
Middle fluid LS (101x101 mesh)	0.1003
CFD result	0.064188

Table 4-7 Minimum Objective value obtained in different simulations

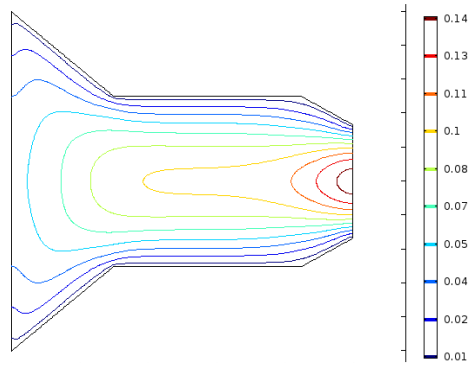


Figure 4-17 Velocity contour on CFD simulation of approximately equivalent diffuser shape

#### 4.4.5 Mesh sensitivity

The mesh sensitivity on the optimised shape is studied for one of the LS initialisation (middle fluid LS) with mesh sizes of 51x51 and 101x101. The results are shown in Figure 4-14 and 4-16. Though the optimum shape is obtained with coarse mesh, the velocity contour shows more non-smoothness and wiggles. Whereas fine mesh results are acceptable as velocity and pressure contours are smooth and have a reasonable agreement with the equivalent CFD simulation.

#### 4.4.6 Summary

The Stokes flow diffuser was designed through level-set based topology optimisation. No-slip condition is not imposed on the solid walls and further flow seepage is observed inside the (porous) walls. Hence the viscous dissipation value is higher by 71% compared to the CFD case. New holes or solid regions are not created inside the fluid region during level-set update, as a topology sensitivity term is not included in the HJ equation. Hence, the final optimum shape obtained depends very much on the initial level-set distribution. Therefore different initializations need to be tried to achieve global optimum. Further, re-initialising the level-sets at regular intervals will improve the accuracy of interface prediction.

## 4.5 Summary

A simple numerical model for the density and level-set method are developed and the topology optimisation of simple test cases are conducted. From this study following points are noted.

1. The developed numerical model of density method makes use of SIMP based material interpolation for penalising the intermediate design variables. Further, the numerical model makes use of the MMA optimiser which is already available in Comsol software. It is observed that the optimised shapes contain some grey cells of intermediate density values and relatively, the density method converges faster than the level-set method.
2. The level-set method numerical model is developed, based on the Hamilton Jacobi equation. This method captures solid boundary properly and for better optimisation results, different LS initialisations had to be tested. The optimised diffuser shapes have solid material distributed at the inlet, which is practically wrong and it is one of the draw backs of porosity approach for modelling solids. LS method with XFEM geometry mapping will be free from this disadvantage, but developing an XFEM solver is difficult and time consuming.
3. Further, the LS method is slightly more advantageous for optimising moderate Reynolds number flows because during the LS initialisation, suitable solid and fluid layout can be chosen to successfully start the flow computation whereas density method faces severe convergence issues hence it is difficult to do optimisation for moderate Re flows.
4. Similar to the density method, the coupled level-set method also has grey cells in the design domain. Regular re-initialisation of the level-set is necessary for accurate interface capture.

## 5 Performance Assessment of Density and Level-set Methods

In this section, numerical models of the density method (DM) and level-set method (LSM) are applied to optimise the topology of a 3 dimensional heat sink subjected to forced convection. The reason for choosing this problem is, it is a three dimensional problem so comparison can give realistic use of these methods. Since the problem is a coupled multiphysics problem the results of the study may be considered universal. The topology optimisation is carried out in Comsol software. The heat sinks are designed for two different material sets or for two different fluid to solid thermal conductivity ratios  $k_f/k_s=0.001$  (Highly conductive solid) and  $k_f/k_s =0.1$  (Less conductive solid). The latter case is significant here because, convective heat transfer will be of comparable magnitude to conductive heat transfer, whereas the former case will be mostly conduction dominant. The optimised heat sinks performance are evaluated and validated through an independent CFD study.

### 5.1 Heat sink design through density method

This topology optimisation is carried out in Comsol using the Method of Moving Asymptote optimiser present in it. The modelling details and results are given in the following sections.

#### Problem formulation

The governing equations of this topology optimisation study are given below.

$$\rho_\gamma(\nabla \cdot u) = 0 \quad (5.1)$$

$$\rho_\gamma(u \cdot \nabla u) = -\nabla p + \nabla \cdot \{\mu\{\nabla u + (\nabla u)^{tr}\}\} - \alpha u \quad (5.2)$$

$$\rho_\gamma C_{p\gamma}(u \cdot \nabla T) = \nabla \cdot (k_\gamma \nabla T) \quad (5.3)$$

$$\text{Heat flux Boundary condition: } (k_\gamma \nabla T) \cdot n = Q \quad (5.4)$$

Where ‘ $\alpha$ ’ is the effective impermeability, and it is zero in the fluid domain and takes higher value ( $10^5$ ) in case of solid domain. Along with impermeability, thermal properties like, thermal conductivity, specific heat capacity, and density are varied depending on whether the grid element becomes solid or fluid. In the Density method, the value of design variable  $\gamma$  determines whether the element is fluid ( $\gamma=0$ ) or solid ( $\gamma=1$ ). The interpolation of thermal and fluid properties are given in Table 5-1 (Yoon [32]).

Name	Expression
$k_\gamma$	$(k_s - k_f) * \gamma^3 + k_f$
$C_{p\gamma}$	$(C_{ps} - C_{pf}) * \gamma^3 + C_{pf}$
$\rho_\gamma$	$(\rho_s - \rho_f) * \gamma^3 + \rho_f$
$\alpha(\gamma)$	$\alpha_{max} \gamma^3$

Table 5-1 Material property interpolation relations for the Density based 3D heat sink design

Name	Value
$\alpha_{max}$	1e5
Volume fraction	0.25
$k_s$	40 [W/(mK)] ( $k_f/k_s = 0.001$ ) 0.4 [W/(mK)] ( $k_f/k_s = 0.1$ )
$\rho_s$	8920 [kg/m <sup>3</sup> ]
$C_{ps}$	385 [J/(kg*K)]
$k_f$	0.04 [W/(mK)]
$\rho_f$	1000 [kg/m <sup>3</sup> ]
$C_{pf}$	4184 [J/(kg*K)]
$\mu_f$	1.002e-3 [Pa.s]

Table 5-2 Parameter values used for the Density based 3D heat sink design

The numerical values of the thermal properties of (porous) solid and fluid are given in Table 5-2. The optimisation problem can be stated as below.

$$\text{Objective function: } \min \int_{\Omega} k_\gamma * \left[ \left( \frac{\partial T}{\partial x} \right)^2 + \left( \frac{\partial T}{\partial y} \right)^2 + \left( \frac{\partial T}{\partial z} \right)^2 \right] d\Omega \quad (5.5)$$

Subjected to

Governing equations (5.1) to (5.4)

$$\text{Volume constraint: } \int_{\Omega} \gamma d\Omega \leq 0.25 * V_{\Omega}$$

where  $V_{\Omega}$  is the design domain volume.

Heat flux is applied at the centre part of the bottom surface and an ideal heat sink has to effectively transfer the heat throughout the design domain to keep the thermal compliance at a minimum.

### Computational details

The computational domain considered for the study is shown in Figure 5-1. The computational domain considered is 1 quadrant of the total domain, making use of symmetry boundary condition on the two sides. The design domain is of size  $0.1 \times 0.1 \times 0.1 \text{m}$  whereas the computational domain is of size  $0.7 \times 0.7 \times 0.3 \text{m}$ . Heat flux is applied at the front corner of the bottom wall ( $10000 \text{W/m}^2$  at an area of  $0.01 \times 0.01 \text{m}^2$ ). Top of the computational domain is assigned velocity inlet ( $4 \times 10^{-5} \text{ m/s}$ ) boundary and a pressure outlet condition is assigned on the two side walls, which are adjacent to symmetry boundaries. The fluid inlet temperature (ambient temperature) is kept as  $293.15 \text{K}$ . The bottom wall is kept insulated, except for the heat flux boundary region. The volume fraction of solid material is constrained at a 25% of design domain volume and the design domain is discretised with  $35 \times 35 \times 35$  cells. The whole computational domain, which encloses the design domain, is discretised with 0.147 millions grid elements.

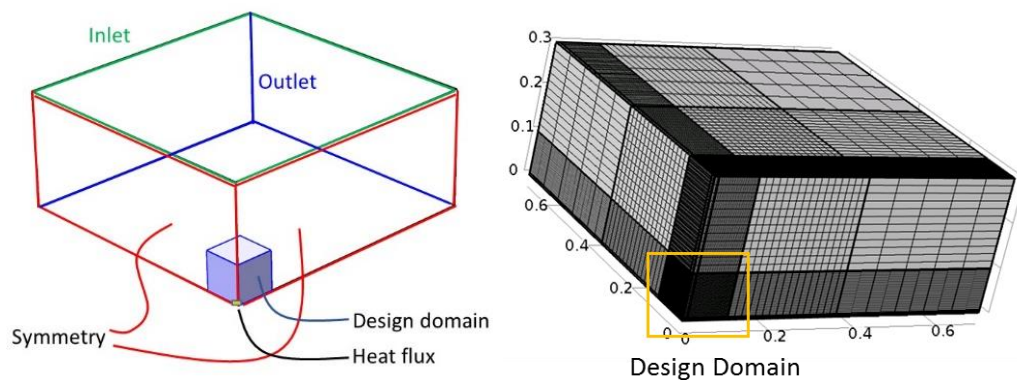


Figure 5-1 Computational domain of 3D heat sink design study

Since the MMA is a gradient based optimiser, in order to find the global optimum, the optimisation study is carried out with different  $\gamma$  initial values namely 0.10, 0.25, 0.45 & 0.55. For details about the MMA optimiser please refer to section 4.4.

### Finite element solver details:

Linear discretisation is used for both velocity and pressure. Temperature and optimisation variable  $\gamma$  are also discretised linearly. The governing equations are

solved in segregated manner. The linear system of equations are solved using GMRES solver. A run is assumed converged if the change in objective value between consecutive iterations remains less than 0.01 for a few iterations.

## 5.2 Results of the density method

### **High conductivity solid:**

The density simulation for  $k_f/k_s = 0.001$  is carried out at initial gamma values of 0.10, 0.25, 0.45 and 0.55. Simulation for gamma initial value higher than 0.55 failed because higher gamma indicates higher solid volume in the domain that leads to lower fluid permeability and hence causing flow instability problems. The simulations are carried out on a design domain mesh of size 35x35x35. In order to assess the sensitivity of the results to mesh, optimisation is carried out on a mesh of 20% lower size. The comparison of the results showed that in both the studies similar optimised shapes were obtained and the difference in the objective value was very small. This ensures that 35x35x35 mesh is free from mesh sensitivity effects.

Figure 5-2 to 5-3 show the optimised heat sink shape for different gamma initial values. It has to be noted that the solution contains some grey regions, hence in the figures  $\gamma$  value of 0.6 is used as a threshold value. The green square surface at the bottom of the heat sink shape indicates the region where the heat flux is applied. The comparison of the objective values and maximum temperature in the domain (given in Table 5-3) shows that  $\gamma=0.25$  has given better optimised solution. The full view (4 quadrant) of this heat sink is shown in Figure 5-4 and the temperature contour in the design domain is shown in Figure 5-5. For this case, the objective (thermal compliance) value is the minimum among the other optimisation results and the objective value is 4.146.

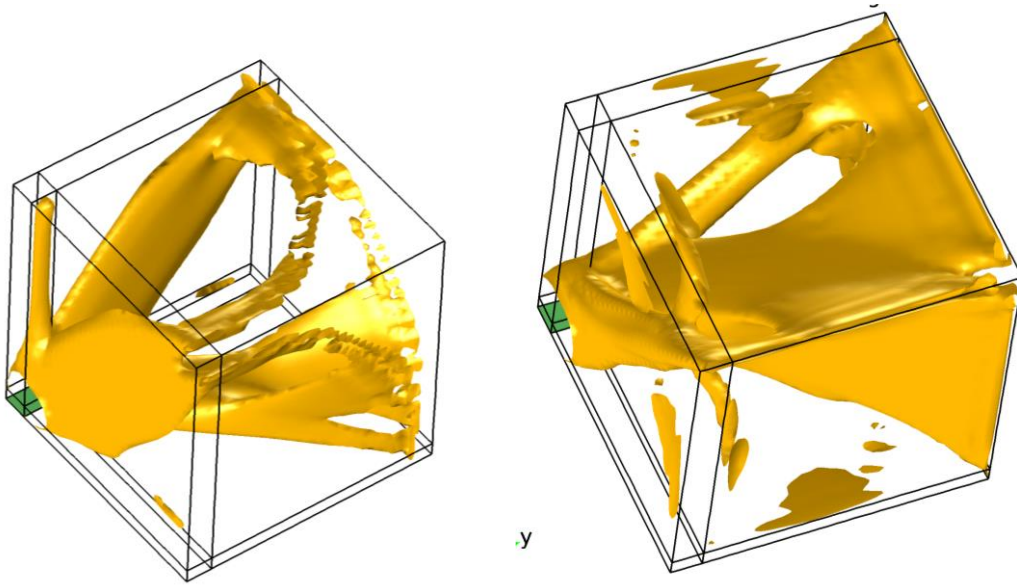


Figure 5-2 Density method optimised heat sink for  $k_i/k_s = 0.001$  at initial  $\gamma$  of 0.1 and 0.25

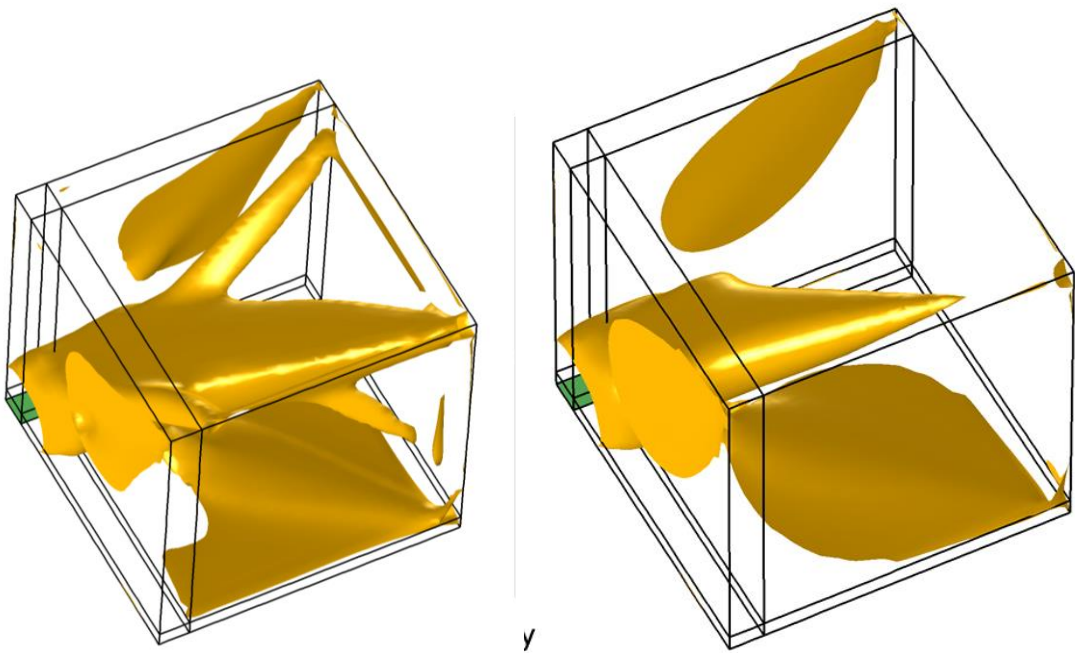


Figure 5-3 Density method optimised heat sink for  $k_i/k_s = 0.001$  at initial  $\gamma$  of 0.45 and 0.55

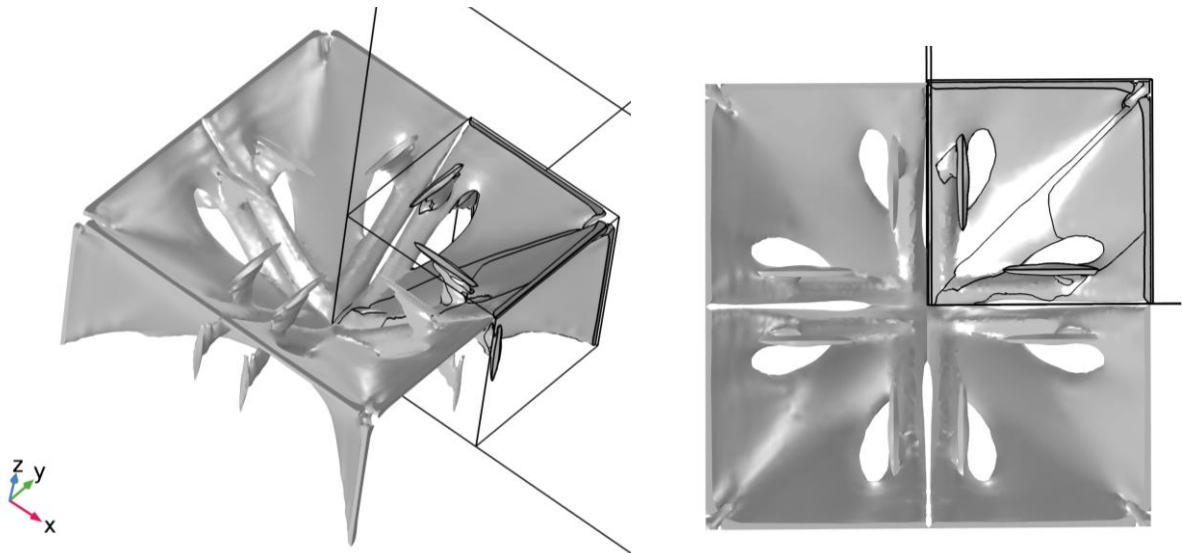


Figure 5-4 Full view of the best optimised heat sink (Isometric, Top view) by Density method for  $k_f/k_s = 0.001$ .

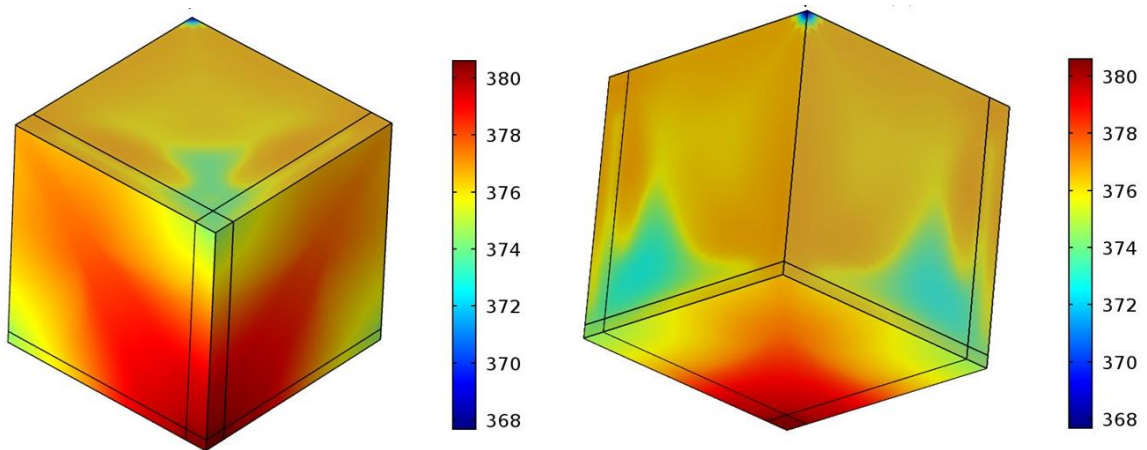


Figure 5-5 Temperature contour in the design domain for  $k_f/k_s = 0.001$  at initial  $\gamma$  of 0.55

**Low conductivity solid case:**

The density method optimisation results for  $k_f/k_s = 0.1$  are shown in Figure 5-6 to 5-7. Note that the shapes corresponds to a  $\gamma$  threshold value of 0.9. In heat transfer involving liquid metal cooling, this kind of conductivity ratio is possible. For example, in copper metal and Gallium liquid cooling, the conductivity ratio is equal to 0.1. The optimised shape nearly remains the same for different optimisation runs with a gamma initial value of 0.25 and higher. A gamma initial value of 0.55 yields minimum objective among the tested values. The full view of this optimised heat sink is given in Figure 5-8 and the corresponding temperature contour is shown in Figure 5-9. The

convergence plot of the objective value for  $k_f/k_s=0.001$  and  $k_f/k_s=0.1$  are shown in Figure 5-10. The correct symmetry boundary condition which has to be imposed on the side walls of the design domain is given in Eqn. 5.6.

$$n \cdot k(\gamma)(\nabla T) = 0 \quad (5.6)$$

But, since the symmetry boundary condition is not editable in Comsol, instead of  $k(\gamma)$ ,  $k$  of the fluid material is used. Hence the optimised shapes have a peak near the symmetry plane.

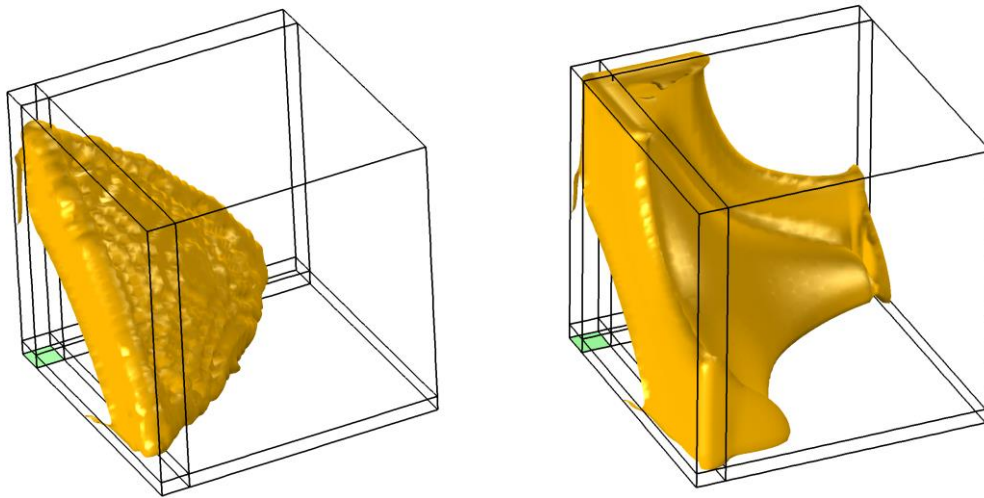


Figure 5-6 Density method optimised heat sink for  $k_f/k_s = 0.1$  at initial  $\gamma$  of 0.1 and 0.25

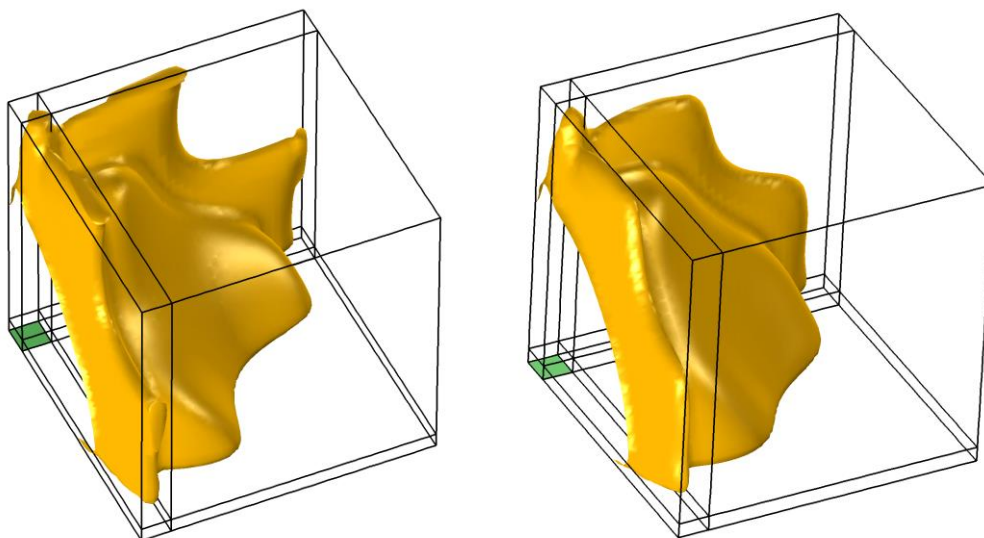


Figure 5-7 Density method optimised heat sink for  $k_f/k_s = 0.1$  at initial  $\gamma$  of 0.45 and 0.55

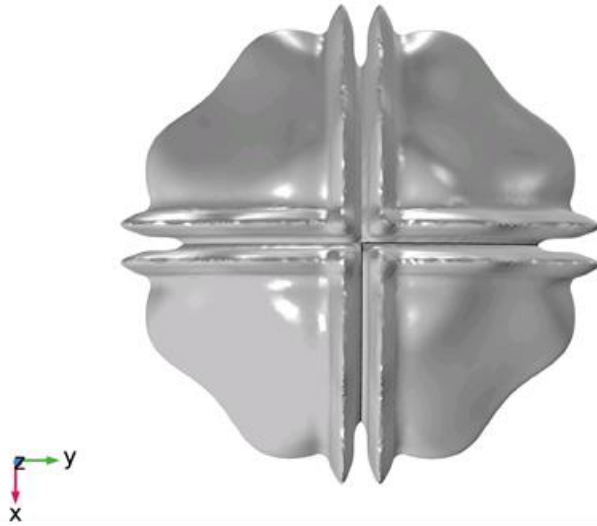


Figure 5-8 Full view of best optimised heat sink by Density method for  $k_f/k_s = 0.1$

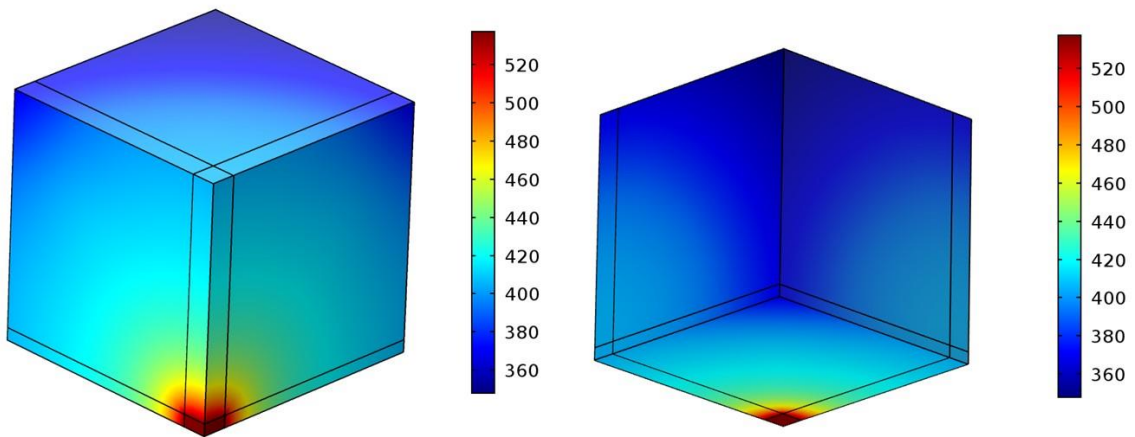


Figure 5-9 Temperature contour in the design domain for best optimised heat sink by DM for  $k_f/k_s = 0.1$  (Top & Bottom view)

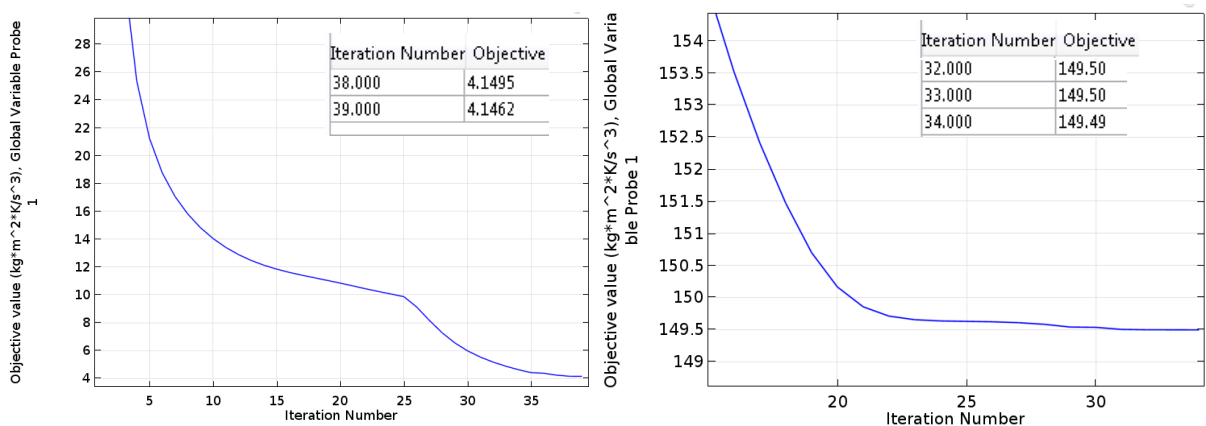


Figure 5-10 Convergence of objective function for  $k_f/k_s = 0.001$  ( $\gamma$  initial = 0.25) and  $k_f/k_s = 0.1$  ( $\gamma$  initial = 0.55)

$k_i/k_s$	Thermal compliance (WK)	$\gamma$	Maximum Temperature (K)	Iterations	Computational time
0.001	6.50	0.10	384	184	32 hours 58mins
	4.146	0.25	378	216	53hours 49mins
	5.091	0.45	379	193	27hours 44mins
	7.70	0.55	382	140	24hours 21mins
0.1	190.51	0.10	573	159	32hours 19mins
	159.24	0.25	545	140	32hours 19mins
	150.66	0.45	534	140	39hours 55mins
	149.5	0.55	532	135	24hours 41mins

Table 5-3 Summary of density method results

### Effect of heat flux on the optimised shape:

The topology optimisation study was also carried out with a  $5500\text{W/m}^2$  heat flux. Comparison of optimised shape for a heat flux of  $10000\text{W/m}^2$  and  $5500\text{W/m}^2$  show that the optimised shape didn't change much for the considered heat flux values.

### 5.3 Heat sink design through coupled level-set method

The level-set based topology optimisation of 3D heat sink was carried out in Comsol in a coupled manner following the works of Liu [48]. The design domain is a cube, with a heat source at the bottom surface and convective cooling surrounding the domain. The design domain and the computational domain are exactly the same as the one used for the density method.

#### Level-set formulation:

The level-set method using the HJ equation is used to optimise the heat sink shape. A signed distance function is used as the level-set function. The region with positive SDF ( $\psi$ ) value is considered to represent (porous) solid and the region with negative

SDF value is considered to represent fluid. This is enforced by the ersatz projection approach [14], using the Heaviside function ( $H$ ).

$$\psi = \begin{cases} = 0 \forall x \in \partial\Omega \text{ (boundary)} \\ > 0 \forall x \in \Omega^+ \text{ (Solid region)} \\ < 0 \forall x \in \Omega^- \text{ (Fluid region)} \end{cases} \quad (5.7)$$

Governing equations are the same as the ones used for topology optimisation by the density method. Brinkman's porosity term ( $\alpha$ ) is used to differentiate solid and liquid regions by modelling as given below.

$$\alpha = (\alpha_{\max} - \alpha_{\min}) * H + \alpha_{\min} \quad (5.8)$$

Where,  $\alpha_{\max} = 1e4$  and  $\alpha_{\min} = 0.001$ . A very low  $\alpha_{\min}$  value is chosen instead of zero to avoid any singularity problems while solving for the physics. The Heaviside function has a smooth transition between the two levels in order to enable differentiability.

$$H(\psi) = \frac{1}{2} + \frac{15}{16} \left(\frac{\psi}{h}\right) - \frac{5}{8} \left(\frac{\psi}{h}\right)^3 + \frac{3}{16} \left(\frac{\psi}{h}\right)^5 \quad (5.9)$$

$$\delta(\psi) = \frac{15}{16h} \left(1 - \left(\frac{\psi}{h}\right)^2\right)^2 \quad (5.10)$$

At any point within the design domain, the thermal properties  $k$ ,  $C_p$  and  $\rho$  take values based on the values of ' $\Psi$ ' and ' $H$ ' as given in Table 5-4.

Property	Expression
$k_\gamma$	$(k_s - k_f) * H + k_f$
$C_{p\gamma}$	$(C_{p_s} - C_{p_f}) * H + C_{p_f}$
$\rho_\gamma$	$(\rho_s - \rho_f) * H + \rho_f$

Table 5-4 Thermal properties interpolation formula in LS method

Problem definition:

Objective function:  $\min \int_{\Omega} k_\gamma * \left[ \left(\frac{\partial T}{\partial x}\right)^2 + \left(\frac{\partial T}{\partial y}\right)^2 + \left(\frac{\partial T}{\partial z}\right)^2 \right] d\Omega$

Subjected to,

Equations (5.1) to (5.3)

Volume constraint = 0.25

### Level-set update scheme:

The HJ equation is marched in time to advect the level-set function in the decreasing direction of the objective value. This is done by taking the velocity of advection equal to the sum of the shape sensitivity, Lagrange multiplier and area constraint terms. Stokes flow equation is self adjoint in nature. Since the flow Re of the present study (Re=8) is of similar order to the Stokes flow Re, this study is also assumed to be self adjoint. The shape sensitivity of this problem is given below.

$$\text{HJ equation :} \quad \frac{\partial \psi}{\partial t} = V_n |\nabla \psi| \quad (5.11)$$

$$V_n = \left[ (k_s - k_f) * \left( \left( \frac{\partial T}{\partial x} \right)^2 + \left( \frac{\partial T}{\partial y} \right)^2 + \left( \frac{\partial T}{\partial z} \right)^2 \right) + \lambda + A \left( \int_{\Omega} H(\psi) d\Omega - V * V_{\Omega} \right) \right] \quad (5.12)$$

where  $\lambda$  is the Lagrange multiplier calculated through,

$$\lambda = - \frac{\int_{\Omega} \left[ (k_s - k_f) * \left( \left( \frac{\partial T}{\partial x} \right)^2 + \left( \frac{\partial T}{\partial y} \right)^2 + \left( \frac{\partial T}{\partial z} \right)^2 \right) \right] \delta(\psi) |\nabla \psi| d\Omega}{\int_{\Omega} \delta(\psi) |\nabla \psi| d\Omega} \quad (5.13)$$

and  $A$  is the area (volume) penalty factor, which needs to be suitably selected to ensure the area constraint is met. This is achieved by trial and error and a suitable value for this problem is -50. It should be noted that the Lagrange multiplier only preserves the volume or it assumes that the initial level-set distribution satisfies the volume constraint.

Typical procedure followed in the level-set based topology optimisation is given below.

1. Mesh the initial structure.
2. Initialize the level-set function to a signed distance function.
3. Map the level-set function values to parameters of the physics.
4. Repeat until convergence:
  - (a) Calculate the solution to the governing equations for the current level-set defined fluid & (porous) solid domain.
  - (b) Calculate the shape sensitivity.

(c) Evolve the level-set function by solving the HJ equation to find a new structure.

Note that the re-initialisation of the level-set function is not carried out in the present study and even in the density method filters are not implemented to reduce the grey regions. This study can be used to obtain a quick first estimate of the topology optimised shape.

### Computational details:

The computational domain used for the study is the same as the one used for the density method (Figure 5-1). Since the problem is symmetric with respect to the x and y axes, only one quarter of the domain is modelled. The design domain is discretised with  $43 \times 43 \times 43$  mesh cells and initially 10 uniform spheres of level-sets are modelled in the design domain.

Three-dimensional simulations are carried out at  $Re=8$  (velocity= $4e-5m/s$ ) and at  $Pr=104.6$ . The fluid inlet temperature (ambient temperature) is kept as 293.15K. The material properties used for this simulation are the same as those used in the Density method, except  $\alpha_{max}$  is taken as  $1e4$  (Table 5-2).

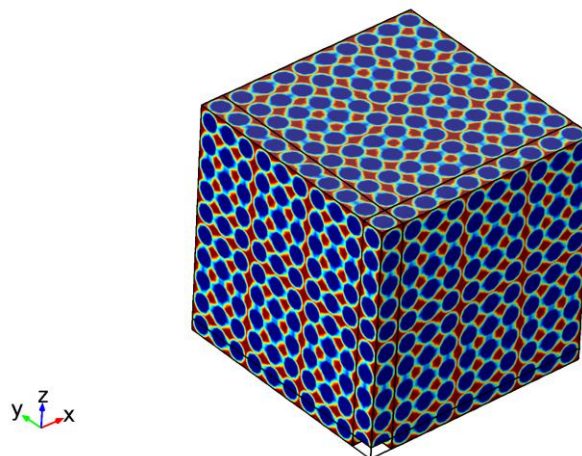


Figure 5-11 Initial Level-set distribution (A) in the design domain (Red- solid, Blue-Fluid)

Allaire [16] has observed that even with the implementation of a hole nucleation capability in the topology optimisation process, the final optimum shape depends on the initial level-set distribution. Since, the method is sensitive to initialisation, two different initialisation strategies have been assessed, namely a uniform distribution of spheres (A) as shown in Figure 5-11 and a uniform distribution of cubes (B) as shown in Figure 5-12.

The cube like SDFs are created using the function,

$$\Psi = -\cos(x*\pi*N/L)*\cos(y*\pi*N/L)*\cos(z*\pi*N/L) \quad (5.14)$$

where x,y,z are coordinate values and N is the number of level-set cubes and 'L' is the side length of the design domain. The computational time taken for this simulation was 23 days and 1 hr on ten real cores/twenty hyper threaded cores on a Dual Xeon CPU cluster node.

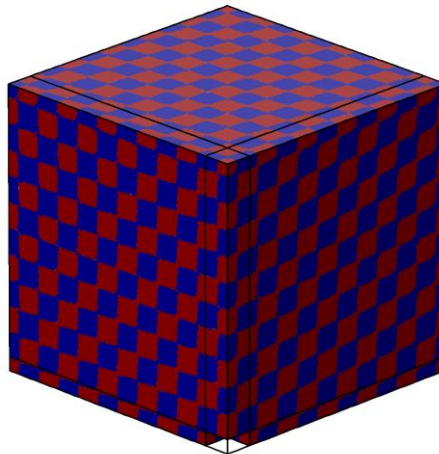


Figure 5-12 Cube like level-set initialisation (B)

#### 5.4 Results of the level-set method

The final optimised shape for  $k_r/k_s$  0.001, with initialisation A, is shown in Figure 5-13, along with the convergence plot. The time at which volume constraint is met is considered as the optimised shape, but the optimised shape obtained is not-smooth at that time. So simulation is run for additional time to obtain a smooth optimised shape for the CFD validation run.

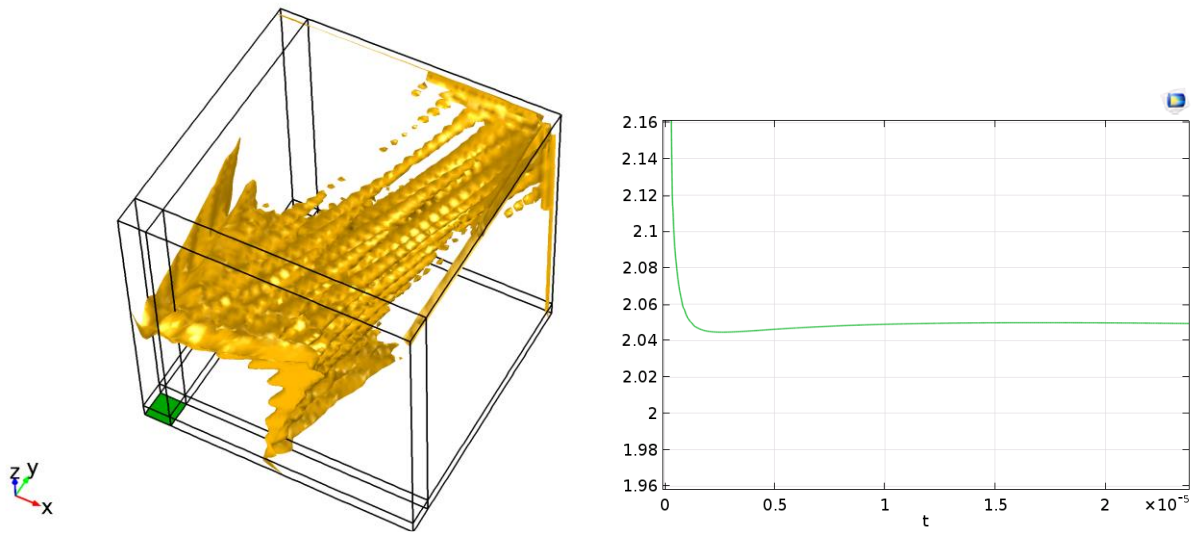


Figure 5-13 Optimised shape for  $k_f/k_s=0.001$  through Level-set method with initialisation A and the convergence plot

The topology optimisation is repeated for the level-set initialisation B. The optimised shape obtained and the convergence history for the high conductive solid case are given in Figure 5-14. This shape overall resembles the optimised shape of the density method (Figure 5-4), but it has many gaps or holes between the radial arms. The shape resembles a web connecting the 3 outer edges of the design domain with the heat flux boundary. In addition to the main web, there are two smaller web-like structures created in the LS design, which were absent in the density design. These additional features make the LS optimised design superior to that obtained using the density method.

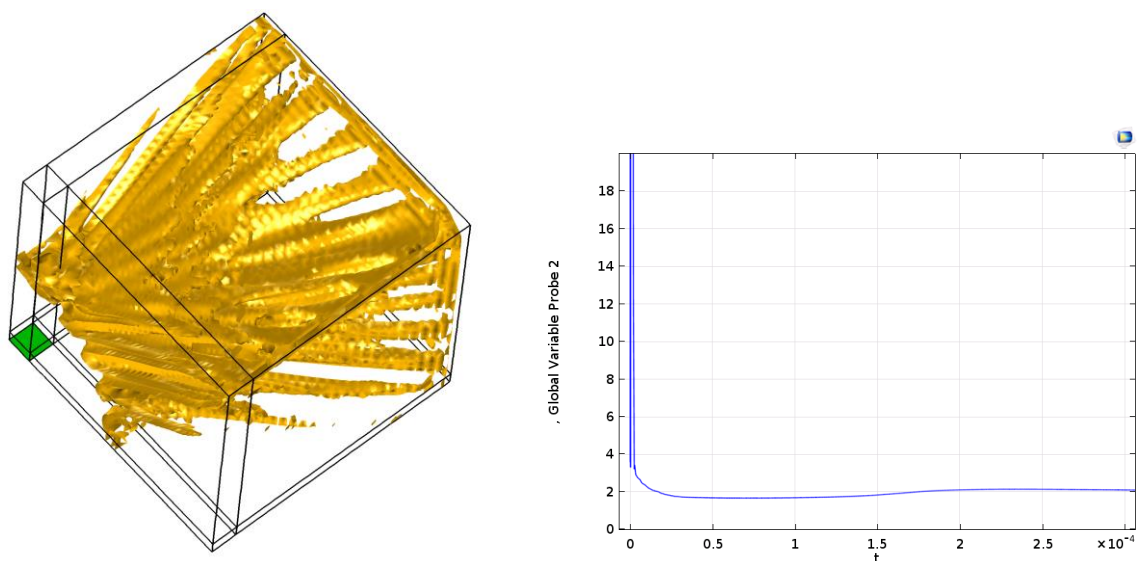


Figure 5-14 Optimised shape for  $k_f/k_s=0.001$  through Level-set method with initialisation B

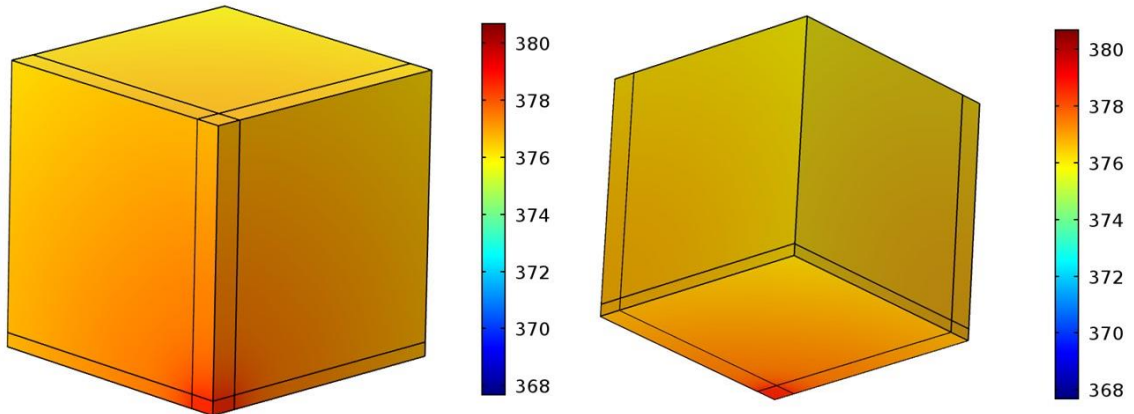


Figure 5-15 Temperature contour on design domain for  $k_f/k_s=0.001$  through LSM with initialisation B

For the low conductivity solid case, optimisation is started with an initial solid volume of 50% and the required volume constraint is 25%, but the minimum objective reached during the optimisation corresponds to a volume constraint of 43%. The optimised shape is given in Figure 5-16.

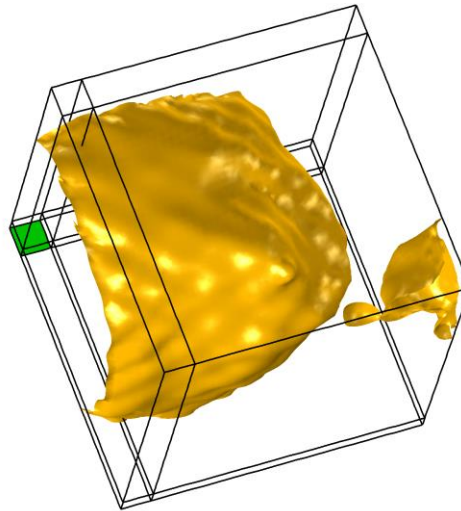


Figure 5-16 Optimised shape for  $k_f/k_s=0.1$  through Level-set method with initialisation B

It is worth noting that, in the density method, the optimised shape of the high conductivity case has more grey regions compared to the low conductivity case. While time marching in the high conductivity solid case, LS front has substantially deviated from the  $45^\circ$  slope, but in the low conductivity solid case, LS front is relatively less deviated from the  $45^\circ$  slope.

The Table 5-5 shows the comparison of the density and LS optimised heat sink performance for the two different conductivity ratios considered. For the  $k_f/k_s=0.001$  case, the LS yields a much lower objective value than the density method; even the maximum temperature within the design domain is lower for the LS shape. However, it should be noted that both the density and LS optimised shapes have grey regions which can impact the final objective value. A CFD validation could better evaluate the effective performance of these designs.

$k_f/k_s$	Thermal compliance (WK)		Maximum Temperature (K)	
	LS	DM	LS	DM
0.001	2.045	4.146	376	378
0.1	163.17	149.5	546.54	532

Table 5-5 Comparison of DM and LS results (Volume fraction 0.25)

## 5.5 CFD based validation

It is necessary to validate the optimised shape obtained because i) gradient based optimisers which are prone to initialization effects are used in the DM, ii) The LS method also has an initialization effect and iii) the threshold parameter for demarcating the (porous) solid from fluid regions is chosen by visual judgement rather than by scientific support. For the purpose of validation, it is planned to compare the cooling effectiveness of the DM and LS optimised heatsinks with a standard heat sink through a Comsol based CFD study.

The standard heat sink is designed based on an article by Yang [100]. He has designed an optimum Pin fin heat sink cooled by air impingement using the Taguchi method. But since, the Reynolds number in the present optimisation study is very much lower than Yang's study, a uniform inter-fin spacing is selected in this study.

### 5.5.1 Validation of the highly conductive solid case ( $k_f/k_s=0.001$ )

As mentioned earlier, the DM result for  $k_f/k_s=0.001$  has more grey regions. To demarcate the (porous) solid and fluid regions, the threshold gamma of 0.5 was

chosen. The resulting heatsink shape has a material volume of 19% of design domain volume. Hence, the standard heat sink is also designed to have a material volume of 19%. In order to compare it with the equivalent DM result, an additional topology optimisation run with a gamma initial value of 0.25 (which yielded best optimal results earlier) & volume constraint of 19% is carried out in the DM method.

The DM optimised heat sink geometry used in the CFD study is a relatively simplified one to enable the meshing. Figure 5-4 denotes the actual optimised shape, but from this shape, unattached regions are removed and very thin plates attached with branches are removed to carry out the meshing. It should be noted that, in general mesh generation over a thin surface will increase the mesh density significantly without increasing the accuracy of the results. Hence, normally thin edges and surfaces are removed while meshing. The simplified geometry obtained is shown in Figure 5-19. A tetrahedral mesh is generated over the geometry, which has 3 different material domains, namely copper near the heatflux region, the (porous) solid region created through optimisation ( $k=40 \text{ W/m/k}$ , density and  $C_p$  are same as copper) and the fluid created through optimisation ( $k=0.04 \text{ W/m/k}$ , density and  $C_p$  are the same as water). In total, 1.3 million tetrahedral elements were used to discretise the DM heat sink, including the outer flow domain. It should be noted that the DM based heat sink geometry had few unconnected surfaces and few very thin sheet like surfaces near the boundaries which were ignored to enable the mesh generation in Comsol.

The pin-fin heat sink is designed in such a manner that it occupies 19% of the design domain volume in order to compare it with the DM heatsink. Geometric details of the pin-fin heat sink are given in Figure 5-17. Each fin has a square cross section of side 0.00703m and a height of 0.1m including the fin base of height 0.01m. The inter-fin space is kept uniform at 0.0125m and the domain is meshed with 1.3 million tetrahedral cells. Total mesh size is kept the same for all the CFD studies to alleviate the mesh effect.

The LS optimised shape has a more complex geometry with many small surfaces and gaps. Conducting a CFD simulation on the actual TO geometry is nearly impossible in Comsol5.1, with the current geometry import features. Hence a simplified geometry has been analysed. However, the mesh and CFD setup are very similar to the DM and pin-fin design. From the CFD study, the thermal compliance of the design domain

(0.1x0.1x0.1m cube) is computed for all the 3 heat sinks and they are compared (Table 5-5) against the values obtained during topology optimisation. The temperature contour of the standard heat sink, DM and LS shape are given in Figures 5-18, 5-19 and 5-20 respectively. The following points can be observed from the table.

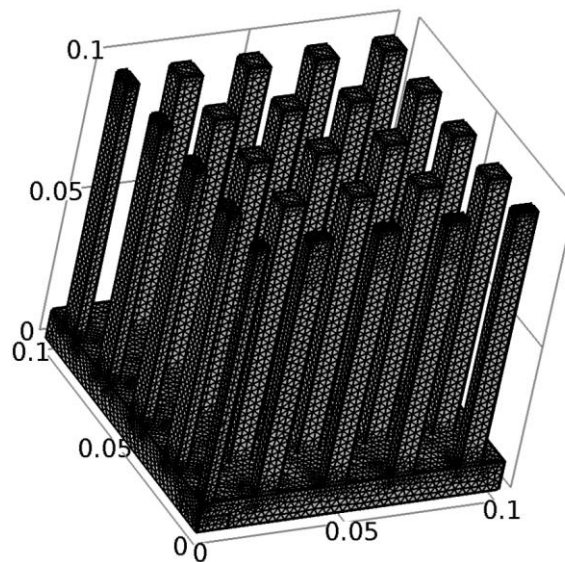


Figure 5-17 3Dimensional Pin-fin heat sink geometry

1. The thermal compliance and maximum temperature of the standard heat sink and DM heat sink are of similar order but the LS heat sink values are slightly higher.
2. The thermal compliance obtained in the CFD study is higher than the compliance obtained during the optimisation study.
3. The maximum Temperature obtained through the CFD study is lower than the temperature obtained during the optimisation study.

	DM optimisation results	LS optimisation results	CFD result of Standard HeatSink	CFD result of DM shape	CFD result of LS shape
Thermal compliance (WK)	6.518	2.05	9.498	10.10	13.86
Maximum Temperature (K)	383.9	378.58	313.89	315.89	314.68

Temperature rise (Max. Temp. - Ambient Temp.)	90.75	85.43	20.74	22.74	21.53
---	-------	-------	-------	-------	-------

Table 5-6 Validation of DM TO results for  $k_f/k_s=0.001$  for volume fraction 19%

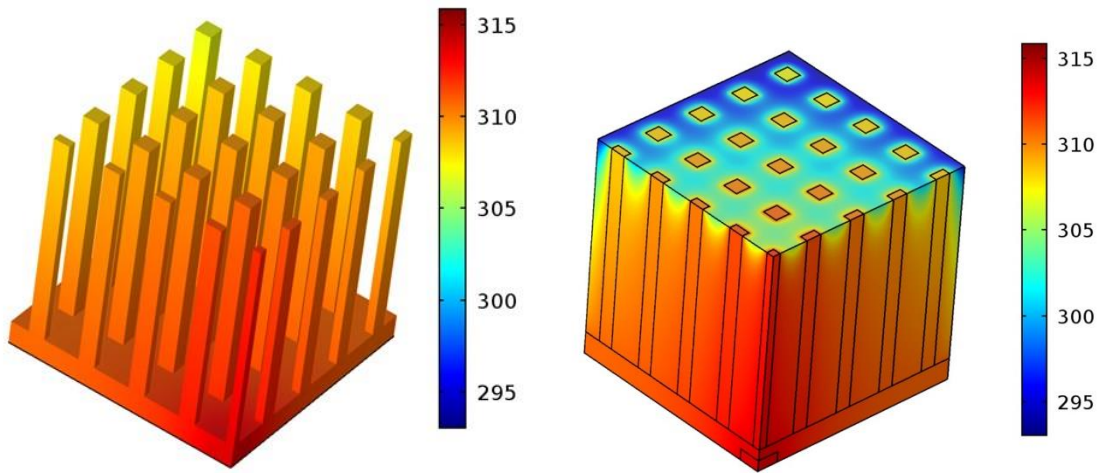


Figure 5-18 Temperature distribution from CFD study on Standard heatsink for  $k_f/k_s=0.001$

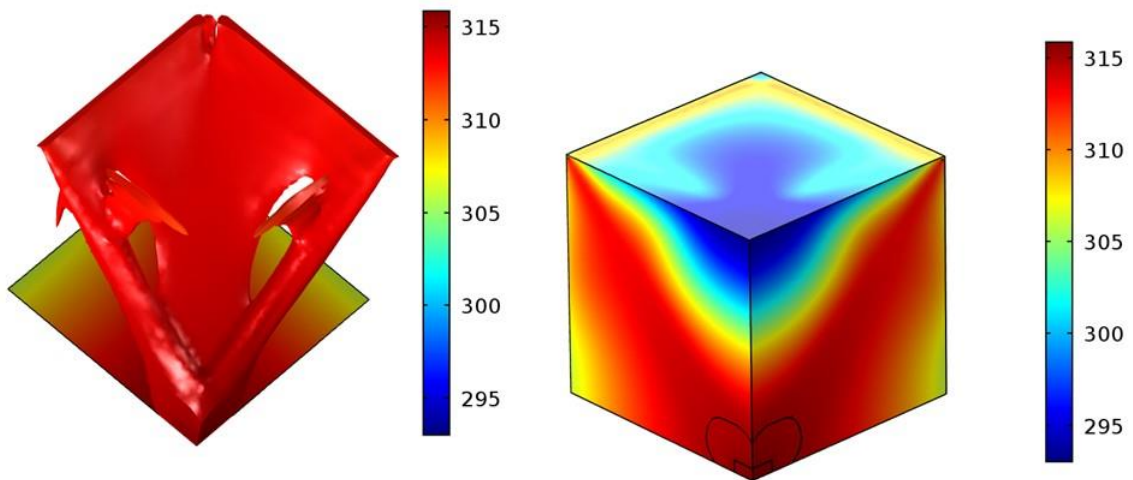


Figure 5-19 Temperature distribution from CFD study on DM heatsink for  $k_f/k_s=0.001$

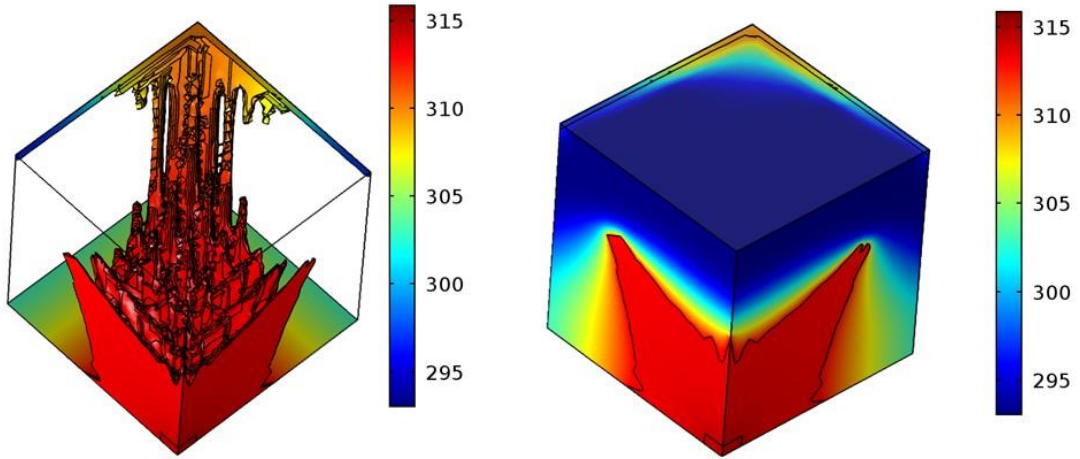


Figure 5-20 Temperature distribution from CFD study on LS heatsink for  $k_i/k_s = 0.001$

The reason for the CFD study on the DM shape reporting a higher objective value is because of the grey regions present during the topology optimisation. The grey cells which act like half-solid (good conductivity) distribute heat effectively within the domain, thereby reducing the objective value during TO. Alexandersen [37] observed a 20% difference in the objective value between the optimisation result and the CFD result. The difference observed in the present study (54.9%) is higher than the value reported by [37], mostly because of the lower  $\alpha_{max}$  ( $1e5$ ) value used during this simulation. This means that in the CFD, solid is perfectly represented as solid: that is with no slip condition, impermeability, and exact thermal conductivity but in the optimisation study solid is approximately modelled.

The surface area exposed to convective cooling is calculated for the 3 heat sinks as obtained in the TO and the simplified shape used for the CFD validation. Table 5-6 shows the comparison.

Heat sink	Surface Area (m <sup>2</sup> ) (volume fraction 19%)	
	TO shape	CFD shape
Standard pin-fin	-	0.06525
Density based heat sink	0.05308	0.04427
LS based heat sink	0.0820	0.03907

Table 5-7 Surface area of different heat sinks for volume fraction 19%

It is noted again that the optimum shape given by the LS is relatively complicated with so many small surfaces. It was difficult to import that geometry in to COMSOL and to do the CFD simulation. Hence a simplified shape with reduced surface area is taken for CFD validation. In the present CFD analysis, both the LS and Density TO shape perform less well than the standard pin-fin. This is because of the geometry simplification carried out to perform the CFD study in COMSOL. It is to be noted that the DM shape, though has 32% less surface area than the pin-fin, its thermal compliance is only 6.3% lower than the standard pin-fin. Hence if the CFD simulation were carried out on the actual TO shape, they would perform better than the standard pin-fin shape but it should also be mentioned that the pin-fin shape used here is not particularly optimised for this flow conditions. So a marginal improvement might be possible by topology optimisation methods.

Figure 5-21 shows, the temperature gradient on the heat sink surfaces obtained through the CFD study. Heat transfer is higher on the outer top edges of the cubic domain when subjected to fluid injection from the top. The DM heat sink has more solid on the outer edges, so as to decrease the temperature gradient. The LS heat sink also has more solid on outer edge, but the simplified LS shape (given in this Figure) didn't have much solid near the top edges. The maximum temperature observed within the domain is 2°K higher for the DM heat sink than the standard heat sink.

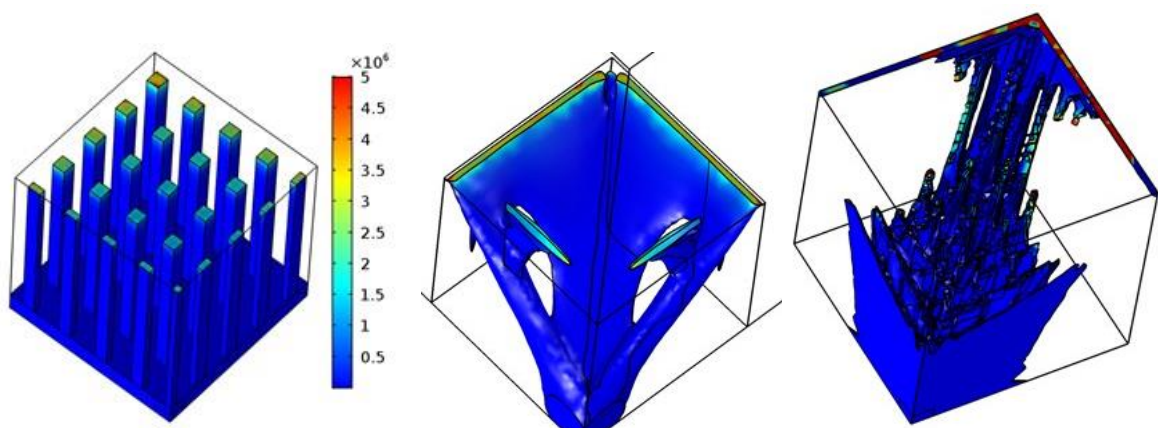


Figure 5-21 Temperature gradient comparison between Standard heatsink, DM & LS heatsinks for  $k_f/k_s=0.001$

### 5.5.2 Validation of low conductivity solid case ( $k_f/k_s=0.1$ )

Since, the LS method did not give an optimised shape for this case, the CFD simulations are only carried out for the standard heat sink and DM heat sink geometries. The DM heat sink geometry with a gamma threshold value of 0.925 had a material volume of 25%. It has to be noted that the DM topology optimisation result for the present case, has less grey cells than the  $k_f/k_s=0.001$  case. A tetrahedral mesh is generated over the computational domain, which has 3 different material domains as mentioned earlier, but now the thermal conductivity of the heat sink material is ( $K_s$ ) 0.4W/m/K. The total number of tetrahedral elements are 0.72million. Using the conjugate Heat transfer module in Comsol, CFD simulations are carried out.

Standard heat sink geometry is the same that is used for the  $k_f/k_s=0.001$  case, but now the solid has a thermal conductivity value of  $k_s=0.4W/m/K$ . From the CFD study, the thermal compliance of the design domain is computed for both the heat sinks and they are compared (Table 5-7) against the value obtained during topology optimisation. The temperature contour of the DM heat sink and standard heat sink are given in Figure 5-22. The following points can be observed from the Table.

1. The DM designed heat sink performs better, that is it attains much lower thermal compliance than the standard heat sink.
2. As for the earlier case, here again, the objective value computed through the CFD simulation of DM heat sink is higher than the value obtained during topology optimisation. The maximum temperature computed through the CFD simulation is lower than the temperature obtained during topology optimisation.

	DM optimisation results	CFD result of Standard Heat Sink	CFD result of DM shape
Thermal compliance (WK)	149.5	248.12	157.74
Maximum Temperature (K)	532	555.81	455.16
Temperature rise (Max. Temp. - Ambient Temp.)	238.85	262.66	162.01

Table 5-8 Validation of DM TO results for  $K_f/K_s=0.1$  for volume fraction 25%

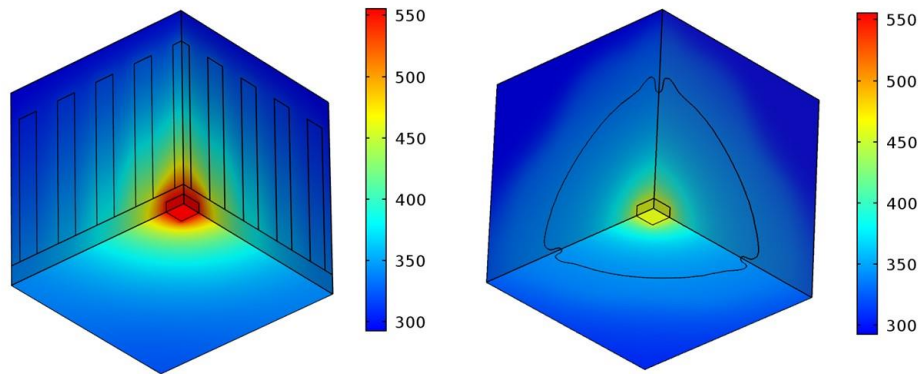


Figure 5-22 CFD based Temperature contour of Standard and DM heat sinks

The difference observed in thermal compliance can be explained from the plot of the temperature gradient given in Figure 5-23. A high value of the temperature gradient is observed near the heat source and a moderate value is observed at the top of the heat source due to convective heat transfer. The DM heat sink has more solid material near the heat source so as to decrease the temperature gradient value. Eventually, the thermal compliance of the design domain also decreases for the DM heat sink than the standard heat sink which has uniform material distribution throughout the design domain.

As the DM heat sink effectively diffuses the heat throughout the design domain it has lower maximum temperature than the Standard heat sink.

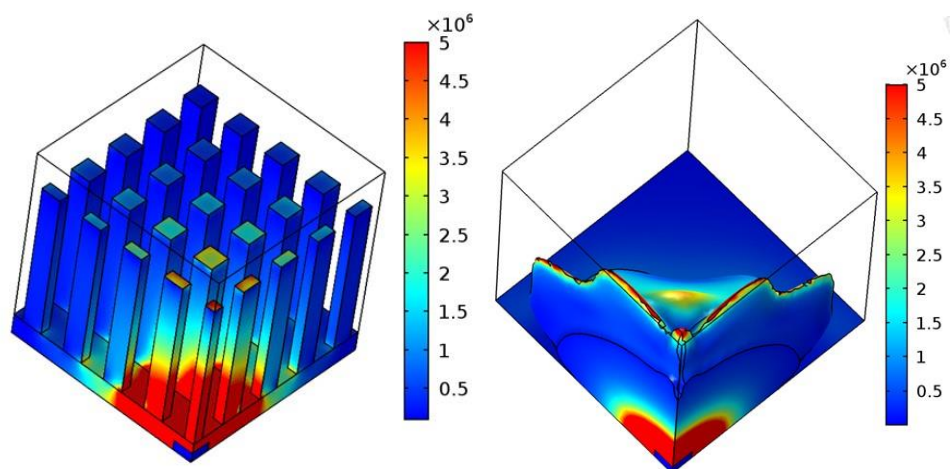


Figure 5-23 Temperature gradient comparison between Standard heatsink and DM heatsink for  $K_f/K_s = 0.1$

## 5.6 Discussion

In this study, the density method has provided optimised solutions for both the conductivity ratios tested. The level-set method has given an optimised solution for the high conductivity ratio case but for the lower conductivity case, only the cubic initialisation yields a solution but this is inferior to the density based solution. In general, the run time of level-set simulation takes longer time than the DM, but the DM requires many different gamma initialisations to be assessed in order to identify the better optimal solution. If the continuation approach is followed for  $\alpha$ , then its value can be gradually increased to higher values ( $1e6$ ) thereby the accuracy of modelling of solids can be improved.

Grey cell regions are observed in both the DM and LS with density-based mapping. The spread of grey cells will come down in LS if the level-set functions are re-initialised frequently. Similarly in DM, by using regularization techniques, the amount of grey cells can be decreased. Alexanderson interpolated the thermal properties using a convex natured relation and also followed the continuation approach to reduce the grey regions and to reach the global optimum. The amount of grey regions present also depends on the nature of the optimisation problem, that is how close it is to a convex optimisation problem. For instance, the  $k_f/k_s = 0.1$  case had less grey regions than the  $k_f/k_s = 0.001$  case. This indicates that the former case could be a convex problem.

It is worth noting that the LS method used here did not use topology sensitivity. Though for a 3D problem without topology sensitivity, holes will emerge through pinching of walls, it is not sufficient to definitely reach a better optimal solution. So to reach a better optimal it is necessary to run LS optimisation with different initialisations.

The LS topology optimisation for the  $k_f/k_s = 0.001$  case is to some extent similar to the 3D LS topology optimisation carried out by Coffin [64], but they have considered a hemi-spherical domain and a simple model for heat transfer computation (Newton's law of cooling). The Biot number in their case is 0.1, whereas in this case it is computed to be 0.03. The Biot number for the  $k_f/k_s = 0.1$  case is calculated to be 524. This indicates that convective heat transfer is relatively stronger than the conduction heat transfer in the latter case.

Optimised shapes obtained from both the DM and LS methods have some disconnected regions. During CFD validation those regions are neglected for ease of meshing. Also, in a practical heat sink, those disconnected regions are meaningless. Implementing regularisation or thin feature control mechanism in the optimiser, will prevent the formation of the disconnected regions and more details about this can be found in reference [72] and [17].

From the optimised heat sinks of  $k_f/k_s = 0.001$  &  $k_f/k_s = 0.1$  some interesting insights can be obtained. Former case is more conduction dominant, so the heat sink is extended to 3 outer edges of cubic domain. Whereas the latter case is not conduction dominant or convection plays a role in spite of  $Re$  being very low. Hence in the latter case heat sink is compact dome like shape to maximise the heat transfer. It is interesting to see that the TO on its own, without any guideline shape, lead to a suitable heatsink shapes depending on the physics of the problem.

## 5.7 Summary

The Topology optimisation of three dimensional heat sink cooled by laminar forced convection is conducted through the i) Density method and ii) Level-set method. Two different types of heat sink materials are considered one with high solid thermal conductivity ( $k_f/k_s = 0.001$ ) and the other with low thermal conductivity solid ( $k_f/k_s = 0.1$ ) and minimum thermal compliance is considered as the objective for optimisation. Complete thermo-fluidic model equations are solved. The Density based optimisation is carried out with the MMA optimiser and the Level-set method used density-based mapping. The optimised shape obtained for high conductivity solid resembles like a web connecting the outer edges of cube with the heat source. The optimised shape is conceptually same in both the methods but there are some differences in the finer details. The LS shape has multiple gaps though maintaining the overall outer shape same, thereby it has much higher surface area for the same material volume. This makes it very difficult to conduct CFD validation simulation on the obtained optimal shape in Comsol. For the low conductivity solid case, the density based method gave good results whereas LS seems to reach a local minima, for the two different initialisations tried.

The optimised shapes are validated through comparison of their CFD performance against the CFD result of standard pin fin heat sink. The CFD validation of  $k_f/k_s = 0.1$  case shows that, the TO heat sink performs better than standard pin-fin heat sink. In the  $k_f/k_s = 0.001$  case, optimised shapes are performing equally to the standard pin-fin heat sink shape. Since the TO heat sink shapes are not directly amenable for CFD simulation, some extent of geometry simplifications or smoothings are made. The simplification reduced the surface area of the optimised shapes considerably. If simulations are performed on the actual un-simplified TO shapes, they might well have a superior performance than the standard one. Further, the objective value calculated through CFD simulation is much higher than that through optimisation study, mainly because of the grey cells present during the optimisation study which understates the objective value significantly. But, this could be avoided by regular re-initialisation of level-set functions.

This performance assessment study also shows that,

1. The LS gives better quality design with much lower objective function value, though the Density method is found to be the robust one.
2. The Density method faces more flow instability problems for 3D problems at moderate Reynolds numbers; because of this optimisation runs with initial gamma value higher than 0.55 could not be carried out. The LS is slightly better as optimisation can be started with suitable solid/fluid area initialisation without destabilising the fluid flow.
3. Computational time taken by the coupled LS method is higher than the DM, but LSM's computational time can be significantly reduced by carrying out the LS advection separately in Matlab and using Comsol only for solving the physics.

This study conducted on a simple numerical framework, indicates that while both the methods experience grey cells, the DM is faster in convergence and robust but the LSM gives better quality design. But more importantly, the DM has more flow instability problems, hence the LSM is chosen as a better method for studying the fluid flow and heat transfer problems. Going forward, the LSM numerical framework will be developed to state-of-the-art level.

## 6 Enhancement of Level-Set Optimisation Framework

### 6.1 Introduction

In the previous chapter it was shown that the Level-set Method gives better quality design with lower objective value than the DM. Hence this method is chosen for further study and it is also planned to improve the LS numerical model in terms of computational time, grey cells and shape sensitivity evaluation. It is planned to do the following changes to the LSM numerical model.

1. De-coupling the solution of physics and advection of LS, in order to reduce the computational time. Consequently, advection of LS will be carried out using the Finite difference method and solution of physics will be carried out using the FE method.
2. Re-initialisation of LS function, in order to reduce the grey cells in the final optimised design.
3. Implementation of adjoint shape sensitivity evaluation.
4. Implementation of Topological derivative based LS advection.

### 6.2 Level-set advection

The LS function is advected by solving the HJ equation (Eqn 5.11). Solving the HJ equation coupled with the problem physics, takes more computational time in Comsol. Hence the HJ equation is solved separately in Matlab and a new LS function (which is the solution of the HJ equation) is passed on to Comsol, to solve for the physics. The HJ equation is solved using an explicit first order upwind scheme. The level-set function is evolved on a grid with ghost elements; the ghost elements surround the 4 sides of the design domain. The physics is solved on the actual design domain mesh. Figure 6-1 shows the design domain with surrounding ghost elements (dotted lines) used for the LS advection. Refer to section 3.2.5 for the finite difference formulas used for the LS time evolution. The time step for time marching the HJ equation should

satisfy the CFL criterion for stability. Every time the physical problem is solved, the HJ equation is marched in time several time steps (~20) in order to obtain the new shape or new level-set function.

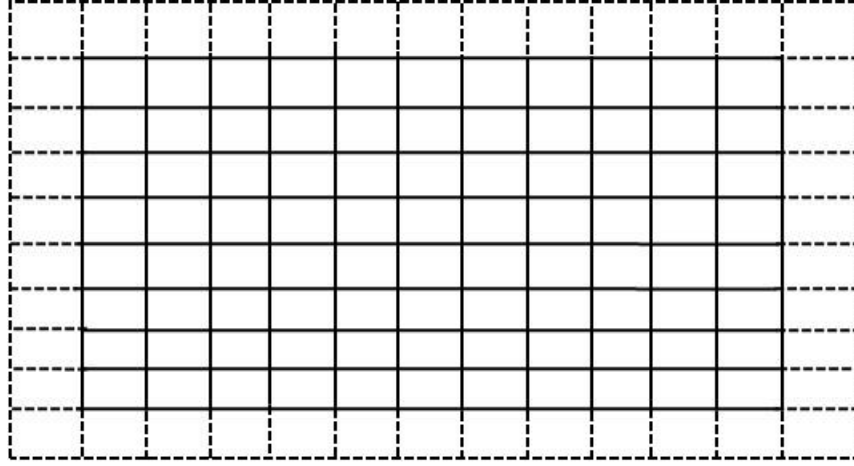


Figure 6-1 Design domain mesh with surrounding ghost elements used for LS advection

### 6.3 Re-initialisation of level-sets

As the LS are propagated during the TO iterations, they become steep or slant. But for accurate interface prediction, the gradient of LS has to be unity; so to bring back the gradient of LS to unity, re-initialisation of LS has to be carried out at regular intervals. In order to re-initialise the LS, the Eikonal equation (6.1) is solved. This unsteady equation is time marched till steady state is obtained and the steady state ensures that the gradient of the level-set has become equal to 1.

$$\frac{\partial \psi}{\partial t} + w \cdot \nabla \psi = S(\psi_0) \quad (6.1)$$

$$w = S(\psi_0) \frac{\nabla \psi}{|\nabla \psi|} \quad (6.2)$$

Where S is the smoothed sign function. For a two dimensional case, the expression for S is given below,

$$S(\psi)_{i,j} = \frac{\psi_{i,j}}{\sqrt{\psi_{i,j}^2 + \left(\left(\frac{a+b}{2}\right)^2 + \left(\frac{c+d}{2}\right)^2\right) * \Delta x^2 + \varepsilon}} \quad (6.3)$$

where  $\Delta x$  is the grid spacing in the x direction and  $\varepsilon$  is a very small number (1e-5). Gradients calculated through forward and backward difference formulas are used to solve the equation. The difference formula used for time marching is given below.

$$a = D_x^- \psi_{i,j} = \frac{\psi_{i,j} - \psi_{i-1,j}}{h} \quad (6.4)$$

$$b = D_x^+ \psi_{i,j} = \frac{\psi_{i+1,j} - \psi_{i,j}}{h} \quad (6.5)$$

$$c = D_y^- \psi_{i,j} = \frac{\psi_{i,j} - \psi_{i,j-1}}{h} \quad (6.6)$$

$$d = D_y^+ \psi_{i,j} = \frac{\psi_{i,j+1} - \psi_{i,j}}{h} \quad (6.7)$$

$$\Delta t = CFL * \min(\Delta x, \Delta y) / \max(abs(S)) \quad (6.8)$$

$$\psi_{i,j}^{N+1} = \psi_{i,j}^N - \Delta t([\max(S, 0) * \nabla^+ + \min(S, 0) * \nabla^-] - S) \quad (6.9)$$

Where 'i' is the node numbering along the x direction, 'j' is the node numbering along the y direction and 'CFL' is the Courant-Friedrichs-Lewy number based on which time step is calculated. The expressions for  $\nabla^+$  and  $\nabla^-$  are given in Eqn. (3.49) and (3.50). The time marching is continued till the stopping criteria described by Sussman [84] is satisfied. The re-initialisation has been implemented in Matlab and typical procedure followed for the topology optimisation with LS re-initialisation is described in the next section.

### 6.3.1 Numerical implementation

The level-set Topology optimisation with the re-initialisation of level-sets at regular intervals is carried out in Comsol software in combination with Matlab Livelink. The various steps involved in this process are given in Figure 6-2, in which the steps enclosed within the dashed line box are carried out in Comsol and the rest of the steps are carried out in Matlab Livelink. It should be noted that in this formulation both the HJ equation and Eikonal equation are solved in Matlab. These equations are solved using an explicit first order upwind scheme. The written Matlab code is inspired from the MATLAB code (TOPLSM) written by Wang [101], which demonstrates the various

steps involved in the level-set based topology optimisation for a simple structural mechanics problem.

In this formulation, first the design domain is initialised with some initial guess of LSF in Matlab and then it is exported to Comsol to solve for the physics.

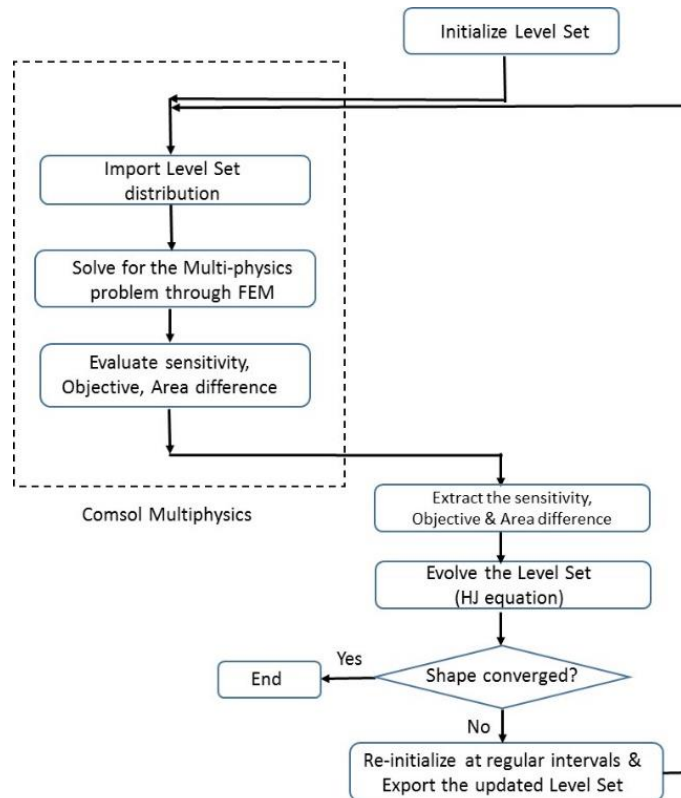


Figure 6- 2 Level-set topology optimisation procedure

In order to import the LS in Comsol from Matlab, “Interpolation” function is used. Since the mesh remains the same and only the level-set function is evolving, no accuracy will be lost due to interpolation. By solving the physical problem in Comsol, the shape sensitivity is calculated and then it is retrieved in Matlab Livelink using the command ‘mpheval’.

The level-set distribution before and after re-initialisation at one instant of optimisation is shown in Figure 6-3. It could be noted that due to re-initialisation, the mean line of the LS boundary is slightly moved.

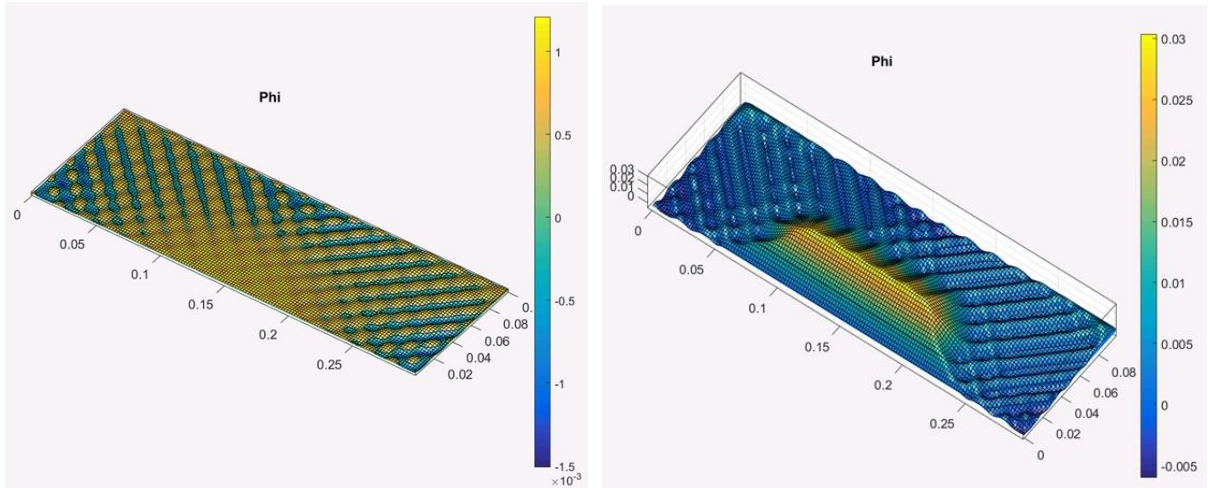


Figure 6- 3 Level-set function before and after re- initialisation

The evolved level-sets are again fed back to Comsol, and this procedure is repeated till convergence.

## 6.4 Heat sink design with re-initialisation of level-set

In this study Two & Three dimensional heat sinks are developed for two different solid-to-fluid thermal conductivity ratios for the objectives of minimum thermal compliance (TC) and viscous dissipation (VD). The level-set formulation is similar to the one described in previous test cases but now re-initialisation is additionally carried out and the HJ equations are solved in the finite difference setup rather than in the finite element setup.

### 6.4.1 Computational details

The design domain is rectangular in shape, with heat source at the bottom of the domain and liquid convection injected from the top of the computational domain as shown in Figure 6-4. The two sides of the computation domain act as outlets.

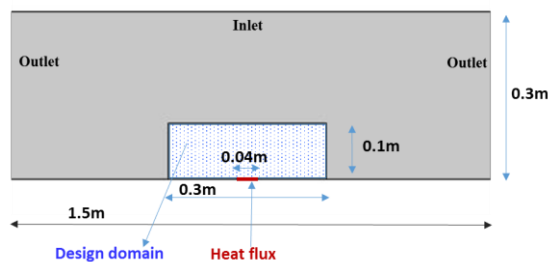


Figure 6- 4 2D Computational domain details

The design domain is discretised with 150x50 rectangular elements. The initial level-set used for the computation is a series of circles. A liquid flow of velocity 0.002m/s and of temperature 293K is applied at the Inlet. The inlet velocity corresponds to a Reynolds number of 600 and a heat flux of 700W/m<sup>2</sup> is specified as heat source in the bottom wall and zero pressure boundary condition is applied at the outlet. No-slip condition is approximately imposed by initialising the velocity equal to zero in solid regions i.e., where H is equal to 1.

$$H(\Psi)u=0 \quad (6.10)$$

At any point on the design domain, material properties are calculated through interpolation based on their Heaviside function value. In this study H=1 denotes (porous) solids, so the interpolation expressions are formulated as given in Table 6-1.

Property	Name	Expression
Thermal conductivity	$k_\gamma$	$(k_s - k_f) * H + k_f$
Specific heat capacity	$C_{p\gamma}$	$(C_{p_s} - C_{p_f}) * H + C_{p_f}$
Density	$\rho_\gamma$	$(\rho_s - \rho_f) * H + \rho_f$
Impermeability factor	$\alpha$	$(\alpha_{max} - \alpha_{min}) * H + \alpha_{min}$

Table 6- 1 Material interpolation formulas

The TO is carried out for two different material sets i.e., fluid to solid conductivity ratios. The material properties are given in Table 6-2.

Parameter	Value
$k_f / k_s$	0.04/40 & 0.04/0.4
$\rho_f / \rho_s$	1000/8920
$C_{p_f} / C_{p_s}$	4184/385
$\mu_f$	1.02e-3 Pa.s

Table 6- 2 Material properties for 2D heat sink design

The computational domain used for the 3D study is shown in Figure6-5. The computational domain considered is 1 quadrant of the total domain, making use of the symmetry boundary condition on the two sides. The design domain is a cube of side 0.1m length and it is discretised by 43x43x43 mesh elements. The heat flux of 10,000W/m<sup>2</sup> is applied at the bottom corner of area 1.353e-4 m<sup>2</sup> of the design domain

base and a fluid flow of velocity  $4e-5\text{m/s}$  is applied at the top surface of the computational domain. The volume fraction of solid material is constrained at 25%. The objective functions of this optimisation study are given below.

$$\text{Objective TC: } \min \int_{\Omega} k_{\gamma} * (\nabla T)^2 d\Omega \quad (6. 11)$$

$$\text{Objective VD: } \min \mu \int_{\Omega} \left(\frac{\partial u_i}{\partial x_j}\right)^2 d\Omega \quad (6. 12)$$

The optimisation is carried out by time marching the HJ equation (Eqn.5.11). The velocity of propagation of LSF is equal to the sum of shape sensitivity, Lagrange multiplier and volume penalty factor (Eqn 6-13). The shape sensitivity of the above objectives are equal to the negative of their objective function values. This is an assumption and this will be true at Stokes flow Reynolds numbers, but in this study the Re (600) is slightly higher than the Stokes flow Re, hence the sensitivities could be slightly erroneous.

$$Vn = F'(\mathcal{Q}) + \lambda + \Lambda \left( \int_{\Omega} H(\psi) d\Omega - V * V_{\Omega} \right) \quad (6. 13)$$

The Lagrangian multiplier and Area penalty factor are updated as follows.

$$\lambda_k = \lambda_{k-1} - \Lambda_{k-1} (\text{Voume Difference}) \quad (6. 14)$$

$$\Lambda_k = \frac{1}{\beta} \Lambda_{k-1} \quad (6. 15)$$

The value of  $\beta$  is 0.9, and the same value is used for all simulations irrespective of the objective of the study but the value of Lagrangian multiplier  $\lambda$ , and the area penalty factor  $\Lambda$ , are chosen differently for different objectives. The reason for choosing different value is the difference in magnitude of the objective values. Suitable value of these factors were chosen by a trial and error method.

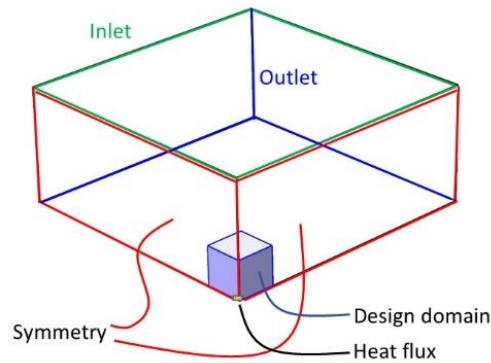


Figure 6- 5 Three dimensional computational domain

For solving the physics, linear elements are used for both velocity and pressure along with stream wise diffusion stabilisation for finite element solution. In the two dimensional case, the governing equations are solved in a coupled way and for three dimensional case, the equations are solved in segregated way. Simulation meeting the area constraint and the objective not varying significantly for a range of iterations is considered as a converged solution.

#### 6.4.2 2D Heat sink results and discussion

Considering only the TC as objective, the TO is carried out for 2 fluid to solid conductivity ratios  $k_f/k_s=0.001$  and  $0.1$ . Since the flow Reynolds numbers are low ( $Re=600$ ), it is expected that at least for the latter case, the convective heat transfer will play a comparable role to conduction. Results obtained for TC minimisation, VD minimisation and combined TC & VD minimisation are given in this section. It is again noted that, though the  $Re$  is slightly higher than Stokes flow  $Re$ , the sensitivities of Stokes flow are used for the optimisation.

##### **Heat sink of higher solid conductivity case ( $k_f/k_s=0.001$ ):**

The optimised shape for higher solid thermal conductivity case, resemble like a tree shape and it is shown in Figure 6-6. The temperature is uniformly distributed throughout the design domain except near the peripheries. The convergence of Lagrange Multiplier, Area difference and Thermal compliance are shown in Figure 6-7.

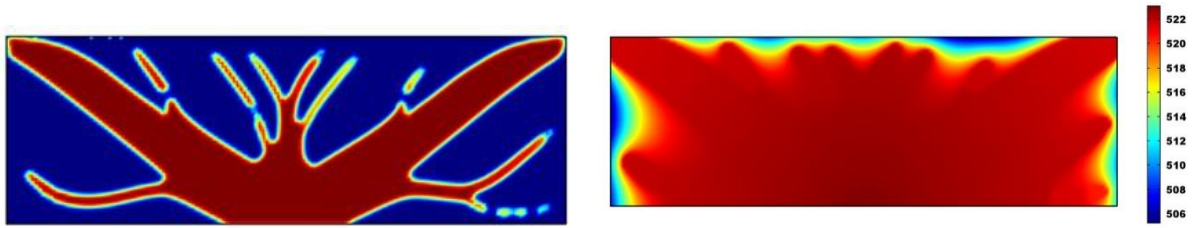


Figure 6- 6 Optimised shape for higher solid conductivity case and Temperature (K) distribution

**Heat sink of lower solid conductivity case ( $k_f/k_s = 0.1$ ):**

The optimised shape and the temperature distribution within the design domain are shown in Figure 6-8. Unlike the high solid conductivity case, this doesn't have many branches but the primary branch connects the heat flux with the corners of the design domain. The objective and maximum temperature observed in the design domain are given in Table 6-3.

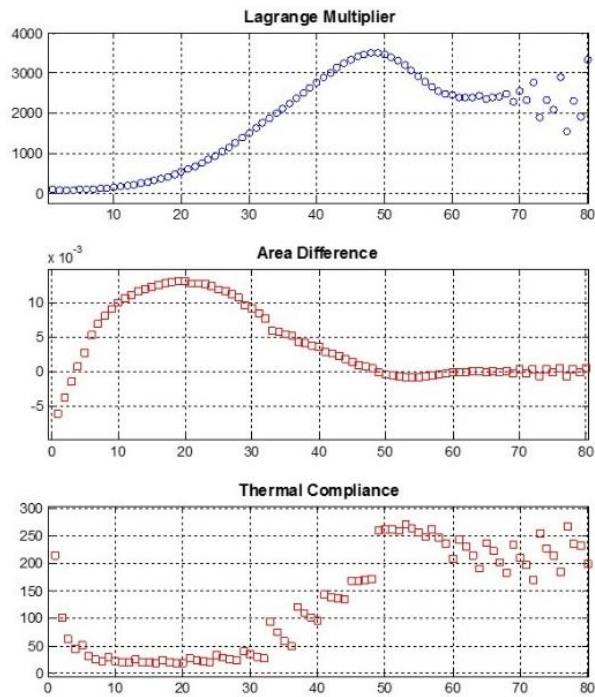


Figure 6- 7 Convergence history of 2D heat sink design using re-initialised LSM

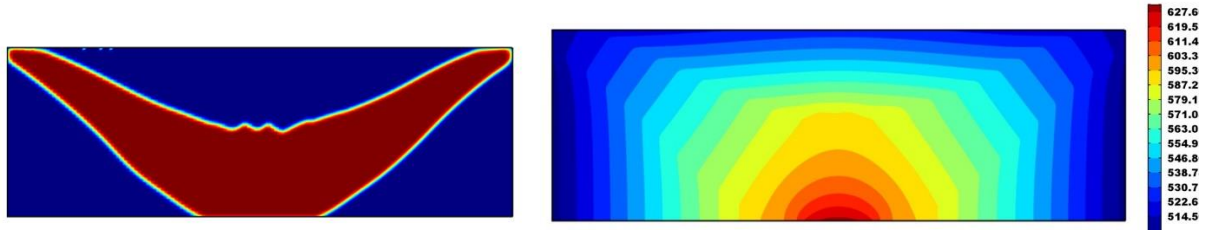


Figure 6- 8 Optimised shape for lower solid conductivity case ( $k_i/k_s=0.1$ ) and Temperature (K) distribution

$k_i/k_s$	Thermal Compliance(WK/m)	Maximum Temperature (K)	Temperature rise (Max. Temp. - Ambient Temp.) (K)
0.001	202.507	523.10	229.95
0.1	3154.40	631.60	338.45

Table 6- 3 Results of minimum thermal compliance objective optimisations

### Combined TC and VD objective:

For this case, the objective for the topology optimisation problem is defined as,

$$\text{Objective} = F1 * TC + F2 * VD \quad (6. 16)$$

Where F1 and F2 are weighting factors and when F1 is equal to zero, the optimisation becomes pure VD minimisation problem and when F2 is zero it becomes pure TC minimisation problem.

Before optimising the heat sink for combined thermal compliance and viscous dissipation, an optimisation is carried out for pure VD minimisation case. The optimised shape and the velocity field in the design domain are shown in Figure 6-9.

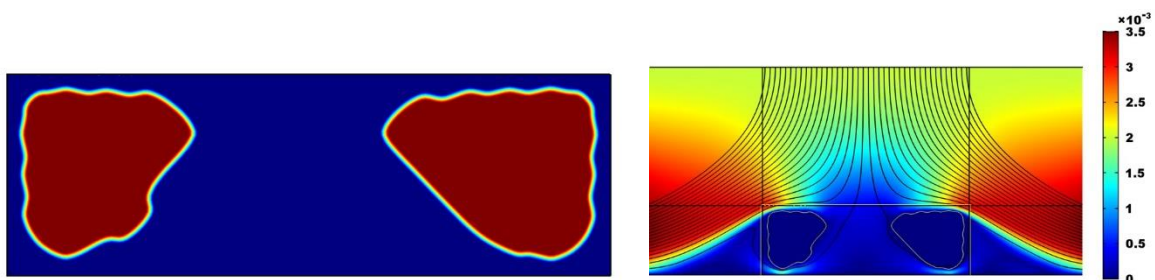


Figure 6- 9 Optimised shape for minimum viscous dissipation and Velocity (m/s) contour

The VD magnitude is many orders lower than TC, as the fluid viscosity (1.02e-3Pa.s) and Re are low. Hence for combined objectives run, F1 is taken as 1e-9 and F2 as 1, so that both the objectives will influence the optimisation. The optimised shape obtained is shown in Figure 6-10. In order to allow the smooth flow passage, branched structure has changed into a rectangular block on top of heat source and two islets of (porous) solid region acting like a guide vane for the incoming flow. The optimised shape along with the velocity and Temperature contour are given Figure 6-10.

(F1,F2)	Thermal Compliance (WK/m)	Viscous Dissipation (N/s)
(0, 1)	-	7.9642e-8
(1e-9,1)	2357.12	8.8307e-8

Table 6- 4 Combined TC and VD optimisation results

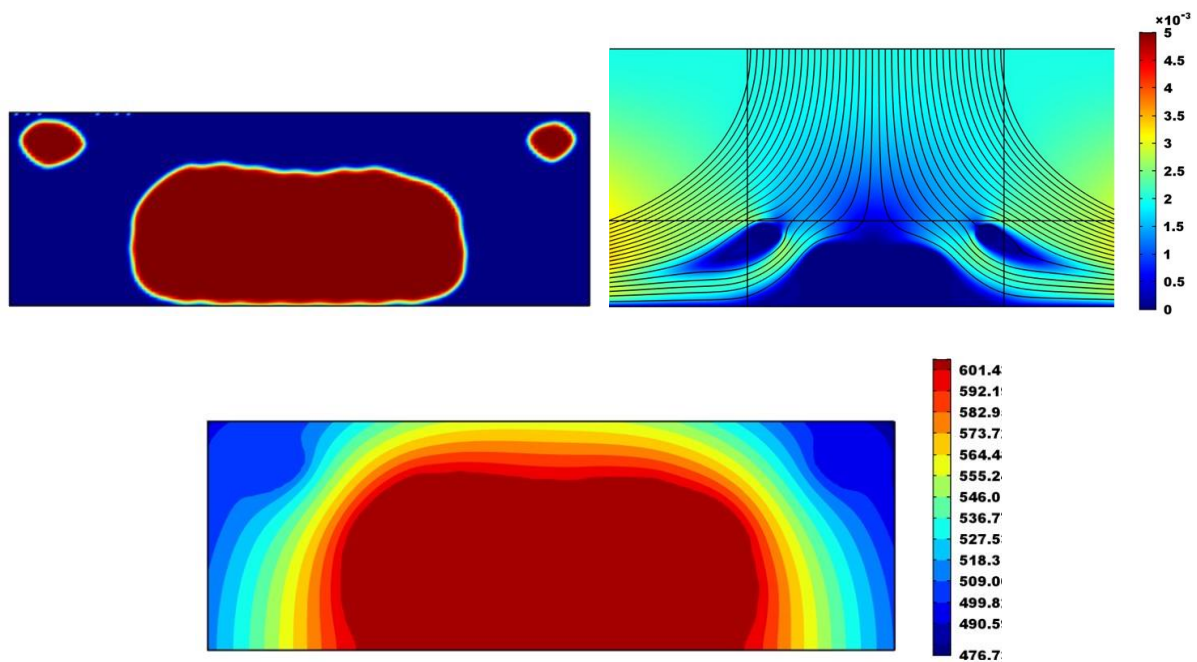


Figure 6- 10 Results of combined TC and VD optimisation: Shape, velocity (m/s) and temperature (K) contours

### 6.4.3 3D Heat sink results and discussion

A three dimensional heat sink is optimised for the TC objective for the conductivity ratio of  $k_f/k_s=0.001$  subjected to laminar forced convection of  $Re=8$ . The temperature of the cooling fluid (ambient temperature) is 293.15K. The computational domain is

exactly the same as the one used in Chapter 5.1. Note in this case, a heat flux of  $20\text{kW/m}^2$  and a solid thermal conductivity of  $400\text{W/(mK)}$  are used. The optimised heat sink shape, velocity, temperature distribution and convergence history are given in Figure 6-11 and 6-12 respectively. This study required about 80 optimisation iterations to converge with a total run time of 140hours on a 10 Xeon core workstation.

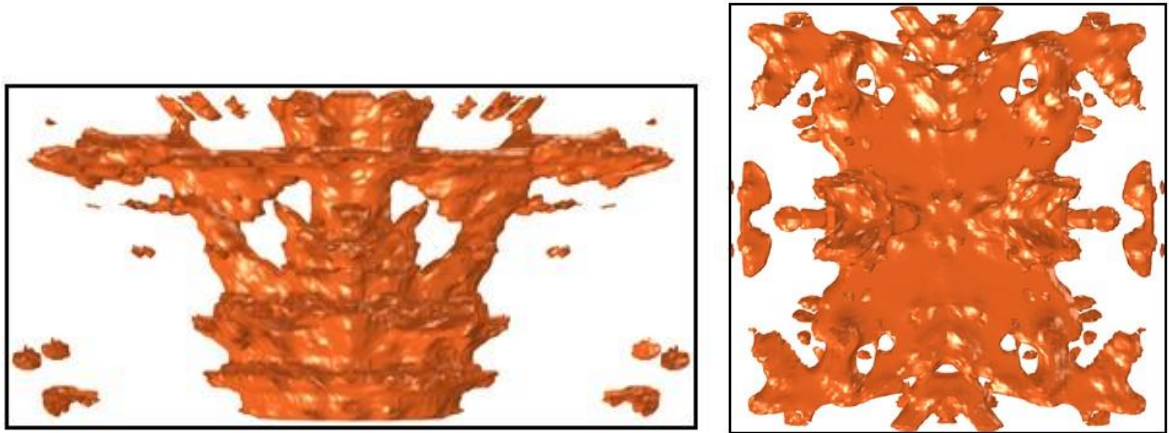


Figure 6- 11 Front and top view of 3D optimised heat sink

The optimised heat sink has two distinct parts, namely the bulk mass of (porous) solid material on top of heat flux boundary and the second part is a flat disk like part near the top of the design domain facing the oncoming fluid injection. The shape is well captured in the complete view of the heat sink.

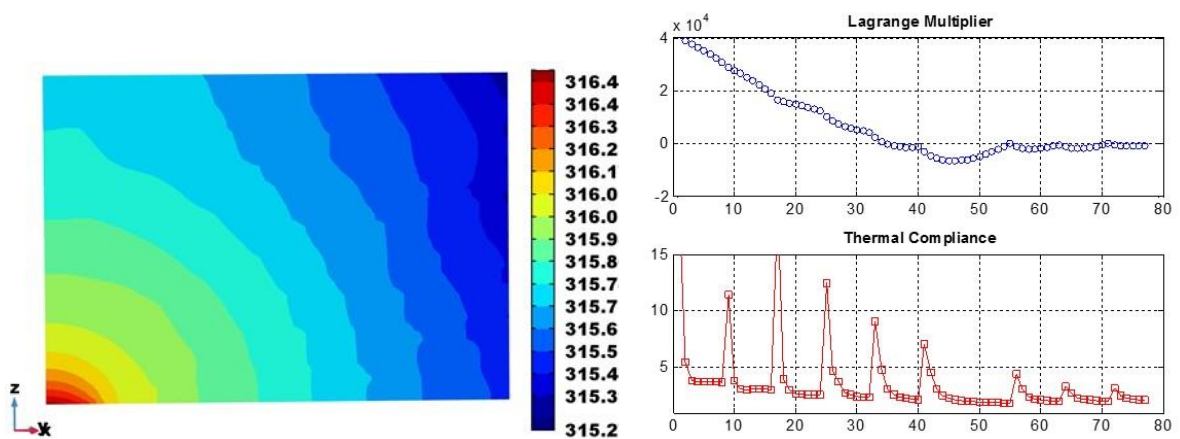


Figure 6- 12 Temperature (K) distribution in the diagonal plane and convergence history

## Discussion

The heat sink shapes obtained for the higher solid conductivity case agrees with the tree like shape reported in the literature. Because of the reduced thermal conductivity, branches are missing in the low solid conductivity case, which is understandable. Similarly for the combined TC and VD minimisation case, the optimiser tried to avoid sharp changes in temperature and velocity throughout the domain.

The 3D heat sink has an inverted wine glass shape. The central part with short branches promotes the conductive heat transfer while the top disk like part promotes the convective heat transfer.

### 6.4.4 Summary

The level-set based topology optimisation is applied to the design of 2D and 3D convectively cooled heat sinks for different material sets. In this formulation, the evolution and re-initialization of level-set are carried out in Matlab while physics is solved in Comsol. This formulation ensures crisp boundary capture and no-slip condition also approximately imposed on the (porous) solid boundaries. The heat sink shape obtained for 2D and 3D higher solid conductivity case agree with the tree like/dendritic shape.

## 6.5 Adjoint based shape sensitivity evaluation

The sensitivity of the objective function with respect to the design variable is the key factor which drives the evolution of shapes. Though sensitivity can be evaluated through Finite difference method, it is very costly as it requires a number of simulations equal to mesh size plus one. The adjoint method is a cheap and easy method, wherein the adjoint equation system has to be solved in addition to the state equations to evaluate the shape sensitivity. The shape sensitivity will be a function of state variables and adjoint variables.

For some simple state equations, state variables are equal to adjoint variables. If the state equation is Laplacian type equation then it will be self-adjoint in nature. Stokes flow problem governed by Stokes equation is an example of this, and here, for the

objective of viscous dissipation, the sensitivity is also equal to negative of viscous dissipation.

If the objectives are volume integrated objectives then the objective related terms will be present in the adjoint equations. On the other hand, if the objectives are surface integrated objectives then its derivative terms will be present in the adjoint boundary conditions. The adjoint equations for the NS equations and combined NS & energy equations are given in this section.

### **Adjoint equations for Navier-Stokes flow:**

The adjoint Navier Stokes equation and its boundary conditions depend on the objective function. For the viscous dissipation objective the adjoint NS and its boundary conditions based on frozen turbulence assumption are given below [102].

$$\text{Objective function, } J(\Omega) = \mu \int_{\Omega} \left( \frac{\partial u_i}{\partial x_j} \right)^2 d\Omega \quad (6.17)$$

Taking ' $u$ ' as the state velocity vector and ' $p$ ' as the state pressure, the adjoint equations are,

$$-(u \cdot \nabla)w + w \cdot (\nabla u) = -\nabla q + \nu \Delta w - 2\nu \Delta u \quad (6.18)$$

$$-\nabla \cdot w = 0 \quad (6.19)$$

$$\text{Boundary conditions at Inlet: } w = 0 \text{ on } \Gamma_D \text{ and } \Gamma_{\text{wall}} \quad (6.20)$$

$$\text{Boundary conditions at Outlet: } (\nu \nabla w + qI)n = -(u \cdot n)w + 2\nu \nabla u \cdot n \text{ on } \Gamma_N \quad (6.21)$$

$$\text{Domain boundary is, } \partial\Omega = \Gamma_D \cup \Gamma_{\text{wall}} \cup \Gamma_N$$

Where, ' $w$ ' & ' $q$ ' are adjoint variables for the velocity vector and pressure. Shape derivative for this problem is,

$$J'(\Omega) = \mu \left[ \left( \frac{\partial u_i}{\partial n} \right)^2 - \left( \frac{\partial u_i}{\partial n} \right) \left( \frac{\partial w_i}{\partial n} \right) \right] \quad (6.22)$$

### **Adjoint equations for the combined NS & energy Equation:**

Generally, adjoint equations are derived from the augmented Lagrangian of the optimisation problem. Kontoleon [58] formulated the adjoint system for turbulent NS equation with energy equation. Hinterberger [103] derived the adjoint equations

for laminar fluid flow with scalar transport, where the scalar variable can be temperature or species concentration. Following these works, the adjoint system is deduced for laminar NS equation with energy equation in this study. For instance, consider the optimisation problem,

$$\text{Minimise } F = -F_1 * \text{Temperature\_Drop} + F_2 * \text{Total Pressure\_Drop} \quad (6. 23)$$

$$\text{Temperature Drop} = \int_I T u \cdot n dA + \int_O T u \cdot n dA \quad (6. 24)$$

$$\text{Total Pressure Drop} = \int_I (p + 0.5\rho u^2) u \cdot n dA + \int_O (p + 0.5\rho u^2) u \cdot n dA \quad (6. 25)$$

Subjected to,

$$\rho(u \cdot \nabla u) = -\nabla p + \nabla \cdot \{\mu \{ \nabla u + (\nabla u)^{tr} \}\} - \alpha u \quad (6. 26)$$

$$\rho(\nabla \cdot u) = 0 \quad (6. 27)$$

$$\rho C_p(u \cdot \nabla T) = \nabla \cdot (k \nabla T) + Q_o T \quad (6. 28)$$

$$H(\Psi)u=0 \quad (6. 29)$$

$$\text{Volume Constraint, } \int_{\Omega} H(\Psi) d\Omega \leq V * V_{\Omega} \quad (6. 30)$$

where  $V_{\Omega}$  is the domain volume, ' $V$ ' is the volume fraction and  $Q_o$  is the volumetric heat source/sink per unit temperature ( $W/(m^3.K)$ ). ' $F_1$ ' and ' $F_2$ ' are weighting factors for each of the objectives. The augmented Lagrangian of this problem is,

$$L_{aug} = F + \int_{\Omega} q R_p d\Omega + \int_{\Omega} w R_u d\Omega + \int_{\Omega} T \hat{a} R_T d\Omega \quad (6. 31)$$

where  $q$ ,  $w$ , and  $T\hat{a}$  are the Lagrangian multipliers or adjoint variables to satisfy the state continuity, momentum and energy equations and ' $F$ ' is the objective function.  $R_p$ ,  $R_v$  and  $R_T$  are continuity, momentum and energy equations. The variation of Lagrangian with respect to porosity variable is,

$$\frac{\delta L_{aug}}{\delta \alpha} = \frac{\delta F}{\delta \alpha} + \int_{\Omega} q \frac{\partial R_p}{\partial \alpha} d\Omega + \int_{\Omega} w \frac{\partial R_u}{\partial \alpha} d\Omega + \int_{\Omega} T \hat{a} \frac{\partial R_T}{\partial \alpha} d\Omega \quad (6. 32)$$

The above equation has to be expanded by substituting state equations and using Gauss divergence theorem. From this, adjoint equations are derived by eliminating all field integrals which depends on  $\frac{\partial p}{\partial \alpha}$ ,  $\frac{\partial u}{\partial \alpha}$  and  $\frac{\partial T}{\partial \alpha}$ .

Since the objectives are surface integrated objectives in this study, the influence of objective is only felt in the boundary conditions of adjoint equations which are given in Eqns (6.33 to 6.42).

Considering 'w' as the adjoint velocity vector, 'q' as the adjoint pressure and 'Ta' as the adjoint temperature the adjoint equations are given as,

$$\rho((\bar{v}u)w - u \cdot \nabla w) = -\nabla q + \nabla \cdot \{\mu\{\bar{v}w + (\bar{v}w)^{tr}\}\} - \alpha w + \rho C_p T \nabla T \hat{a} \quad (6.33)$$

$$\rho(\nabla \cdot w) = 0 \quad (6.34)$$

$$\rho C_p (u \cdot \nabla T \hat{a}) = -\nabla \cdot (k \nabla T \hat{a}) + Q_o T \hat{a} \quad (6.35)$$

Boundary conditions:

$$\text{Wall: } w=0 \text{ and } T \hat{a} = 0 \quad (6.36)$$

$$\text{Outlet: } \frac{(u \bar{v} w - q) n}{\rho} = -(u \cdot n) w - (u \cdot w) n - C_p (T \hat{a}) n - \frac{\partial F}{\partial u} \quad (6.37)$$

$$(k \nabla T \hat{a}) n = -\rho C_p (u \cdot n) T \hat{a} - \frac{\partial F}{\partial T} \quad (6.38)$$

$$\text{Inlet: } w \cdot n = -\frac{\partial F}{\partial p}, T \hat{a} = 0 \text{ and } w_t = 0 \quad (6.39)$$

$$\frac{\partial F}{\partial p} = F_2 u \cdot n \quad (6.40)$$

$$\frac{\partial F}{\partial u} = F_2 ((0.5 * \rho u^2 + p) \cdot n + u(u \cdot n)) - F_1 T n \quad (6.41)$$

$$\frac{\partial F}{\partial T} = -F_1 u \cdot n \quad (6.42)$$

Where 'n' is the normal vector,  $w_t$  is the tangential component of adjoint velocity vector.

From the solution of state equations Eqns. (6.26 to 6.28) and adjoint equations Eqns. (6.33 to 6.35), the topology sensitivity can be calculated using the below formula [58],

$$F'(\Omega) = -\alpha_{max} (u \cdot w) - Q_o(T \cdot T \hat{a}) \quad (6.43)$$

Othmer [5] has shown that the shape sensitivity for the NS problem is equal to the dot product between tangential flow velocity and tangential adjoint velocity which is quite similar to the topology sensitivity expression given in Eqn 3.45, without the temperature terms.

### 6.6 Topology optimisation of ‘Bend channel’ using adjoint sensitivity

In order to demonstrate the applicability of adjoint based shape sensitivity, topology optimisation of 90° bend channel design is considered. Geometry is a square domain with inlet on left side wall and outlet at bottom wall (Figure 6-13). Minimum viscous dissipation is considered as the objective and this is a volume integrated objective.

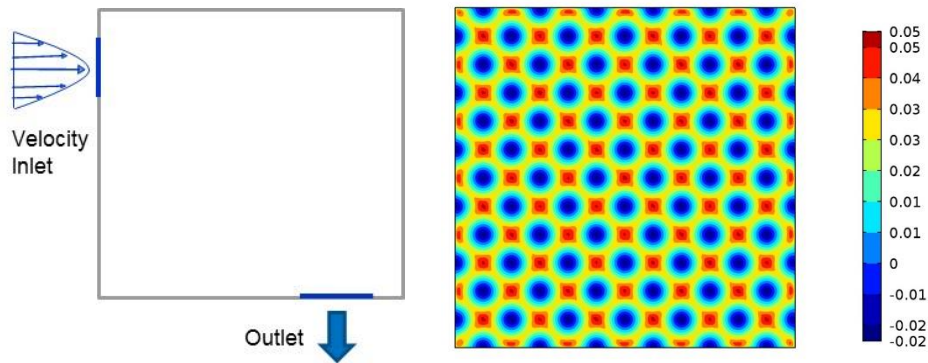


Figure 6- 13 Design domain geometry for 90° bend channel and initial LS distribution

#### 6.6.1 Computational details

The design domain is discretized by 100x100 cells. The re-initialized Level-set framework described in the previous section is used for this optimisation. The initial level-set distribution is given in Figure 6-13. The volume constraint is set as 21%. In the design domain, density and impermeability factor are interpolated based on the Heaviside function (H) value. Here,  $H=1$ , denotes fluid, so formulas in Table 6-1, are modified accordingly.

The adjoint equations for this objective are given in Eqn.(6.18) to (6.21). The State NS equation and adjoint NS equations are modelled using general form PDE model in Comsol5.2. One PDE model to solve for velocity and another one for pressure, so totally 4 PDE models are used including 2 for state NS and 2 for adjoint NS equations. First state equations alone are solved, then adjoint NS are solved using the state NS

solution, as the adjoint NS equation involves state variable terms. This is done because there is only one way coupling present between NS and adjoint NS equations. The shape sensitivity is calculated from the state and adjoint variables using the below equation.

$$F'(\Omega) = \mu \left( \left( \frac{\partial u_i}{\partial x_j} \right)^2 - \left( \frac{\partial u_i}{\partial x_j} \right) \left( \frac{\partial w_i}{\partial x_j} \right) \right) \quad (6.44)$$

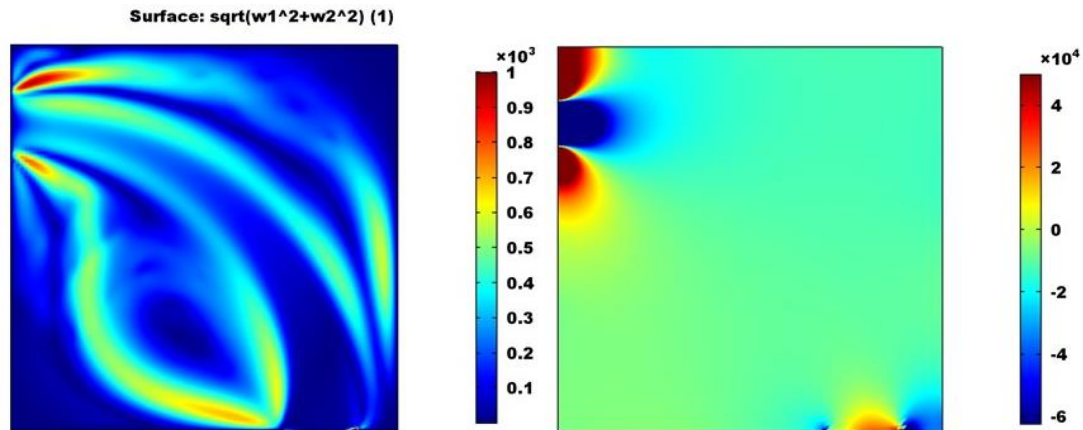


Figure 6- 14 Adjoint velocity and adjoint pressure at an instant during optimisation

The contour of adjoint variables at one instant of optimisation are given in Figure 6-14. The adjoint variables doesn't have any physical meaning but the contours are produced here to get a feel for these variables.

The level-set function is advected by solving the HJ equation as mentioned earlier and the level-sets are re-initialised at regular intervals. The optimisation is carried out for different Reynolds numbers from 5.33 to 622. Beyond this Re, laminar flow becomes unstable and flow doesn't converge in the present problem setup.

### 6.6.2 Results

The optimisation is carried out for different Reynolds numbers namely 5.33, 266.7 and 622.2. The obtained shapes are shown in Figure 6-15. As reported in the literature, at lower Reynolds numbers for minimum viscous dissipation objective, the optimum flow path, a straight line connecting the inlet and outlet, is obtained. For the same objective, at higher Re, a parabolic arc like flow path is obtained and this is also in agreement with the literature.

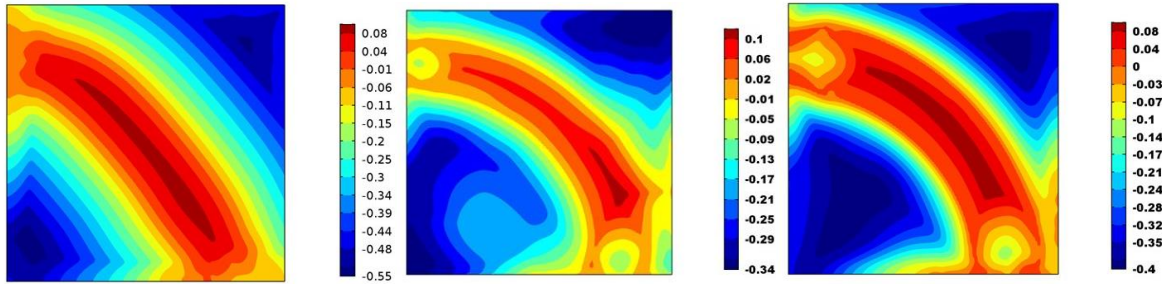


Figure 6- 15 Optimised level-set function distribution at Re5.33, Re266.7 and Re622.2

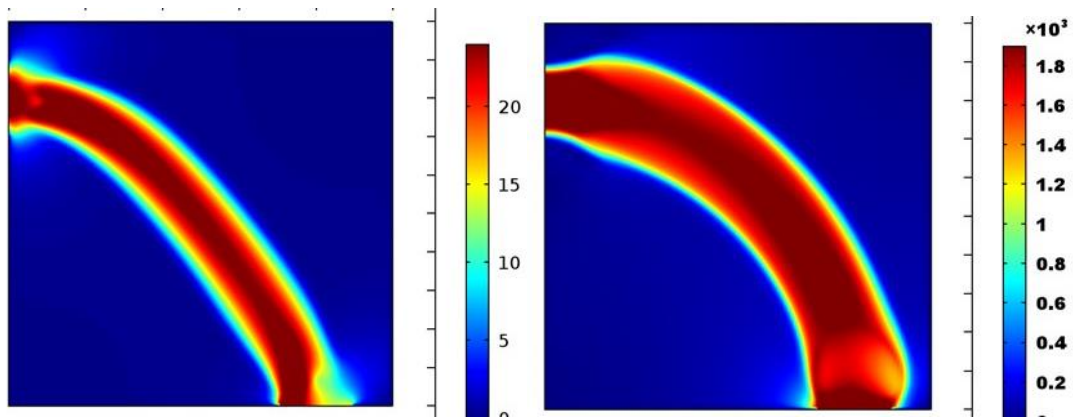


Figure 6- 16 Velocity contours on optimised shapes for Re5.33 and Re 622.2

The pressure contours on the optimised shape at these 3 Reynolds numbers are given in Figure 6-17. Since the solids formed during optimisation are porous solid, pressure diffusion occurs and this is clearly evident in the contours. Another interesting thing to note is, the pressure levels are higher than the pressure that would be required to maintain a flow of the given Reynolds numbers. This is because small islets of (porous) solid regions are formed near the inlet and outlet and to maintain the required inlet velocity, inlet pressure is increased. High inlet pressure makes the flow pass through the porous solid at the required velocity condition. This increases the pressure drop required to maintain a flow of given velocity. Combined minimum pressure drop and minimum viscous drop objective may prevent the formation of these (porous) solid regions at the inlet. Alternatively imposing an additional constraint on inlet pressure ( $P_{in} < 100\text{Pa}$ ) in the optimisation problem might avoid this problem.

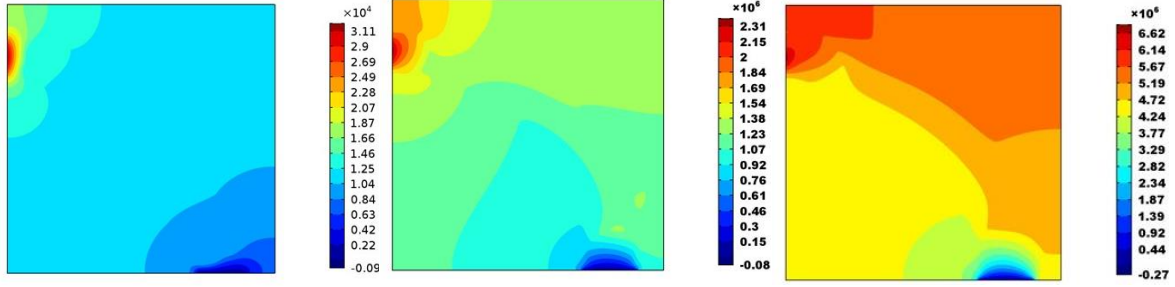


Figure 6- 17 Pressure (Pa) distribution over optimised shape at Re5.33, Re266.7 and Re622.2

## 6.7 Topology derivative based optimisation

One of the drawbacks of the LS TO is, the final optimum shape obtained is sensitive to the initial level-set function used. This is because new holes cannot be generated during the convection of level-set by the solution of the HJ equation. This drawback, restricts the optimiser, as it cannot fully change the design topology. By adding a topology derivative term in the HJ equation as a reaction term (Eqn 3.44), new holes can be generated in the design domain during the LS evolution.

The topology derivative at a point is defined as the change in objective value occurred when an infinitesimal hole is inserted at that point. For fluid flows, hole insertion is equivalent to inserting a solid obstacle in the fluid domain. Updating the level-set function considering both the shape sensitivity and topology derivative will give more chance to reach to global optimum but still that cannot be guaranteed. In this section, the topology optimisation of fluid flow problem considering the topology derivative has been carried out and the results are discussed.

The topology derivative of a given problem can be evaluated by topological asymptote method and Amstutz [82] derived the topological derivative for the NS flows. That is given as,

$$d_T J(\Omega) = 4\pi\rho\mu u \cdot w + 4\pi\rho\mu u \cdot u + \pi[\lambda - \Lambda(\text{Vol. Difference})] \quad (6.45)$$

Where ‘ $u$ ’ is state velocity vector and ‘ $w$ ’ is adjoint velocity vector. The optimisation problem is solved by updating the LSF using the Eqn 6.46. Note, this equation is obtained by omitting the shape sensitivity term from the complete HJ equation (3.49).

$$\frac{\partial \Psi}{\partial t} = -w * d_T J(\Omega) \quad (6.46)$$

The same, first order upwind difference method, which is used to solve the HJ equation is used to solve the above equation. The geometry and computational setup are same as the one given in section 6.6. The flow velocity corresponds to Re 31. To successfully run the simulation, the weighting factor ‘ $w$ ’ has to be suitably selected. This factor influences the amount of (porous) solid regions created while time marching the Eqn. (6.46). After few trial and errors, suitable ‘ $w$ ’ value is found to be ‘1200’.

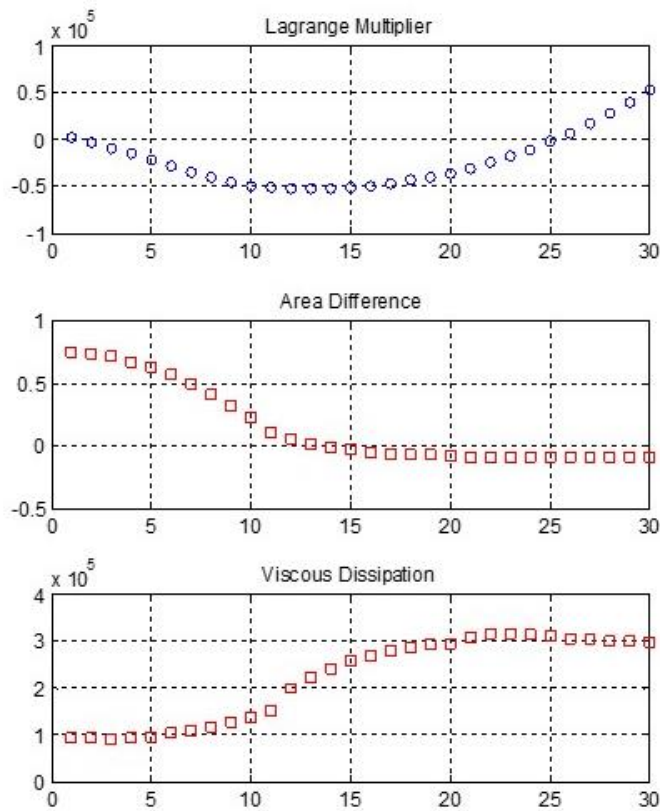


Figure 6- 18 Convergence history

The optimisation run is started with full fluid initialisation in the design domain. The the convergence plot is shown in Figure 6-18 and the obtained optimal shape is shown in Figure 6-19.

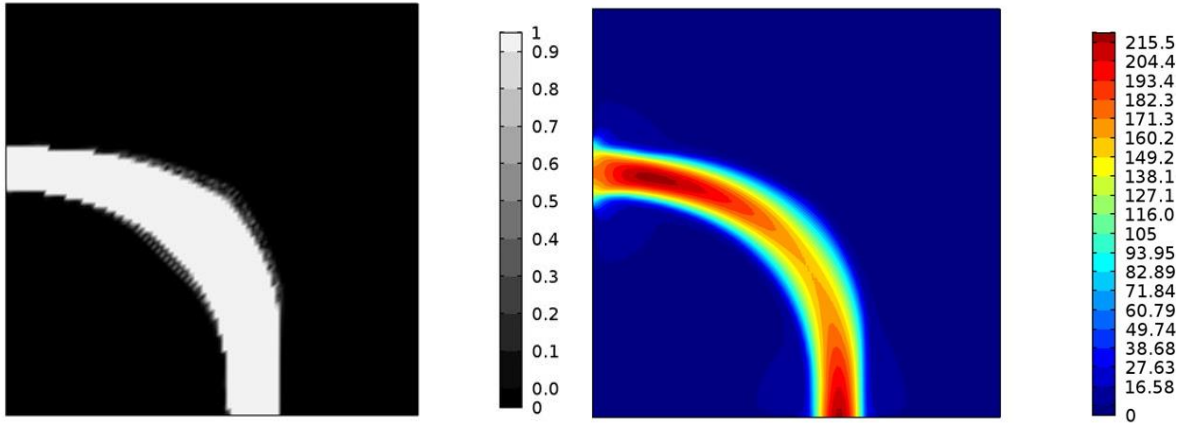


Figure 6- 19 Optimised pipe bend and the velocity contour

## 6.8 Topology optimisation of irregular design domain

So far most of the optimisation problems were carried out on a simple square or rectangular domains, which are easy for meshing and for advecting the level-set functions with ghost elements. In this section, an irregular geometry is considered for the topology optimisation. The main challenges in this problem are meshing the geometry, generating the ghost elements surrounding the geometry and advecting the level-set function within the design domain.

### Problem details:

The problem considered here, is the design of a straight duct from an initially given complex geometry. The design domain considered is shown in Figure 6-20, wherein the flow enters and leaves the domain with the same velocity. Minimum viscous dissipation is considered as the objective for this optimisation. As the focus of this work is to generate mesh for this irregular domain and for the LSF advection, this optimisation problem is simplified by considering the Stokes flow. The Stokes flow equation is self-adjoint in nature for which shape sensitivity is given as,

$$F'(\Omega) = 0.5 * \mu * \left( \left( \left( \frac{\partial u}{\partial x} \right)^2 + \left( \frac{\partial u}{\partial y} \right)^2 + \left( \frac{\partial v}{\partial x} \right)^2 + \left( \frac{\partial v}{\partial y} \right)^2 \right) \right) \quad (6.47)$$

The flow Reynolds number considered in this study is 0.004.

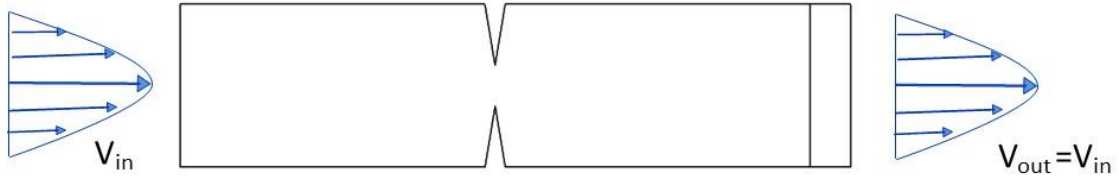


Figure 6- 20 Irregular geometry for topology optimisation

### Implementation and results:

The computational domain is meshed in multi-block structured way. The throat region of the channel is split into suitable quadrilateral blocks and the mesh is generated in Matlab (Figure 6-21). Over the mesh, additional single layer mesh is generated on all edges to create the ghost elements. These are used for advecting the LSF.

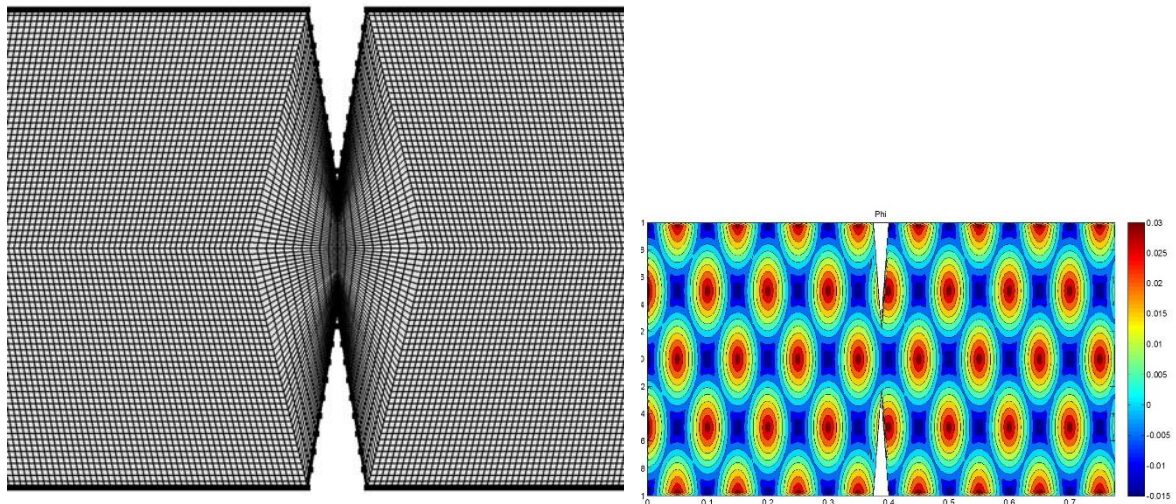


Figure 6- 21 Multi-block mesh and initial level-set distribution in the design domain

The optimised flow path and the pressure contour are shown in Figure 6-22. The pressure drop between inlet and exit is found to be 1.505Pa, which is a reasonable value for Stokes flow with  $Re=0.004$ . This study validates that the developed LS TO framework is capable to do optimisation for irregular geometries also.

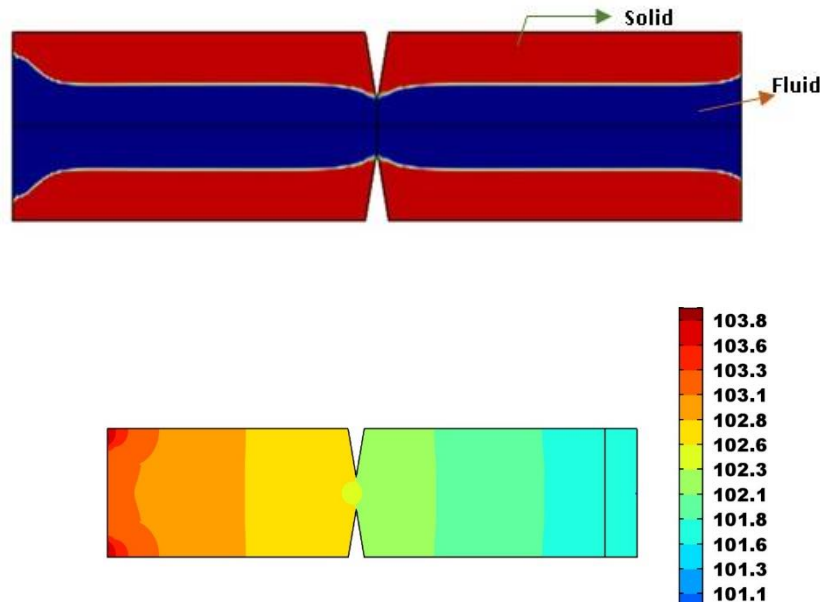


Figure 6- 22 Optimised flow path shape and its pressure (Pa) contour

## 6.9 Summary

The enhanced level-set framework produces better results than the level-set framework discussed in chapter 5. The re-initialisation enables crisp capture of the interface boundary, reduces grey cell regions and the LS advection in Matlab has reduced the computational time significantly.

The adjoint sensitivity calculation for the coupled NS and energy equation is implemented in the framework and it is validated with a 90° pipe bend optimisation. The topology derivative based optimisation is also demonstrated. Topology optimisation of irregular geometry also made possible through multi-block meshing of the given geometry in Matlab.

In the subsequent sections, the enhanced LS TO model is used to optimise some of the novel fluid flow and heat transfer coupled applications.

## 7 Topology Optimisation of Heat Recovery Channel

### 7.1 Introduction

Heat recovery channels are used in engine exhausts of automobiles and power plants to recover the residual heat leaving the system. This heat could be later used to generate electricity using thermo-electric generators (TEG). Thermo-electric generators are solid state devices, made up of thermoelectric materials which convert temperature difference into electricity. The challenge in the heat recovery channel design is that the fluid should exchange maximum heat with the solid and at the same time the pressure difference required to maintain the flow has to be minimum. Hence, the 'temperature drop' maximisation and 'total pressure drop' minimisation together are considered as the objective for this optimisation.

In heat exchangers, the amount of heat exchange depends on the solid-to-fluid thermal conductivity ratio ( $k_s/k_f$ ). Hence this thermal conductivity ratio can influence the optimum shape of the heat recovery channels significantly. Another important factor which can influence the heat recovery channel shape is the flow Reynolds number ( $Re$ ). So, in this study, the effect of thermal conductivity ratio and  $Re$  on the optimised heat recovery channel shape has been studied in 2D. Apart from this, for the  $k_s/k_f=1$  case, the effect of actual thermal conductivity value of the material on the optimised shape is also studied in detail (in 2D and 3D). Since the value of 'temperature drop' objective is much lower than the value of 'total pressure drop' objective, two different weightage factors for the 'temperature drop' objective are studied. Two and three dimensional studies are conducted using fictitious materials of different thermal conductivity values.

Unlike Yaji [63], who considered maximising the heat generation rate as an objective, in this study, maximising the temperature drop and minimising the total pressure drop between the inlet and outlet is considered as the objective. Further, he has used the RD equation based LSM, but in this case the HJ equation based LSM is used. The computational details of the 2D study are given in section 7.2 and corresponding

results are given in section 7.3. The computational details and results of the three dimensional study are given in section 7.4 and the study is summarised in section 7.5.

## 7.2 Two-dimensional optimisation

The combined temperature drop and total pressure drop is considered as the objective for this optimisation. The optimisation problem is stated below.

$$\text{Temperature Drop} = \int_I T u \cdot n dA + \int_O T u \cdot n dA \quad (7.1)$$

$$\text{Total Pressure Drop} = \int_I (p + 0.5\rho u^2) u \cdot n dA + \int_O (p + 0.5\rho u^2) u \cdot n dA \quad (7.2)$$

$$\text{Objective, } F = -F_1 * \text{Temperature Drop} + F_2 * \text{Total Pressure Drop} \quad (7.3)$$

$$\text{Volume Constraint, } \int_{\Omega} H(\Psi) d\Omega \leq V * V_{\Omega} \quad (7.4)$$

The governing equations for this coupled fluid flow and heat transfer problem are given in below equations.

$$\rho_{\gamma}(\nabla \cdot u) = 0 \quad (7.5)$$

$$\rho_{\gamma}(u \cdot \nabla u) = -\nabla p + \nabla \cdot \{\mu\{\nabla u + (\nabla u)^{tr}\}\} - \alpha u \quad (7.6)$$

$$H * \rho_{\gamma} C_{p\gamma}(u \cdot \nabla T) = \nabla \cdot (k_{\gamma} \nabla T) + Q_o T \quad (7.7)$$

The shape sensitivity is evaluated through continuous adjoint method. The adjoint equations, given in section 6.5 are reproduced here and the variables  $w$ ,  $q$  and  $T\hat{a}$  are adjoint variables for velocity, pressure and temperature respectively.

$$\rho_{\gamma}((\nabla u)w - u \cdot \nabla w) = -\nabla q + \nabla \cdot \{\mu\{\nabla w + (\nabla w)^{tr}\}\} - \alpha w + \rho_{\gamma} C_{p\gamma} T \nabla T \hat{a} \quad (7.8)$$

$$\rho_{\gamma}(\nabla \cdot w) = 0 \quad (7.9)$$

$$H * \rho_{\gamma} C_{p\gamma}(u \cdot \nabla T \hat{a}) = -\nabla \cdot (k_{\gamma} \nabla T \hat{a}) + Q_o T \hat{a} \quad (7.10)$$

$$Q_o = Q_{o1} * (1-H) \quad (7.11)$$

$$\alpha = \alpha_{\max} * (1-H) \quad (7.12)$$

The thermal properties, density, thermal conductivity, specific heat capacity in the above equations are expressed as given in Table 7-1. These relations ensures that, a given element takes either solid or fluid material properties depending on its Heaviside

function value. Since this is a heat recovery problem, a temperature dependent heat sink term ( $Q_o$  [ $W/(K.m^2)$ ]) is present in the energy equation. The temperature dependent heat sink ensures that the heat extraction rate at a given point is proportional to the fluid temperature at that location. Further, to ensure that the thermal convection is present only in the fluid region and not in the (porous) solid region, the convective term of the energy equation is multiplied with the Heaviside function (H) as given in Eqn. (7-10). Note that, in this study  $H=1$ , denotes a fluid and  $H=0$  denotes a (porous) solid and a similar modification is also done on the convection term of the adjoint energy equation.

Name	Expression
$k_\gamma$	$(k_s - k_f)^*(1-H) + k_f$
$Cp_\gamma$	$(Cp_s - Cp_f)^*(1-H) + Cp_f$
$\rho_\gamma$	$(\rho_s - \rho_f)^*(1-H) + \rho_f$

Table 7-1 Thermal properties interpolation for heat recovery channel design

The expression for the shape sensitivity is given in Eqn (7.13).

$$F'(\Omega) = -\alpha_{max} (u \cdot w) - Q_o (T \cdot T \hat{a}) \quad (7.13)$$

where  $\alpha$  is the material impermeability and  $Q_o$  is the heat generation/extraction rate in solids. The optimisation is carried out by time marching the HJ equation and the velocity of propagation of LSF is evaluated using the equation (7.15).

$$\text{HJ equation :} \quad \frac{\partial \psi}{\partial t} = V_n |\nabla \psi| \quad (7.14)$$

$$V_n = F'(\Omega) + \lambda + A \left( \int_{\Omega} H(\psi) d\Omega - V * V_{\Omega} \right) \quad (7.15)$$

The rest of the steps in the optimisation are very similar to the one described in section 6.4.

### Two-dimensional numerical model

The computational domain used for the study is shown in Figure 7.1. The domain is square in shape with the inlet width being  $1/3^{\text{rd}}$  of the domain width. At the inlet, a specified velocity and temperature are imposed and at the outlet, a zero pressure condition and zero heat flux condition are imposed. The inlet velocity has a parabolic velocity profile as in a fully developed laminar flow. The inlet temperature of the fluid is 360K. A temperature dependent heat source ( $Q_o$ ) is considered only in the solid

region and its heat flux value is  $-1500\text{W}/(\text{K}\cdot\text{m}^2)$ . To reduce the computational cost, only half of the design domain is computed using the symmetry boundary condition at the midline of the domain. The boundary conditions for the adjoint equation system, which are imposed on the design domain are shown in Figure 7.2. The derivative of the objective function with respect to state variables, which are used in the boundary conditions of adjoint equations are given in Eqn (6.40) to (6.42).

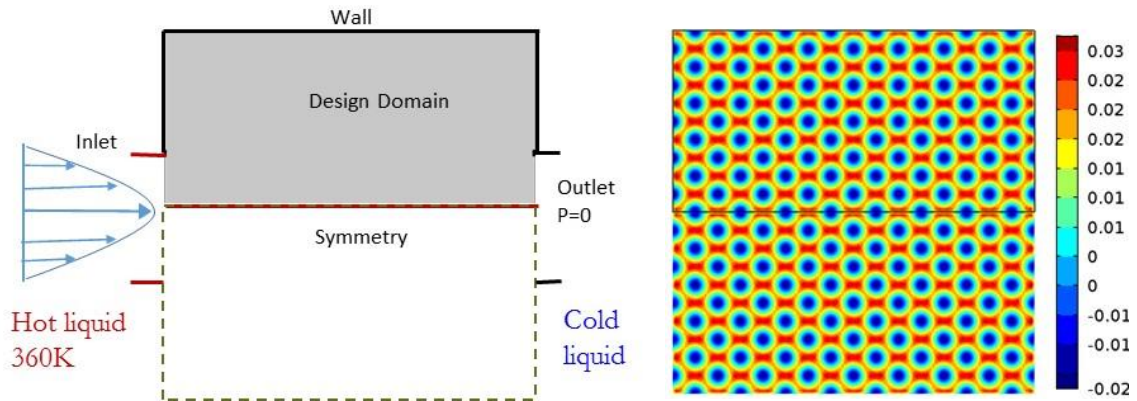


Figure 7- 1 Computational domain of 2D study and initial LS function

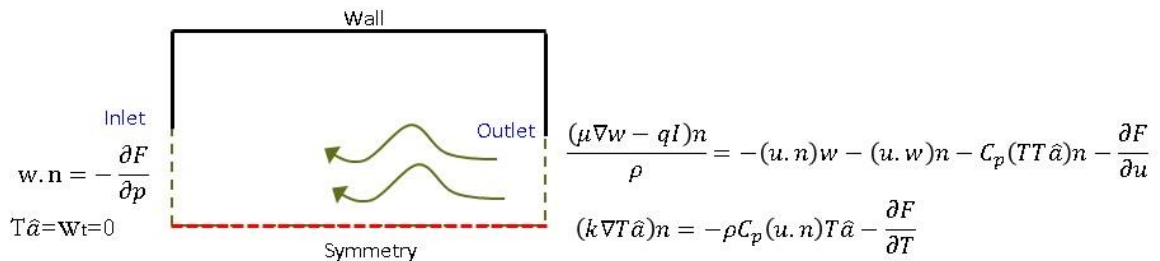


Figure 7- 2 Computational domain with boundary conditions for adjoint equations

The domain is discretised with square cells of size  $1/132$  units. For the adjoint equations, a flux or source boundary is applied at the outlet and the Dirichlet boundary condition is applied at the inlet as given in Figure 7-2. The state momentum equations are non-linear but they are not coupled with the energy equation whereas adjoint momentum equations are linear but they are coupled with their energy equation. A quadratic discretization for velocity and a linear discretization for pressure and all other variables are used for the computation. The schematic of quadratic and linearly discretised finite elements are shown in Figure 7-3. The state and adjoint equations are solved in Comsol using general form PDE modules.

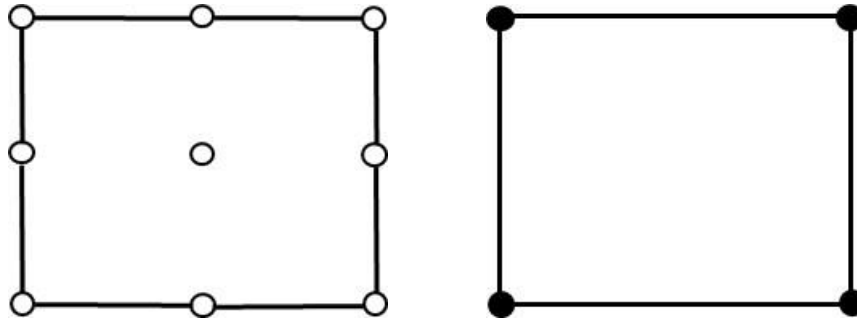


Figure 7- 3 Schematic of Quadrilateral and Linear elements for Finite element discretisation

The initial level-sets used for the computation is a series of circles as shown in Figure 7-1. A positive LS function represents a fluid and a negative LS function represents a (porous) solid. The level-set function is evolved on a mesh with ghost elements, these elements surround the 4 sides of the design domain. The HJ equations are solved by finite difference method and the re-initialization of level-set is applied for every 6 iterations. A fluid volume constraint of 45% of the design domain volume is imposed.

The optimisation is carried out for solid-to-fluid conductivity ratios ( $k_s/k_f$ ) of 10 and 1. The  $k_s/k_f = 1$  case denotes, both solid and fluid have same thermal properties. In this case the effect of changing the thermal conductivity of the materials ( $k_s=k_f$ ) on the optimised shape is studied for 3 different values, they are 4, 0.4 and 0.04 W/m/K. The two dimensional simulations are carried out at the Reynolds numbers (Re) of 70, 174, 326 and 521 (Reference length is 0.3m). Since the value of the ‘temperature drop’ objective is much lower than the ‘total pressure drop’ value, two different weightage factors ( $F_1=1$  & 100) for ‘temperature drop’ objective are studied. The thermal properties of the solid and fluid, which are used in this study are given in Table 7-2.

Name	Value
$\alpha_{max}$	1e5
Volume fraction	0.45
$k_s/k_f$	10 and 1
$\rho_s/\rho_f$	8.92 and 1
$C_{ps}/C_{pf}$	9.20 and 1
$\mu_f$	0.08 [Pa.s]

Table 7- 2 Properties of solid and fluid used in the 2D heat recovery channel design

A typical convergence history of the TO run is given in Figure 7-4. Generally in the augmented Lagrangian method, as the iterations proceed, the material volume oscillates and finally settles to the required material volume. At this point, the objective value might also become stationary and at this point, the optimisation is considered to be converged. But in general, a flat or invariant curve in material volume and objective function indicates the presence of a local optimum.

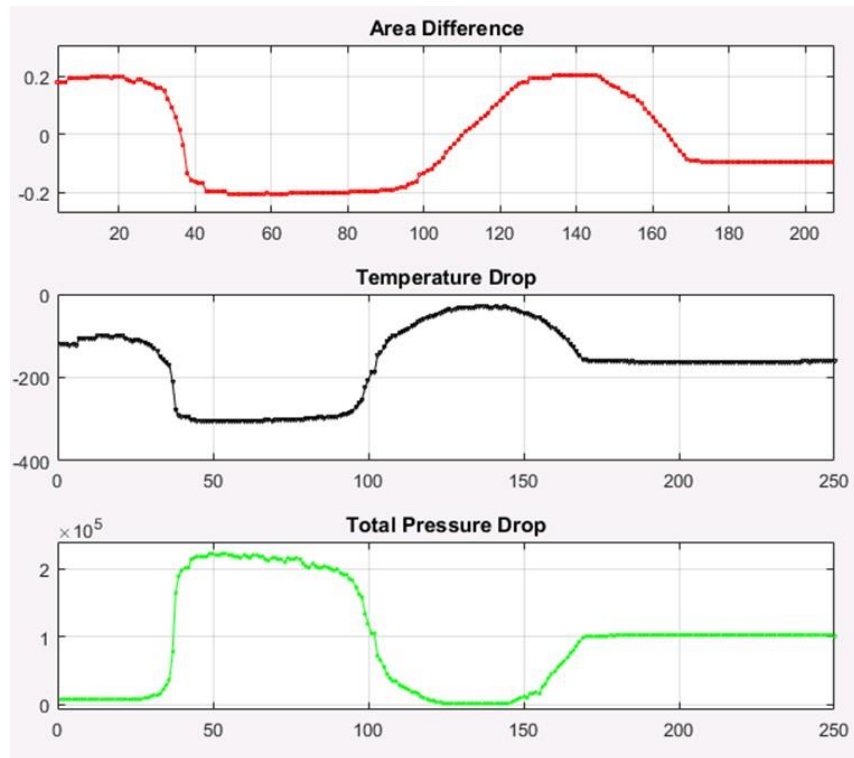


Figure 7- 4 Convergence history of a TO run

#### **Validation of the numerical framework:**

The LS TO numerical framework with adjoint NS and energy equation system is validated by performing a single objective optimisation of total pressure drop minimisation, for which the analytical solution is a straight line duct. The optimisation is carried out at  $Re=140$  for a fluid volume fraction of 35%. The optimisation yielded a straight line duct and that is shown in Figure 7-5. The optimised objective value (Pressure drop) for this channel is 59.69Pa.



Figure 7- 5 Optimised shape (LSF contour) and velocity contour for total pressure drop minimisation at Re=140

### 7.3 Two-dimensional results and discussion

In this section the effect of thermal conductivity ratio and Re are studied for 2D channel design. In addition, the effect of actual thermal conductivity of the materials in the  $k_s/k_f=1$  case, is also studied.

#### 7.3.1 $k_s/k_f=10$ case:

This study is conducted for  $k_s/k_f = 10$  for the Reynolds numbers 35 and 70. The optimisation is carried out with weightage factors  $F_1$  and  $F_2$  equal to 1.

#### Results:

The results obtained for  $k_s/k_f=10$  at Re=35 and Re=70 along with its temperature contours are shown in Figure 7-6. It is surprising to see that, the optimised shape has got (porous) solid material at the inlet and exit. This is because the solid is having higher thermal conductivity than the fluid; hence the (porous) solid is distributed directly at the inlet face, so that heat transfer can be maximised and yet since the solid is porous, by increasing the pressure, the required flow rate can be maintained. Because of this, almost all of the heat transfer has happened near the inlet, as observed in the temperature contour (Figure 7-6). This is the drawback of modelling solid as a porous material in topology optimisation and this leads to un-practical design solutions for the internal flow problems. Similar results are expected for other thermal conductivity ratios ( $k_s/k_f > 1$ ) also. Hence they were not carried out.

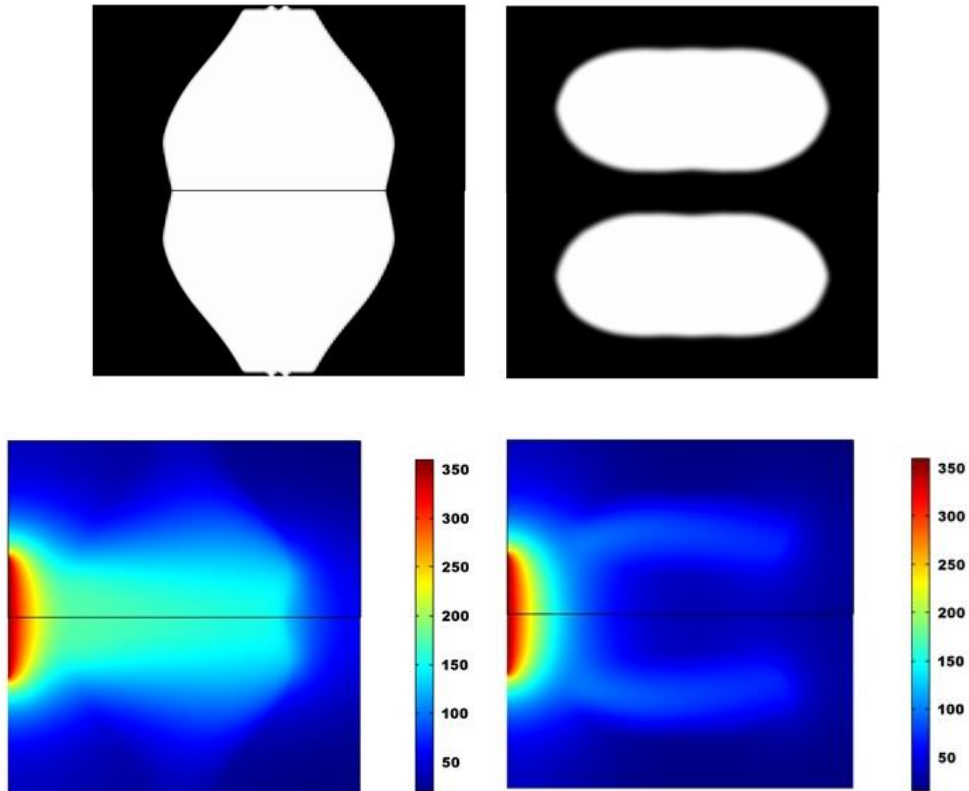


Figure 7- 6 Optimised shapes and corresponding temperature contour for Re=35 (Left) and Re=70 (Right) for  $k_s/k_f = 10$

In order to get realistic shapes and to avoid the formation of (porous) solid at the inlet, few optimisations are carried out with the ‘pressure drop’ objective weightage factor,  $F_2$ , set as  $1e4$  and  $1e5$ . These results are shown in Figure 7-7. In spite of using such a high weightage for the pressure drop objective, thin (porous) solid layer is still distributed at the inlet and outlet. The objective values of the optimised shapes are given in Table 7-3. Though the shape corresponding to  $F_2=1e5$  appears to be a poor local optima, its pressure drop value is realistic.

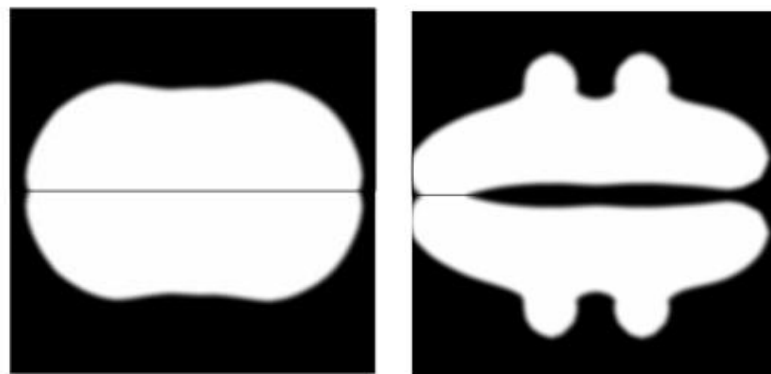


Figure 7- 7 Optimised shapes for Re=70 with  $F_2=1e4$  (Left) and  $F_2=1e5$  (Right) for  $k_s/k_f = 10$

	Temperature Drop (K)		Pressure Drop (Pa)	
	Re=35	Re=70	Re=35	Re=70
$F_2=1$	-305.9	-330.6	26832.6	60336.0
$F_2=1e4$	-	-93.1	-	17957.0
$F_2=1e5$	-	-148.9	-	9820.3

Table 7-3 Objective values of optimised shapes for  $k_s/k_f=10$

### 7.3.2 $k_s/k_f=1$ case:

In this case both solid and fluid have same thermal conductivity, hence it is expected that the optimiser might give some practically usable channel designs compared to the  $k_s/k_f=10$  case. Even when the solid and fluid have same thermal conductivity, depending upon its actual value, the heat recovery from fluid to solid could vary. To study this, the optimisation is carried out for thermal conductivity values of 4, 0.4 and 0.04[W/m/K]. For each of the thermal conductivity value, topology optimisation is carried out for different Reynolds numbers and different 'Temperature drop' objective weightage factors ( $F_1$ ).

#### Thermal conductivity $k_f=k_s=4$ [W/m/K]:

The optimal shapes obtained for different Reynolds numbers and different weightage factor  $F_1$  values are shown in Figure 7-8. The corresponding temperature contours are shown in Figure 7-9. For this case, unlike the  $k_s/k_f=10$  case, realistic channel shapes are obtained. The shape obtained for  $Re=174$ ,  $F_1=1$  resembles a channel flow over a cone-cylinder body. As the  $Re$  is increased, channel becomes more lengthy and curvy. But when the weightage factor  $F_1$  is increased to 100, the optimised shape has (porous) solid material distributed at the inlet and exit. Even though, the solid has the same thermal conductivity as the fluid, heat exchange to the solid will be more when flow passes through it (like in porous medium flow) than the flow passing over the solid. This could partially explain the reason for distributing the (porous) solid at the inlet and exit. Another reason for this is, the amount of heat transferred to solid is inversely proportional to fluid inertia. If the fluid inertia ' $uL$ ' is lower then higher heat exchange is possible. So by blocking the exit, flow velocity/inertia is decreased and hence the heat exchange is increased. Flow velocity contour for  $Re=174$ ,  $F_1=100$

shown in Figure 7-10 supports this argument. The optimised objective values are given in Table 7-4.

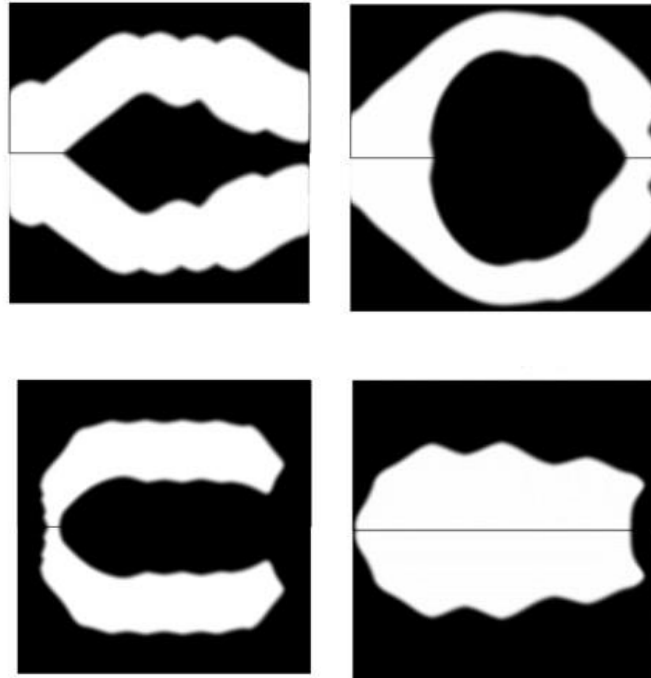
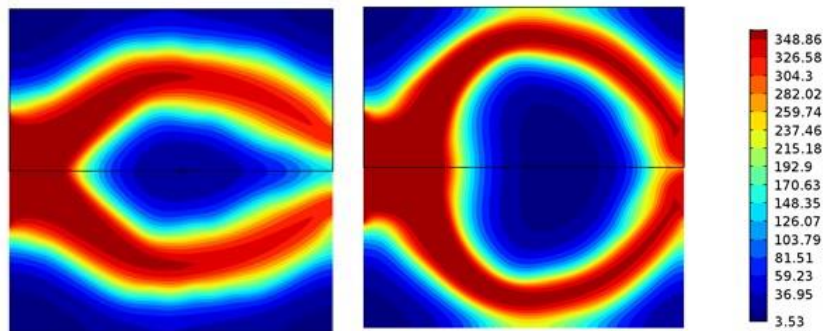


Figure 7- 8 Optimised shapes for  $Re=174$  (Left) and  $521$  (Right) for  $F_1=1$  (Top row) and  $100$  (Bottom row) for  $k=4$  [W/m/K].



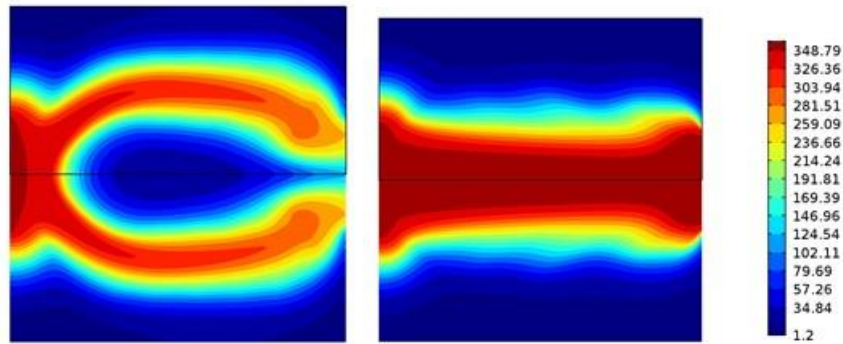


Figure 7- 9 Temperature (K) distribution on optimised shapes at Re=174 (Left) and 521 (Right) for  $F_1=1$  (Top row) and 100 (Bottom row) for  $k_f=4$  [W/m/K]

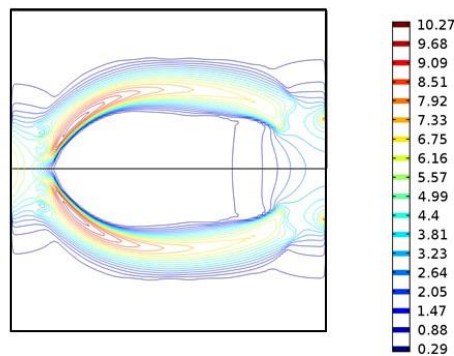


Figure 7- 10 Velocity contour in the design domain for Re=174,  $F_1=100$  for  $k_f=4$  [W/m/K]

By conducting the optimisation for different weightage factors,  $F_1$ , a Pareto of optimal shapes and results are obtained. In a practical situation depending upon the requirement of temperature drop and pressure drop, suitable optimised shape can be chosen and used.

	Temperature Drop (K)		Pressure Drop (Pa)	
	Re=174	Re=521	Re=174	Re=521
$F_1=1$	-73.5	-35.7	325.7	5547.6
$F_1=100$	-148.5	-23.2	94034.0	98106.6

Table 7- 4 Optimised objective values of optimised shapes for  $k_f=4$  [W/m/K]

### 7.3.3 $k_s/k_f=1$ case with $k_s=k_f=0.4$ [W/m/K]:

The optimised shapes obtained for Re=70, 174 and 326 are shown in Figure 7-11. Generally, the optimised shape obtained depends on the initial level-set distribution, initial Lagrange multiplier and its rate of updatment and volume penalty factor. The results shown here are obtained from the carefully chosen Lagrange multiplier and its

updatment, so as to reach a better optimised shape; yet a much better result or a global optimum could also be obtained, by refining these parameters further.

The optimised shape for  $Re=70$  is a flow around a centre body as observed for  $k_f=4$  case. The optimised shape of  $Re=174$  for  $F_1=1$ , is a through channel, the shape is a local minima which is good in terms of the 'pressure drop' objective but not good in terms of the 'temperature drop' objective. In two objective optimisation problems, the optimiser tends to do a trade-off and may give more importance to the first objective or to the second objective, depending on the problem nature and objective's magnitude. An interesting feature to note in these cases is that the optimised channels have a dead flow region, and the observation at the corresponding temperature contour (Figure-7-12) shows that, these regions aid in heat exchange from the fluid to solid. The isolated fluid region in the optimised shape of  $Re=174$  and  $F_1=100$ , is an impractical solution, and it is obtained because of the porous nature of the solid modelled.

Generally, in the augmented Lagrangian method, as the iteration proceeds, the

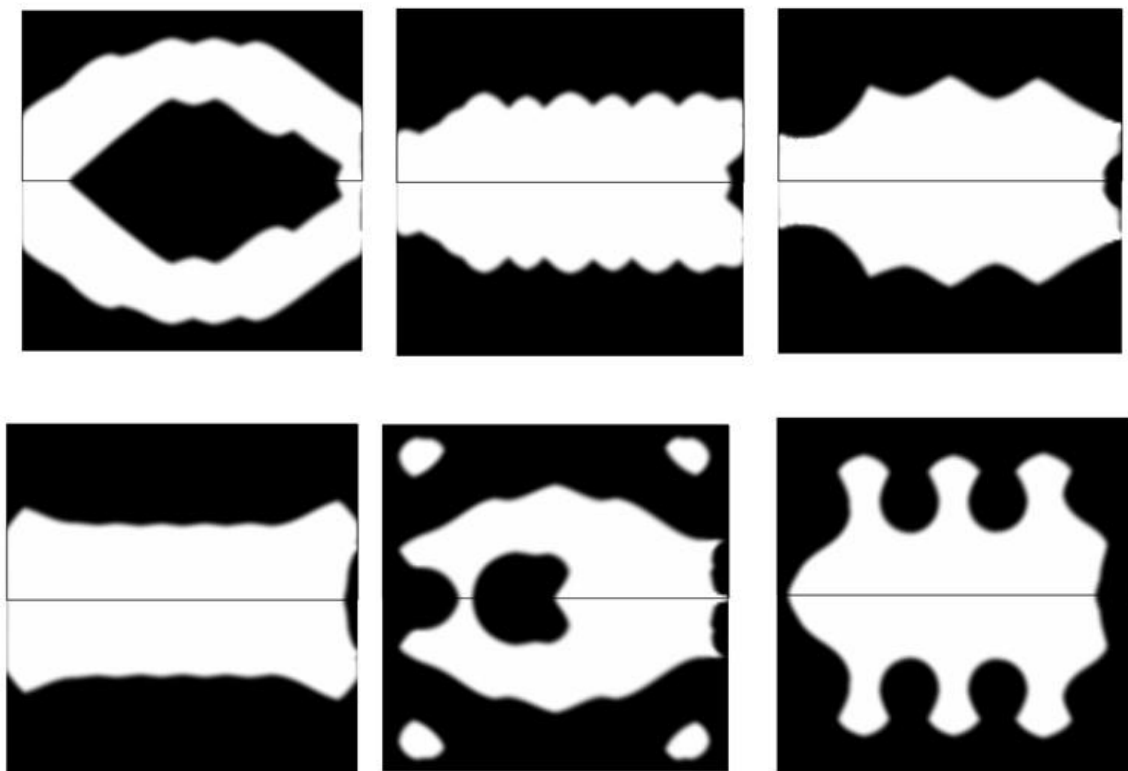


Figure 7- 11 Optimised shapes for  $Re=70$  (Left),  $Re=174$  (centre) and  $326$  (Right) for  $F_1=1$  (Top row) and  $100$  (Bottom row) for  $k_f = 0.4$  [W/m/K]

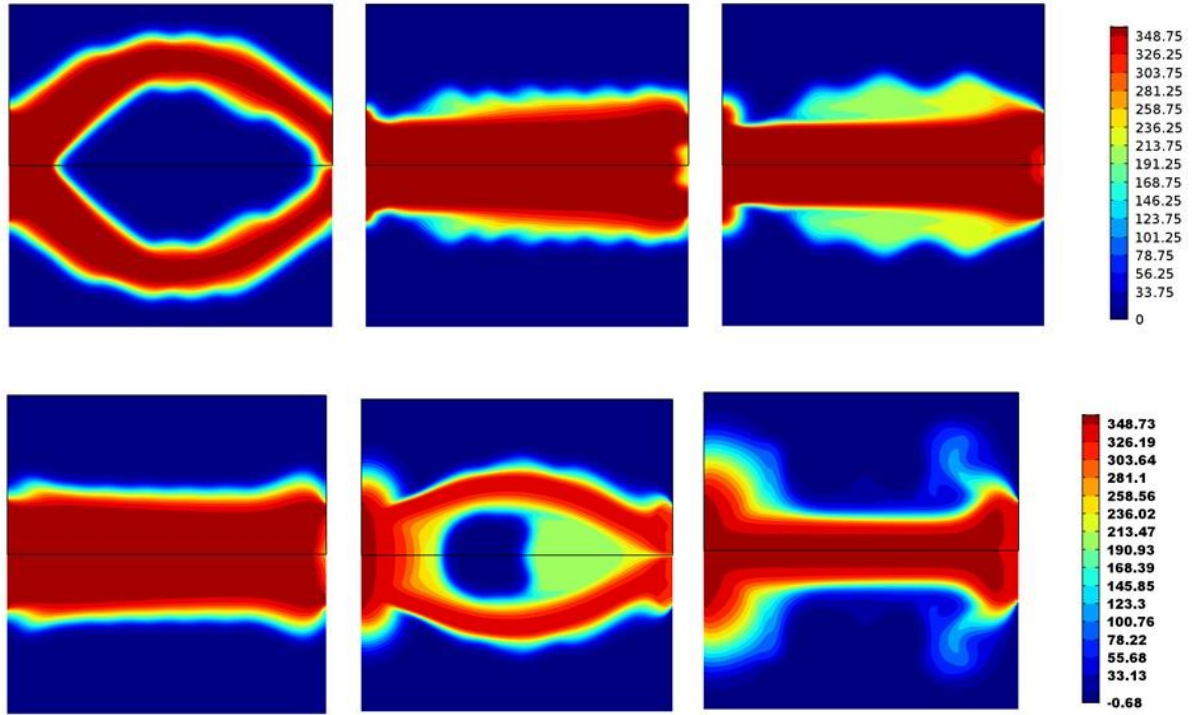


Figure 7- 12 Temperature (K) distribution on optimised shapes at Re=70 (left), Re=174 (centre) and Re=326 (right)

material (fluid) area will oscillate around the required amount and will finally settle to the required value. However, in some cases, material volume continuously decrease and become zero, then it cannot increase due to the lack of solid insertion capability is this numerical model. The initial values of the Lagrange multiplier and volume penalty factor, play an influential role in deciding the convergence nature. The objective values of the optimised shape for  $k_f=0.4$  case are given in Table 7-5.

	Temperature Drop (K)			Pressure Drop (Pa)		
	Re=70	Re=174	Re=326	Re=70	Re=174	Re=326
$F_1=1$	-43.7	-12.0	-10.4	299.8	801.9	5853.7
$F_1=100$	-30.1	-50.7	-49.8	1616.5	46681.1	110298.0

Table 7- 5 Objective values of optimised shapes for  $k_f=0.4$  [W/m/K]

### 7.3.4 $k_s/k_f=1$ case with $k_f=k_s=0.04$ [W/m/K]:

The optimised shapes obtained for Re=70, 174 and 326 for the  $F_1$  values of 1 and 100 are shown in Figure 7-13 and the corresponding temperature contours are shown in Figure 7-14. The objective values corresponding to the optimised shapes are given in

Table 7-6.

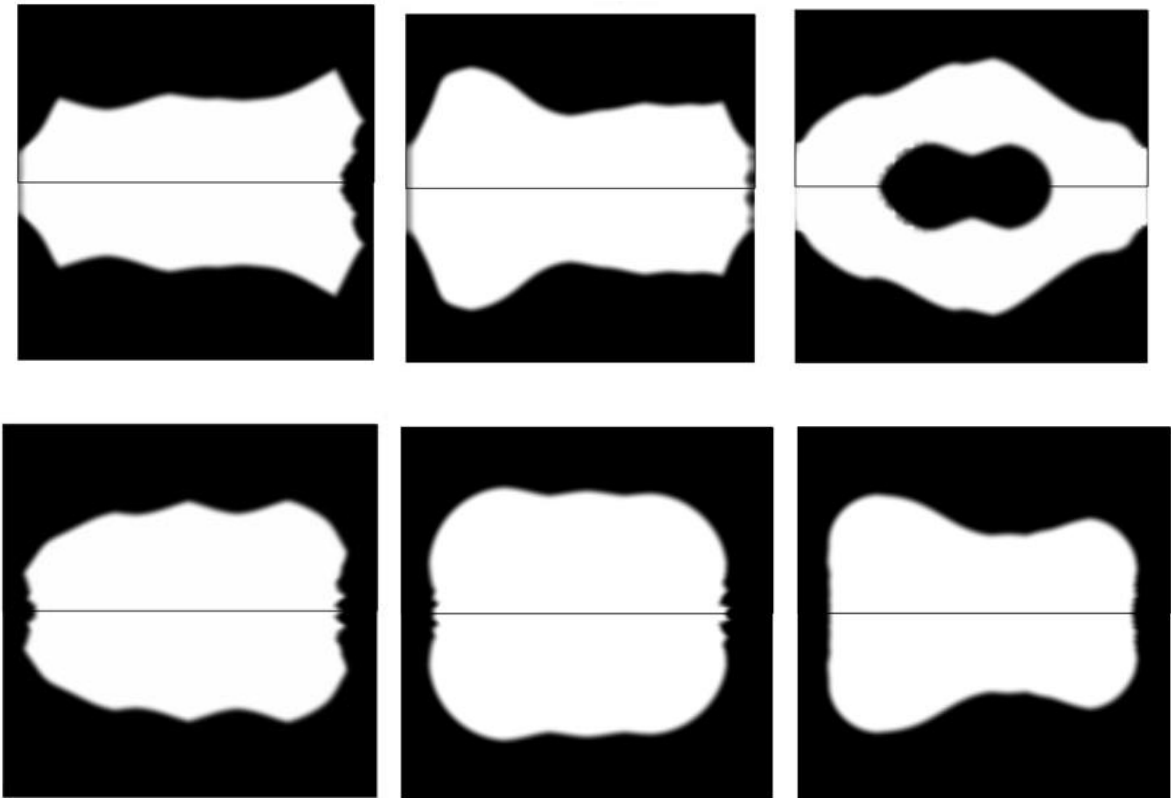


Figure 7- 13 Optimised shapes for  $Re=70$  (Left),  $Re=174$  (Centre) and  $326$  (Right) for  $F_1=1$  (Top row) &  $100$  (Bottom row) for  $k_f=0.04$  [W/m/K]

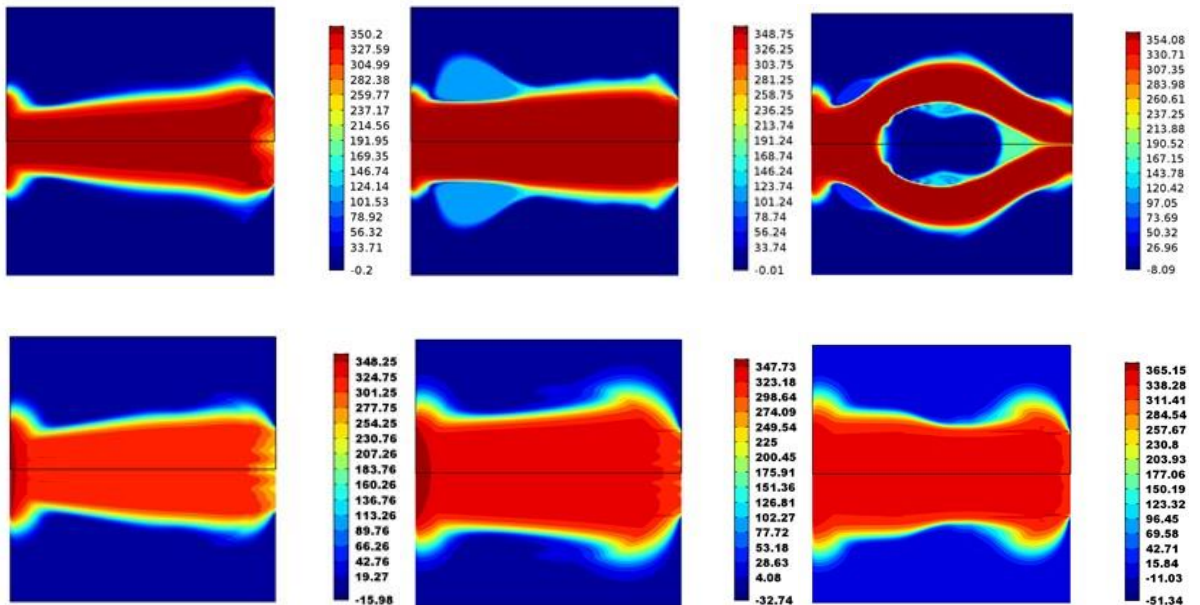


Figure 7- 14 Temperature (K) distribution on optimized shapes for  $Re=70$  (Left),  $Re=174$  (Centre) and  $326$  (Right) for  $F_1=1$  (Top row) &  $100$  (Bottom row) at  $k_f=0.04$  [W/m/K]

	Temperature Drop (K)			Pressure Drop (Pa)		
	Re=70	Re=174	Re=326	Re=70	Re=174	Re=326
$F_1=1$	-64.2	-14.7	-7.3	11447.0	10983.3	2317.2
$F_1=100$	-134.2	-94.1	-47.4	28647.3	87662.9	146788.3

Table 7- 6 Objective values of optimised shapes for  $k_f=0.04$  [W/m/K]

From the convergence plot of  $Re=70$ ,  $F_1=100$ , given in Figure 7-15, it is observed that it has more than one local optimal shape. The first two shapes haven't met the volume constraint but they have considerably higher temperature drop. Among the three shapes, middle shape requires the lowest pressure drop yet it yields considerable temperature drop (Table 7-7). This shape is almost a through channel with least amount of porous solid at the inlet and exit and hence could be a practically feasible solution.

	Temperature Drop (K)	Pressure Drop (Pa)
Iteration=120	-207.43	41444.93
Iteration=180	-59.13	7914.41
Iteration=300	-134.21	28647.32

Table 7- 7 Objective values of optimised shapes for  $k_s/k_f=1000$ ,  $F_1=100$  at  $Re=70$

A Comparison of the optimised objective values for the materials with different thermal conductivity values shows that, material with highest thermal conductivity has highest heat recovery; which is on the expected lines. As the material thermal conductivity decreases, temperature drop decreases. As the flow  $Re$  is increased, temperature drop decreases, this indicates that less heat transfer has taken place from the fluid to solid at high  $Re$ .

The level-set framework used for this study, doesn't have a capability to insert a solid in the fluid region. The HJ equation, used in this study, only has the shape sensitivity term and not the topology gradient term. As this problem domain has many local minima, a solid insertion capability (by using topology gradient term) could improve the result and hence slightly better shapes could be obtained. The optimised shapes with solid at the inlet and outlet are not practically acceptable solutions. These solutions are obtained because solids are modelled using porosity approach.

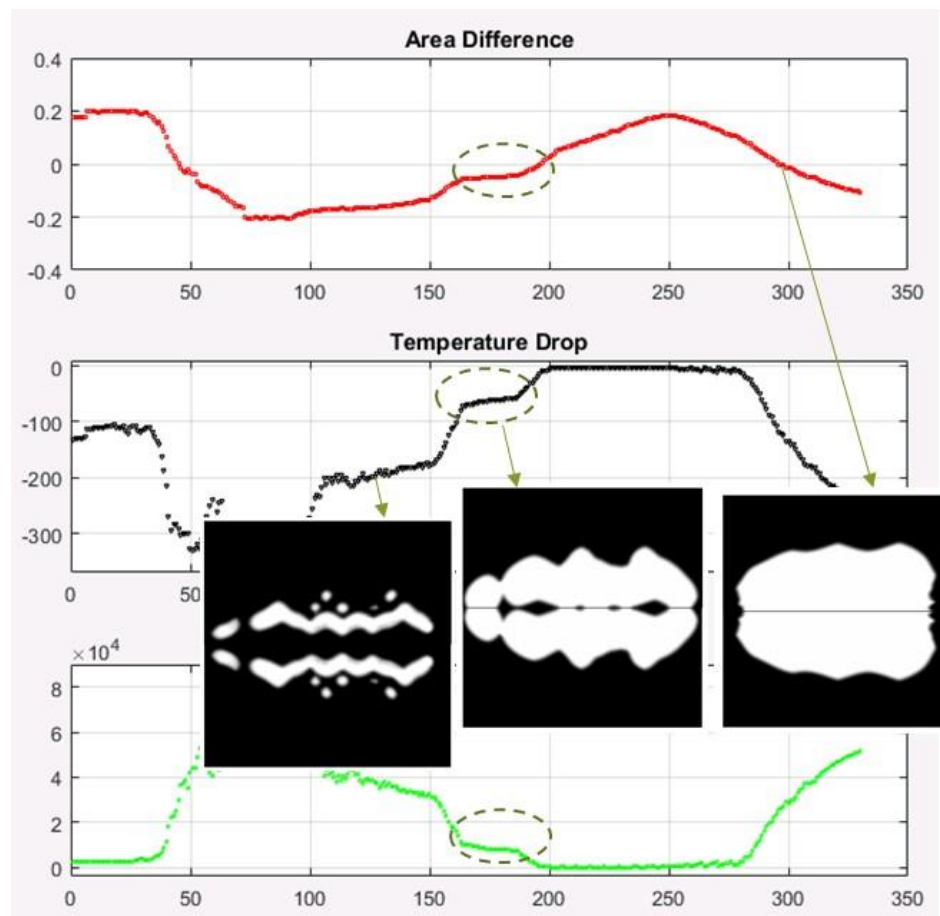


Figure 7- 15 Evolution of optimised shapes during optimisation for  $k_s/k_f=1000$ ,  $F_1=100$  at  $Re=70$

## 7.4 Three-dimensional optimisation

### 7.4.1 Three-dimensional numerical model

The three-dimensional heat recovery channels are designed for  $k_s/k_f=1$  case with two different thermal conductivity values. The computational domain used for the 3D study is shown in Figure 7-16. The inlet of the domain has an extended channel in order to let the development of the laminar profile velocity to some extent. The region excluding the extended channel comprises the design domain. It has a square cross section of side length 20cm and a depth of 6.67cm. A symmetry boundary condition is used to model and solve only one-quarter of the domain in order to save the computation time.

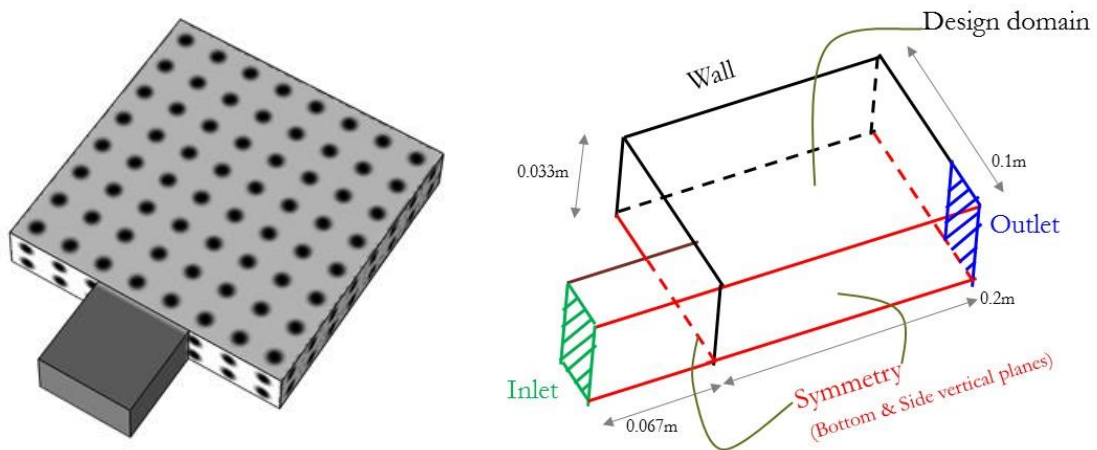


Figure 7- 16 Full domain with initial LSF and computational domain for 3D heat recovery channel design

The 3D heat recovery channel optimisation is conducted for  $k_s/k_f=1$ . The solution of state and adjoint equations for low viscosity fluid like water takes very high time in Comsol (>20hrs) hence a slightly low viscous, glycol is used as the working material. Glycol finds more application in heat exchanger design because of its high specific heat capacity and very low freezing point. As one of the objective of this study is to analyse the effect of thermal conductivity of the material (fluid) on the heat recovery channel shape, along with glycol a fictitious fluid of lower thermal conductivity is also considered. The thermal properties of both the materials are listed in Table 7-8.

Working Material	Density (Kg/m <sup>3</sup> )	Specific heat capacity (J/(kg-K))	Thermal conductivity ( $k_s=k_f$ ) (W/(m-K))
Glycol	1113.2	2470	0.258
Low conductivity fictitious fluid	1113.2	2470	0.00258

Table 7- 8 Thermal properties of materials used for 3D heat recovery channel design

The inlet temperature of the fluid is set as 360K and a heat flux of  $-5000\text{W/m}^3$  is applied on the solid regions. In this 3D study, both the objective values are of same order, hence the weightage factors  $F_1$  and  $F_2$  are taken as 1. The volume fraction of the fluid is constrained at 45% of the design domain volume. The design domain is discretised by  $90 \times 45 \times 15$  hexahedral cells. The study is conducted at two different Reynolds numbers, 19 and 38. Note that, the reference length is 0.067m for calculating the Re. The design domain is initialised with sphere like LS distribution (Figure 7-16). The state and adjoint

equations are solved using the finite element method.

At convergence, the volume constraint is satisfied and the objective become invariant for a range of 5-10 iterations. Each iteration takes about 52mins and the number of iterations required for convergence depends on the Lagrange multiplier and volume penalty factor used for the simulation. So a simulation requiring 125 iteration will take a run time of 108.3 hours on ten real cores / twenty hyper-threaded cores on a Dual Xeon CPU cluster node. In a single iteration, major time taking steps are solving for the state and adjoint equations. The time taken for solving the state and adjoint equations will vary depending upon the nature of flow passage and Reynolds number.

#### **7.4.2 Three-dimensional results and discussion ( $k_s/k_f=1$ )**

The results obtained for 3D optimisations along with the mean velocity iso-contour shapes are shown in Figure 7-17 and 7-19 for glycol and fictitious fluid respectively. By making use of the fact that the Heaviside function value of 1 denotes a fluid and 0 denotes a (porous) solid, the iso-surface of both fluid and solid are plotted with the fluid in grey colour and the solid in black color. Since the flow can take place even through the (porous) solid, for better understanding of the channel shape, the iso-contour of 40% of the inlet velocity is plotted next to the shape. Choosing an higher velocity to plot the iso-contour velocity profile may lead to a discontinuous shape, as the porous solid at the exit is slowing down the flow. The results show that, like in 2D, the 3D optimised shapes also have a solid material at the exit but at the inlet (porous) solid distribution is slightly reduced. Apart from this, the comparison of shapes for  $Re=19$  and  $Re=38$  show that, as  $Re$  increases channel length increases to maximise the heat transfer. Since it is a 3D study, to understand the channel shape in third dimension (depth), the velocity contour on vertical planes for  $Re=38$ , is plotted in Figure 7-18. The figure also contains the corresponding temperature contour.

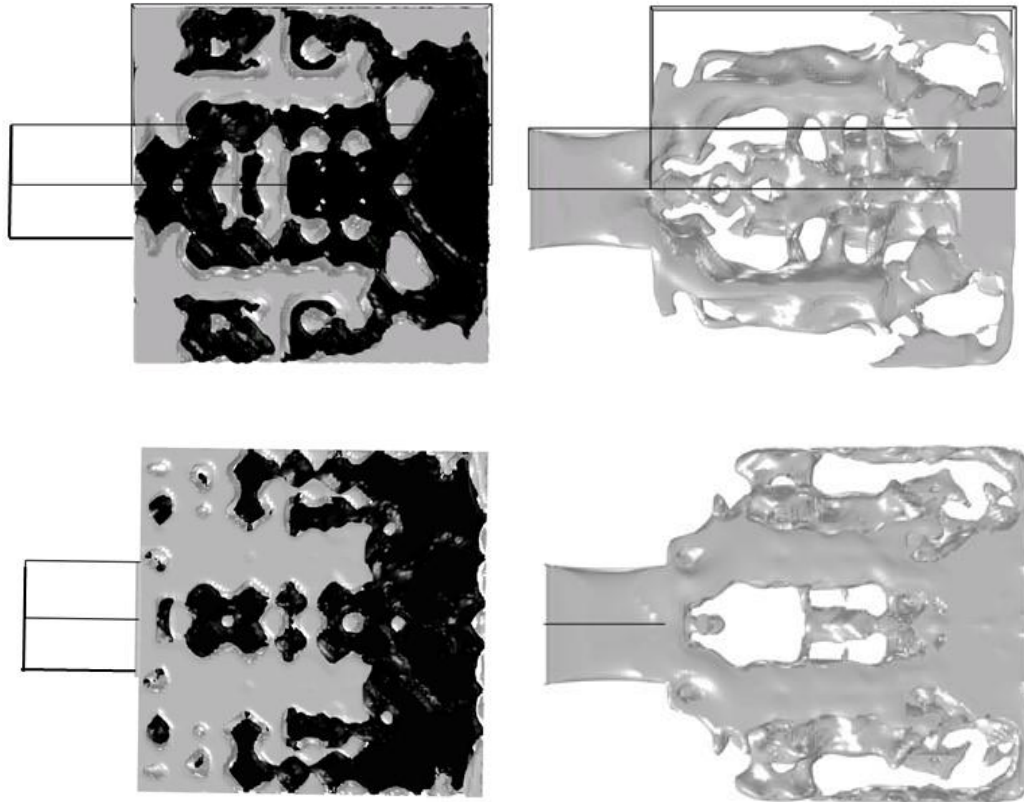


Figure 7- 17 Optimised shapes for glycol ( $k_s=k_f$ ) at Re=19 (Top) and Re=38 (Bottom) and their velocity iso-surface.

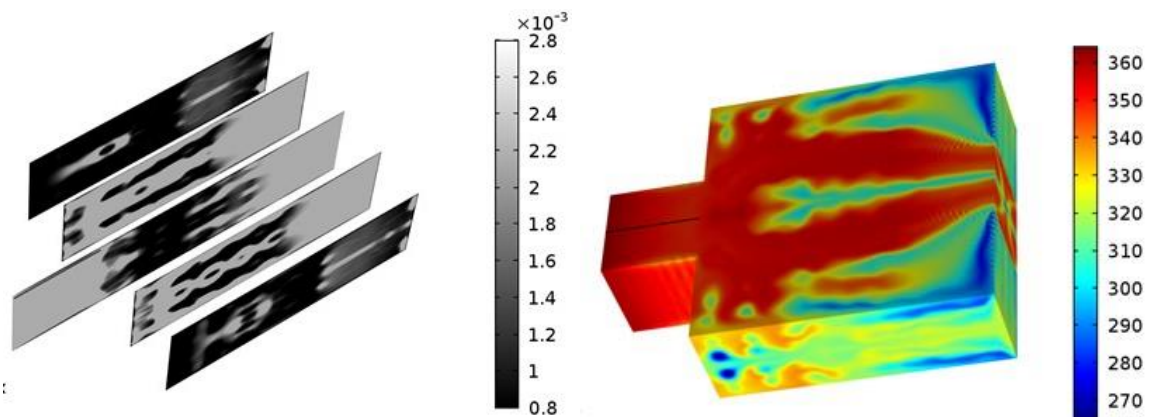


Figure 7- 18 Velocity and temperature contour for glycol ( $k_s=k_f$ ) at Re=38

Heat recovery channel for lower thermal conductivity (fictitious) material has more number of channels than the optimised shape of glycol. This behaviour is observed for both the Reynolds numbers. The final objective values for all the four cases are given in Table 7-9. The table shows that, at a given Reynolds number, low conductivity fictitious fluid recovers more heat than glycol. This is in contrast to the results obtained

for 2D cases and with the common knowledge. The anomaly could be because this design problem has got many local optima, and the optimised shape obtained for low conductivity material is a better one than the optimised shape obtained for glycol. But these shapes require higher pressure drop than the shapes corresponding to glycol to maintain the flow. Hence the low conductivity fluid is reporting a better performance.

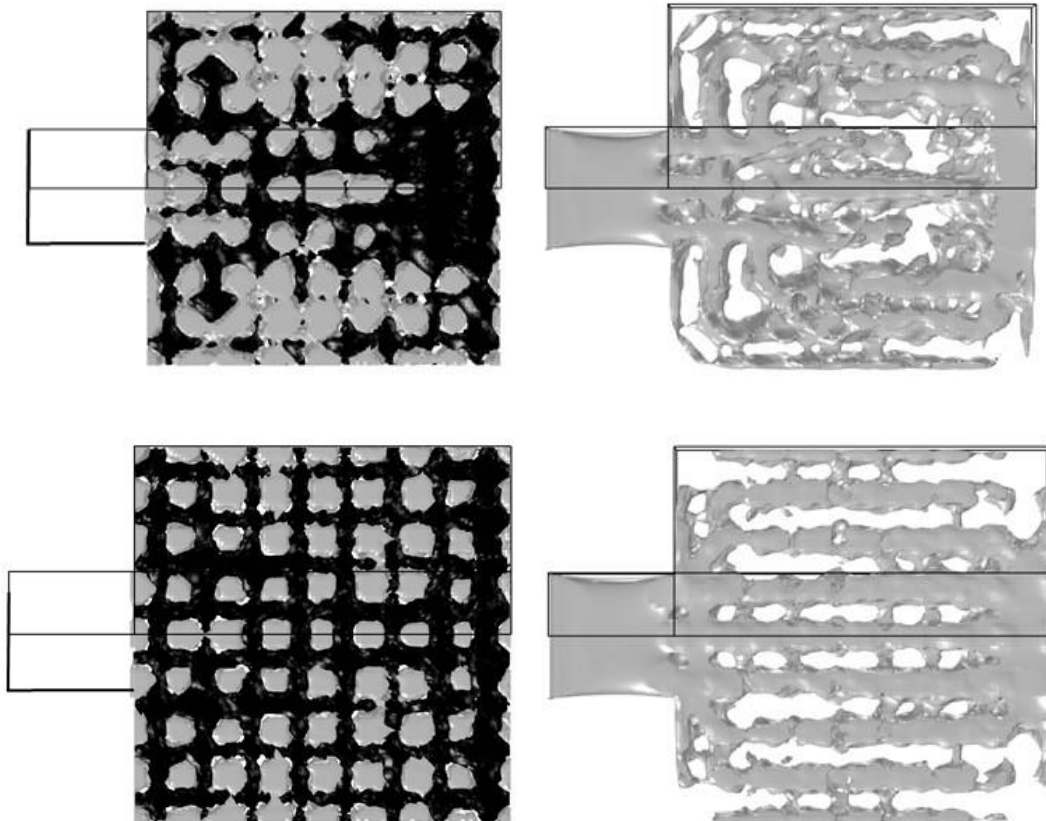


Figure 7- 19 Optimised shapes for low conductivity material ( $k_s=k_f$ ) at  $Re=19$  and  $Re=38$  and its velocity iso-surface

	Temperature Drop (K)	Total pressure Drop (Pa)
Glycol, $Re=19$	-47.83	13.56
Glycol, $Re=38$	-27.45	33.78
Low conductivity fictitious fluid, $Re=19$	-53.87	15.75
Low conductivity fictitious fluid, $Re=38$	-28.39	34.28

Table 7- 9 Objective values obtained for optimised 3D heat recovery channels

## 7.5 Summary

In this study, heat recovery channels are designed for different thermal conductivity ratios ( $k_s/k_f$ ) and for different Reynolds numbers for a fully developed laminar flow. The effect of actual thermal conductivity of the material on the optimised channel shape for  $k_s/k_f=1$  case is also studied. The combined objective of maximum temperature drop and minimum total pressure drop between the inlet and outlet is considered as the objective. Since the two objectives' magnitudes are very different, weightage factor for temperature drop objective is increased from 1 to 100 and its effect on the optimised shape and objective values are also studied. The level-set method uses density-based mapping and the shape sensitivity is calculated through the continuous adjoint method. Following conclusions are drawn from this study.

1. As the flow Re increases, the temperature drop (heat recovery) decreases in both 2D and 3D. As the Re increases, the inertial diffusivity increases (in comparison to thermal diffusivity), hence the flow has to take a lengthy route to enable heat transfer, before the flow exits out of the design domain. But if the Re increases further, since the domain size is fixed, the channel length cannot be increased further. In these cases, the optimiser distributes the (porous) solid material at the inlet and outlet to slow down the flow velocity and thereby to increase the heat recovery.
2. The porosity modelling of solid used in this LSM prevents or discourages the design of practically feasible channel shapes when the solid-to-fluid thermal conductivity ratio ( $k_s/k_f$ ) is greater than 1. Since the solid has higher thermal conductivity (than the fluid) in this case, the optimiser distributes more (porous) solid materials at the inlet and exit to improve the heat recovery. Hence these shapes become practically unfeasible.
3. For  $k_s/k_f=1$  case, practically feasible heat recovery channels shapes are obtained. As expected, in this case if actual thermal conductivity of the material is higher, then higher heat recovery is possible.
4. As expected, when the 'temperature drop' weightage factor increases, higher temperature drops are achieved in most of the cases (Exception  $Re=70$  design). This is achieved by having dead flow regions in the channel or by slowing down the flow velocity by placing the (porous) solid at the inlet and exit. On the similar

- lines, increasing the 'pressure drop' weightage factor leads to straight line channel designs (in most of the cases) to achieve lower pressure drop objective.
5. The 3D study is conducted for  $k_s/k_f=1$  case and this also confirms that with increase in  $Re$ , the temperature drop decreases. But an interesting feature is that as the  $Re$  increases, the channel length increases to improve the heat recovery.
  6. The HJ equation, used in this study, only has the shape sensitivity term and not the topology derivative term. But using both the terms in the HJ equation, will enable to insert a solid material inside the fluid region during the optimisation process; this could improve the result and hence slightly better shapes could be obtained. Alternate option is introducing additional constraint (upper limit) on the inlet total pressure values.
  7. The distribution of solid materials at the inlet and exit is the drawback of porosity modelling and this is observed mostly in the internal flow optimisation problems but not in the external flow optimisation problems. The LS method with an xFEM mapping, is more accurate for solid modelling, hence this method can provide practically suitable shapes for these flow problems.

Overall, in this study heat recovery channels are designed for different scenarios and the influence of the  $k_s/k_f$  and  $Re$  on the heat recovery channel shape is clearly brought out. The study also highlighted the drawback of the porosity approach for internal flow problems.

## 8 Topology Optimisation of Multi-material Heat Sink

### 8.1 Introduction

The rapid development taking place in additive manufacturing, enables multi-material manufacturing, with spatial variation in material properties achieved through selective deposition. Topological optimisation techniques can be utilised to determine the optimal distribution of one or more materials within a given design space for a prescribed set of constraints. However, this technique has so far not been applied to the design of multi-material convectively cooled heat sinks. This study is important as it will pave way for the design of composite copper-aluminium or copper-steel heat sinks which will be cheap and very effective in heat dissipation. This study is challenging as it has more than one volume constraint to be satisfied at the optimal solution. In this chapter, LS TO is used to design two and three solid material heat sinks. The design is carried out for different combinations of solid and fluid properties. Section 8.2 describes the optimisation formulation for 2 materials and section 8.3 describes the optimisation formulation for 3 materials. Section 8.4 describes the computational details. Two dimensional and three dimensional study results are presented in sections 8.5 and 8.6 respectively. A summary of this study is given in section 8.7.

### 8.2 Two-material topology optimisation formulation

Topology optimisation has been used for multi material structural optimisation for more than 2 decades [104]. This technique is particularly useful for multi-material optimisation as it can simultaneously change the shape and layout of the materials. Sigmund [6] used the density method for the topology optimisation of 3 phase thermal expansion materials. Hvejsel and Lund [105] generalised the density method material interpolation schemes for an arbitrary number of pre-defined materials with given

properties. Wang [7] presented a level-set based multi-material topology optimisation method for structural optimisation, wherein he used ' $l$ ' level-sets for modelling ' $2^l$ ' distinct material phases. There are alternate ways for modelling multi-phase materials using level-sets including Wang's [68] proposed model wherein ' $l-1$ ' level-sets are used to model ' $l$ ' phases of materials.

Allaire et al. [106] gave a more rigorous shape derivative for multi-material level-set topology optimisation problems. Generally in multi-material TO, the material interface between two solids is assumed to be perfectly bonded, but this need not be the case in practice. Michailidis [107] gives a description of different methods for modelling the material interface with relevant numerical examples. Liu et al. [108] presented an optimisation strategy considering the cohesive constitutive relationship of the interface for the level-set method with XFEM geometry mapping. This model enables possible separation of material interfaces, which is realistic in nature.

Apart from the density and level-set methods, other methods are also used for multi-material TO. Notable ones are the peak function method of Yin and Ananthasuresh [109] and the bi-value coding parameterisation scheme of Gao et al. [110]. Bruyneel [111] proposed a new parameterisation based on shape functions. Phase-field approaches based on the Cahn-Hilliard equation are also used for multi-material TO. Tavakoli and Mohseni [112] implemented an alternative active-phase algorithm for multi-material problems in a MATLAB code. Zhou and Wang [113] introduced a general method for multi-phase material TO using the phase field method. The main drawback of phase-field approaches is their slow convergence rate. Typically thousands of iterations are required for a good level of convergence.

In this section, the multi-material level-set model of Wang [68] is extended to two-material convectively cooled heat sink design. To model two different solids and a fluid, two level-set functions are used. A positive SDF ( $\psi_1$ ) is considered to represent a solid and negative SDF is considered to represent a fluid (Figure 8-1). The second level-set function  $\psi_2$  is used to differentiate the two solids. The region where both the SDFs are positive represents solid2 and the region where  $\psi_1$  is positive and  $\psi_2$  is negative indicates solid1, as illustrated in Figure 8-1.

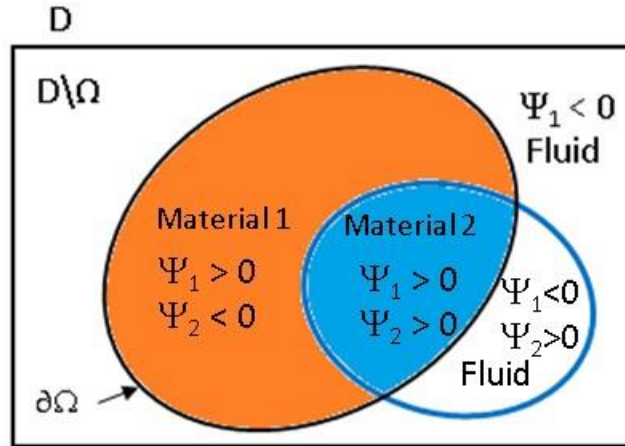


Figure 8- 1 Design domain with level-set representation for two-material structure

At any point within the design domain, the thermal properties  $k$ ,  $C_p$  and  $\rho$  take values based on the values of  $\Psi_1$ ,  $\Psi_2$  and their respective Heaviside functions, as given in Table 8-1.  $H_1$  is the Heaviside function corresponds to  $\Psi_1$  and  $H_2$  is the Heaviside function corresponding to  $\Psi_2$ . In this chapter, subscript 1 refers to property corresponding to solid 1 and subscript 2 refers to property corresponding to solid2.

Name	Expression
$k_\gamma$	$H_1*(H_2*k_{s2}+(1-H_2)*k_{s1})+k_f*(1-H_1)$
$C_{p\gamma}$	$H_1*(H_2*c_{ps2}+(1-H_2)*c_{ps1})+c_{pf}*(1-H_1)$
$\rho_\gamma$	$H_1*(H_2*\rho_{s2}+(1-H_2)*\rho_{s1})+\rho_f*(1-H_1)$

Table 8- 1 Thermal properties interpolation formula for two-material LSM

In single material LS TO, level-sets are updated by solving a single Hamilton Jacobi (HJ) equation. Here, since more than one LS function is used, each LSF is updated by solving its respective HJ equation. The shape sensitivity of each of the LSF is calculated and the velocity of advection of the LSF is equal to the sum of shape sensitivity, Lagrange multiplier and area constraint terms as per the augmented Lagrangian method of optimisation (Eqn-3.24). For the heat sink design, minimum thermal compliance is considered as the objective and the constraints are governing thermo-fluidic equations (Eqn 5.1 to 5.4) and volume constraints of respective solids.

The objective of optimisation and its augmented Lagrangian are given in following equations.

$$\text{Objective } F(\Omega) = \int k_\gamma * (\nabla T)^2 d\Omega \quad (8.1)$$

$$L = F(\Omega) + \lambda_1 \left( \int_\Omega H(\psi_1) d\Omega - V_1 * V_\Omega \right) + \lambda_2 \left( \int_\Omega H(\psi_1) H(\psi_2) d\Omega - V_2 * V_\Omega \right) \quad (8.2)$$

The HJ equations of the two LSF are given below and they are solved using an explicit first order upwind scheme. The same solution methodology described in previous chapters are followed for solving them.

$$\text{HJ equation:} \quad \frac{\partial \psi_1}{\partial t} = V_{n1} |\nabla \psi_1| \quad (8.3)$$

$$\frac{\partial \psi_2}{\partial t} = V_{n2} |\nabla \psi_2| \quad (8.4)$$

The velocity of advection of LSF is obtained by differentiating the Lagrangian with respect to corresponding LSF.

$$V_{n1} = F'_1(\Omega) + \lambda_1 + \lambda_2 H(\psi_2) + \Lambda_1 \left( \int_\Omega H(\psi_1) d\Omega - V_1 * V_\Omega \right) \quad (8.5)$$

$$V_{n2} = F'_2(\Omega) + \lambda_2 H(\psi_1) + \Lambda_2 \left( \int_\Omega H(\psi_1) H(\psi_2) d\Omega - V_2 * V_\Omega \right) \quad (8.6)$$

In the above equations,  $F'_1(\Omega)$ ,  $F'_2(\Omega)$  are shape sensitivities,  $\lambda_1$ ,  $\lambda_2$  are Lagrangian multipliers and  $\Lambda_1$ ,  $\Lambda_2$  are volume penalty factors.  $V_1$  is the volume constraint of total solid material,  $V_2$  is the volume constraint of solid2 alone and  $V_\Omega$  is the design domain volume. Shape sensitivities are obtained by differentiating the objective function with respect to the corresponding LS functions. Since the flow Reynolds number is of comparable order to Stokes flow, the self-adjoint nature of Stokes flow equations are exploited and the contribution of the NS and energy equations to shape sensitivity is ignored though the equations are solved to evaluate the state variables.

$$F'_1(\Omega) = (H_2 * k_{s2} + (1 - H_2) * k_{s1} - k_f) * \delta_I * (\nabla T)^2 \quad (8.7)$$

$$F'_2(\Omega) = (k_{s2} - k_{s1}) * H_1 * \delta_2 * (\nabla T)^2 \quad (8.8)$$

The Lagrangian multiplier and volume penalty factor are updated similar to single material LS TO. Also, the two LSFs are re-initialised at regular intervals by solving respective Eikonal equations.

### 8.3 Three-material topology optimisation formulation

For optimising three solids and a fluid, three level-set functions are used. The definition of 3 solid materials in terms of the 3 level-set function values are depicted in Figure 8-2. Each of the three LSFs are evolved by solving their respective HJ equation. Thermal conductivity definition is given in Eqn (8.9), and following this definition other thermal properties like  $C_p$  and  $\rho$  are also defined.

$$k_y = H_1*(H_2*((1-H_3)*k_{s2}+H_3*k_{s3})+(1-H_2)*k_{s1})+k_f*(1-H_1) \quad (8.9)$$

The augmented Lagrangian of this problem is given as,

$$L = F(\Omega) + \lambda_1 \left( \int_{\Omega} H(\psi_1) d\Omega - V_1 * V_{\Omega} \right) + \lambda_2 \left( \int_{\Omega} H(\psi_1)H(\psi_2)(1 - H(\psi_3)) d\Omega - V_2 * V_{\Omega} \right) + \lambda_3 \left( \int_{\Omega} H(\psi_1)H(\psi_2)H(\psi_3) d\Omega - V_3 * V_{\Omega} \right) \quad (8.10)$$

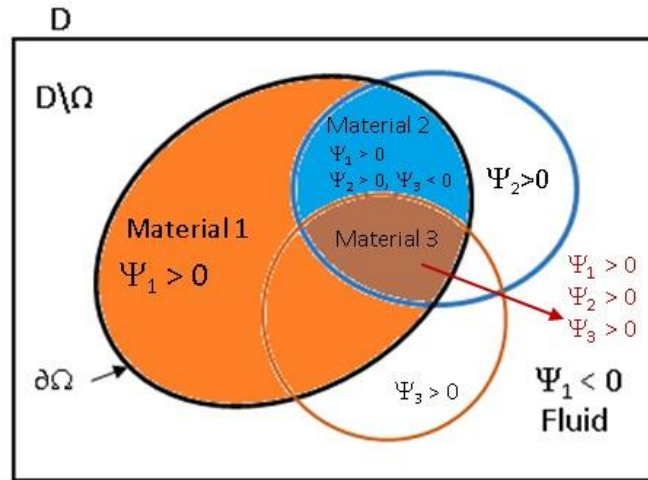


Figure 8- 2 Design domain with level-set representation for three-material structure

Velocity of advection for the three LSFs are obtained by differentiating the Lagrangian and adding the volume penalty terms.

$$V_{n1} = F'_1(\Omega) + \lambda_1 + \lambda_2 H(\psi_2)(1 - H(\psi_3)) + \lambda_3 H(\psi_2)H(\psi_3) + \lambda_1 \left( \int_{\Omega} H(\psi_1) d\Omega - V_1 * V_{\Omega} \right) \quad (8.11)$$

( 8. 12)

$$V_{n2} = F_2'(\Omega) + \lambda_2 H(\psi_1)(1 - H(\psi_3)) + \lambda_3 H(\psi_1)H(\psi_3) + \Lambda_2 \left( \int_{\Omega} H(\psi_2) d\Omega - V_2 * V_{\Omega} \right)$$

( 8. 13)

$$V_{n3} = F_3'(\Omega) - \lambda_2 H(\psi_1)H(\psi_2) + \lambda_3 H(\psi_1)H(\psi_2) + \Lambda_3 \left( \int_{\Omega} H(\psi_3) d\Omega - V_3 * V_{\Omega} \right)$$

In the above equations,  $F_1'(\Omega)$ ,  $F_2'(\Omega)$ ,  $F_3'(\Omega)$  are shape sensitivities,  $\lambda_1$ ,  $\lambda_2$ ,  $\lambda_3$  are Lagrangian multipliers and  $\Lambda_1$ ,  $\Lambda_2$ ,  $\Lambda_3$  are volume penalty factors.  $V_1$  is the volume constraint of total solid material,  $V_2$  is the volume constraint of solid2 alone,  $V_3$  is the volume constraint of solid3 alone and  $V_{\Omega}$  is the design domain volume. The shape sensitivities of the 3 LSFs are given in below equations.

$$F_1'(\Omega) = H_2 * (H_3 * ks_3 + (1 - H_3) * ks_2) + (1 - H_2) * ks_1 - k_f * \delta_1 * (\nabla T)^2 \quad (8. 14)$$

$$F_2'(\Omega) = H_1 * (H_3 * ks_3 + (1 - H_3) * ks_2) - ks_1 * \delta_2 * (\nabla T)^2 \quad (8. 15)$$

$$F_3'(\Omega) = H_1 * H_2 * (ks_3 - ks_2) * \delta_3 * (\nabla T)^2 \quad (8. 16)$$

For optimisation, the HJ equation of all 3 LSFs are solved and all the LSFs are re-initialised at regular intervals to maintain their slope. The rest of the formulation is similar to two material TO formulation given in the previous section.

## 8.4 Computational details

### Two dimensional study:

The design domain is same as the one used for heat sink design in Chapter 4. It is rectangular in shape, with heat source at the bottom of the domain and liquid convection injected from the top of the computational domain as shown in Figure 8-3. The two sides of the computation domain act as outlet.

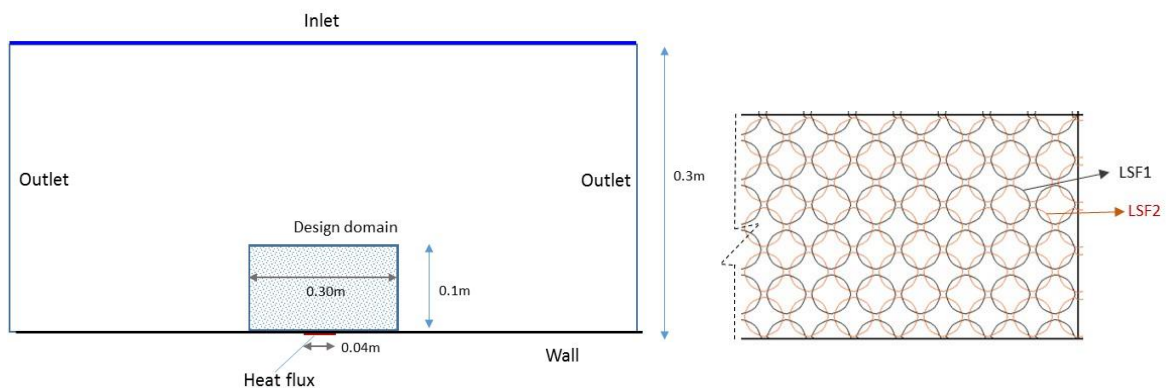


Figure 8- 3 Computational domain and initial distribution of two LSFs

The design domain is discretised with 150x50 rectangular elements. The initial level-set used for the computation is a series of circles. The level-set function is evolved on a grid mesh with ghost elements. A liquid flow of velocity 0.002m/s and temperature 293K is applied at the inlet. The inlet velocity corresponds to a Reynolds number of 600 and a heat flux of 3500W/m<sup>2</sup> are specified; zero pressure boundary condition is applied at the outlet. The properties of the solid and fluid materials used in this study are shown in Table 8-2.

Property	Value
C <sub>ps1</sub>	385 J/(kgK)
C <sub>ps2</sub>	770 J/(kgK)
C <sub>ps3</sub>	460 J/(kgK)
C <sub>pf</sub>	4184 J/(kgK)
ρ <sub>s1</sub>	8920 kg/m <sup>3</sup>
ρ <sub>s2</sub>	4460 kg/m <sup>3</sup>
ρ <sub>s3</sub>	7800 kg/m <sup>3</sup>
ρ <sub>f</sub>	1000 kg/m <sup>3</sup>
Volume fraction	0.4
Solid2 volume fraction	0.2
α <sub>max</sub>	1e4

Table 8- 2 Material properties

The TO are carried out for 1 single material, 6 two material and 1 three material cases; the thermal conductivity and volume fractions of solid and fluid for each of the cases are listed in Table 8-3. The total solid volume is constrained at 40% of design domain volume. Among the two solids, two different volume ratios are considered between solid1 to solid2: 50:50, and 20:80. The thermal conductivities of the three solids, considered in this study are 400 W/(mK), 200 W/(mK) and 40 W/(mK). Note that they closely represents the thermal conductivities of copper (Cu), aluminium (Al) and steel respectively. A single material heat sink is designed with high thermal conductivity material (copper) and this results will be used to benchmark the results obtained for other multi-material heat sinks. The thermal conductivity of fluid considered is 0.4 W/(mK), which closely represents water. Only for two cases (case4 and case5), an artificially high conductivity fluid of thermal conductivity 4 W/(mK) is considered.

	Single Material	Two Material cases						Three Material case
	$V_{solid1}=0.4V_{\Omega}$	$V_{solid1}=0.20V_{\Omega}, V_{solid2}=0.20V_{\Omega}$				$V_{solid1}=0.08V_{\Omega}, V_{solid2}=0.32V_{\Omega}$		$V_{s1}=0.06 V_{s2}=0.12$ $V_{s3}=0.22V_{\Omega}$
	Case 1	Case2	Case3	Case4	Case5	Case6	Case7	Case 8
$ks_1$	400	400	400	400	400	400	400	400
$ks_2$	-	40	200	40	200	40	200	200
$ks_3$	-	-	-	-	-	-	-	55
$k_f$	0.4	0.4	0.4	4	4	0.4	0.4	0.4

Table 8- 3 Thermal conductivity used in different simulations

The typical convergence history of two material TO run is given in Figure 8-4 and the evolution of heat sink shape with respect to iterations is given in Figure 8-5. At convergence, the area constraint of both the solids are satisfied and both area difference and thermal compliance remain stationary at the convergence point.

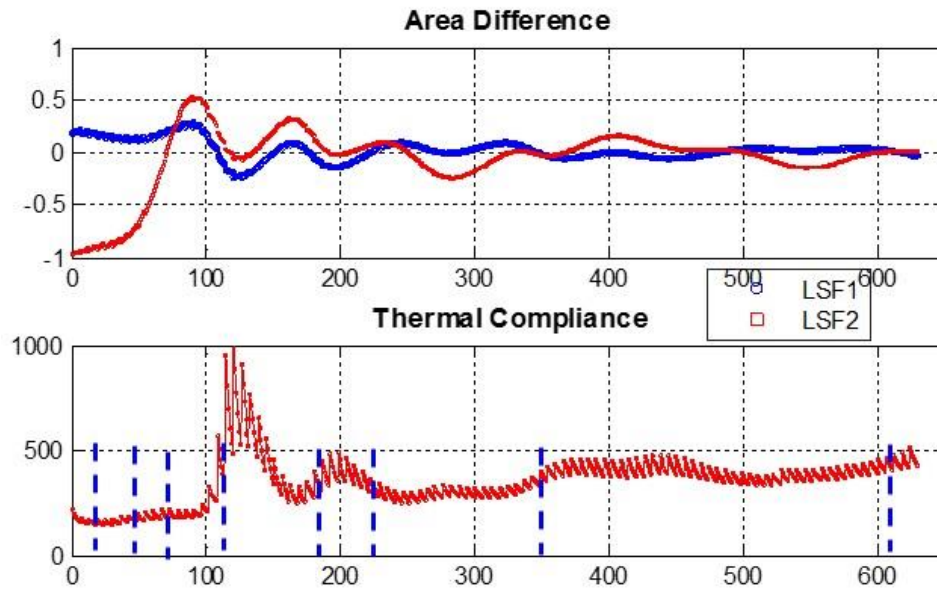


Figure 8- 4 Convergence history of two material topology optimisation

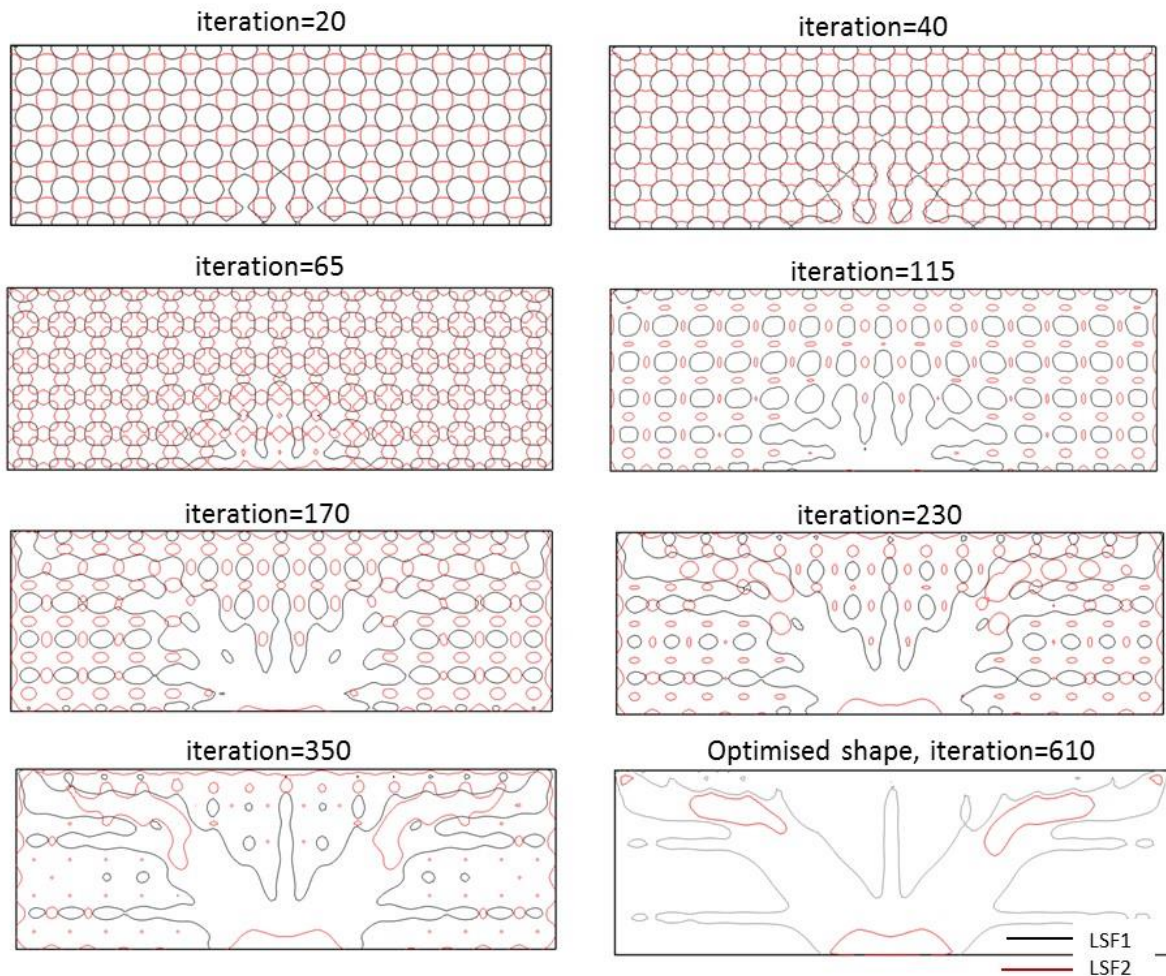


Figure 8- 5 Evolution of two-material heat sink shape with iterations

### 3D Computational details:

The computational domain used for the 3D study is the same as the one shown in Figure 6.5. Fluid velocity corresponding to a Re of 8 and heat flux of  $20\text{kW/m}^2$  is applied at the bottom corner of the design domain. The mesh size and boundary conditions are the same as the one used in section 6.4. Initial level-sets are spherical in shape and level-sets of different radii are tried to reach the better optimised shape.

Three dimensional optimisation study is carried out to design two material copper-aluminium and copper-steel heat sinks. Their performance are compared against single material (copper) heat sink designed in section 6.4.3. In these optimisations, solid1 (copper) and solid2 (aluminium or steel) material volumes are constrained at 10% and 15% of design domain volume respectively.

## 8.5 Two dimensional study results

### Single material copper heat sink (Case1):

Single material heat sink is designed with copper and its material volume is constrained at 40% of design domain volume. The heat sink shape obtained along with the temperature distribution in the design domain is shown in Figure 8-6.

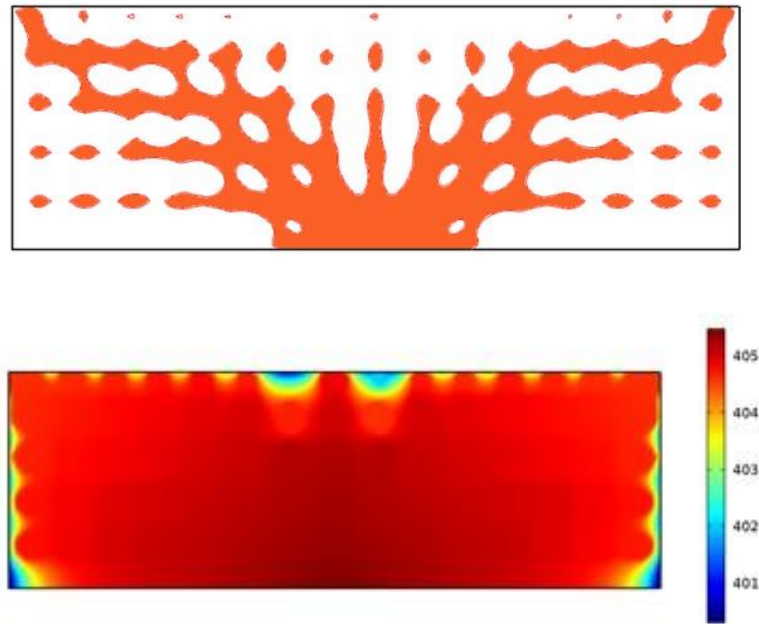


Figure 8- 6 Optimised shape and the Temperature contour (K) for single material heat sink

### Two material, equal solid volume ratio heat sinks (Case2 & 3):

In case2 to case5, solid1 and solid2 material volumes are constrained at a ratio of 20:20. The optimised shape obtained for these cases along with their temperature distributions are given in Figures 8-7 to 8-10. The objective value achieved and maximum temperature in the design domain are tabulated and given in Table 8-4. The following points are observed from the results.

In the copper-steel two material heat sink (case2), the high conductivity copper tends to have a branched structure and the steel is mostly distributed surrounding the copper and also over the heat flux boundary. The shape obtained for copper-aluminium two material heat sink (case3) is slightly different from this. Overall, this heat sink has

smooth and branched structure but there are subtle differences which can be observed from Figures 8-7 and 8.8.

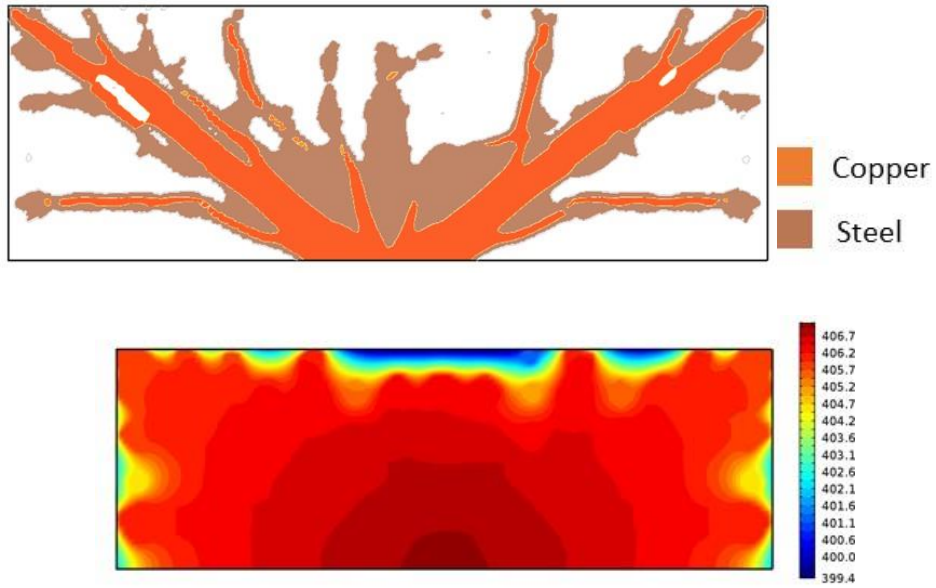


Figure 8- 7 Optimised shape and its temperature contour for case2

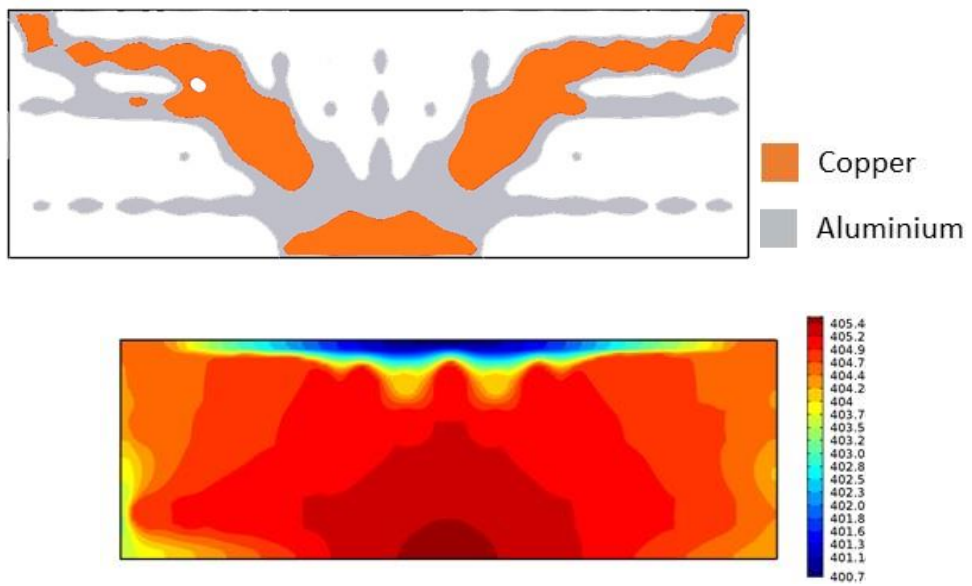


Figure 8- 8 Optimised shape and its temperature contour for case3

Name	Description	Volume Fraction	Maximum Temperature(K)	Thermal Compliance (wK/m)	Max. Temperature-Ambient Temperature (K)
Case1	Single material: Cu, water	0.40	405.48	261.79	112.33
Case2	Cu-steel, water	0.20, 0.20	407.18	464.98	114.03
Case3	Cu-Al, water	0.20, 0.20	405.56	293.12	112.41
Case4	Cu-steel, High conductivity fluid	0.20, 0.20	305.66	198.15	12.51
Case5	Cu-Al, High conductivity fluid	0.20, 0.20	305.59	190.80	12.44
Case6	Cu-steel, water	0.08, 0.32	409.08	735.78	115.93
Case7	Cu-Al, water	0.08, 0.32	406.83	429.63	113.68
Case8	Cu-Al-steel, water	0.06, 0.12, 0.22	406.38	379.33	113.23

Table 8- 4 Summary of 2D multi-material heat sink design results

### Two material disparate solid volume ratio heat sinks (Case 6 & 7):

In these cases, solid1 and solid2 material volumes are constrained at a ratio of 8:32. These cases relate to economic heat sink design with a small fraction of highly conductive solid used along with a low cost medium conductivity solid. So the results yield economic, water cooled heat sink shapes. Results obtained for case6 and case7 are shown in Figures 8-9 and 8-10 respectively.

The results show that in spite of very low usage of highly conductive copper, these two material heat sinks are performing on par with a single material copper heat sink of the same material volume. The maximum temperature of the disparate solid volume Cu-Al heat sink is only 1.3°K higher than the single material Cu heat sink, and on similar lines, the maximum temperature of the Cu-steel heat sink is only 3.5°K higher than the Cu heat sink. This point proves the heat dissipation capability of multi-material heat sinks. Another point to be noted is, the shape of disparate volume ratio heat sinks are quite similar to equal solid volume ratio heat sinks, but only the copper has taken a thinner shape now.



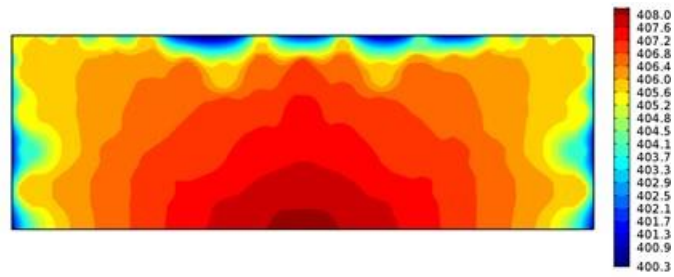


Figure 8- 9 Optimised shapes and its temperature contour for case6

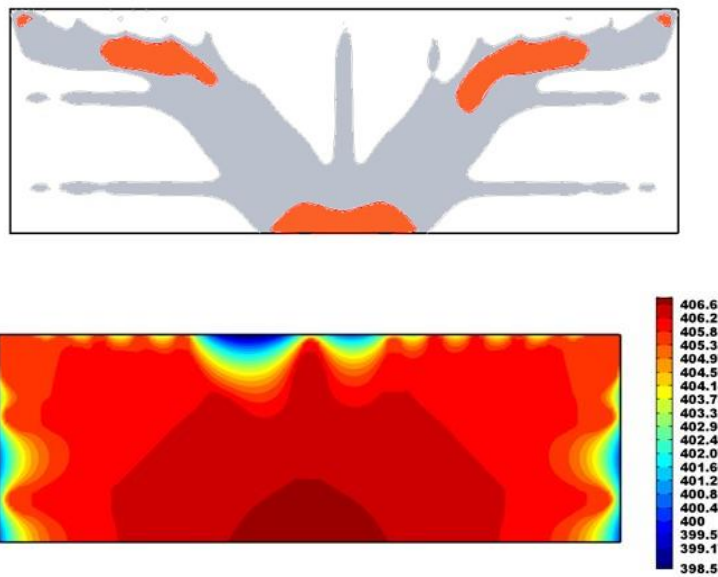


Figure 8- 10 Optimised shapes and its temperature contour for case7

The results obtained for the LS TO depend on the initial LS distribution, indicating that many local minima appear to be present. So the shapes have to be investigated further to determine the global optima.

**Two material heat sinks for high conductivity fluid (Case4 &5):**

Two optimisations are carried out with fluid thermal conductivity of 4 W/(mK), to study the effect of solid-to-fluid thermal conductivity ratio. Since the fluid conductivity is increased, the convective heat transfer is expected to play a significant role in these cases. The results obtained are shown in Figure 8-11 and 8-12.

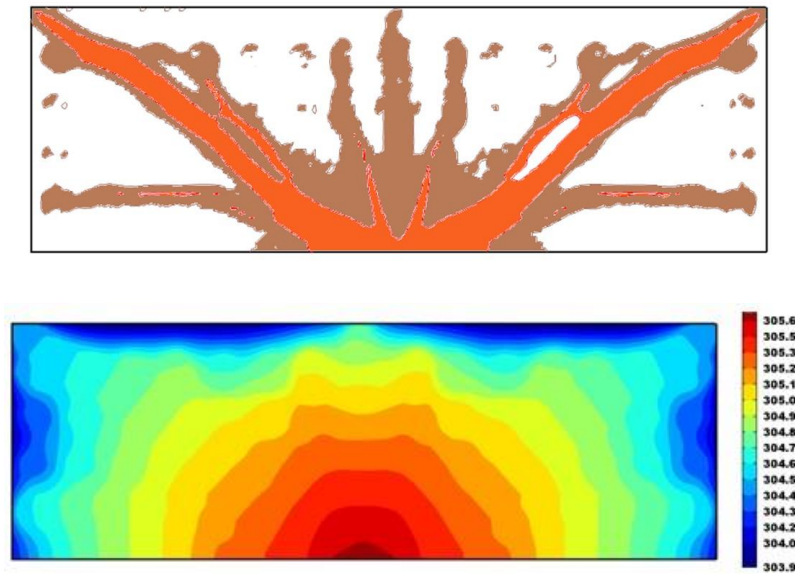


Figure 8- 11 Optimised shape and its temperature contours for case4

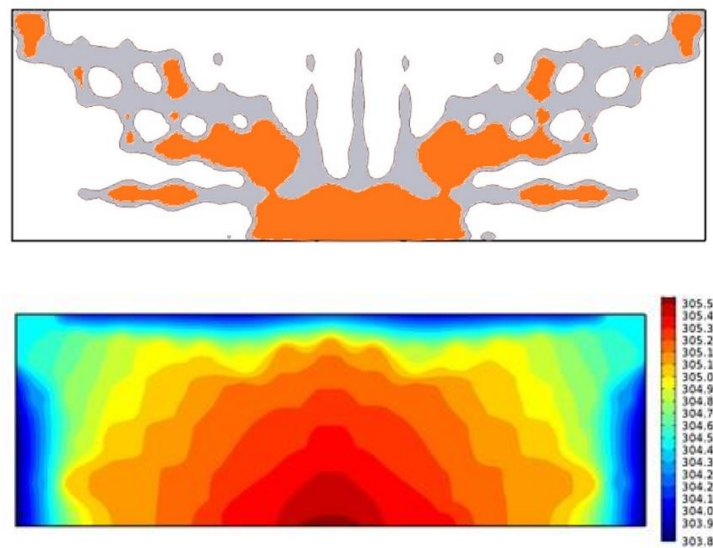


Figure 8- 12 Optimised shape and its temperature contour for case5

These heat sinks tend to have more flat base than the other cases. The optimised shape obtained for case5 is non-intuitive in nature with highly conductive solid placed at specific places discretely and fluid gaps are present within the heat sink structure.

### Three material heat sink:

The three solid material heat sink design is carried out considering copper, aluminium and steel. The volume of 3 solids are constrained at 6, 12 and 22% of design domain

volume. The volume constraint of copper is minimum in order to make the heat sink cost minimum. The heat sink shape is shown in Figure 8-13. From Table 8-4 it can be observed that the maximum temperature of 3 material heat sink is only 1°K higher than the single material heat sink, in spite of using only 6% copper. This is a remarkable result which shows that multi-material heat sinks are very effective in heat dissipation and yet can be made very cheaply by using small quantities of costly, high conductivity material.

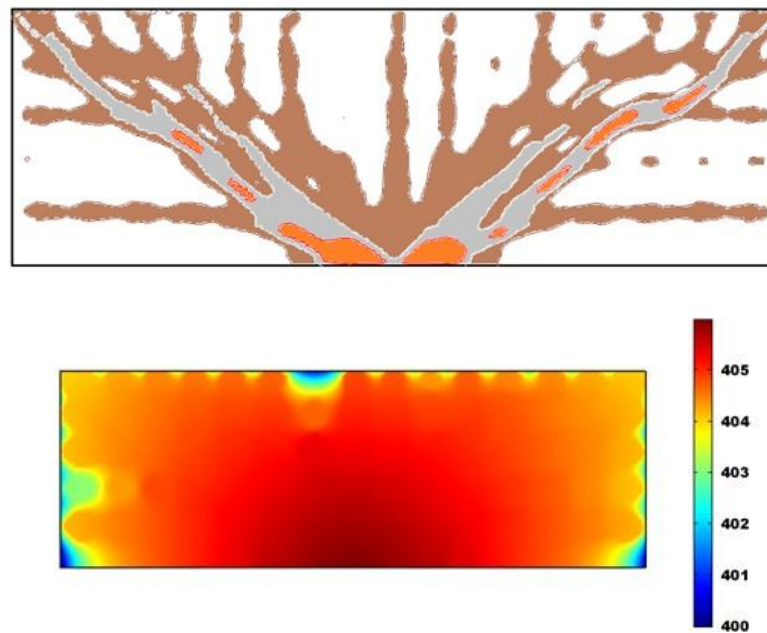


Figure 8- 13 Optimised shape and its temperature contour for case8

### 8.6 Three dimensional study results:

Results obtained for three dimensional two-material optimisation study are compared with single material (Cu) heat sink optimisation results (Case 1) already reported in section 7.4.3. The optimised shape is reproduced in Figure 8-14, for ease of comparison. Each 3D optimisation run takes about 140 hours (for 75 iterations) on ten real cores/twenty hyper threaded cores on a Dual Xeon CPU cluster node, while 2D runs take about 7 hours on the same machine for 600 iterations. Table showing the details of different 3D TO carried out is given in Table 8-5.

#### **Two material (copper, aluminium) heat sink (Case 2&3):**

The three dimensional, two material (Cu-Al) heat sink design is carried out with 2 different initial LSF set-ups. In the first set-up (A), solid1 is considered as copper and

solid2 is considered as aluminium/steel. In the second set-up (B) solid1 and solid2 materials are swapped. That is, solid1 is considered as aluminium/steel and solid2 is considered as copper; this is illustrated in the Figure 8-15.

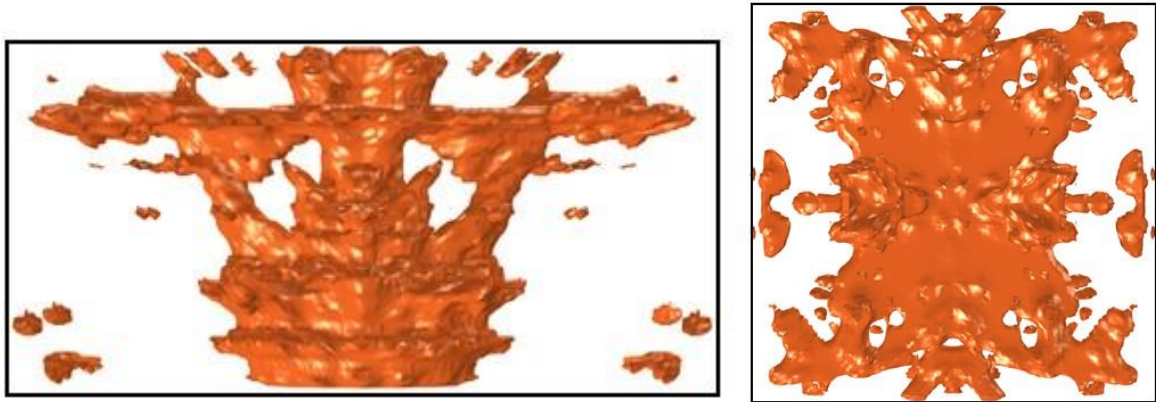


Figure 8- 14 Optimised shape of single material (Cu) 3D heat sink (Front view & Top view) (Case1)

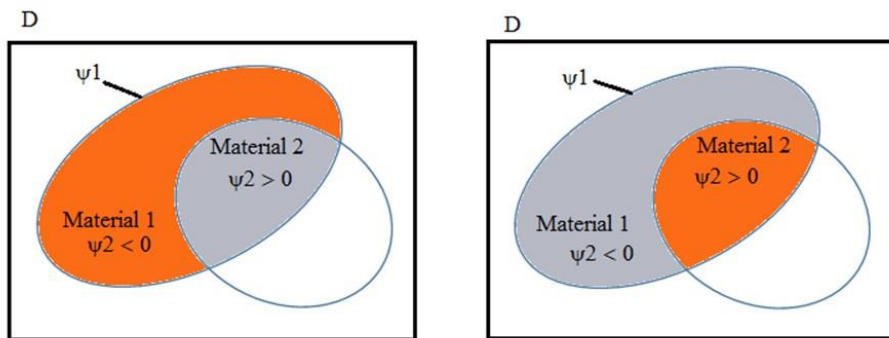


Figure 8- 15 Illustration of initial set-up 'A' (left, Case2) and initial set-up 'B' (right, Case3)

The optimised two material (Cu-Al) heat sink shape for initial setup 'A' and 'B' are given in Figure 8-16 and 8-17 respectively. It can be observed that, for set-up 'A', the low conductivity aluminium has occupied the region above the heat flux boundary and high conductivity copper has branching structure connecting the aluminium boundary with all corners of the design domain. This shape is quite opposite to the heat sink shape obtained for initial set-up 'B', where copper is placed on top of the heat source and aluminium is distributed everywhere (Figure 8-17). In the figure, for the sake of clarity, the layout/shape of aluminium and copper are separately visualised then a complete view of Cu-Al heat sink is also provided.

The thermal compliance, maximum temperature and rise in temperature relative to the ambient temperature (293.15K) in the design domain for these two shapes are listed

in Table 8-5. Comparison shows that the shape of setup 'B' is the best optimised shape compared to that of setup 'A'. The maximum temperature of setup 'B' shape is 0.6°K lower than the setup 'A' shape.

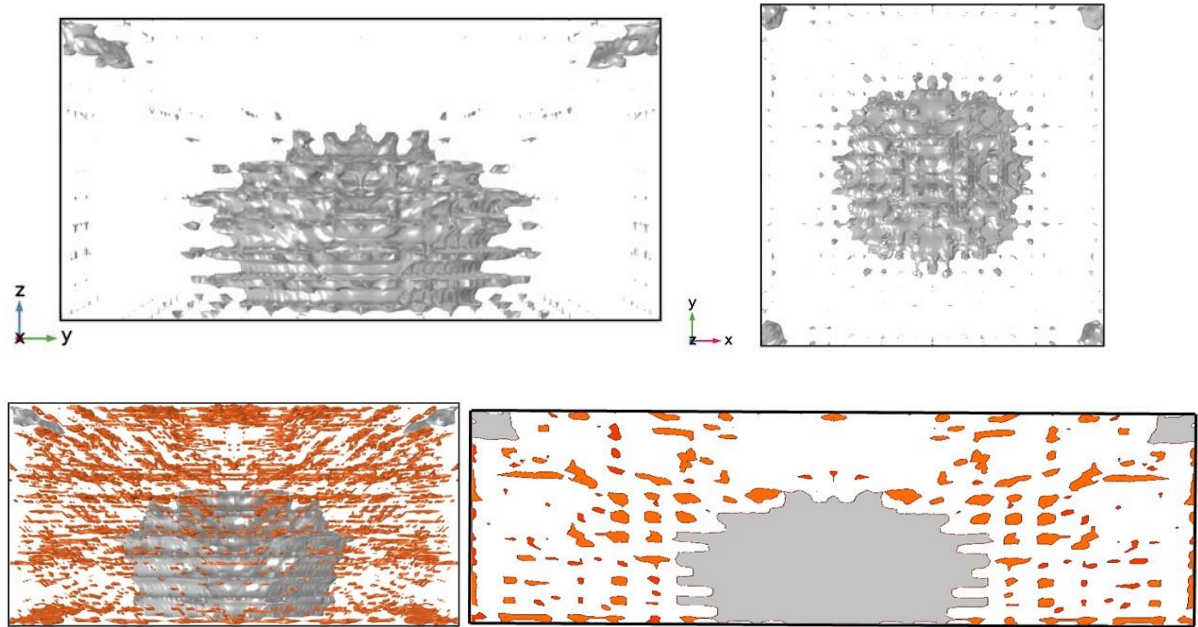


Figure 8- 16 Optimised copper-aluminium heat sink shape for set-up 'A' (Case2). Top row: Front & topview of Al layout; Bottom row: Complete view and diagonal plane view of Cu-Al heat sink

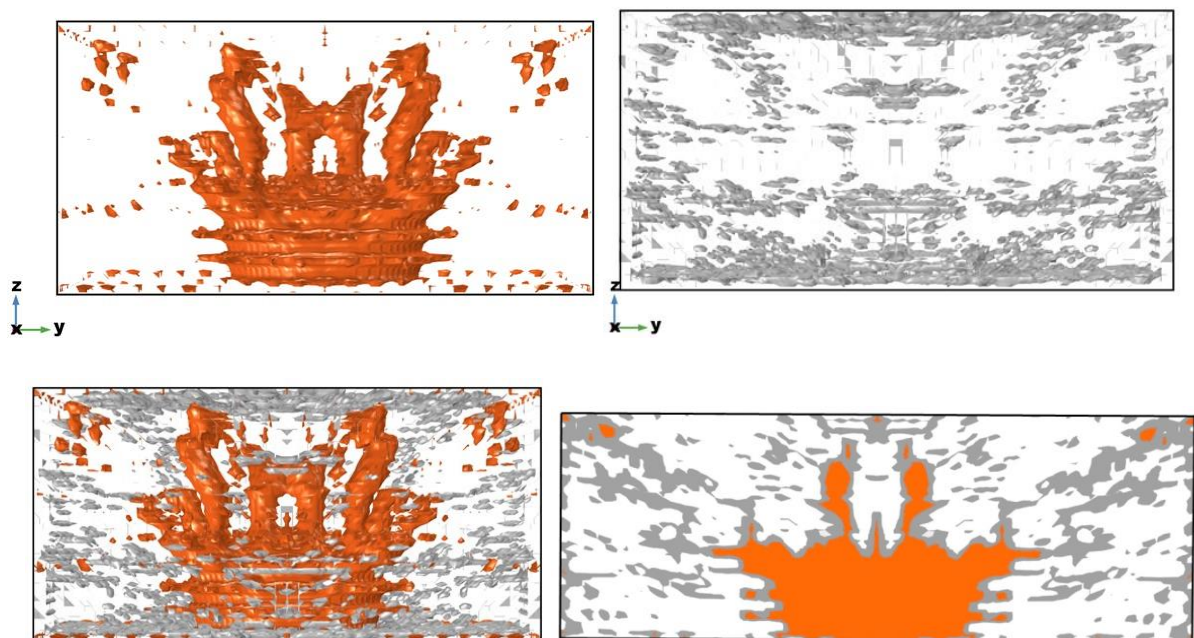


Figure 8- 17 Optimised copper-aluminium heat sink shape for set-up 'B' (Case3). Top row: Copper layout and aluminium layout; Bottom row: Complete view & diagonal plane view of Cu-Al heat sink.

Case Name	Description	Thermal Conductivities	Volume Fraction	Thermal Compliance (WK)	Maximum Temperature (K)	Temperature Rise (Max. Temperature-Ambient Temperature) (K)
Case1	Single material	400, 0.4	0.25	2.300	316.5	23.35
Case2	Cu-Al (setup A)	400, 200, 0.4	0.10,0.15	3.52	317.1	23.95
Case3	Cu-Al (setup B)	400,200, 0.4	0.10,0.15	2.16	316.5	23.35
Case4	Cu-Steel (setup A)	400, 40, 0.4	0.10,0.15	13.91	321.8	28.65
Case5	Cu-Steel (K <sub>f</sub> =4,80kW) setup B	400, 40, 4	0.10,0.15	42.60	306.8	13.65

Table 8- 5 3D multi-material heat sink design results

### **Two material (copper, steel) heat sink (Case 4 & 5):**

The optimised heat sink shape for the copper-steel combination with initial set-up 'A' is shown in Figure 8-18. The shape is similar to the copper-aluminium heat sink of setup 'A', but with some minor differences. The centre part of the steel heat sink is thicker and shorter than the aluminium and this is because steel is less conductive material than aluminium. Copper takes a prominent disk like shape near the top region. Since the conductivity of steel is less, the optimiser tries to improve the convective cooling (by forming a thicker disk near the top surface) to maximise the heat dissipation capability of the heat sink. The design of a copper-steel heat sink with the initial setup 'B' could not be successfully completed, as the optimisation failed in the Comsol flow solver. Porosity modelling used for the topology optimisation also complicates the flow solution.

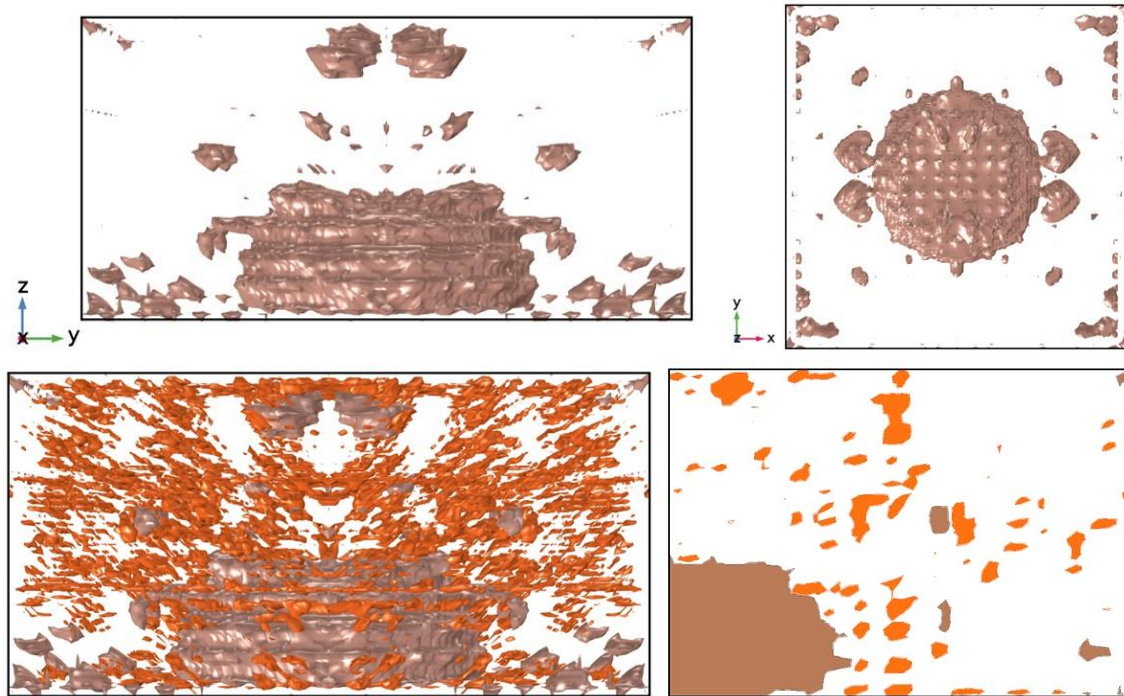


Figure 8- 18 Optimised copper-steel heat sink shape for set-up 'A'(Case4). Top row: Front & topview of steel; Bottom row: Complete view and diagonal plane view of Cu-steel heat sink.

In order to make the problem more benign and solvable, fluid thermal conductivity is increased from  $0.4\text{W}/(\text{mK})$  to  $4\text{W}/(\text{mK})$ . The fluid considered, is a fictitious one, chosen mainly for academic interest. Results obtained for this case are shown in Figure 8-19. With setup 'B', copper occupies the centre region on top of the heat source (as in copper-aluminium case with set-up 'B') and steel takes the disk-like shape on top and also branches are formed connecting the copper part with the top disk. Since the fluid conductivity is higher in this case, convective heat transfer is significant hence, the copper takes a shorter shape.

The maximum temperature in the design domain for copper-steel heat sink of setup 'A' is  $5.3^\circ\text{K}$  higher than the single material copper heat sink. If optimisation for setup 'B' was successful, it might have given much lower maximum temperature than setup 'A' case, because for copper-aluminium heat sink design, setup 'B' has produced better shape than setup 'A'.

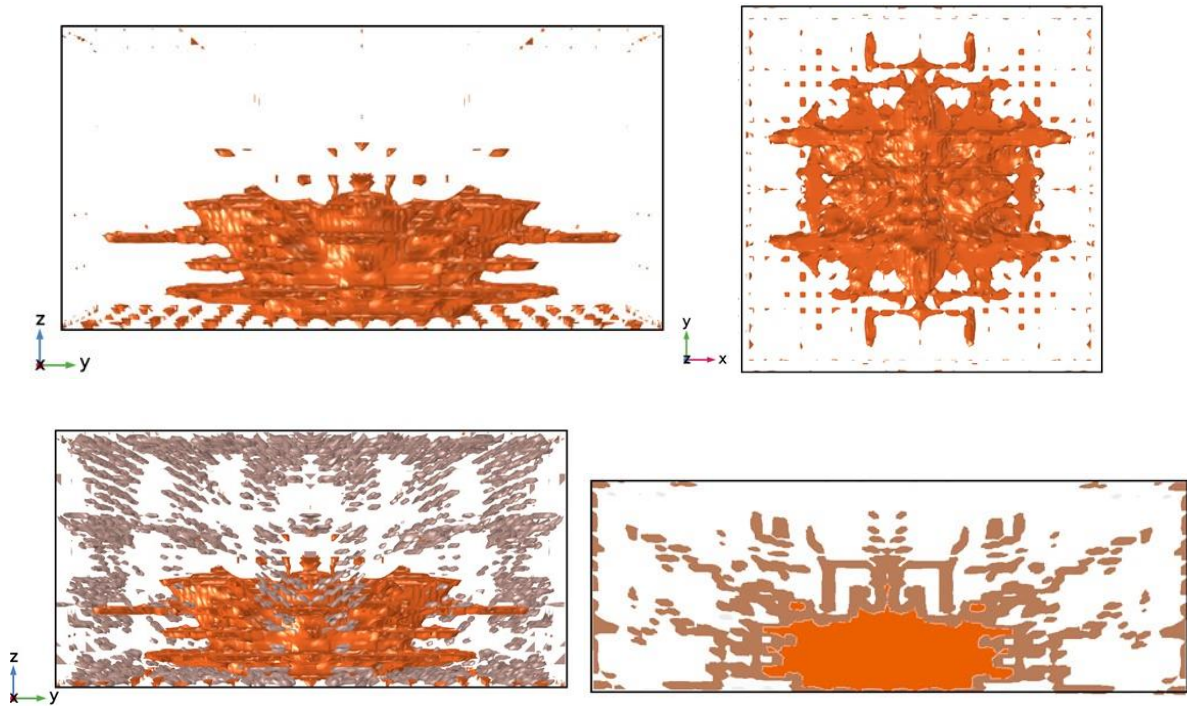


Figure 8- 19 Optimised copper-steel heat sink for high conductivity fluid with initial set-up 'B' (Case5). Top row: Copper front & top view; Bottom row: Complete view and diagonal plane view of Cu-steel heat sink.

### Discussions:

The study shows that for 3D applications, two material Cu-Al heat sink performance is equivalent to that of single material copper heat sink. Hence by the two-material heat sink design, copper of 15% design domain volume can be saved and instead the same volume of a cheaper material like aluminium or steel can be used. This will definitely lead to considerable cost reduction provided manufacturing technology enables this at a nominal cost.

The optimised 3D heat sink shape had few disconnected (porous) solid regions. Practically, these are unsupported solid mass hence not manufacturable. Formation of these isolated (porous) solid regions could be avoided by optimising for a relaxed objective function. Purpose of these isolated regions is to minimise the thermal compliance further, so by optimising for a shape corresponding to a relatively higher objective value, then a connected shape – free from isolated regions, can be obtained. Alternatively, regularisation techniques such as perimeter filtering [114], Tikhonov regularization [17] or sensitivity filtering [72] could be integrated into the algorithm.

Further, it is observed that Heaviside functions,  $H1 \cdot H2$  and  $H1 \cdot (1 - H2)$  are taking intermediate values between 0 and 1 and this led to slight in-accuracy in the material

boundary definition. This could be avoided by further refining the design domain mesh and by frequent re-initialisations. But due to the limitation on computational resources available, much finer meshes are not studied.

## 8.7 Summary

The design of two and three solid material convectively cooled heat sinks is carried out at low Reynolds numbers for minimum thermal compliance objective. The optimisation is carried out for different solid-solid and solid-fluid thermal conductivity ratios. Overall, the study results show that, the heat dissipation capability of a single material (copper) heat sink is achievable by a multi-material heat sink even with very low percentage use of copper in it.

The two material two dimensional Cu-Al heat sink has a smooth branched structure extending from the heat source location to the farthest corners of the design domain. Whereas in the copper-steel heat sink, copper takes a branching structure and steel is mostly distributed surrounding the copper, on top of the heat source location.

In the 3D study, the single material copper heat sink shape approximately resembles an inverted 'filled-wine glass'. The disk-like shape near the top side of the design domain enhances the convective cooling. In two material 3D heat sink, high conductivity solid (copper) takes a branching structure on top of the heat flux boundary. The low conductivity solid (aluminium/steel) forms a disk like shape near the top of the design domain and also connects the copper structure with the disk. The two material Cu-Al heat sink performance is exactly equivalent to the single material copper heat sink inspite of using 15% less copper. If a technology enables the manufacture of these designs, considerable cost reduction can be achieved by saving the high conductivity, costly materials.

Since the study minimises only thermal compliance and does not consider convective cooling, the shapes may not be the optimal for high Reynolds number flows where convective cooling will be predominant.

To summarise, the multi-material heat sink design technique opens the possibility of using copper at minimal amounts in combination with aluminium or steel to enhance its performance while keeping the cost low.

## 9 Conclusions and Future Work

In this study, after assessing the performance of two popular TO methods, a numerical model for better performing TO method, for fluid flow and heat transfer application, has been developed. Using this framework, heat recovery channels and the novel multi-material convectively cooled heat sinks are designed.

Two popular topology optimisation methods namely the Density method and Level-set method (coupled formulation) are assessed for the quality of design results, computational time and robustness by designing 3 dimensional convectively cooled heat sinks. The results have shown that both the methods with their basic numerical formulation gave optimised shapes with grey cells. Among them, the level-set method yields a better quality design and the density method is found to be more robust in yielding the results. Because the LS with re-initialisation captures crisp material boundaries and is less susceptible to flow instabilities at moderate and high Reynolds numbers, the level-set method is chosen and the numerical framework for this technique is developed further.

The level-set TO numerical framework is based on the HJ equation for advecting the level-sets and it uses the density-based material mapping. The framework is developed in Matlab and it uses Comsol for solving the PDE equations of physics. The following state-of-the-art features are implemented in the level-set numerical model.

1. The re-initialisation of level-sets by solving Eikonal equations.
2. Adjoint based shape sensitivity evaluation for NS and energy equations.
3. Topology derivative based optimisation.
4. Capability for handling multi-material topology optimisation problems.

Using the developed LS TO numerical framework, heat recovery channels and multi-material convectively cooled heat sinks are designed.

### **Heat recovery channels design:**

The heat recovery channel design which requires heat recovery maximisation without penalising the pump pressure requirements was carried out for different solid-to-fluid thermal conductivity ratios and flow Reynolds numbers. The optimisation studies are

carried out in 2D and in 3D and the effect of Reynolds number, conductivity ratio and objective function weightage factor on the channel shape are critically studied. Further, heat transfer model is fully solved in this study, without resorting to simplified convective cooling models.

As the flow Reynolds number is increased, the heat recovery and temperature drop are decreasing. But at high Re, the optimised shape has more number of lengthy flow channels than at low Reynolds number. In the  $k_s/k_f=1$  case, increasing the thermal conductivity of the material leads to increase in heat recovery of the channel. Since, the porosity approach is used for solid modelling, the optimiser distributes (porous) solid at the inlet and outlet to reduce the flow velocity and thereby to increase the heat exchange. This may not be a practically suitable design solution and it is one of the drawbacks of the porosity approach.

#### **Multi-material convectively cooled heat sink design:**

Multi-material convectively cooled heat sinks are designed for the minimum thermal compliance objective at low Reynolds numbers. This study envisions the design of heatsinks using copper and aluminium or copper and steel at right proportions to achieve excellent cooling performance while keeping the cost low.

The optimisation is carried out for different solid-fluid material conductivities and volume constraints in 2D and 3D. The thermal conductivity ratio of solid-to- solid and solid-to-fluid play a significant role in the shape of the final optimum. The study shows that, even with very low percentage use of the high conductivity material (copper), the multi-material heat sinks can perform equivalent to the single material copper heat sinks. So, for the same heat dissipation capability, the amount of high cost copper used can be decreased leading to cost reduction of the heat sinks.

This research study has significantly broadened the understanding of the application of topology optimisation to fluid flow and heat transfer problems. Further study is still necessary to approach a wide range of heat exchanger design problems.

#### **Future work:**

The following can be taken as an extension of the present study.

- It is observed that during the convectively cooled heat sink design, the optimiser yields designs with isolated (porous) solid regions. Though theoretically this may reduce the thermal compliance of the design domain, practically these heat sinks are not manufacturable. Hence, to avoid this, regularisation or thin feature control mechanism has to be implemented in the numerical framework.
- The topology optimisation field is rapidly growing and a number of researchers are working on coupled fluid flow and heat transfer problems. So, soon the design of industrial heat exchanger problem has to be handled. For this a turbulent flow optimisation capability has to be implemented. Turbulent flows call for increased mesh refinement near the solid walls hence these optimisation runs will involve increased computational cost.
- In relation to the preceding point, currently solved optimisation problems are benign (well-posed) problems. The material properties are so chosen that the optimiser runs without divergence and yields a well-defined optimum solution. Therefore, to handle industrial geometries and materials, the optimisation algorithm needs to be improved and made more robust, to handle a wider range of problems.
- All of the topology optimisations were carried out using the density-based material mapping method and hence the solids created are porous solids. A drawback of this method is that, no-slip condition cannot be properly imposed on the solid walls and there will be pressure diffusion across the solid walls. The LS method with an xFEM mapping is free from these disadvantages, hence implementation of an xFEM mapping would be a natural future extension of this study.
- In this study, the augmented Lagrangian method is used for the level-set optimisation. It is observed that, for the multi-material optimisation problem, the rate of convergence of this method is very low and it takes approximately 600 iterations (for 2D problem) to yield a converged solution. Hence, it is necessary to develop a numerical strategy to increase the convergence rate of this method.
- The optimisation work can be extended to the design of heat exchangers like shell and tube heat exchanger, and co-flow and counter flow heat exchangers.

## 10 References

- [1] Z. Luo, "A Short Survey: Topological Shape Optimization of Structures Using Level Set Methods," *Journal of Applied Mechanical Engineering*, vol. 2, no. 2, 2013.
- [2] L. Frattari, "The Structural Form : Topology Optimization in Architecture and Industrial Design," Altair engineering.
- [3] T. Borrvall and J. Petersson, "Topology optimisation of fluids in Stokes flow," *International Journal of Numerical Methods in Fluids*, vol. 41, no. 1, p. 77–107, 2003.
- [4] X. Duan, Y. Ma and R. Zhang, "Shape-topology optimisation for Navier–Stokes problem using variational level set method.," *Journal of Computational and Applied Mathematics* , vol. 222, p. 487–499, 2008;.
- [5] C. Othmer, "A continuous adjoint formulation for the computation of topological and surface sensitivities of ducted flows," *International Journal of Numerical methods in fluids*, vol. 58, pp. 861-877, 2005.
- [6] O. Sigmund and S. Torquato, "Design of materials with extreme thermal expansion using a three-phase topology optimization method," *Journal of Mechanics and Physics of Solids*, vol. 45, no. 6, p. 1037–1067, 1997.
- [7] M. Y. Wang and X. Wang, "Color level sets: a multi-phase method for structural topology optimization with multiple materials," *Computer methods in Applied Mechanics and Engineering*, vol. 193, pp. 469-496, 2004.
- [8] M. Bendsoe and N. Kikuchi, "Generating optimal topologies in structural design using a homogenization method.," *Computer Methods in Applied Mechanics and Engineering*, vol. 71(2), p. 197–224, 1988.

- [9] M. Bendsoe, "Optimal shape design as a material distribution problem," *Structural Optimization*, vol. 1, p. 193–202, 1989.
- [10] O. Sigmund, "A 99 line topology optimisation code written in MATLAB," *Structural and Multidisciplinary Optimization*, vol. 21, p. 120–127, 2001.
- [11] L. Osher and J. Sethian, "Fronts propagating with curvature dependent speed : algorithms based on Hamilton-Jacobi formulations.," *Journal of Computational Physics*, Vols. 79,, 1988.
- [12] S. Osher and F. Santosa, "Level-set methods for optimisation problems involving geometry and constraints: frequencies of a two density inhomogeneous drum," *Journal of Computational Physics*, vol. 171, p. 272–288, 2001.
- [13] J. Sethian and A. Wiegmann, "Structural boundary design via level-set and immersed interface methods," *Journal of Computational Physics*, vol. 163, p. 489–528, 2000.
- [14] G. Allaire, F. Jouve and A. Toader, "Structural optimisation using sensitivity analysis and a level-set method," *Journal of Computational Physics*, vol. 194, no. 1, p. 363–393, 2004.
- [15] M. Wang, X. Wang and D. Guo, "A level set method for structural topology optimisation," *Computer Methods in Applied Mechanics and Engineering*, vol. 192, p. 227–246, 2003.
- [16] G. Allaire, F. Gournay, F. Jouve and A. Toader, "Structural optimisation using topological and shape sensitivity via a level set method," *Control and Cybernetics*, vol. 34, no. 1, pp. 59-80, 2005.
- [17] T. Yamada, K. Izui and S. Nishiwaki, "Topology optimization method based on the level set method incorporating a fictitious interface energy," *Computer Methods in Applied Mechanics and Engineering*, vol. 199, no. 45-48, pp. 2876-2891, 2010.

- [18] . H. Eschenauer, V. Kobelev and A. Schumacher, "Bubble method for topology and shape optimisation of structures," *Structural Optimization*, vol. 8, p. 42–51, 1994.
- [19] S. Amstutz, "Connections between topological sensitivity analysis and material interpolation schemes in topology optimisation.," *Structural and Multidisciplinary Optimization*, vol. 43, no. 6, p. 755–765, 2011.
- [20] O. Sigmund and K. Maute, "Topology optimisation approaches: A comparative review," *Structural and Multidisciplinary Optimization*, vol. 48, pp. 1031-1055, 2013.
- [21] A. Takezawa, S. Nishiwaki and M. Kitamura, "Shape and topology optimisation based on the phase field method and sensitivity analysis," *Journal of Computational Physics*, vol. 229, pp. 2697-2718, 2010.
- [22] A. Gain and G. Paulino, "Phase field based topology optimisation with polygonal elements: a finite volume approach for the evolution equation," *Structural and Multidisciplinary Optimization*, vol. 46, pp. 327-342, 2012.
- [23] G. Rozvany, "A critical review of established methods of structural topology optimisation," *Structural and Multidisciplinary Optimization*, vol. 37, pp. 217-237, 2009.
- [24] Y. Xie and G. Steven, "A simple evolutionary procedure for structural optimization," *Computers and Structures*, vol. 49, pp. 885-896, 1993.
- [25] O. Querin, G. Steven and Y. Xie, "Evolutionary structural optimization (ESO) using a bi-directional algorithm," *Engineering computations*, vol. 15, pp. 1031-1048, 1998.
- [26] C. Jog, "Topology design of structures subjected to periodic loading.," *Journal of Sound and Vibrations*, vol. 253, no. 1, p. 687–709, 2002.
- [27] O. Sigmund, "On the design of compliant mechanisms using topology optimisation," *Mechanics of Structures and Machines*, vol. 25, p. 493–524, 1997.

- [28] J. Deaton and R. Grandhi, "A survey of structural and multidisciplinary continuum topology optimisation: post 2000," *Structural and Multidisciplinary Optimization*, vol. 49, pp. 1-38, 2014.
- [29] L. Olesen, F. Okkels and H. Bruus, "A high-level programming-language implementation of topology optimisation applied to steady-state Navier-Stokes flow.," *International Journal for Numerical Methods in Engineering* , vol. 65 , no. 7, p. 957–1001, 2006.
- [30] Y. Deng, Z. Liu, P. Zhang, Y. Liu and Y. Wu, "Topology optimization of unsteady incompressible Navier-Stokes flows," *Journal of Computational Physics*, vol. 230, pp. 6688-6708, 2011.
- [31] E. Dede, "Multiphysics topology optimisation of heat transfer and fluid flow systems," in *Proceedings of the COMSOL Conference*, Boston, 2009.
- [32] G. H. Yoon, "Topological design of heat dissipating structure with forced convective heat transfer," *Journal of Mechanical Science and Technology* , vol. 24, no. 6, p. 1225–1233, 2010.
- [33] A. A. Koga, E. C. C. Lopes and H. F. V. Nova, "Development of heat sink device by using topology optimisation.," *International Journal of Heat and Mass Transfer*, vol. 64, pp. 759-772, 2013.
- [34] F. H. Burger, J. Dirker and J. P. Meyer, "Three dimensional conductive heat transfer topology optimisation in a cubic domain for the volume to surface problem," *International Journal of Heat and Mass Transfer*, vol. 67, pp. 214-224, 2013.
- [35] T. V. Oevelen and M. Baelmans, " Numerical topology optimisation of heat sinks," in *Proceedings of the 15th International Heat Transfer Conference, IHTC*, Japan, 2014.
- [36] J. Alexandersen, N. Aage, A. C. S and O. Sigmund, "Topology optimization of natural convection problems," *International Journal for Numerical Methods in Fluids*, vol. 00, pp. 1-23, 2013.

- [37] J. Alexandersen, O. Sigmund and N. Aage, "Large scale three dimensional topology optimisation of heat sinks cooled by natural convection," *International Journal of Heat and Mass Transfer*, vol. 100, pp. 976-891, 2016.
- [38] J. Alexandersen, "Topology optimisation for coupled convection problems," 2013.
- [39] T. Matsumori, T. Kondoh, A. Kawamoto and T. Nomura, "Topology optimisation for fluid-thermal interaction problems under constant input power," *Structural and Multidisciplinary optimization*, vol. 47, pp. 571-581, 2013.
- [40] J. H. K. Haertel, K. Engelbrecht, B. S. Lazarov and O. Sigmund, "Topology optimization of thermal heat sinks," in *Comsol conference*, Grenoble, France, 2015.
- [41] J. H. K. Haertel and G. F. Nellis, "A fully developed flow thermofluid model for topology optimisation of 3D printed air cooled heat exchangers," *Applied thermal engineering*, vol. 119, pp. 10-24, 2017.
- [42] A. Pizzolato, A. Sharma and e. al, "Topology optimization for heat transfer enhancement in Latent Heat thermal energy storage," *International Journal of Heat and Mass transfer*, vol. 113, pp. 875-888, 2017.
- [43] J. Alexandersen, O. Sigmund and K. E. Meyer, "Design of passive coolers for light-emitting diode lamps using topology optimisation," *International Journal of Heat and Mass transfer*, vol. 122, pp. 138-149, 2018.
- [44] M. Zhou, J. Alexandersen and O. Sigmund, "Industrial application of topology optimization for combined conductive and convective heat transfer problems," *Structural and Multidisciplinary optimization*, vol. 54, pp. 1045 -1060, 2016.
- [45] C. B. Dilgen, S. B. Dilgen, D. R. Fuhrman and O. Sigmund, "Topology optimisation of turbulent flows," *Computer Methods in Applied Mechanics and Engineering*, vol. 331, pp. 363-393, 2018.

- [46] T. Dbouk, "A review about the engineering design of optimal heat transfer systems using topology optimisation," *Applied thermal engineering*, vol. 112, pp. 841-854, 2017.
- [47] V. Challis, "A discrete level-set topology optimisation code written in Matlab," *Structural and Multidisciplinary Optimisation*, vol. 41, p. 453–464, 2010.
- [48] Z. Liu, J. G. Korvink and R. Huang, "Structure topology optimisation: fully coupled level set method via FEMLAB," *Structural and Multidisciplinary Optimisation*, vol. 29, p. 407–217, 2005.
- [49] A. Kawamoto, T. Matsumori, T. Nomura, T. Kondoh, S. Yamasaki and S. Nishiwaki, "Topology optimisation by a time dependent diffusion equation," *International Journal for Numerical methods in Engineering*, vol. 93, pp. 795-817, 2013.
- [50] S. Zhou and Q. Li, "A variational level set method for the topology optimisation of steady-state Navier–Stokes flow," *Journal of Computational Physics* , vol. 227, p. 10178–10195, 2008.
- [51] V. Challis and J. K. Guest, "Level set topology optimisation of fluids in Stokes flow," *International Journal of Numerical Methods in Engineering*, vol. 79, no. 10, p. 1284–1308, 2009.
- [52] S. Kreissl and K. Maute, "Level set based fluid topology optimisation using the extended finite element method," *Structural and Multidisciplinary Optimisation*, vol. 46, no. 3, p. 311–326, 2012.
- [53] Y. Deng, Z. Liu, J. Wu and Y. Wu, "Topology optimisation of steady Navier Stokes flow with body force," *Computer methods Applied Mechanical Engineering*, vol. 255, pp. 306-321, 2013.
- [54] Y. Deng, P. Zhang, Y. Liu, Y. Wu and Z. Liu, "Optimization of unsteady incompressible Navier-Stokes flow using variational level set method," *International Journal of Numerical Methods for Fluids*, vol. 71, pp. 1475-1493, 2013.

- [55] M. Burger, B. Hackl and W. Ring, "Incorporating topological derivatives into level set methods," *Journal of Computational Physics*, vol. 194, pp. 344-362, 2004.
- [56] A. S. Zymaris, D. I. Papadimitriou, K. C. Giannakoglou and C. Othmer, "Continuous adjoint approach to the Spalart–Allmaras turbulence model for incompressible flows," *Computers & Fluids*, vol. 38, no. 8, p. 1528–1538, 2009.
- [57] E. M. Papoutsis-Kiachagias, E. A. Kontolentos, A. S. Zymaris, D. I. Papadimitrou and K. C. Giannakoglou, "Constrained topology optimization for laminar and turbulent flows including heat transfer," in *EDMDOC conference*, Italy, 2011.
- [58] E. A. Kontoleontos, E. M. Papoutsis-Kiachagias and A. S. Zymaris, "Adjoint-based constrained topology optimization for viscous flows including heat transfer," *Engineering Optimization*, vol. 45, no. 8, pp. 941-961, 2013.
- [59] E. M. Papoutsis-Kiachagias and K. C. Giannakoglou, "Continuous Adjoint methods for Turbulent flows, Applied to shape and topology optimisation: Industrial Applications," *Archives of Computational Methods Engg*, vol. 23, pp. 255-299, 2016.
- [60] G. K. Karpouzas and E. D. Villiers, "Level set based topology optimisation using continuous adjoint method," in *ICEASO conference*, Greece, 2014.
- [61] G. H. Yoon, "Topology optimization for turbulent flow with Spalart-Allmaras model," *Computer Methods in Applied Mechanics and Engineering*, vol. 303, pp. 288-311, 2016.
- [62] T. Yamada, K. Izui and S. Nishiwaki, "A level set based topology optimisation method for maximizing thermal diffusivity in problems including design dependent effects," *Journal of Mechanical design*, vol. 133, 2011.
- [63] K. Yaji, T. Yamada, S. Kubo and S. Nishiwaki, "A topology optimisation method for a coupled thermal-fluid problem using level set boundary expressions," *International Journal of Heat and Mass transfer*, vol. 81, pp. 878-888, 2015.

- [64] P. Coffin and K. Maute, "Level set topology optimisation of cooling and heating devices using a simplified convection model," *Structural and multidisciplinary optimisation*, vol. 53, no. 5, pp. 985-1003, 2016.
- [65] P. Coffin and K. Maute, "A level-set method for steady-state and transient natural convection problems," *Structural and Multidisciplinary Optimization*, vol. 53, no. 5, pp. 1047-1067, 2016.
- [66] K. Yaji, T. Yamada, M. Yoshino, T. Matsumoto, K. Izui and S. Nishiwaki, "Topology optimization in thermal-fluid flow using the lattice Boltzmann method," *Journal of Computational Physics*, vol. 307, pp. 355-377, 2016.
- [67] C. Zhuang, Z. Xiong and H. Ding, "Topology optimization of multi-material for the heat conduction problem based on the level set method," *Engineering Optimization*, vol. 42, no. 9, pp. 811-831, 2011.
- [68] Y. Wang, Z. Luo and Z. Kang, "A multi-material level set based topology and shape optimisation method," *Computer Methods in Applied Mechanics and Engineering*, vol. 283, pp. 1570-1586, 2015.
- [69] Q. Li, G. Steven, Y. Xie and O. Querin, "Evolutionary topology optimization for temperature reduction of heat conducting fields," *International Journal of Heat and Mass Transfer*, vol. 47, pp. 5071-5083, 2004.
- [70] R. Bornoff and J. Parry, "An additive design heat sink geometry topology identification and optimisation methodology," in *SEMI-THERM Conference*, San Jose, 2015.
- [71] R. Bornoff, J. Wilson and J. Parry, "Subtractive design: A novel approach to heatsink improvement," in *SEMITHERM Conference*, San Jose, 2016.
- [72] O. Sigmund and J. Petersson, "Numerical instabilities in topology optimisation: a survey on procedures dealing with checker-boards, mesh-dependencies and local minima.," *Structural Optimization*, vol. 16:, p. 68–75, 1998.

- [73] M. Stolpe and K. Svanberg, "An alternative interpolation scheme for minimum compliance topology optimization," *Structural and Multidisciplinary Optimization*, vol. 22, pp. 116-124, 2001.
- [74] F. vanKeulen, R. T. Haftka and N. H. Kim, "Review of options for structural design sensitivity analysis. Part 1: linear systems.," *Computer Methods in Applied Mechanics and Engineering*, vol. 194(30–33), p. 3213–3243, 2005.
- [75] D. A. Tortorelli and P. Michaleris, "Design sensitivity analysis: Overview and Review," *Inverse problems in Engineering*, vol. 1, no. 1, 1994.
- [76] T. E. Bruns and D. A. Tortorelli, "Topology optimisation of non-linear elastic structures and compliant mechanisms," *Computer methods in Applied Mechanics and Engineering*, vol. 190, pp. 3443-3459, 2001.
- [77] J. Guest, J. Prevost and T. Belytschko, "Achieving minimum length scale in topology optimisation using nodal design variables and projection functions," *International Journal of Numerical Methods in Engineering*, vol. 61, no. 2, p. 238–254, 2004.
- [78] A. Jameson, "Aerodynamics shape optimization using the Adjoint method," Lectures at the Von Karman Institute, Brussels, 2003.
- [79] M. B. Giles and N. A. Pierce, "An Introduction to the adjoint approach to design," *Flow Turbulence and combustion*, vol. 65, pp. 393-415, 2000.
- [80] V. Challis, "Multi-Property Topology optimisation with the level set method," 2009.
- [81] P. H. Guillaume and I. K. Sid, "Topological sensitivity and shape optimisation for the Stokes equations," *SIAM Journal on Control and Optimisation*, vol. 43, no. 1, p. 1–31, 2004.
- [82] S. Amstutz, "The topological asymptotic for the Navier Stokes equations," *ESAIM: Control Optimisation and Calculus of Variations*, vol. 11, pp. 401-425, 2005.

- [83] X. Xing, P. Wei and M. Y. Wang, "A finite element based level set method for structural optimisation," *International Journal for Numerical methods in Engineering*, vol. 82 , pp. 805-842, 2010.
- [84] M. Sussman, P. Smereka and S. Osher, "A level set approach for computing solutions to incompressible two phase flow," *Journal of computational physics*, vol. 114, pp. 146-159, 1994.
- [85] S. Chen, M. Y. Wang and A. Q. Liu, "Shape feature control in structural topology optimisation," *Computer-Aided Design*, vol. 40, no. 9, p. 951–962, 2008.
- [86] G. Allaire, F. Jouve and G. Michailidis, "Thickness control in structural optimisation via a level set method," *Structural and Multidisciplinary optimization*, vol. 53, pp. 1349-1382, 2016.
- [87] X. Guo, W. Zhang and W. Zhong, "Explicit feature control in structural topology optimisation via level set method," *Computer Methods in Applied Mechanics and Engineering*, vol. 272, no. 0, pp. 354-378, 2014.
- [88] Z. Luo, L. Tong, M. Y. Wang and W. S, "Shape and topology optimisation of compliant mechanisms using a parametrization level set method," *Journal of Computational Physics*, vol. 227, pp. 680-705, 2007.
- [89] M. Otomori, T. Yamada, K. Izui and S. Nishiwaki, "Level set based topology optimisation of compliant mechanism design using mathematical programming," *Mechanical Sciences*, vol. 2, no. 1, pp. 91-98, 2011.
- [90] J. Nocedal and S. J. Wright, *Numerical Optimization*, New York: Springer-Verlag, 1999.
- [91] S. S. Rao, *Engineering Optimisation- Theory and Practice*, John Wiley & Sons, 2009.
- [92] P. W. Christensen and A. Klarbring, *An Introduction to structural optimisation*, Springer publications, 2009.

- [93] C. Fleury and V. Braibant, "Structural optimisation: A new dual method using mixed variables," *International Journal for Numerical Methods in Engineering*, vol. 23, p. 409–428, 1986.
- [94] K. Svanberg, "Method of Moving Asymptotes - a New Method for Structural Optimisation," *International Journal for Numerical Methods in Engineering*, vol. 24, no. 2, pp. 359-373, 1987.
- [95] K. Svanberg, "A class of globally convergent optimisation methods based on conservative convex separable approximations," *SIAM Journal of Optimization*, vol. 12, no. 2, p. 555–573, 2002.
- [96] R. Haftka and Z. Gurdal, *Elements of Structural Optimisation*, Kluwer Academic Publishers, 1990.
- [97] J. N. Reddy, *An introduction to the finite element method*, Third edition ed., McGraw Hill Higher Education, 2006.
- [98] A. Bejan, "Constructal-theory network of conducting paths for cooling a heat generating volume," *International Journal of Heat and Mass Transfer*, vol. 40, p. 799–816, 1996.
- [99] K. Lee, "Topology optimization of convective cooling systems," 2012.
- [100] Y. T. Yang, H. S. Peng and H. T. Hsu, "Numerical optimisation of Pin-Fin Heat sink with forced cooling," *International journal of electrical, computer, energetic, electronic and communication engineering*, vol. 7, no. 7, 2013.
- [101] M. Y. Wang, "TOPLSM199 Matlab code," [Online]. Available: <http://www2.acae.cuhk.edu.hk/~cmdl/download.htm>.
- [102] X. Liu, B. Zhang and J. Sun, "An improved implicit re-initialization method for the level set function applied to shape and topology optimisation of fluid," *Journal of Computational and Applied Mathematics*, vol. 281, pp. 207-229, 2015.

- [103] C. Hinterberger and M. Olesen, “Industrial application of continuous adjoint flow solvers for the optimization of automotive exhaust systems,” in *ECCOMAS Thematic conference*, Antalya, Turkey, 2011.
- [104] J. Thomsen, “Topology optimization of structures composed of one or two materials,” *Journal of structural optimisation*, pp. 108-115, 1992.
- [105] C. Hvejsel and E. Lund, “Material interpolation schemes for unified topology and multi-material optimization,” *Struct Multidiscip Optim*, vol. 43, no. 6, p. 811–825, 2011.
- [106] G. Allaire, C. Dapogny, G. Delgado and G. Michailidis, “Multi-phase Structural Optimization via a Level-Set Method,” *ESAIM: Control, Optimization and Calculus of Variations*, vol. 20, no. 2, p. 576–611, 2014.
- [107] G. Michailidis, “Manufacturing Constraints and Multi-phase shape and Topology Optimization via a Level-set method,” Ecole Polytechnique, 2014.
- [108] P. Liu, Y. Luo and Z. Kang, “Multi-material topology optimization considering interface behavior via XFEM and level set method,” *Computer methods Applied Mechanical Engineering*, vol. 308, pp. 113-133, 2016.
- [109] L. Yin and G. Ananthasuresh, “Topology optimization of compliant mechanisms with multiple materials using a peak function material interpolation scheme,” *Structural Multidisciplinary Optimization*, vol. 23, no. 1, p. 49–62, 2001.
- [110] T. Gao, W. Zhang and P. Duysinx, “A bi-value coding parameterization scheme for the discrete optimal orientation design of the composite laminate,” *International Journal of Numerical Methods Engineering*, vol. 91, no. 1, p. 98–114, 2012.
- [111] M. Bruyneel, “SFP—A new parameterization based on shape functions for optimal material selection: application to conventional composite plies,” *Structural Multidisciplinary Optimization*, vol. 43, no. 1, p. 17–27, 2011.
- [112] R. Tavakoli and S. Mohseni, “Alternating active-phase algorithm for multimaterial topology optimization problems: a 115-line MATLAB

implementation,” *Structural Multidisciplinary Optimization*, vol. 49, no. 4, p. 621–642, 2014.

[113] S. Zhou and M. Wang, “Multimaterial structural topology optimization with a generalized Cahn-Hilliard model of multiphase transition,” *Structural Multidisciplinary Optimization*, vol. 33, no. 2, p. 89–111, 2006.

[114] R. Haber, C. Jog and M. Bendsoe, “A new approach to variable-topology shape design using a constraint on perimeter,” *Structural and multidisciplinary optimisation*, vol. 11, no. 1, pp. 1-12, 1996.